


UNIVERSITY OF
BIRMINGHAM

# Prediction of Structural Integrity of the Ground Using Numerical Simulation of Soil Erosion around a Leaking Pipe

by

Ali Monzer

A thesis submitted to the University of Birmingham for the degree of

DOCTOR OF PHILOSOPHY

Department

School of Engineering

College of Engineering and Physical Sciences

University of Birmingham

June 2023

UNIVERSITY OF
BIRMINGHAM

## University of Birmingham Research Archive

### e-theses repository

This unpublished thesis/dissertation is copyright of the author and/or third parties. The intellectual property rights of the author or third parties in respect of this work are as defined by The Copyright Designs and Patents Act 1988 or as modified by any successor legislation.

Any use made of information contained in this thesis/dissertation must be in accordance with that legislation and must be properly acknowledged. Further distribution or reproduction in any format is prohibited without the permission of the copyright holder.

*"My Lord, increase me in knowledge"*

Quran - Surah Ta ha - Verse 114

I would like to dedicate this thesis to my loving family

# Abstract

Underground buried pipes are extensively used in water and sewer networks to fulfil domestic and agricultural demands. Leakage is a common issue associated with underground water networks that occurs due to cracks and holes in pipes which can lead to economic, environmental, health, and safety predicaments. Leakage can induce soil fluidisation resulting in severe consequences to the urban environment where pipes are commonly buried in and supported by the ground.

Soil fluidisation is the process of transition of soil particles from solid-like to liquid-like behaviour that can eventually lead to the failure of the surrounding ground and buried utilities. Understanding and predicting the initiation and propagation mechanisms of soil fluidisation around a leaking pipe is of particular importance for risk assessment of ground and buried assets. In addition, it is essential to determine the crucial parameters contributing to the fluidisation process to prevent severe damage and fatal consequences.

There have been considerable studies in the field of soil fluidisation process; however, majority of these research concentrated on the initiation of soil fluidisation around defective pipes, lacking fundamental studies addressing the soil-fluid interaction during the progression of soil fluidisation until it reaches the ground surface. The onset and progress of the soil fluidisation mechanism are significantly detrimental in identifying the severity of pipe leakage, maintenance of underground pipes, support of the ground, and transportation infrastructure. Therefore, a thorough understanding of soil fluidisation due to leakage should be achieved via a robust modelling method that properly addresses the influence of different soil and pipe parameters on fluidisation phenomenon. Physical modelling is expensive and time consuming whilst analytical modelling cannot be used to analyse complex problems. As such, often, numerical simulation is the preferred approach. Meanwhile, numerical simulation of pipe leakage problems often entails several challenges due to complexity of modelling associated with large deformations, soil-fluid interaction, and mesh distortions associated with traditional numerical methods such as the standard Lagrangian Finite Element Method (FEM). To overcome this, advanced computational

approaches such as Material Point Method (MPM) can be used. This method has proven to be a powerful technique in simulating large deformations in various multi-material and multi-phase geotechnical and hydraulic problems.

In this research, the soil fluidisation mechanism induced by a pressurised leaking pipe embedded in fully saturated soil is numerically modelled using MPM formulations, namely two-phase single-point (2P-SP) and two-phase double-point (2P-DP) approaches. Additionally, advanced inflow/outflow Boundary Conditions (BCs) are implemented in the double-point formulation to prescribe a velocity-controlled inflow of water into the domain.

The capabilities of two MPM approaches to simulate the onset and progression of soil fluidisation are presented and discussed. Displacement field and failure mechanism around a leaking pipe are analysed in terms of change in pore water pressure and soil porosity. The results have demonstrated that the 2P-SP MPM formulation is applicable for identifying the leak pressure required for the initiation of the local fluidisation in the vicinity of the orifice. The results of 2P-SP MPM approach were compared against standard FEM for reference which revealed both are not capable of capturing the post-local fluidisation mechanism due to numerical instabilities. However, the 2P-DP MPM formulation has proven to be an effective tool in capturing the progression of this phenomenon until it reaches the ground surface.

This thesis has successfully replicated an experimental pipe leakage problem using 2P-DP MPM approach. The observed results and fluidisation mechanism are consistent with the experimental data. The model is further developed to conduct an extensive parametric assessment of the impacts of different soil and pipe parameters on the soil fluidisation process. It has shown that the inflow velocity required for the onset and development of fluidisation decreases with the increase in orifice size and soil porosity. The bed height increases the resistance of the soil bed against fluidisation. Furthermore, the onset and progression of soil fluidisation are controlled by the flow direction and the burial depth of the pipe.

The numerical model presented in this thesis provides useful information that buried utilities companies and asset managers can utilise to improve and evaluate aspects associated with maintenance, operations, and remediation of pipe leakage problem and the supporting ground.

# Acknowledgements

First and foremost, I would like to express my sincere gratitude to my academic supervisors at the University of Birmingham, Dr Asaad Faramarzi and Prof. David Chapman for the opportunity and their invaluable support and guidance throughout my PhD studies.

An immense thank you to my external supervisor, Dr Alba Yerro Virginia Tech University, for introducing me to the Anura3D Research Community. Her unlimited support and unconditional guidance during my PhD journey. The completion of this research would not have been possible without her enthusiasm for the valuable advice and ideas implemented in this thesis.

I would like to convey my great thanks to my reviewers, Dr Bruno Fraga and Dr Dexter Hunt at the University of Birmingham, for their useful feedback and suggestions during the annual progress reviews.

I would like to extend my appreciation to my fellow researchers at Virginia Tech University, that I have collaborated with them to develop my numerical model. I would like to highlight John Murphy at the University of California, Berkeley for his kind guidance in terms of double-point MPM code. The output of this collaboration was published in a well-known academic journal (Journal of Geotechnical and Geoenvironmental Engineering-ASCE) and conference papers (Geo-Congress 2022 and NUMGE 2023).

I would like to acknowledge the School of Engineering scholarship for PhD in Geotechnical Engineering at the University of Birmingham for their financial support. It has been an honour to be the inaugural recipient of this scholarship. I must highlight the support of the School of Engineering as well as the National Buried Infrastructure Facility (NBIF) at the University of Birmingham for providing the necessary support to complete this research. I want to give my deepest appreciation to the British Geotechnical Associated (BGA) Fund Award for their financial support towards my attendance and presentation of my paper "Simulation of Soil Fluidisation Around a Pressurised Leaking Pipe Using the Material Point Method" in the Geo-Congress 2022 conference in North Carolina, United States. My sincere thanks to the exceptional

community, colleagues and friends: Ahmed Alagha, Asaad Kassem, Farough Rahimzadeh, Fatemeh Ardakani, Kassem El Cheikh Ali, Koohyar Faizi and Sahin Gunes. for their support, for being a great bunch of people and for making my doctoral degree enjoyable and for memories that I shall cherish for the rest of my life.

Special thanks and dedication to my family and my wife, Jana, who cheered me up in the difficult moments and I will always be in debt for all the love and support. My final thanks to all the people who believed in me and encouraged me to be the best that I could be.

# List of Publications

The following publications were prepared from this research during the course of the author's study.

- Monzer, A., Murphy, J., Yerro, A., Faramarzi, A., and Chapman, D. (2022).'Simulation of Soil Fluidisation Around a Pressurised Leaking Pipe Using the Material Point Method.' In *Geo-Congress 2022*, North Carolina, United States, pp. 363-374. Available at: https://ascelibrary.org/doi/abs/10.1061/9780784484050.038

- Monzer, A., Faramarzi, A., Yerro, A. and Chapman, D. 'MPM Investigation of the Fluidisation Initiation and Post-Fluidisation Mechanism Around a Pressurised Leaking Pipe', *Journal of Geotechnical and Geoenvironmental Engineering*. [Accepted]

- Monzer, A., Faramarzi, A., Yerro, A. and Chapman, D. 'Influence of Leakage Direction and Pipe Depth on the Soil Fluidisation Using the MPM', In *10th European Conference on Numerical Methods in Geotechnical Engineering*, London, UK. [Accepted]

- Monzer, A., Faramarzi, A., Yerro, A. and Chapman, D. 'A Review of Soil Fluidisation Triggered by a Defective Pipe'. [In preparation]

# Table of Contents

**List of Figures** **xi**

**List of Tables** **xvii**

**List of Abbreviations** **xviii**

**List of Symbols** **xix**

**1 Introduction** **1**

1.1 Background and motivation . . . . . 1

1.2 Aim and objectives . . . . . 6

1.3 Contribution to knowledge . . . . . 7

1.4 Layout of the thesis . . . . . 8

**2 Literature Review** **10**

2.1 Introduction . . . . . 10

2.2 Background . . . . . 10

2.3 Fluidisation . . . . . 11

2.4 Pipe Leakage . . . . . 12

2.5 Experimental studies on soil fluidisation around leaking pipes . . . . . 18

2.6 Numerical studies on soil fluidisation around leaking pipes . . . . . 34

2.6.1 Finite Element Method (FEM) coupled with Discrete Element Method (DEM) . . . . . 35

2.6.2 DEM coupled with Darcy fluid flow (DFF) . . . . . 36

2.6.3 DEM coupled with computational fluid dynamics (CFD) . . . . . 37

2.6.4 DEM coupled with lattice Boltzmann method (LBM) . . . . . 37

2.6.5 DEM coupled with smoothed particle hydrodynamics (SPH) . . . . . 38

2.6.6 Coupled Eulerian-Lagrangian (CEL) Method . . . . . 38
2.6.7 Particle Finite Element Method (PFEM) . . . . . 38
2.6.8 Material Point Method (MPM) . . . . . 39
2.7 Parameters involved in soil-leakage interaction . . . . . 44
2.7.1 Pipe-material behaviour . . . . . 44
2.7.2 Flow rate . . . . . 45
2.7.3 Leakage pressure . . . . . 47
2.7.4 Orifice size . . . . . 48
2.7.5 Orifice position . . . . . 49
2.7.6 Bed height . . . . . 50
2.7.7 Soil properties . . . . . 51
2.8 Key gaps of knowledge . . . . . 55
2.9 Summary . . . . . 58

**3 Methodology** **59**
3.1 Introduction . . . . . 59
3.2 Research methodology . . . . . 59
3.3 The Material Point Method: basic concept . . . . . 60
3.4 MPM multi-phase approaches . . . . . 63
3.4.1 Two-phase single-point MPM approach . . . . . 64
3.4.2 Two-phase double-point MPM approach . . . . . 67
3.5 MPM simulation process . . . . . 74
3.6 Summary . . . . . 75

**4 Capability of Different MPM Approaches in Modelling Soil Fluidisation** **77**
4.1 Introduction . . . . . 77
4.2 Numerical model . . . . . 77
4.2.1 Two-phase single-point (2P-SP) model . . . . . 79
4.2.2 Two-phase double-point (2P-DP) model . . . . . 82

4.3 Results and discussion . . . 86
4.3.1 Two-phase single-point (2P-SP) MPM results . . . 86
4.3.2 Two-phase double-point (2P-DP) MPM results . . . 92
4.4 Summary . . . 94

**5 Implementing the Proposed 2P-DP MPM Approach for Modelling Pipe Leakage 95**
5.1 Introduction . . . 95
5.2 Numerical model . . . 95
5.3 Results and discussion . . . 98
5.3.1 Soil fluidisation mechanism . . . 99
5.3.2 Parametric study . . . 106
5.4 Summary . . . 133

**6 Conclusions and Future Research 135**
6.1 Research outcomes and conclusions . . . 135
6.2 Recommendations for future research . . . 139

**References 142**

**Appendix A MPM numerical implementation 158**
A.1 2P-SP MPM approach . . . 158
A.1.1 Spatial discretisation . . . 158
A.1.2 Discretisation of the momentum balance equations . . . 159
A.1.3 Time discretisation . . . 161
A.2 2P-DP MPM approach . . . 161

**Appendix B Pipe leakage modelling using a water reservoir 164**

**Appendix C Mesh sensitivity analysis 167**

**Appendix D Boundary condition analysis 169**

**Appendix E Lateral leakage simulation** **171**

# List of Figures

Figure 1.1 Sinkhole in San Antonio, Texas caused by a buried pipe leakage (Cleve R. Wootson Jr., 2016) . . . . . 5

Figure 1.2 Sinkholes induced by water network leakages in the United Kingdom: (a, b) sinkhole in Selly Oak, Birmingham, November, 2016 (Campbell and Belcher-BM, 2016); (c, d) sinkhole in Islington, London, August 2022 (Telegraph, 2022) 6

Figure 2.1 Water leakage percentage across European countries [data retrieved from (EurEau, 2021)] . . . . . 13

Figure 2.2 Types of failure in pipes (Mora-Rodríguez et al., 2014) . . . . . 17

Figure 2.3 Schematic representation of transition stages of the fluidisation zone (Niven and Khalili, 1998) . . . . . 19

Figure 2.4 Schematic diagram of the experimental setup Zoueshtiagh and Merlen (2007) . . . . . 20

Figure 2.5 Experimental setup for fluidisation study (Alsaydalani, 2010) . . . . . 21

Figure 2.6 Stages of fluidisation of granular material (Alsaydalani, 2010) . . . . . 23

Figure 2.7 Schematic drawing of the experimental setup (van Zyl et al., 2013) . . . 24

Figure 2.8 Development of the fluidised region with the increase in the flow rate (van Zyl et al., 2013) . . . . . 25

Figure 2.9 Experimental model for internal fluidisation mechanism (Bailey and van Zyl, 2015) . . . . . 27

Figure 2.10 Plot of the velocity distribution in the Ballotini bed (Bailey and van Zyl, 2015) 28

Figure 2.11 Experimental model [after He et al. (2017)] . . . . . 29

Figure 2.12 Evolution of sand-bed erosion at different flow rates; (a) no cavity, stable cavity, (c) unstable cavity and (d) full fluidisation (He et al., 2017) . . . . . 30

Figure 2.13 Schematic presentation of the experimental setup and (b) range of the scouring volumes for different parameters at 180 h (Pike et al., 2018) . . . . . 31
Figure 2.14 Schematic section of the experimental setup (Latifi et al., 2022) . . . . . 32
Figure 2.15 (a) The observed fluidised and mobile bed zones around the leakage zone and (b) schematic drawing of the fluidised zones caused by leakage (Latifi et al., 2022) . . . . . 33
Figure 2.16 Three zones associated with fluidisation with a leak from an orifice (van Zyl et al., 2013) . . . . . 46
Figure 2.17 The variation in pressure (kPa) at the initiation of fluidisation with the change in orifice size (mm) (Alsaydalani and Clayton, 2014) . . . . . 49
Figure 2.18 The change in water flow rate, $q_w$, for different orifice positions, $\alpha$, with time (Tang, 2017) . . . . . 50
Figure 2.19 The variation in pressure (kPa) at the initiation of fluidisation with the change in bed height (m) and particle size (mm) (Alsaydalani and Clayton, 2014) 51
Figure 2.20 Sand vertical displacement ($U_z$) profile during the soil fluidisation for (a) loose soil with DR = 31%, (b) medium dense soil with DR = 61%, dense soil with DR = 88% (Tehrani et al., 2018) . . . . . 54

Figure 3.1 Overview of the research methodology followed in this research work . 60
Figure 3.2 Schematic representation of the spatial discretization of MPM (Fern and Soga, 2016) . . . . . 62
Figure 3.3 The computational strategy of MPM (Fern and Soga, 2016) . . . . . 63
Figure 3.4 Schematic diagram of different multi-phase MPM approaches [after Yerro et al. (2015)] . . . . . 64
Figure 3.5 Scheme of the two-phase single-point formulation [after Yerro and Rohe (2019)] . . . . . 65
Figure 3.6 Scheme of the two-phase double-point formulation [after Yerro and Rohe (2019)] . . . . . 68
Figure 3.7 Schematic of (a) inflow BC and (b) outflow BC . . . . . 74

Figure 3.8 Flowchart illustration of the implemented MPM simulation . . . . . 75

Figure 4.1 Experimental setup for internal fluidisation mechanism by Alsaydalani (2010) . . . . . 78

Figure 4.2 Discretised domain employed in the single-point modelled problem where 'p' is the applied water pressure, 'H' is the height, 'L' is the length, 'O' is the orifice, and 'E' is the empty space . . . . . 80

Figure 4.3 Effect of the number of elements at the orifice on the transmitted water pressure under different imposed excess water pressure (EWP) . . . . . 82

Figure 4.4 Discretised domain employed in the double-point modelled problem . . 84

Figure 4.5 Schematic of the effect of (a) two elements and (b) four elements at the orifice on the MPM simulation . . . . . 85

Figure 4.6 Effect of the number of elements at the orifice on the transmitted water velocity under different inflow velocities ($v_i$) . . . . . 86

Figure 4.7 Excess pore water pressure distribution in a submerged soil bed based on (a) MPM and (b) FEM results where an excess water pressure (10 kPa) is imposed at an orifice . . . . . 88

Figure 4.8 Excess of pore water pressure distribution at different heights (H) for a centred cross-section considering different applied pressures. FEM versus single-point MPM results . . . . . 89

Figure 4.9 Soil vertical displacement after 2s of simulation in a submerged soil bed where an excess water pressure of (a) p=10 kPa or (b) p=14.5 kPa is imposed at the orifice . . . . . 90

Figure 4.10 Soil vertical displacement during the post-local fluidisation mechanism in submerged soil bed where an excess water pressure of 16 kPa is imposed at the orifice . . . . . 91

Figure 4.11 Soil porosity after 2s of simulation at the SMPs (a) at the onset of fluidisation considering an inflow of $10^{-3}$ m/s and (b) when the fluidisation reaches the surface considering an inflow velocity of $10^{-2}$ m/s . . . . . 93

Figure 4.12 Soil vertical displacement after 2s of simulation at the SMPs when fluidisation reaches the surface (inflow velocity of $10^{-2}$ m/s) . . . . . 94

Figure 5.1 Geometry of the MPM model (unit: millimetres) . . . . . 97

Figure 5.2 Porosity distribution at different inflow velocities ($v_i$) through the centre-line of the soil bed . . . . . 102

Figure 5.3 Fluidised zone at the onset of fluidisation for (a) Alsaydalani (2010)'s experimental result with an orifice of 0.336 mm and (b) MPM result with an orifice of 10 mm after 2s of simulation (c) Fully developed fluidised zone based on MPM simulation after 2s of simulation . . . . . 103

Figure 5.4 Change in soil bed expansion ratio with different prescribed inflow velocities at a 10 mm orifice . . . . . 104

Figure 5.5 Soil vertical displacement at the onset of fluidisation for (a) Alsaydalani (2010)'s experimental result and (b) MPM result at an inflow velocity of 0.04 m/s. (c) MPM soil vertical displacement when fluidisation reaches the surface at an inflow velocity of 0.10 m/s . . . . . 105

Figure 5.6 Effective stress at different inflow velocities ($v_i$) through the centreline of the soil bed . . . . . 106

Figure 5.7 Porosity distribution at different inflow velocities ($v_i$) through the centre-line of the soil bed with different orifice sizes (o) . . . . . 109

Figure 5.8 Inflow velocity through different orifice sizes at the onset of fluidisation and when the fluidisation reaches the surface of the soil bed. The vertical lines demonstrate the variability of the inflow velocity . . . . . 110

Figure 5.9 Change of soil bed expansion ratio at different inflow velocities through different orifice sizes (o) . . . . . 110

Figure 5.10 Inflow velocity through different soil bed height at the onset of fluidisation and when the fluidisation reaches the surface in soil bed . . . . . 112

Figure 5.11 Change of soil bed expansion ratio at different inflow velocities through different soil-bed height (H) . . . . . 112

Figure 5.12 (a) Inflow velocity at the onset of fluidisation and when the fluidisation reaches the surface in soil bed with different initial soil porosity. (b, c, d and e) Soil porosity in soil bed with different initial porosity . . . . . 115

Figure 5.13 (a) Change in soil bed expansion ratio at different inflow velocities in soil bed with different initial soil porosity (n). Soil vertical displacement at an initial porosity of (b) 0.30 and (c) 0.45 . . . . . 116

Figure 5.14 (a) Inflow velocity at the onset and surface fluidisation in soil with different effective cohesion. Soil porosity at an inflow velocity of (b) 0.10 m/s and (c) 0.20 m/s in soil with the cohesion of 1 kPa and 50 kPa, respectively. The LMPs are represented with blue dots . . . . . 118

Figure 5.15 Change of soil bed expansion ratio at different inflow velocities in soil bed with different effective cohesion (c') . . . . . 119

Figure 5.16 Geometry of the MPM model of soil bed subjected to (a) upward leakage and (b) lateral leakage where Hp is the pipe burial depth (unit: millimetres) . . 121

Figure 5.17 Soil porosity at the onset and surface fluidisation in soil bed subjected to upward (a, b) and lateral (c, d) leakage at the different inflow velocities . . . . . 122

Figure 5.18 Different phases of the failure mechanisms of granular beds caused by lateral leakage: (a) static bed, (b) outwards movement of the grains, (c) creation of cavity, (d) and (e) enlargement of cavity, (f) cavity breaking the surface of the bed with a height of 200 mm and a defect opening of 0.23 mm (Alsaydalani, 2020) 123

Figure 5.19 Change of soil bed expansion ratio is soil bed subjected to different flow directions . . . . . 124

Figure 5.20 Soil porosity at the SMPs in the soil bed subjected to an upward leakage from a pipe with different burial depths . . . . . 127

Figure 5.21 Upward inflow velocity through a pipe located at different burial depths at the onset of fluidisation and when the fluidisation reaches the bed surface . . 128

Figure 5.22 Change of soil bed expansion ratio through a pipe located at different depths 128

Figure 5.23 Soil porosity at the SMPs in soil bed subjected to a lateral leakage from a pipe with different burial depths . . . . . 131
Figure 5.24 Lateral inflow velocity through a pipe located at different depths at the onset of fluidisation and when the fluidisation reaches the surface of the soil bed 132
Figure 5.25 Change of soil bed expansion ratio through a pipe located at different depths 132

Figure B.1 Discretised domain of pipe leakage problem . . . . . 164
Figure B.2 Soil vertical displacement in pipe leakage problem at different time; (a) 1s, (b) 2s, and (c) 3s . . . . . 166

Figure D.1 Soil vertical displacement when fluidisation reaches the surface at an inflow velocity of 0.10 m/s for MPM model with (a, b) fixed boundary and (c, d) contact boundary at the base of the soil bed . . . . . 170

Figure E.1 Geometry of the lateral leakage model (unit: mm) . . . . . 171
Figure E.2 Change of soil porosity in the soil bed subjected to a lateral leakage at different inflow velocities . . . . . 173
Figure E.3 Change of soil porosity in the soil bed subjected to a lateral leakage at different inflow velocities . . . . . 174

# List of Tables

Table 2.1 Pipe failure causes and the influence factors . . . . . 14

Table 2.2 Summary of the different numerical methods that have been used for soil-water interaction . . . . . 40

Table 4.1 Material parameters of the model, equivalent for the silica sand and water (* parameters only required for the double-point formulation) (Alsaydalani, 2010) 79

Table C.1 Mesh sensitivity analysis parameters . . . . . 168

# List of Abbreviations

| | |
|---|---|
| 2D | Two Dimensional |
| 2P-DP | Two-Phase-Double-Point |
| 2P-SP | Two-Phase Single-Point |
| BCs | Boundary Conditions |
| CEL | Coupled Eulerian Lagrangian |
| CFD | Computational Fluid Dynamics |
| CPU | Central processing unit |
| DEM | Discrete Element Method |
| DEM-LBM | Discrete Element Method-Lattice Boltzmann Method |
| DFF | Darcy Fluid Flow |
| DP | Double Point |
| EWP | Excess Water Pressure |
| FDM | Finite Difference Method |
| FEM | Finite Element Method |
| GB | Gigabyte |
| GDP | Gross Domestic Product |
| GHz | Gigahertz |
| HDPE | High-density Polyethylene |
| LBM | Lattice Boltzmann Model |
| Leighton Buzzard-A | Leighton Buzzard Sand – Fraction A |
| Leighton Buzzard-B | Leighton Buzzard Sand – Fraction B |
| LMPs | Liquid Material Points |
| MC | Mohr-Coulomb |
| MPM | Material Point Method |
| MPs | Material Points |
| NRW | Non-Revenue Water |
| OECD | Organisation for Economic Co-operation and Development |
| OS | Orifice/soil |
| PFEM | Particle Finite Element Method |
| pH | Potential Hydrogen |
| PIC | Particle-In-Cell |
| PIV | Particle Image Velocimetry |
| PSD | Particle size distribution |
| RAM | Random-access memory |
| SMPs | Solid Material Points |
| SPH | Smoothed Particle Hydrodynamics |
| TFM | Two-Fluid Model |
| uPVC | Unplasticised Polyvinyl Chloride |

# List of Symbols

| Symbol | Variable name | Unit measure |
|---|---|---|
| $a_L$ | Acceleration of the pore liquid | $m/s^2$ |
| $a_S$ | Acceleration of the solid skeleton | $m/s^2$ |
| $H_p$ | Buried depth | mm |
| $\sigma$ | Cauchy stress tensor | $Pa$ |
| $\kappa_L$ | Constant intrinsic permeability | $m^2$ |
| $\mu_L$ | Constant liquid viscosity | $Pa.s$ |
| $\sigma_{dev,L}$ | Deviatoric part of the stress tensor of the liquid | Pa |
| $\psi$ | Dilatancy angle | degree |
| $C_d$ | Discharge coefficient | - |
| $f^d$ | Drag force | N |
| $K_0$ | Earth pressure coefficient at rest | - |
| $c'$ | Effective Cohesion | $Pa$ |
| $\phi'$ | Effective friction angle | degree |
| $\nu'$ | Effective Poisson ratio | - |
| $\sigma'$ | Effective stress tensor | $Pa$ |
| $E'$ | Effective Young's modulus | $Pa$ |
| $\mu_{eq}$ | Equivalent viscosity | $Pa.s$ |
| q | Flow rate | $m^3/s$ |
| g | Gravitational acceleration | $m/s^2$ |
| H | Height | mm |
| h | hour | - |
| $v_i$ | Inflow liquid velocity | $m/s$ |
| $H_0$ | Initial bed height | $mm$ |
| $n_0$ | Initial porosity | - |
| $\tilde{n}^L_{S,el}$ | Interpolated element solid concentration ratio | - |
| $N_1$ | Leakage exponent | - |
| L | Length | mm |
| $\rho_L$ | Liquid density | $kg/m^3$ |
| $v_L$ | Liquid velocity | m/s |
| $n_{max}$ | Maximum porosity | - |
| $\rho_m$ | Mixture density | $kg/m^3$ |
| $\beta$ | Non-Darcy flow coefficient | - |
| $v_{io}$ | Onset inflow velocity | $m/s$ |
| o | Orifice | - |
| A | Orifice area | $m^2$ |
| $\alpha$ | Orifice position | degree |
| $\bar{\sigma}_L$ | Partial stress for the liquid phase | $Pa$ |
| $\bar{\sigma}_S$ | Partial stress for the solid phase | $Pa$ |
| p | Pore pressure | $Pa$ |

| Symbol | Variable name | Unit measure |
|---|---|---|
| h | Pressure head differential over the orifice | $mm$ |
| $D_R$ | Relative density | $\%$ |
| $D_p$ | Soil grain diameter | $mm$ |
| $\rho_S$ | Solid density | $kg/m^3$ |
| n | Solid porosity | - |
| $v_S$ | Solid velocity | $m/s$ |
| $v_{is}$ | Surface inflow velocity | $m/s$ |
| $D^L(.)/D_t$ | Time derivative of material for the liquid phase | - |
| $D^s(.)/D_t$ | Time derivative of material for the solid phase | - |
| $v_o$ | Velocity at the orifice | $m/s$ |
| $u_z$ | Vertical displacement | $mm$ |
| $n_L$ | Volumetric concentration ratio of liquid | - |
| $n_S$ | Volumetric concentration ratio of solid | - |
| $\varepsilon_{vol,L}$ | Volumetric strain of the liquid phase | - |
| $K_l$ | Water bulk modulus | $Pa$ |
| $q_w$ | Water flow rate | $m^3/s$ |
| $\mu_d$ | Water viscosity | $Pa.s$ |

# Chapter 1

# Introduction

## 1.1 Background and motivation

Every city is maintained operationally using a network of water, energy, and sewer infrastructure. With the expansion of cities, on one hand, and the advances in technology and engineering, on the other hand, this infrastructure network undergoes continual expansion and transformation. This continuous development of infrastructure systems, comprising both surface transportation infrastructure and subsurface utilities, offers substantial opportunities for further prosperous growth of urbanised cities' economy, as well as health and wellbeing of society. An important element of these systems are underground pipelines which are critical components of infrastructure in modern developed cities that are used for the transportation of water, sewage, gas and liquid fuels (Liu, 2017; Dave and Solanki, 2020). Both in the United Kingdom (UK) and worldwide, water main networks are considered the primary method to distribute potable water to citizens safely (Giustolisi et al., 2006). According to DiscoverWater (2022), the length of the water mains owned by water companies in the UK is approximately 347,636 km, mostly buried underground, supported by the ground and buried underneath surface transportation infrastructure. Given their significant role in urban systems, underground pipe networks need to be adequately maintained throughout their designed life span. However, the anticipated and designed life span and the performance of water networks can be adversely impacted by pipeline defects caused by several factors, including but not limited to pipe aging, corrosion, material defects, excavation, external loads, and internal pressure (Makar, 2001; Fang et al., 2011).

Among various reasons for pipe defects, pipe leakage is perceived to be a serious issue by water-management authorities, i.e., 35% of the transmitted water in the world is wasted as a

result of leakage (Hecke, 2020). For instance, the average water leakage is 24% in Europe (EurEau, 2021). In the United Kingdom, this problem amounts to 3,113 million litres of water that are lost daily (DiscoverWater, 2022). A leakage loss of 70% has been reported in the utilities of lower Gross Domestic Product (GDP) countries (Barbosa, 2022). Beside the loss of valuable fluids during transmission due to damaged pipes, water leakage in buried water distribution mains may result in other severe problems such as water shortage, subsurface contamination, and ground collapse (Xu et al., 2014; Peche et al., 2017; Karoui et al., 2018). Furthermore, water leakage can have significant economic consequences that adversely influence under-represented communities by damaging the structural integrity of the water networks and the quality of the water to the customers (Rogers, 2014). According to the World Bank, the cost of water leakage is valued at approximately $15 billion per year (Liemberger et al., 2008). In extreme cases, water leakage can damage the structural integrity of buried pipes and the surrounding infrastructure (Nath, 1983; Clarke et al., 2017). These negative consequences resulting from pipe leakage have been reported all over the world (Colombo and Karney, 2002).

Soil fluidisation is one of the consequences of water leakage which occurs when soil particles lose their interlocking forces and move freely within the pore (Richards Jr et al., 1990; Alsaydalani, 2010). Soil fluidisation and cavity formation in the leakage zone result from fluid seepage from cracks, joint openings, and other forms of pipeline structural failure (Li, 2013). This process results in reduction of bearing capacity and, subsequently, leads to surface subsidence usually in form of sinkholes. For example, Figure 1.1 demonstrates a deadly sinkhole triggered by an aging sewer pipe of 54-inches (1372 mm) diameter located in the industrial region of San Antonio, United States, 2016. This 12-feet (3658 mm) wide sinkhole caused injury and death to multiple civilians, as well as irreparable damage to several cars that collapsed into the sinkhole (Stelloh and Bacallao, 2016). Figure 1.2 presents two severe cases of water leakage leading to ground surface failure in the United Kingdom. The burst of a 42-inches (1067 mm) water main resulted in damaging various city roads and houses in Birmingham, UK, in November 2016 (Figure 1.2a and Figure 1.2b). Millions of litres of water caused the collapse of a traffic junction and flooded around ten houses. Apart from the financial consequences relevant to infrastructural damage, this

incident caused other severe socio-environmental impacts such as the disruption of businesses, major transportation lines, and civil services. Another example is a serious water leakage case in London, reported by the Telegraph (2022), that was caused by the burst of a 36-inches (915 mm) damaged water main (Figure 1.2c and Figure 1.2d). This case resulted in damaging fifty properties and injuring four people.

As a result of the rapid increase in the reported cases of ground collapses triggered by leaking pipes, sinkholes have been identified as a critical risk that can significantly damage underground infrastructures and cause significant social and economic drawbacks (Ali and Choi, 2019). Thus, understanding the dynamics and governing processes of underground pipe leakages, including the soil-fluid interaction, is an essential factor for maintaining the infrastructure, and consequently preventing the aforementioned disasters.

Pipelines are commonly buried underground, which hinders their visual inspection and the observation of fluidisation caused by water leakages. Numerous laboratory studies have been conducted to investigate the soil fluidisation mechanism around leaking pipes (Rogers et al., 2008; Teeluckdharry, 2017). However, difficulties and uncertainties at the data acquisition phase inhibited these studies from determining essential factors for interpreting the soil-fluid behaviour, including the fluidising pressure and soil displacement aspects (Li, 2013; Cui et al., 2014). To undertake more effective measures, further studies are required to fill knowledge gaps of the soil-fluid behaviour, for example the transition to the post-fluidisation process under the above mentioned circumstances (Zhu et al., 2018).

At the same time, considerable efforts have been made to develop numerical simulation of the soil fluidisation around a leaking pipe through different approaches. This includes Finite Element Method (FEM) analyses (for example the work by Zhu et al. (2018) investigating the effects of various parameters including water pressure, crack lengths and location, and soil layering on the flow regime. From previous experimental work, it has been observed that once fluidisation occurs, a localised cavity forms near the leakage zone that is characterised by large deformations. Due to the localised large soil displacements, standard FEM suffers from mesh distortion and tangling (Wang et al., 2015), and it is not capable of simulating the

entire mechanism. Accordingly, alternative methods are more suitable for the simulation of large deformations. For example, Cui (2013) investigated the inhomogeneities of granular particle behaviour in the soil fluidisation around a leaking pipe using coupled Discrete Element Method-Lattice Boltzmann Method (DEM-LBM). However, for real-scale pipe leakage problems, DEM is computationally expensive. Therefore, a thorough understanding of the soil fluidisation around a leaking pressurised pipe should be established through an efficient numerical method that is applicable to simulate such a "multiphase" large deformation problem (Bolognin et al., 2017). Such methods should be capable of addressing the influence of different soil and pipe parameters on the soil-leakage system and the evolution of the soil fluidisation mechanism with effective computational time.



(a)




(b)

**Figure 1.1:** Sinkhole in San Antonio, Texas caused by a buried pipe leakage (Cleve R. Wootson Jr., 2016)




**Figure 1.2:** Sinkholes induced by water network leakages in the United Kingdom: (a, b) sinkhole in Selly Oak, Birmingham, November, 2016 (Campbell and Belcher-BM, 2016); (c, d) sinkhole in Islington, London, August 2022 (Telegraph, 2022)

## 1.2 Aim and objectives

The aim of this research is to accurately capture and simulate the fluidisation mechanisms of soil due to leakage from a buried pressurised water pipe using an advanced computational modelling method. To attain this aim, the following objectives were defined.

1. To conduct a comprehensive assessment of studies on soil fluidisation associated with leakage from a pressurised water pipe, including experimental and numerical approaches, and to identify the advantages and disadvantages of each method.

2. To review soil fluidisation mechanism induced by a leaking buried pressurised water pipe, as well as the parameters involved within these mechanisms and the role of soil-fluid interaction and their overall effect on ground stability.

3. To develop a robust numerical model to capture the soil-fluid interaction associated with water discharge from leaking pressurised water pipes.

4. To validate the proposed model against previous experimental and numerical studies and compare its capability to other numerical methods in modelling the soil fluidisation mechanism.

5. To employ the proposed model to investigate the impact of different soil and pipe properties on the soil fluidisation process, such as the leakage pressure/velocity, the orifice size, the bed height, the soil porosity, the soil cohesion, the leakage orientation, and the pipe depth.

## 1.3 Contribution to knowledge

This PhD makes advances in the field of simulating fluidisation through computational modelling of ground and water flow from a leaking pipe. Soil fluidisation triggered by leakage from a defective pressurised pipe exhibiting complex behaviour that involves multiphase interaction. Therefore, this PhD focuses on developing an advanced numerical model, using Material Point Method (MPM), capable of simulating the multiphase interaction associated with a leaking underground water pipe. The fulfilment of the described objectives produced the following novelty and contributions to the field of knowledge.

1. Developing MPM numerical models to simulate leakage from a pressurised water pipe into the soil bed, in which the limitations of previous studies in capturing the initiation and progression of the soil fluidisation mechanism were addressed and rectified.

2. Integrating and comparing the different multiphase MPM approaches to model the initiation and development of soil fluidisation around the leaking pipe. In addition, advanced

inflow/outflow Boundary Conditions (BCs) for simulating the water inflow to the domain were implemented in the two-phase double-point (2P-DP) MPM formulation.

3. Investigating the effect of different soil and pipe parameters on the soil fluidisation phenomenon. The model considers the impact of the leakage velocity, the orifice size, the orifice location/depth, the bed height, the soil porosity and the soil cohesion on the soil fluidisation mechanism. This will provide a strong tool for prioritising the controlling parameters in leakage assessments.

4. The model developed in this study can be used as a prediction tool to estimate the significance and progress of fluidisation zone and to determine the critical state that leads to ground failure.

## 1.4 Layout of the thesis

The thesis is divided into six chapters, starting with an introduction to put the research problem into context, followed by reviewing the relevant studies, introducing the developed numerical model for the pipe leakage problem, presenting parametric analysis and the obtained results, research conclusions, and finally recommendations for future works. The content of the six chapters of this thesis is outlined below:

**Chapter 1** (this chapter) provides a brief background on the pipe leakage problem and states the aim, objectives, and overview of the research;

**Chapter 2** reports a critical and comprehensive review of the literature relevant to the soil-fluidisation mechanism triggered by a leaking pipe. This chapter summarises the published experimental and numerical modelling attempts available in literature conducted on soil-leakage interaction, including the parameters that contributed to this phenomenon. This helps in demonstrating the importance of current research and to identify the key findings and the gaps in knowledge;

**Chapter 3** presents the developed numerical modelling approaches, i.e., two-phase single-point Material Point Method (MPM) and two-phase double-point Material Point Method (MPM), that were utilised to accomplish the aim of this research. The basis of the Material Point Method (MPM) multiphase formulations is reviewed in this chapter, followed by a description of the computational solution in each approach;

**Chapter 4** investigates the capability of two-phase single-point MPM and two-phase double-point MPM approaches in modelling the soil fluidisation mechanism around a leaking pressurised water pipe. Moreover, a comparison between the MPM and Finite Element Method (FEM) results is conducted to validate the advantages of the MPM model over the FEM in the prediction of the fluidisation phenomenon initiation;

**Chapter 5** presents and discusses the results obtained with the advanced two-phase double-point MPM technique to study the initiation and progression of soil fluidisation induced by a leaking pipe. This chapter also reports the validation of the MPM results against previous experimental data. Parametric sensitivity analyses are then presented to investigate the influence of different soil and pipe properties on soil fluidisation;

**Chapter 6** summarises the conclusions derived from this study, the contributions to the literature, and the suggestions for future works.

# Chapter 2

# Literature Review

## 2.1 Introduction

This chapter summarises the literature review of the previous experimental and numerical research on soil fluidisation mechanism induced by pipe leakage. Key findings and identified gaps in the literature are highlighted at the end of this chapter.

## 2.2 Background

Non-revenue water (NRW) refers to the water that is not delivered to intended consumers. These water losses can be physical losses induced by pipe leakage or apparent losses due to inaccuracies in metering, theft, or unmetered usage. Whilst water utilities in developed countries have systems for monitoring these losses, majority of NRW losses occur due to physical leaks and breaks. Water loss due to pipe leakage is a rising predicament in many urban areas. According to a survey conducted by the Organization for Economic Co-operation and Development (OECD, 2016), leakage rates range from 4% in Amsterdam to 65% in Mexico City. Pipe leakage is caused by poor construction, deterioration, external loads, lack of maintenance, geological hazards, and seasonal soil variations. According to the World Bank, the world's pipe leakage amounts to over 8 billion US dollars in loss annually (Kingdom et al., 2006). Furthermore, leaks may cause damage to underground and surface infrastructure by weakening the surrounding soils (Waltham, 1993) which can cause significant financial damages or even fatal injuries (Rogers, 2014).
Previous studies have shown that pipe leakage may result in soil fluidisation when a sufficient leakage rate is present (Alsaydalani, 2010; Li, 2013). Soil fluidisation due to underground pipe

water leakage can mobilise and displace the surrounding soil particles, generating an underground cavity in the leakage region (Guo et al., 2013). Under continuous leakage, the formed cavity can further develop and propagate to the soil surface leading to ground failure (Tang, 2017). Considering the potential severity of the pipe leakage problem, it is essential to understand the water-soil interaction around a leak to maintain safety of urban infrastructure.

## 2.3 Fluidisation

The fluidisation mechanism is a multidisciplinary phenomenon occurring in different fields of study including chemical engineering, ocean engineering, geology and civil engineering. In chemical engineering, the fluidisation phenomenon occurs when solid particles are separated by a flow of gas or fluid and transformed into a liquid-like state (Cathala, 1953). This phenomenon has been investigated by different researchers in chemical engineering to regulate the behaviour of reactors in chemical reactions (Taghipour et al., 2005; Al-Farraji, 2017). In the field of ocean engineering, fluidisation has been proven as a useful navigable tool for the maintenance of waterways at tidal inlets and harbour mouths (Weisman et al., 1988; Ledwith et al., 1990). Weisman et al. (1988) observed that the flow emerging from perforations in source pipes can fluidise a sand bed when a local boil of sand is induced by the greatest hydraulic pressure. Similarly, fluidisation has been studied in geology, where upward forces exerted by fluid flowing through a loose bed drag the grains deposited by gravity (Lowe, 1976). A significant number of studies have been conducted on fluidisation in this field to explain tectonic movements (Mourgues and Cobbold, 2006) and the formation of volcaniclastic materials (Gernon et al., 2009). Nevertheless, soil fluidisation can be caused by fluid flow in different situations in civil engineering. Soil fluidisation is defined as the process by which soil particles lose their interlocking forces and turn into a viscous fluid or fluid-like state (Richards Jr et al., 1990). This process initiates in the leak region as the effective stresses reduce to zero due to an increase in pore water pressure. Usually, in urban underground applications, the fluidisation process can occur when a soil bed is subjected to water flow. Leva (1959) stated that soil fluidisation occurs when

the seepage flow is sufficient to drag the soil bed. Soil fluidisation occurs as the hydraulic gradient reaches its critical value due to the increase in pore water pressure (Das and Sivakugan, 2018). There are various cases where soil fluidisation can occur in the geotechnical field, for example, in shaft construction during jetting works (Alsaydalani and Clayton, 2014). The post-construction leakage around seepage barriers results in soil fluidisation which may reduce the bearing strength and the stability of the foundations. Examples of these are the Navajo Dam (Dewey, 1988) and Twin Buttes Dam (Bruce et al., 2006) in the United States. Both cases suffered postconstruction cracking in seepage barriers. Tsinker (1988) showed that a driven pile might suffer from the fluidisation phenomenon in the surrounding ground due to water flow. In addition, leakage from a fractured (pressurised) water pipe into the surrounding soil may increase pore water pressures and potentially lead to soil fluidisation (Awad and Karni, 2000; Noack and Ulanicki, 2008; van Zyl et al., 2013). After reaching a certain threshold of the flow rate and pore water pressure, the upward flow force at the pipe opening will dominate the weight of overlying saturated soil (van Zyl et al., 2013) leading to soil movement where soil particles will fluidise (Alsaydalani and Clayton, 2014). Despite the fact that soil fluidisation was studied extensively as mentioned, the significant influence of pipe leakage on ground stability was not addressed clearly, in particular the evolution of soil fluidisation with time was not shown.

## 2.4 Pipe Leakage

The extent of the underground water supply network throughout the world is countless. In the United Kingdom, water companies are responsible for 347,636 kilometres of pipes (Discover-Water, 2022). Water leakage in the distribution system is a rising and serious concern faced by water companies (Ali and Choi, 2019). Leakage is the loss of treated water from the water supply system including losses from industrial and domestic networks (OFWAT, 2022). Water loss due to pipe leakage is a major issue for various countries around the world, with a global leakage rate of 35% (Global Water Leakage Summit, 2008). Figure 2.1 shows the leakage rate by percentage in water distribution systems in 24 European countries (EurEau, 2021). According to the water

service suppliers across Europe (EurEau), the average value for water leakage is 24% and this value for the United Kingdom is 23% which is about the average.

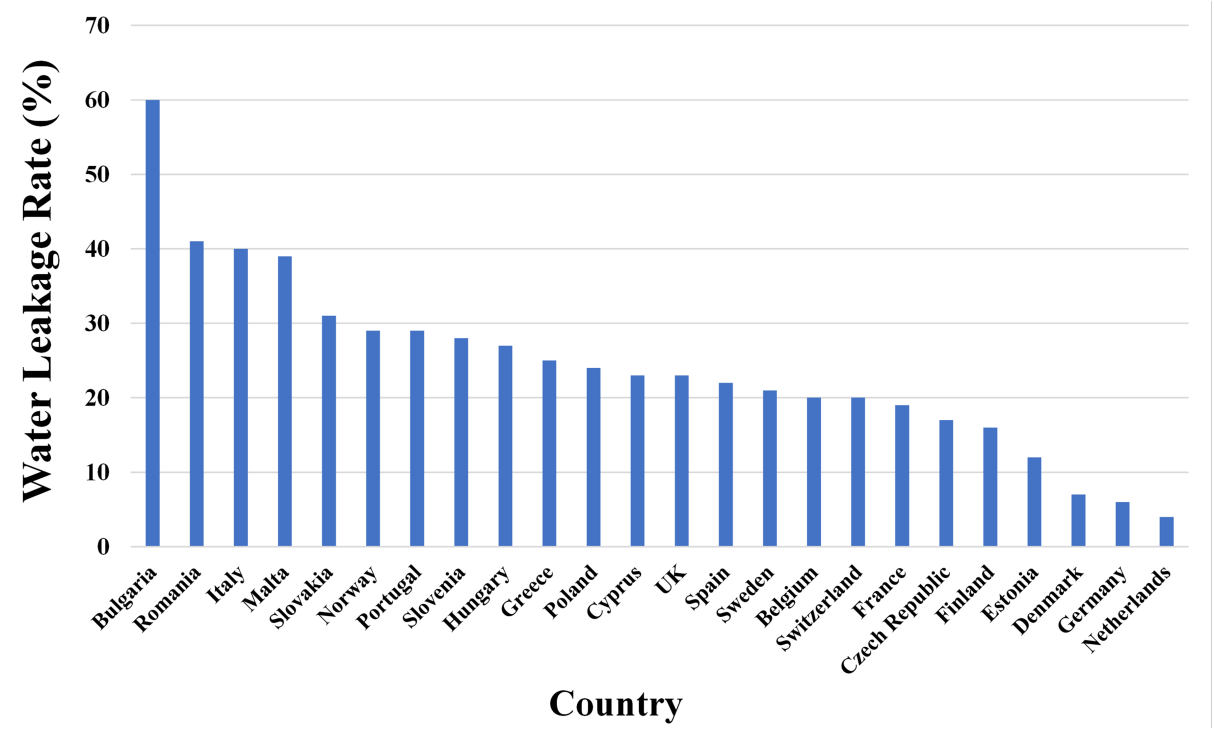



**Figure 2.1:** Water leakage percentage across European countries [data retrieved from (EurEau, 2021)]

Pipe failures are the most common causes of leakage that are associated with pipe material, environmental and operating conditions. Leakage from pipe cracks may fluidise the surrounding soil when there is sufficient flow (van Zyl et al., 2013; Bailey and van Zyl, 2015). Table 2.1 presents the most important reasons of pipe breakage and the contributing parameters. Pipe leakage can result from pipe properties (diameter, material, age, length and wall thickness), excessive loading (internal and external), corrosion, degradation (internal and external) and climate (temperature, groundwater level and soil) (Almeida and Ramos, 2010; Rezaei, 2016).

**Table 2.1:** Pipe failure causes and the influence factors

| Failure cause | Influence factor | Comments |
|---|---|---|
| Pipe properties | Diameter | Smaller diameter pipes with lower strength and wall thickness are characterised by higher failure rate (Andreou et al., 1987; Rajani and Kleiner, 2001). |
| | Material | Pipe material affects strength properties and corrosion resistance. Cast Iron is a strong and brittle pipe while Ductile Iron is more resistant to breakage and corrosion (Makar, 2001). Polyvinyl chloride and polyethylene pipes are vulnerable to corrosion by organic contaminants (St. Clair and Sinha, 2014). |
| | Age | Pipe age contributes to its deterioration and failure (Clark et al., 1982; Berardi et al., 2008). It is an indicator of the service length, loading and environmental exposure, manufacturing process and installation methods (Malm et al., 2012). |
| | Length | The probability of pipe failure increases with the increase in pipe length (Boxall et al., 2007; Yamijala et al., 2009). |
| | Wall thickness | Thinner walls are highly influenced by external stresses (Røstum, 2000). |

| Failure cause | Influence factor | Comments |
|---|---|---|
| Loading | Internal | Internal pressure including pressure transients may result in excessive stresses leading to pipe failure (Mora-Rodríguez et al., 2014). |
| | External | Traffic and cyclic loading results in non-uniform stress distribution around the pipe and ultimately pipe breakage (Rajeev et al., 2014). External stresses from the surrounding ground during construction works increase the failure rate (Jenkins et al., 2015). |
| Corrosion | Internal | The water quality (pH, alkalinity, temperature, chlorine residual, etc.) and interaction with the internal pipe contribute to the rate of internal corrosion (Rajani and Kleiner, 2001; Yamini and Lence, 2010). |
| | External | The soil-pipe interaction commonly deteriorates and weakens the pipe (Doyle et al., 2003). The soil contaminants including sulfates and alkalis result in concrete corrosion of pipes (Rezaei, 2016). The presence of inorganic and organic acids accelerates external corrosion in metallic pipes (Liu et al., 2010). Pipe failure is highly caused by the absence of cathodic protection (Kleiner et al., 2003). |

| Failure cause | Influence factor | Comments |
|---|---|---|
| Climate | Temperature | The pipe breakage rate exacerbates in severe winter (Wols and Van Thienen, 2014) and the presence of high-temperature changes between the water and surrounding soil (Rajani and Tesfamariam, 2004). Frost heave could lead to pipe failure by increasing the vertical loads (Rajani and Kleiner, 2001). |
| | Groundwater level | Groundwater lowering due to an extreme deficit of rain may increase the ground differential settlements and eventually break the pipes (Kakoudakis, 2019). |
| | Soil | Soil behaviour is controlled by weather extremes (Hu and Hubble, 2007). The ground movement caused by soil shrinking or swelling results in pipe degradation and failure (Gould et al., 2011). The pipe depth and freeze or thaw vulnerability highly affect the pipe breaks (Stuart, 2011). |

Leakage can occur in various components of the water distribution systems depending on the types of failures of pipes. The typical failure modes of water distribution pipes (Figure 2.2) are categorised into circumferential breaks, longitudinal breaks, joint failure, and holes (O'Day, 1989; Jesson et al., 2017).

The circumferential failures often occur in smaller diameter pipes (< 200 mm) that are caused by tensile forces including differential soil settlement, thermal contraction and expansion, inadequate installation and external loadings (Mordak and Wheeler, 1988; Wengström Rd, 1993; Bruaset and Sægrov, 2018). The internal pressure within the pipe can lead to circumferential breaks when it is accompanied with external tensions (Rajani and Kleiner, 2001). Longitudinal fractures are commonly observed in cast iron pipes (up to 600 mm diameter) as a consequence of radial and transverse stresses resulting from internal pressure, traffic loads, ground forces and seasonal

changes (Rajani and Kleiner, 2001; Kunkel et al., 2008). Joint pipe breaks including leakage, fracture, disconnection, and gasket failure are mainly caused by tensile or compressive stresses. Poor installation, corrosion, chemical degradation and ground movement can impose joint failure (Mordak and Wheeler, 1988; Twort et al., 2001; Vreeburg et al., 2013; Ruchti, 2017). Holes leaks (blowouts and pinholes) result from radial stresses associated with corrosion (Makar, 2001; Rajeev et al., 2014). On average, circumferential breaks account for 70% of total pipe failures, whereas the other 30% are longitudinal, joint and hole failures (Rajani et al., 1996).

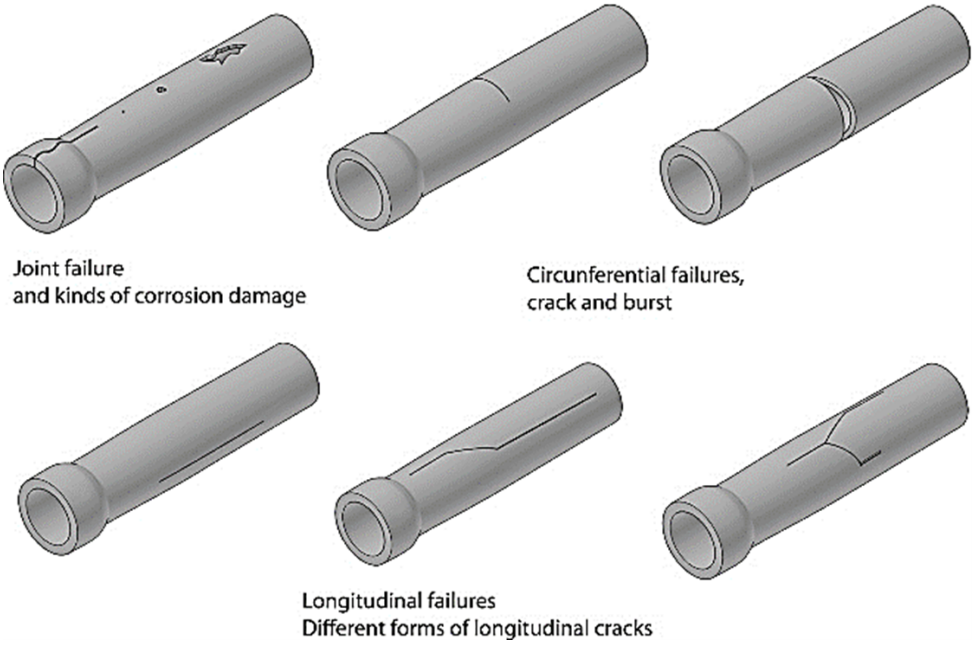



**Figure 2.2:** Types of failure in pipes (Mora-Rodríguez et al., 2014)

There are several methods for leakage classification depending on pipe diameter, leakage pressure, crack size, etc. According to Daoudi et al. (2005), leakage can be classified based on the leakage flow rate into small leaks for a flow rate lower than 5 l/min and large leaks for a flow rate greater than 5 l/min. Adedeji et al. (2017) categorised leaks into three groups specifically reported, unreported, and background. Reported and unreported leakages are induced by the structural failure of the pipe. The reported type of leakage to the water authority is normally surface related; while the unreported leakage does not reach the ground surface but is detectable. On the other hand, background leakage is hidden loss through creeping joints or small cracks along a pipe (Adedeji et al., 2017). This latter type of leakage is difficult to detect; therefore, can

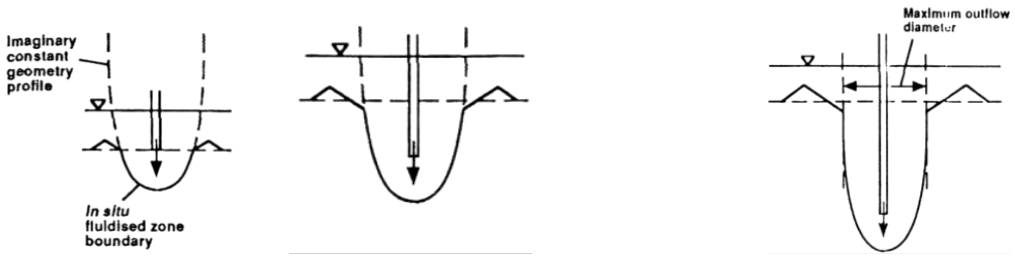
concur continuously for a longer time. In this contribution, an overview of pipe leakage and information necessary to understand the various causes and types of failure of pipe are presented and analysed. A comprehensive review of the previous experimental and numerical studies performed to understand the soil fluidisation mechanism due to pipe leakage is provided in the next section.

## 2.5 Experimental studies on soil fluidisation around leaking pipes

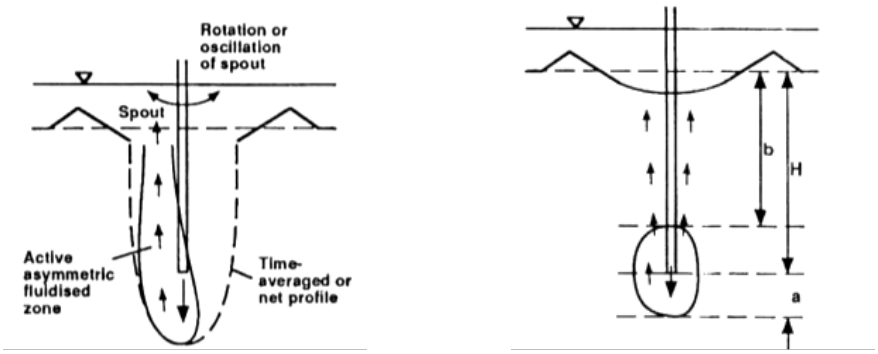
Previous experimental studies have focused on the soil fluidisation mechanism induced by a pipe leakage (Germanopoulos and Jowitt, 1989; Lennon and Weisman, 1995; Awad and Karni, 2000; Lambert, 2001; Mukunoki et al., 2012; Pike et al., 2018; Latifi et al., 2022). These existing studies further expanded understanding of soil-leakage problems through examining effects of different soil and pipe parameters on soil fluidisation. Ledwith et al. (1990) performed an experiment to examine the water pressure and flow rate required for the initiation and full development of fluidisation. These experiments were conducted in sand with different grain sizes (fine, medium and coarse) at varied bed heights (254 and 420 mm). Twelve different orifice sizes, ranging between 1.59 mm and 6.35 mm, were drilled opposing one another in a pipe with a diameter of 50.8 mm. The observations from this study demonstrated that significant pressure head could be sustained in the soil bed without reaching the bed surface, even only in the 420 mm soil bed.

Niven and Khalili (1998) investigated the fluidisation of granular material induced by a vertical jet. The scour of granular soil was triggered by a vertically downward jet ultimately leading to soil fluidisation. They studied the impact of granular material and jet diameters on the fluidisation zone. Experiments were designed using five granular samples, including fine sand, medium to coarse sand, coarse sand, very coarse sand and silty clayey sand. The jet diameter was varied between 4 mm and 14 mm. The results showed that the fluidisation mechanism is defined by the deposition of granular soil in the form of a circular ridge surrounding the fluidised region.

(Niven and Khalili, 1998) observed that the fluidised profile progresses from an open stable zone to cavity formation with the increase of jet depth as shown in Figure 2.3. Their analysis indicated that a uniform fluidised zone is formed independently of the size of granular material and jet diameter.




(a) Initiation (b) Stable fluidisation (c) Maximum depth of stable (open) fluidisation




(d) Asymmetric unstable (open) fluidisation (e) Submerged fluidised cavity

**Figure 2.3:** Schematic representation of transition stages of the fluidisation zone (Niven and Khalili, 1998)

Zoueshtiagh and Merlen (2007) studied the behaviour of a granular bed subjected to a vertically flowing water jet. They evaluated the effect of bed height, orifice size, and flow rate on the fluidisation mechanism. The experiment was conducted using a 240 mm diameter vertical Plexiglas cylinder tank that is shown in Figure 2.4. A disk that formed the bottom of the tank consists of interchangeable sub-cylinders with varied diameter (3, 15 or 35 mm). All experiments were conducted in a fully saturated condition and a 210 $\mu$ m grid was used above each sub-cylinder to prevent grains from falling into the jet. Three distinct regimes of the granular bed were observed depending on the flow rate. At a low flow rate, the bed behaved similar to a rigid

porous medium and thus remained motionless (Regime 1). Local distortion of the granular bed was recognised at higher flow rates (Regime 2). Zoueshtiagh and Merlen (2007) defined this regime as the transitional stage where the local fluidisation is initiated around the jet. The bed exploded and the fluidisation reached the bed surface as the flow rate was increased (Regime 3). The authors defined the fluidised region as a cylindrical chimney in which the grains within this zone moved vertically while the surrounding grains remained stable and behaved as a solid skeleton. The investigations showed that the initiation of fluidisation and the diameter of the chimney were independent of the size of the jet. Furthermore, the bed height significantly influenced the flow rate required for the onset of soil fluidisation.

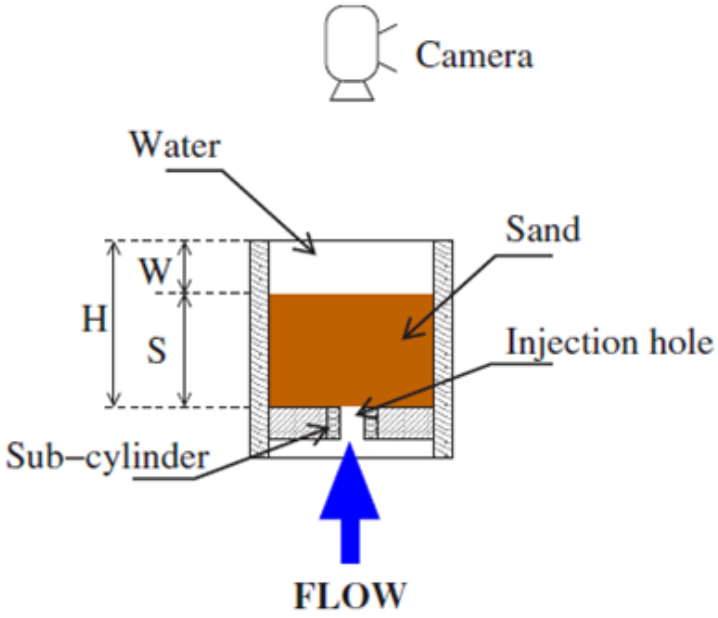



**Figure 2.4:** Schematic diagram of the experimental setup Zoueshtiagh and Merlen (2007)

Alsaydalani (2010) adopted an experimental approach using a small-scale model to investigate the soil fluidisation mechanism around a vertical jet emanating from a leak. Experiments were carried out using a 1060 mm x 550 mm x 153 mm Plexiglas tank that was attached to the bottom of an aluminium box, of dimensions 330 mm in length, 152 mm in height, and 105 mm in width. In the box, the orifice was designed as an adjustable longitudinal crack that allowed flexibility in the orifice opening. A soil bed measuring 600 mm x 300 mm x 146.6 mm was tested in all experiments. The schematic representation of the experimental apparatus is shown in Figure 2.5

which consisted of pressure gauges to record the upstream pressure of the orifice and sight tubes to measure the excess pore water pressure in the soil bed. Particle Image Velocimetry (PIV) was used to monitor the behaviour of the soil bed, particularly the movement of the granular particles during the fluidisation process.

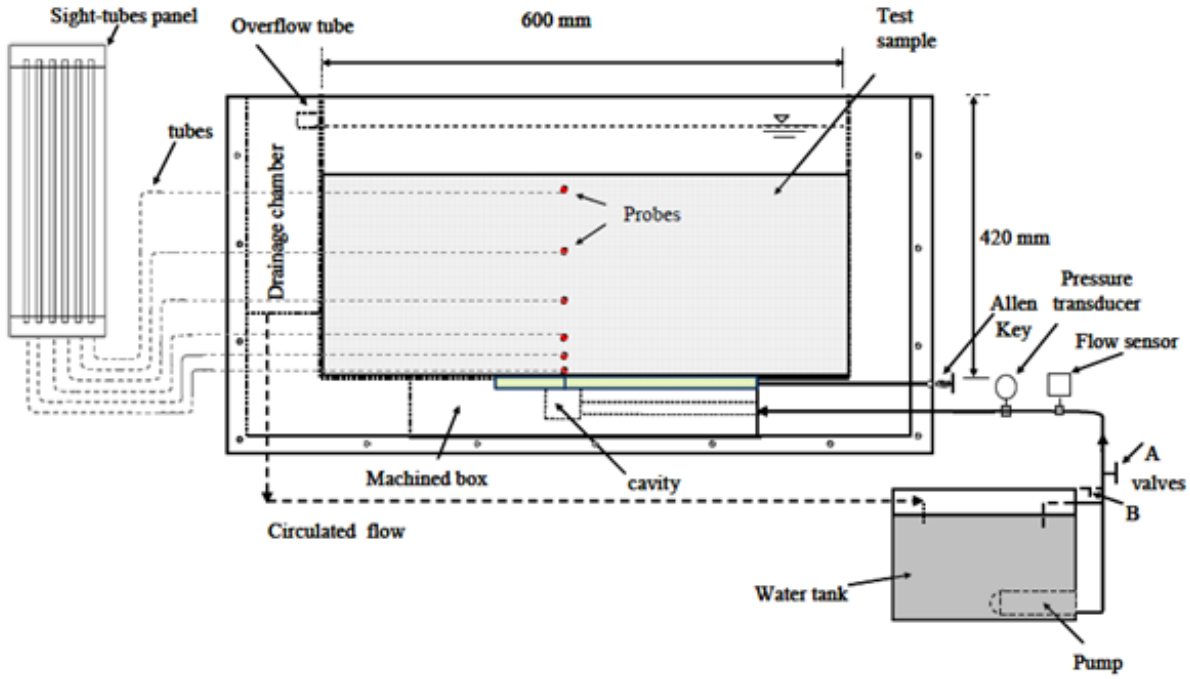



**Figure 2.5:** Experimental setup for fluidisation study (Alsaydalani, 2010)

In the tests previously outlined, the leakage rate at the orifice into a granular soil layer was incrementally increased until the initiation of internal fluidisation. It was observed that by increasing the flow rate, the excess pressure in the soil bed increased up to a peak point. Immediately after the peak, an abrupt drop in excess pore water pressure was observed which was associated with the onset of fluidisation in the vicinity of the orifice. The experimental sequence of the fluidisation mechanism is shown in Figure 2.6. The fluidised region progressively enlarged with the increase in the flow rate until it ultimately reached the soil bed surface. This study demonstrated that the onset of soil fluidisation is controlled by the flow rate, the size of the particles, the particle shape, and the bed height. Four types of granular materials were studied: Glass Ballotini, Leighton Buzzard-A, Leighton Buzzard-B, and Silica Sand. It was observed that

the soil properties (i.e. size and shape) unlike the orifice size, strongly impacted the fluidisation mechanism.

Experimental tests conducted by Alsaydalani (2010) compared the ratio of total head loss through the orifice to that in the soil bed. The total head loss due to flow through the orifice was obtained by estimating the difference between the head upstream of the orifice and the head in the orifice. Alsaydalani observed that most of the energy losses occurred through the orifice (98% of the total energy losses) while a relatively small amount (2%) dissipated through the soil bed. This is consistent with Walski et al. (2006)'s experimental verification that total head losses due to Darcy's flow through the soil mass in the leakage problem are generally much smaller than that in the orifice. Alsaydalani (2010) successfully investigated different parameters involved in the soil fluidisation process such as particle size, particle velocity, cavity size and pore water pressure distribution. However, essential factors for interpreting the soil-fluid behaviour including the particle contact forces and the fluid-particle forces were not determined in the conducted laboratory tests. The study focused solely on uniform granular material, highlighting the need for further investigation into materials like widely graded material and clay to explore different mechanisms. Furthermore, while water was used as the injection fluid in upward seepage flow tests, future research could enhance the understanding by exploring different flow directions, such as horizontal or downwards.

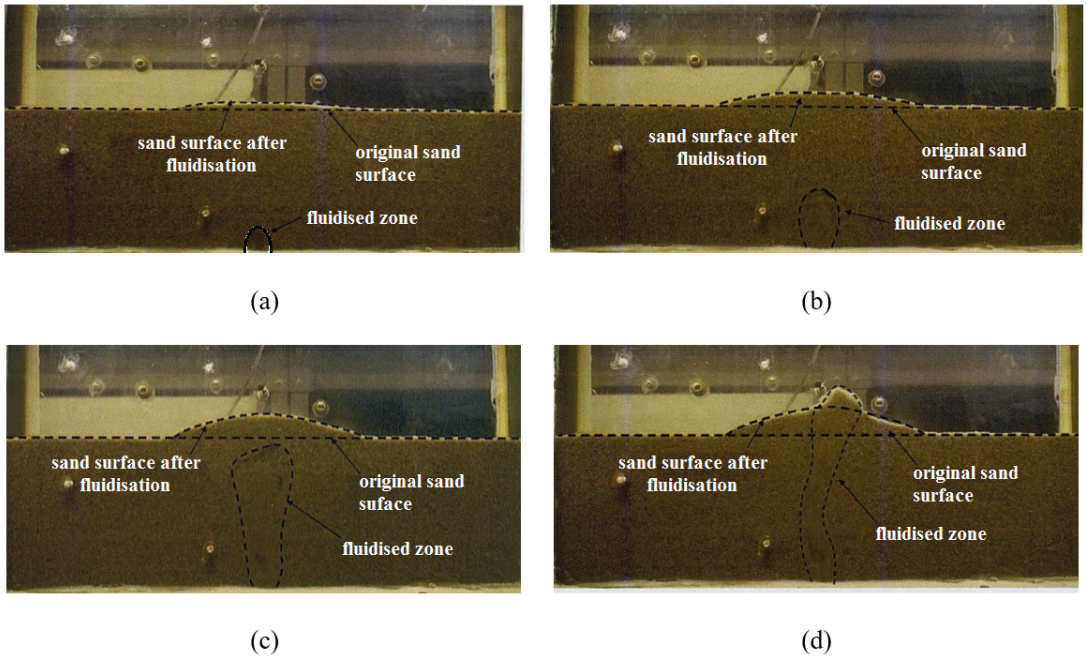



**Figure 2.6:** Stages of fluidisation of granular material (Alsaydalani, 2010)

van Zyl et al. (2013) conducted a series of experimental studies on the fluidisation of a Glass Ballotini bed induced by a vertical interchangeable jet with different diameters (2,4 and 8 mm). The schematic of the experimental model is shown in Figure 2.7 where a Perspex tank of dimensions 1000 mm x 200 mm x 500 mm was used for the tests. The interchangeable jet was positioned at a 2 mm distance from the front face of the tank. The excess water pressure in the soil bed was measured through the pressure tapings that were connected to sight tubes. The authors expected a symmetrical fluidisation zone and thus the pressure tapings were drilled on one side of the orifice centreline. All experiments were carried out on a saturated Ballotini with a height of 400 mm. The bed was subjected to leakage at a controlled flow rate ranging between 220 l/h and 850 l/h recorded using an electromagnetic flowmeter. The progressive development of the fluidised region and the pressure head within the bed were measured for the applied flow rates.

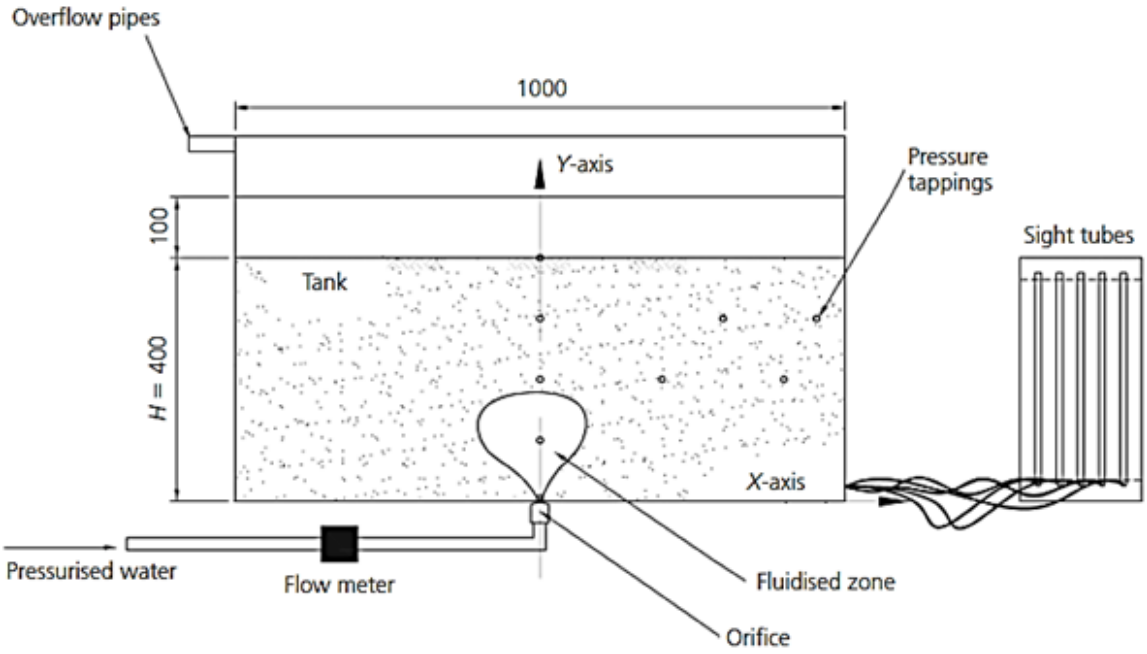



**Figure 2.7:** Schematic drawing of the experimental setup (van Zyl et al., 2013)

Furthermore, van Zyl et al. (2013) identified three zones in the vicinity of the leak: (a) a fluidised zone with mobilised soil particles caused by the water that flows from the region of the leak to the soil surface, (b) a mobile soil zone in which the particles are tightly packed, and (c) a static zone that might move but very slowly. The three zones can be distinguished in Figure 2.8 with increasing in flow rate. Consistently, this study observed that most energy losses in the jet occurred through the orifice. van Zyl et al. (2013) also concluded that in some cases substantial pressure can be maintained within the leaking pipe without the fluidised zone reaching the soil surface. In this study, it was noticed that the pressure head in the bed and the extent of the fluidised zone were controlled by the flow rate rather than the orifice size. Additionally, it was observed that the pressure–leakage behaviour of the orifice was slightly affected by the surrounding idealised Ballotini. Nevertheless, further investigations are required for the latter results validation.

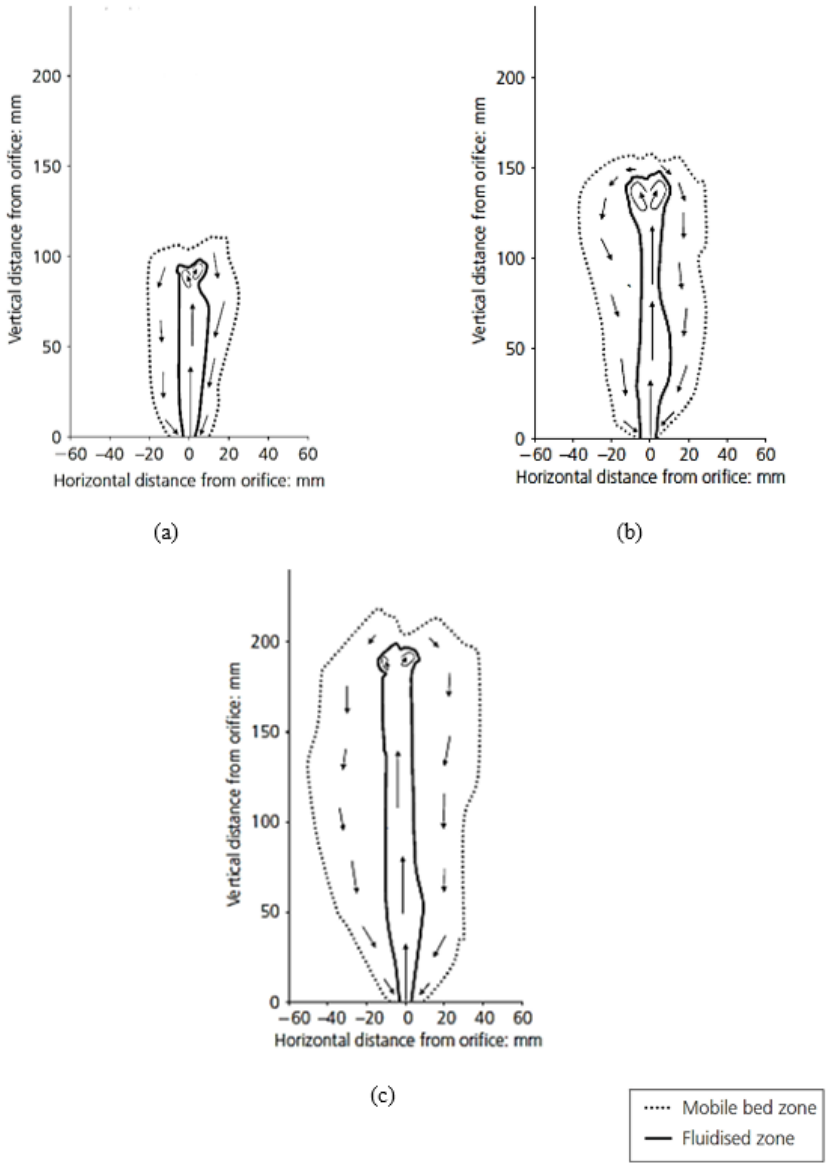



**Figure 2.8:** Development of the fluidised region with the increase in the flow rate (van Zyl et al., 2013)

Bailey and van Zyl (2015) developed an experimental model to monitor the excess pore water pressure and flow velocity in a uniform Glass Ballotini bed subjected to leakage from a vertical water jet. The experimental setup is presented in Figure 2.9 which consisted of a Glass Ballotini filled in a glass tank and Pitot tubes. A central inlet was drilled in the base of the tank representing the orifice in a water-distributing pipe in addition to an outlet hole to drain the tank at the end of the experiment. The Pitot tubes were utilised to measure the pore and dynamics pressures within the Ballotini bed.

The velocity vectors were plotted as shown in Figure 2.10. From the observation, the largest velocities with a maximum of 0.524 m/s (in red) occurred in the fluidised region around the jet. The velocities substantially decreased outside the fluidised zone. In the surrounding mobile bed zone, the flow circulated down towards the orifice. Bailey and van Zyl (2015) found that the highest pore water pressure observed in the fluidised region while this pressure decreased rapidly outside the influence zone. Therefore, high energy occurred in the fluidised zone to then decrease considerably in the surrounding mobile and static bed zones.

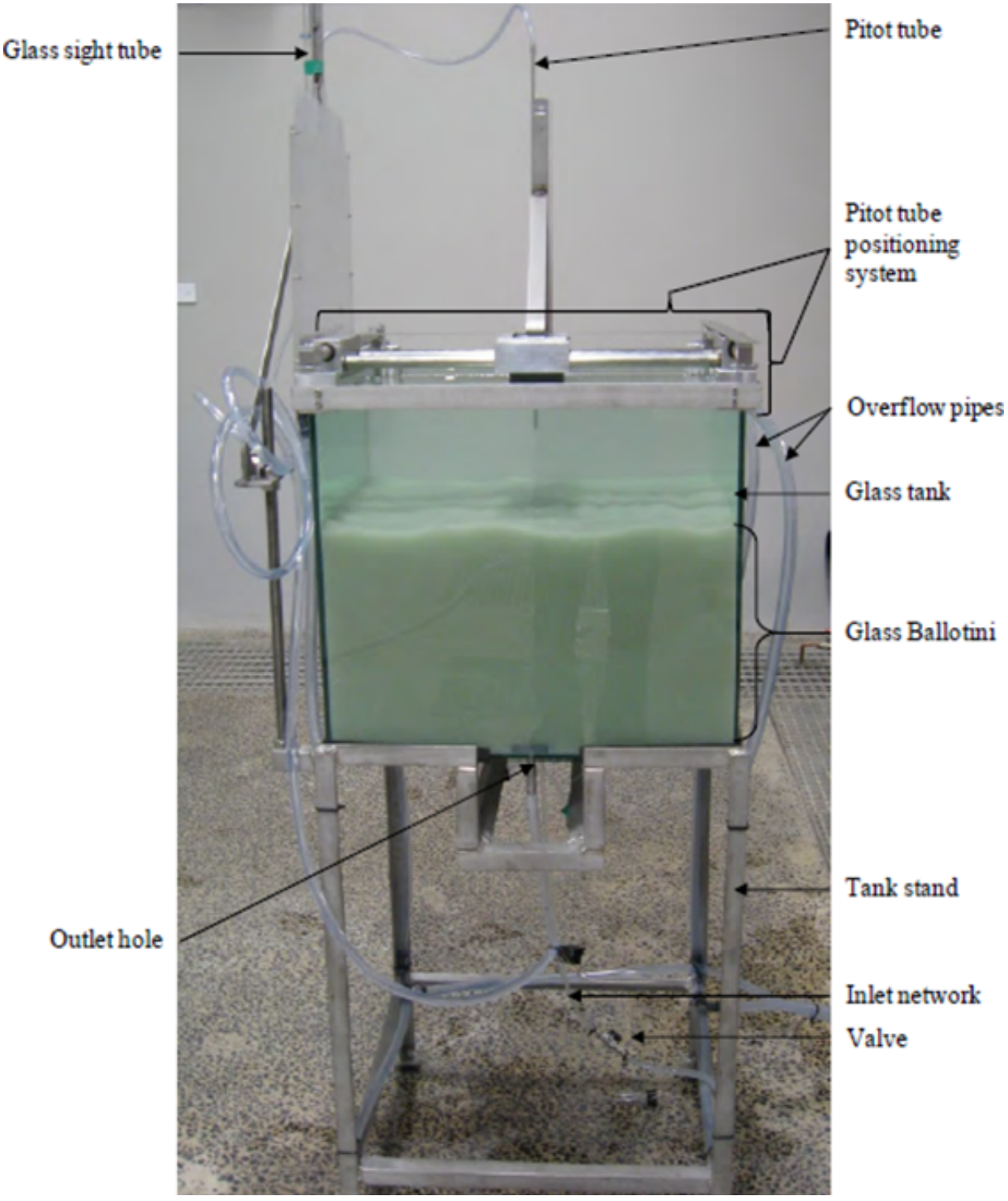



**Figure 2.9:** Experimental model for internal fluidisation mechanism (Bailey and van Zyl, 2015)

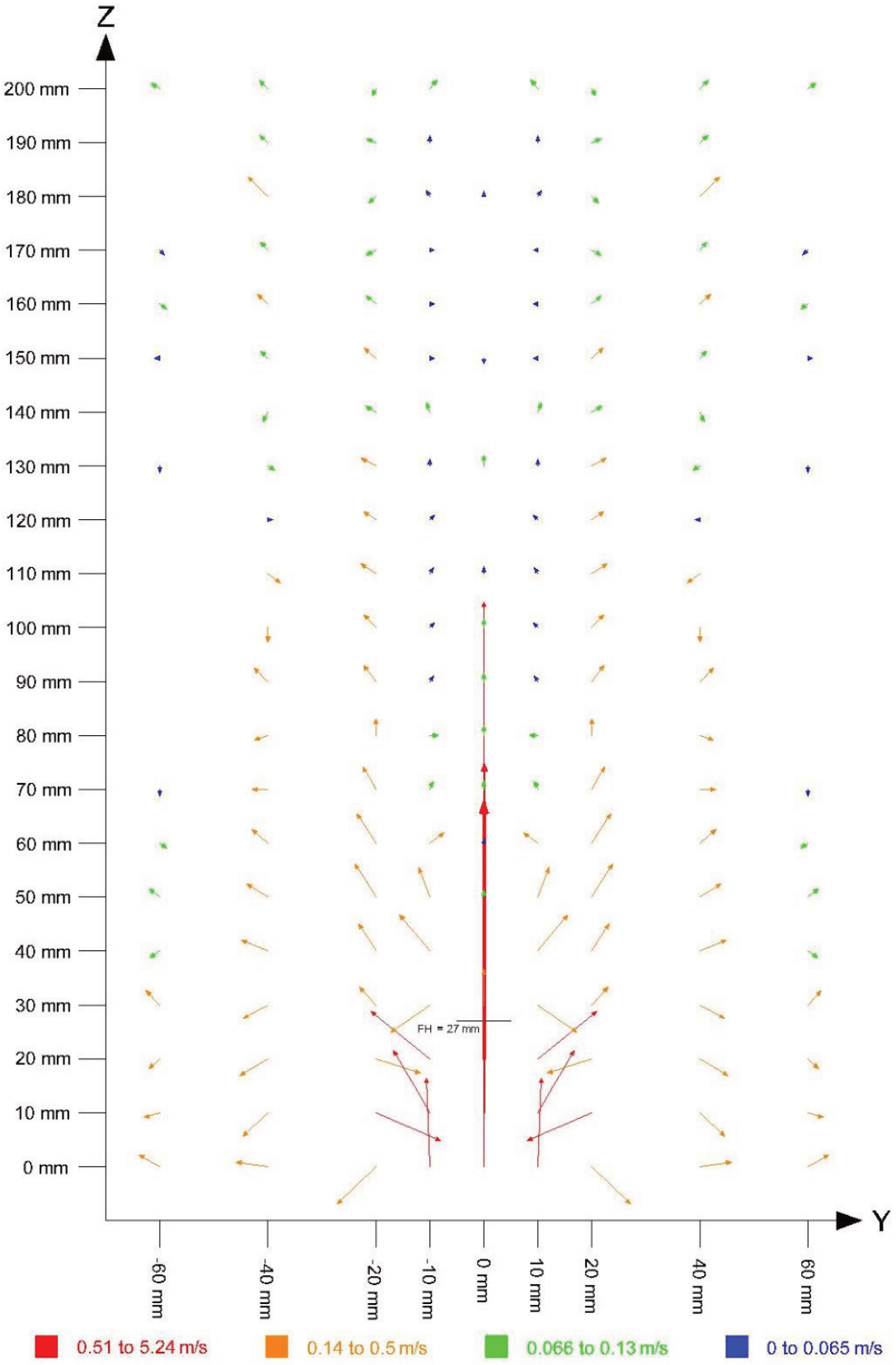



**Figure 2.10:** Plot of the velocity distribution in the Ballotini bed (Bailey and van Zyl, 2015)

He et al. (2017) studied erosion of a saturated sand-bed triggered by a vertical upward jet through an orifice. The authors examined the effect of the flow rate on the sand bed behaviour and identified the critical fluidisation flow rate. The geometry of the developed experimental setup is presented in Figure 2.11.

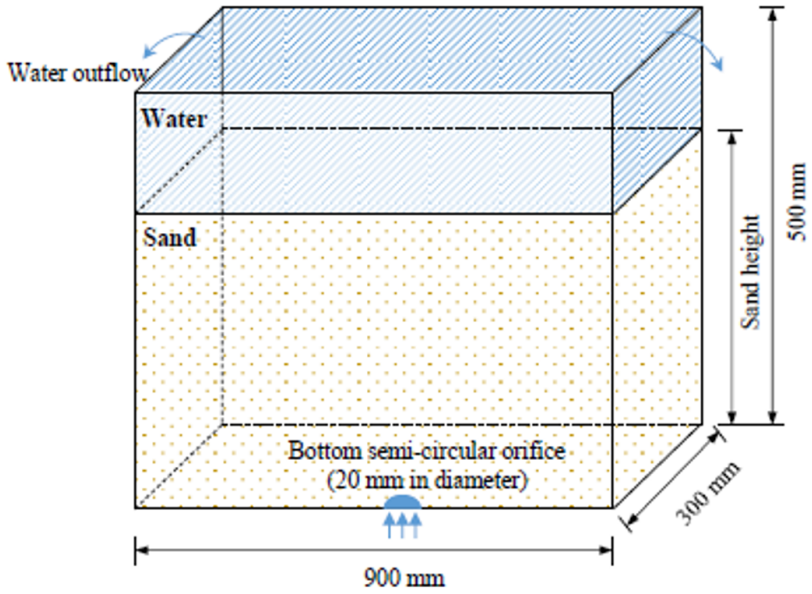



**Figure 2.11:** Experimental model [after He et al. (2017)]

He et al. (2017) showed the different soil fluidisation stages associated with the increase in leakage rate through an upward water jet into a granular soil bed by a set of experiments. These are revealed in Figure 2.12 that included (a) no cavity, (b) a stable cavity in the vicinity of the jet, (c) an unstable cavity, and (d) full fluidisation. The increase in the flow rate resulted in the formation of a cavity that expanded vertically until eventually reaching the bed surface at a critical flow rate. This observation was consistent with the findings of Alsaydalani (2010) for the fluidisation process in granular material. Similarly, He et al. (2017) developed an analytical model to identify the critical fluidisation leakage rate based on the equilibrium of forces and Darcy's law which used to predict the pore pressure distribution in experiments with different sand-bed heights.

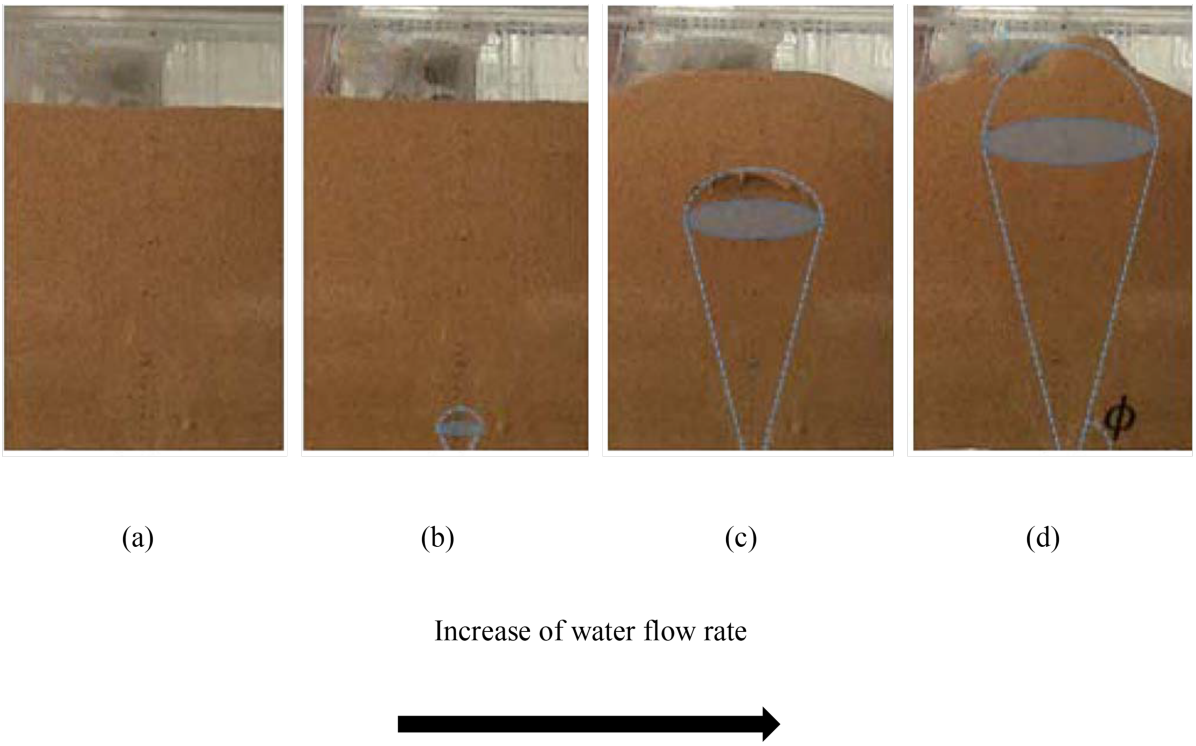
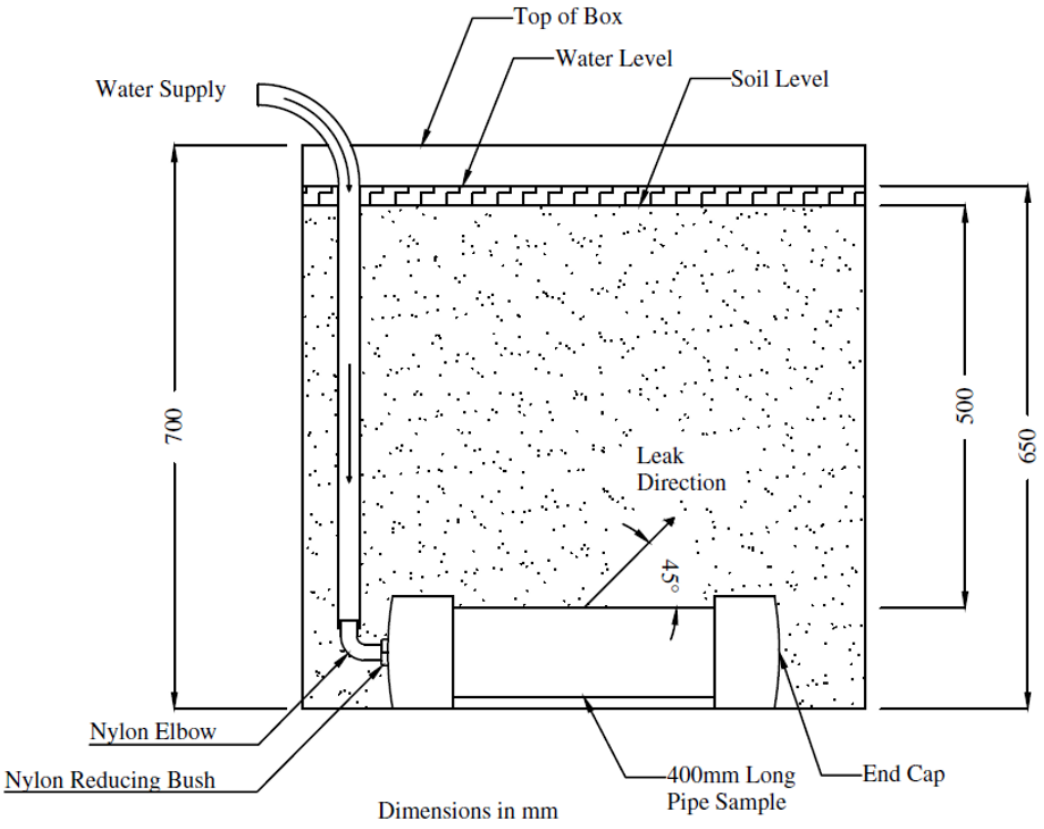
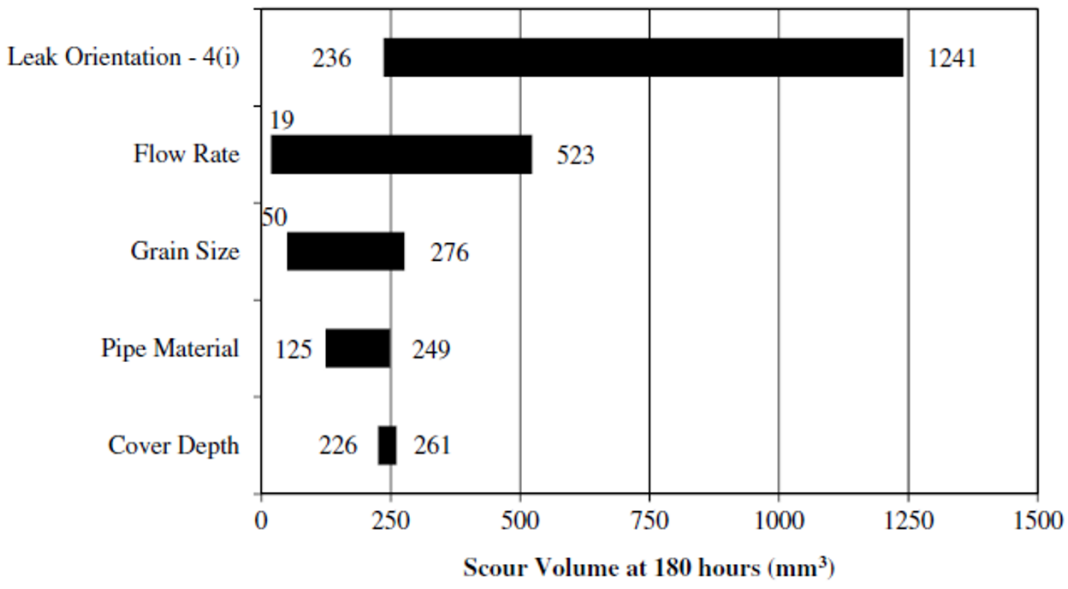



**Figure 2.12:** Evolution of sand-bed erosion at different flow rates; (a) no cavity, stable cavity, (c) unstable cavity and (d) full fluidisation (He et al., 2017)

Pike et al. (2018) conducted a series of experiments on the scouring of pipe materials at leaking regions induced by soil fluidisation. The base experimental setup is presented in Figure 2.13 that consisted of a 110 mm unplasticised polyvinyl chloride (uPVC) pipe with a 45 ° oriented hole of a 3 mm diameter buried in an aluminum box filled with silica sand. Pike et al. (2018) investigated the effect of the leak jet orientation, leakage discharge rate, soil particle size, pipe material and sand cover depth on the scouring pattern around the leaking zone. It was observed that the volume of pipe scouring was mostly affected by the leak orientation followed by leakage flow rate, grain size, pipe material and cover depth (Figure 2.13b). A greater scouring rate was observed with a high leakage discharge from a pipe buried in a deep soil bed with coarse soil grains. In addition, uPVC and steel pipes are characterised by high erosion rates compared to the high-density polyethylene (HDPE) pipe material. This study clearly shows the scouring damage to buried pipes that might be triggered by soil fluidisation.




(a)




(b)

**Figure 2.13:** Schematic presentation of the experimental setup and (b) range of the scouring volumes for different parameters at 180 h (Pike et al., 2018)

Latifi et al. (2022) examined the parameters impacting the geometric properties of the formed zones around a leaking pipe via experiments. The soil behaviour surrounding a 40 mm unplasticised polyvinyl chloride (uPVC) pipe with a longitudinal crack buried in a soil bed was investigated using the experimental setup shown in Figure 2.14. A longitudinal crack was artificially created with a length of 8 mm and a width of 1 mm. The stabilised dimensions of the identified fluidised zone and mobile bed zone caused by pipe leakage were assessed at different leakage pressure values and in different soil types (Figure 2.15) and it was observed that the leakage zones were enlarged with the increase in the water pressure. Moreover, the effect of different soil properties including the particle size, Atterberg limit, soil porosity, and hydraulic conductivity were also assessed. The height and area of the obtained fluidised and mobile bed zones were greatly affected by the soil gradation. The maximum height and the cross-sectional area of the studied zones increased as the soil became finer. Also, the leakage water quickly dissipated in highly permeable and coarser soils. The study performed by Latifi et al. (2022) aided in the understanding of the effect of particular soil characteristics and leakage pressure on soil-leakage interaction.

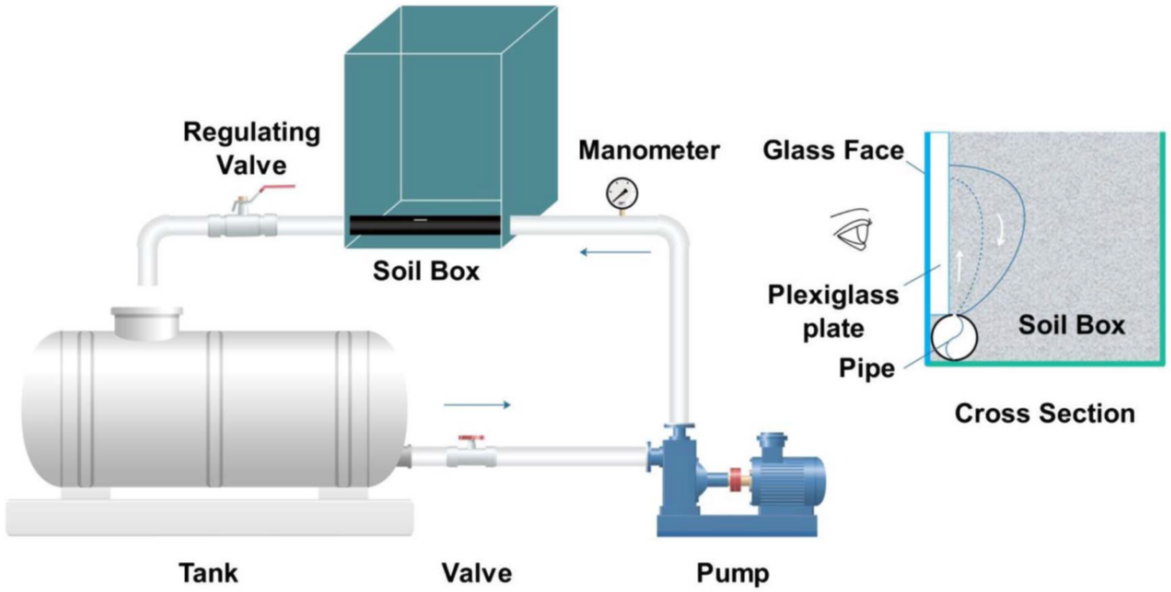
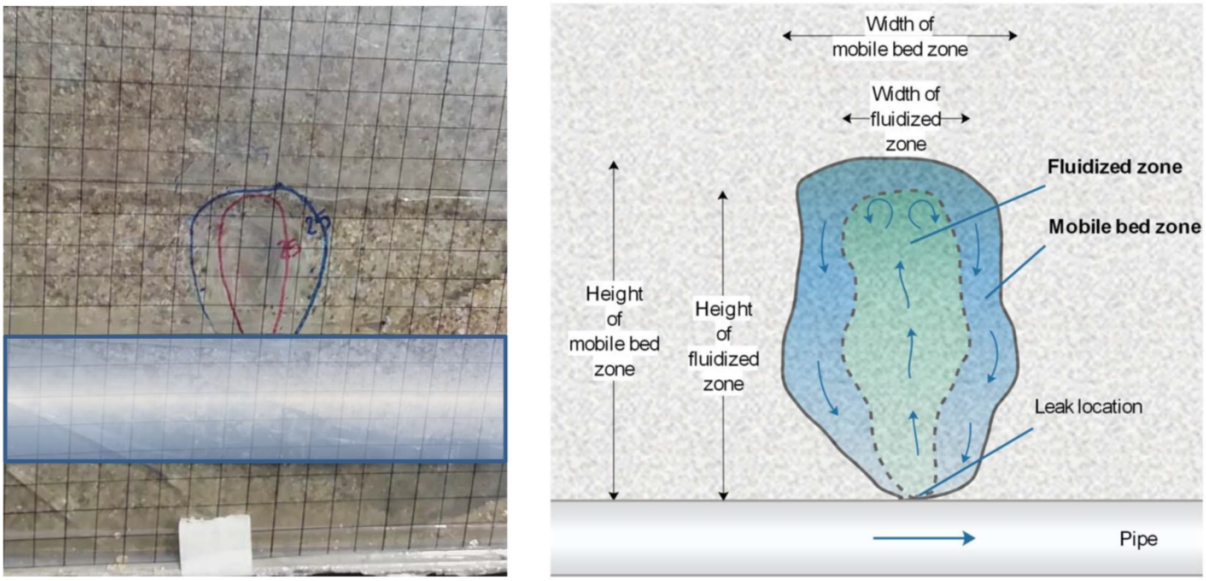



**Figure 2.14:** Schematic section of the experimental setup (Latifi et al., 2022)




(a) (b)

**Figure 2.15:** (a) The observed fluidised and mobile bed zones around the leakage zone and (b) schematic drawing of the fluidised zones caused by leakage (Latifi et al., 2022)

These studies demonstrate the considerable efforts undertaken by researchers to investigate and understand the soil fluidisation process. However, changes in the flow regime, pipe-material behaviour, and hydraulic fracturing increase the complexity of the interaction between the leaking pipe and the surrounding soil (van Zyl and Clayton, 2005). The difficulties and uncertainties in the data acquisition prevented these studies from determining essential factors for interpreting the soil-fluid behaviour, including the soil effective stresses and fluidising pressure. Further research is required to acquire a complete understanding of soil behaviour and the transition to the post-fluidisation stage. Challenges associated with pipe leakage problems make analytical and theoretical approaches to simulate the soil-fluid interaction difficult due to the heterogeneous and discontinuous behaviour. Therefore, numerical simulations are highly recommended by (Cui et al., 2012; Tang, 2017; Ibrahim and Meguid, 2020) to efficiently understand the complicated soil-leakage system due to the possibility and repeatability of data acquisition under different settings.

## 2.6 Numerical studies on soil fluidisation around leaking pipes

Investigation of the soil fluidisation mechanism requires an understanding of the micromechanics of the problem and resolving the soil-fluid interactions. Soil fluidisation around a leaking pipe has also been studied using different numerical approaches with various assumptions. The continuum approach and coupled discrete continuum modelling are the most applied numerical methods in modelling the soil-leakage problem. In a pure continuum study, a single continuum is used to simulate the solid and liquid phases with their collective properties. On the other hand, in the Two-Fluid Model (TFM), the solid and fluid phases are considered as inter-penetrating continua (Anderson and Jackson, 1967; Kuipers et al., 1992; Ibrahim and Meguid, 2021). Alternatively, in a coupled discrete continuum approach, the fluid phase is interpreted as a continuum while the solid phase is treated as a discrete Lagrangian. The Discrete Element Model (DEM) that represents the solid phase is coupled with other methods such as Computational Fluid Dynamics (CFD) (Tsuji et al., 1993) and Lattice Boltzmann Model (LBM) (Cook et al., 2004) that simulates the liquid phase. The utilisation of coupled discrete approaches helps in a relatively more precise simulation of the soil-fluid interaction compared to the continuum methods. However, DEM is computationally expensive and timely expensive, particularly for large-scale problems (Han and Cundall, 2013; Ibrahim and Meguid, 2020). Considerable efforts to numerically model the soil fluidisation around a leaking pipe using different approaches have been made including FEM analysis conducted by Zhu et al. (2018) to investigate the effect of different water pressure, crack lengths and locations, and soil layering on the flow regime. From previous experimental work, it has been observed that once fluidisation occurs, a localised cavity forms near the leak area that is characterised by large deformations. Due to the localised large soil displacements, FEM suffers from mesh tangling (Wang et al., 2015), and it is not capable of simulating the whole mechanism. Alternative methods are suitable for the simulation of large deformations. For example, Cui (2013) used the coupled Discrete Element Method-Lattice Boltzmann Method (DEM-LBM) to capture the inhomogeneities of cohesive soil behaviour in the soil fluidisation around a leaking pipe. In their studies, the developed two-dimensional (2D) numerical model

demonstrated pipe leakage resulted in the formation of a local cavity near the pipe crack that evolved continuously until it reached the surface of the soil bed. DEM is ideal for studying micro-mechanical particulate soil behaviour, but it becomes computationally too expensive for real-scale pipe leakage problems (Han and Cundall, 2013). Several point-based computational approaches were developed in recent decades to model problems that involve large deformation together with solid-fluid interaction. These are meshless numerical methods where a set of points is defined to solve the solution independently or in combination with a background grid that is used in the traditional finite element method (FEM) or finite difference method (FDM). Furthermore, smoothed particle hydrodynamics (SPH), particle finite element method (PFEM) and material point method (MPM) are numerical approaches that can be used to model soil-fluid interaction. The different numerical methods that have been used to model soil-fluid interaction during the past decades are reviewed in the following section.

### 2.6.1 Finite Element Method (FEM) coupled with Discrete Element Method (DEM)

The Finite Element Method (FEM) have been robustly and extensively applied in various engineering problems including geotechnical engineering (Zienkiewicz and Morice, 1971). In this numerical method, the material geometry is modelled using a lagrangian finite element grid. The model could be discretised into diverse types and shapes of elements depending on the integration order (Bathe and Wilson, 1976). In addition, interpolation functions are used to determine the state parameters at the nodes of the grid. Although FEM is widely used as a valuable technique in different engineering fields, due to mesh distortions, the standard FEM has serious challenges in simulating large deformation problems (Armero and Love, 2003). The DEM method was developed to study the granular material that is represented as an assembly of discrete particles (Cundall, 1971). Duran (2012) mentioned that DEM models can be categorised into the original DEM model “soft-sphere”, and the “hard-sphere” that was initiated by Campbell and Brennen (1985). In the original (soft-sphere) model, a dynamic process characterises the particle-particle interaction with slight deformation allowance during collisions. In this

model, different collisions and various contact behaviour can be treated which is applicable in the geotechnical field (O'Sullivan, 2011). However, an impulsive process is assumed for the particle-particle interaction in the (hard-sphere) model without particle overlap during contacts (Deen et al., 2007). In contrast to traditional numerical methods including FEM, DEM is an explicit technique that enables tracking particle interactions (Tang, 2017). The recent studies have taken the advantage of DEM modelling in a continuum framework including the FEM for solving engineering problems(Andrade et al., 2011; Guo and Zhao, 2014; Guo and Yu, 2016; Wang and Sun, 2016). The FEM is employed to discretise the region and find the solutions to boundary value problems, while DEM provides the local material behaviors at the nodes of FEM mesh. This development helps in bypassing the phenomenological constitutive laws of the FEM and overcoming the DEM challenge regarding the amount of discrete bodies (Pirnia et al., 2020). Guo and Zhao (2014) applied FEM-DEM to simulate the nonlinear behaviour of sand in saturated media. Furthermore, Pirnia et al. (2019) investigated the internal erosion during a permeameter test using this multiphase method. However, the model was limited to a small laboratory specimen due to the heavy computational cost associated with the FEM-DEM method.

### 2.6.2 DEM coupled with Darcy fluid flow (DFF)

Coupled DEM-DFF method was initiated by Hakuno and Tarumi (1988) to study the fully saturated soil characteristics in an undrained setting. In this method, the fluid-induced force depends on the value of fluid pressure on each particle (Preece et al., 1999). DEM method is used to update the particle locations in which permeability and pore pressure values can be estimated from the change in volume fraction (Hakuno and Tarumi, 1988). The evolution of pore pressure must be treated as a dynamic process that gives accurate results (Olivera Bonilla, 2004). The liquefaction mechanism in the 3D model was studied by Meguro and Ravichandran (2000) using the coupled DEM-DFF method. This method was also proved to be efficient in simulating soil-fluid systems in laminar flow (Goodarzi et al., 2013). Tang (2017) used this technique to

model the soil fluidisation around leaking pipes where a 3D model was developed to study the deformational characteristics of soil particles.

### 2.6.3 DEM coupled with computational fluid dynamics (CFD)

CFD is based on the computational solution of the Navier-Stokes equations. The coupled CFD-DEM method was developed by Tsuji et al. (1993) in which the fluid domain is split into cells. At the cell scale, the Navier-Stokes equations are solved, and the volume fraction is averagely estimated based on the DEM updated particle locations (Xu and Yu, 1997). The fluid pressure and velocity are computed, and the drag force is then estimated and added to identify the resultant force on each particle. The three-dimensional combination of DEM with CFD was extended by Kawaguchi et al. (1998) to simulate the bed fluidisation in which the numerical results were compatible with the experimental findings. In addition to simulating fluidised beds (Kafui et al., 2002; Feng and Yu, 2006), DEM-CFD simulation can be used in seepage flows (El Shamy, 2002; Suzuki et al., 2007) and soil piping to understand the soil fluidisation mechanism (Tao, 2018).

### 2.6.4 DEM coupled with lattice Boltzmann method (LBM)

The Lattice Boltzmann Method (LBM) is a numerical fluid simulation that divides the fluid domain into a regular lattice (Chen et al., 1995). Fluid flow is simulated based on solving the discrete Boltzmann equation instead of the Navier-Stokes equation (Chen and Doolen, 1998). Thus, LBM is considered an alternative method to DFF, CFD, and other conventional macroscopic fluid models (Han et al., 2007). LBM is a microscopic method that can be used for multiphase or a turbulent flow simulation with high resolution (Premnath et al., 2005). Cook et al. (2004) highlighted that the coupled DEM-LBM technique can be efficiently used to simulate fluid-particle interactions where it can accurately reproduce the physically realistic behaviour of the erosion process. Lominé et al. (2013) used the coupled DEM-LBM method to simulate the piping fluidisation in two dimensions. In addition, Cui (2013) and Li (2013) modelled the leaking-soil interaction problem using DEM–LBM method integrated with the Immersed

Moving Boundary (IMB) scheme (Kwon and Hosoglu, 2008). They developed a 2D computer code (FPS-BHAM) where soil and fluid are modelled following the soft-sphere DEM and LBM approaches respectively.

### 2.6.5 DEM coupled with smoothed particle hydrodynamics (SPH)

Lucy (1977) and Gingold and Monaghan (1977)have developed a Smoothed Particle Hydrodynamics (SPH) as one of the Mesh-free Particle Methods that is based on the Lagrangian approach. This is a macroscopic fluid method in which the fluid phase is represented by finite discrete particles with kernel function (Liu and Liu, 2003). This fluid technique is capable of capturing large displacement or discontinuous materials (Morris and Johnson, 2009). Therefore, Li et al. (2007) and Robinsona et al. (2013) employed this method for the solid-fluid simulation. Furthermore, the DEM-SPH technique has been used widely for fluid-structure interaction problems (Wu et al., 2016).

### 2.6.6 Coupled Eulerian-Lagrangian (CEL) Method

The Coupled Eulerian-Lagrangian method has been developed to solve the limitation of the classical Finite Element Method (FEM) in simulating soil-structure interaction issues involving large deformation (Wang et al., 2015; Aubram et al., 2017). In the CEL technique, the Eulerian approach is used to describe the fluid phase and the Lagrangian approach is applied to solid phase (Mercier et al., 2015). Solid and fluid phases are separated by a Level-Set interfere function (Osher and Sethian, 1988). CEL has been widely used for soil fluidisation (Donea et al., 1982).

### 2.6.7 Particle Finite Element Method (PFEM)

A Particle Finite Element Method (PFEM) uses an updated Lagrangian approach to represent the motion of particles (nodes) in regions consisting of liquid and solid subregions (Oñate et al., 2006). Nodes are identified as material particles that can move freely and detach from the liquid and solid subregions. The nodes that define the discretised zone in the liquid and solid domains

are connected by a background mesh where the governing equations are computed as in the classical FEM.

### 2.6.8 Material Point Method (MPM)

The material point method (MPM) is a particle-based technique that models the continuum by Eulerian meshes and Lagrangian points (material points, MP) that hold the physical characteristics such as stress, load, strain, momentum, etc. (Al-Kafaji, 2013). In MPM, material motion and deformation are represented by the movement of Lagrangian MP through the fixed Eulerian meshes (Yerro et al., 2016). This numerical method is based on Newton's principal equations. It combines the advantages of Lagrangian and Eulerian approaches (Fern et al., 2017). It is applicable for solving problems with large and small deformations (Sulsky and Schreyer, 1996; Nairn, 2003; Coetzee et al., 2005). It has been developed to simulate multi-phase and soil-structure interactions. Jassim et al. (2013) and Yerro et al. (2016) show the application of the MPM in saturated and unsaturated porous media respectively. The MPM hasn't been applied yet for simulating the soil fluidisation around a leakage pipe to predict the structural integrity of the ground and buried utilities. However, based on conducted literature review, the MPM method has proven to be the most suitable and efficient method in simulating the soil fluidisation around leaking pressurised pipe. The advantages and disadvantages of different numerical methods used to model soil-fluid interaction during the past decades are summarised in Table 2.1. This includes DEM-DFF, DEM-CFD, DEM-LBM, DEM- SPH, coupled Eulerian-Lagrangian, PFEM and MPM methods.

ragged2e

**Table 2.2:** Summary of the different numerical methods that have been used for soil-water interaction

| Method | Advantages | Disadvantages |
|---|---|---|
| FEM-DEM | • Applicable for the modelling of internal erosion (Pirnia et al., 2020)<br>• Capable of capturing the macro-micro behavior of suffusion in saturated soil (Hu et al., 2022) | • Require extremely fine mesh for accurate results (Hazay and Munjiza, 2016)<br>• Not applicable for large scale problems (Owen and Feng, 2001)<br>• Challenges in calculating the interfacial interactions among the multiphase flow with suspended particles (Wang et al., 2022) |
| DEM-DFF | • Low computational cost (Li, 2013)<br>• Rapid in terms of computational time compared to the classical analytical methods (Goodarzi et al., 2013; Cui, 2013) | • Limited to the fluid flow with low Reynolds number (Shafipour and Soroush, 2008).<br>• Not applicable for large scale simulation model (Goodarzi et al., 2013)<br>• Difficult to describe the fluidisation process (Jensen and Preece, 2000)<br>• Require the determination of additional parameters e.g. permeability (Bear, 1988) |

| Method | Advantages | Disadvantages |
|---|---|---|
| DEM-CFD | • Capable of interpreting the internal soil fluidisation mechanism (Guo and Yu, 2016; Tao, 2018)<br>• CFD is effectively used to simulate soil fluidisation in combination with the kinetic granular flow approach Tang et al. (2017) | • Difficult to simulate the fluid-particle interaction where the fluid flow simulation required extremely fine cells (Li, 2013)<br>• High computational cost (Hu, 1996)<br>• Not applicable to all particle sizes (He et al., 2018) |
| DEM-LBM | • Higher efficiency compared to the CFD (Cui, 2013)<br>• Detailed lattice description of soil particles (Li, 2013)<br>• Results can be qualitatively validated experimentally and analytically (Cui et al., 2014)<br>• Applicable for multiphase or turbulent flows (Premnath et al., 2005)<br>• Owen et al. (2011) showed its capability in simulating soil fluidisation | • Large computational time and memory space for a large-scale problem (Han and Cundall, 2013)<br>• Computationally expensive particularly in three dimensions (Han and Cundall, 2013; Cui et al., 2014) |

| Method | Advantages | Disadvantages |
|---|---|---|
| DEM-SPH | • Applicable for complicated geometries due to its Lagrangian nature (Crespo, 2008)<br>• Simple where SPH is better than grid-based techniques in simulating material with large deformation (Bui et al., 2007)<br>• Reliable and flexible in handling large deformation problems (Morris and Johnson, 2009)<br>• Applicable to flows of large Reynolds Numbers (Robinsona et al., 2013) | • Crespo (2008) mentioned that compared with mesh-based methods, SPH is more expensive and of lower computational accuracy.<br>•Complicated implementation (Cui, 2013)<br>• Useful only for laminar flow in which artificial viscosity is assumed (Crespo, 2008) |
| CEL | • High accuracy in estimating the mechanical characteristics such as shear stress to strain and velocity (Donea et al., 1982)<br>• Interface between variable materials can be easily determined following the Lagrangian approach (Priyadarshini et al., 2012) | • Mesh distortion in large deformation problems (Priyadarshini et al., 2012)<br>• Requirement of frequent re-meshing particularly in following large distortion(Chenot and Massoni, 2006)<br>• Complexity in identifying the boundary conditions (Jain et al., 2015)<br>• Difficult to simulate the soil-fluid interaction (Al-Kafaji, 2013) |

| Method | Advantages | Disadvantages |
|---|---|---|
| PFEM | • Suitable to model multi-physics problems including fluid-fluid, fluid-solid or free surfaces (Cremonesi et al., 2020)<br>• Mesh distortion problem is overcome by remeshing as the current mesh gets too distorted (Oñate et al., 2006) | • Pressure oscillations at the fluid-solid boundaries (Cerquaglia et al., 2015)<br>• Perturbations in the velocity field caused by remeshing (Oñate et al., 2006; Cerquaglia et al., 2015) |
| MPM | • Capable of simulating multi-phase flows and multi-material interactions (Kashiwa, 2001)<br>• Applicable to large deformation problems (Bardenhagen et al., 2000)<br>• Avoids the Lagrangian and Eulerian disadvantages such as the mesh distortion and advection errors respectively (Zhang et al., 2008)<br>• Accurate and reliable for real-scale problems (Ceccato et al., 2018) | • Computationally more expensive than FEM (Kularathna, 2018)<br>• Possibility of error accumulation due to the numerical approximations, grid resolution, interpolation schemes, and constitutive modelling (Sulsky et al., 1994) |

Although several numerical investigations have been undertaken to investigate soil-fluid interaction, due to its complexity, little knowledge is available in regard to soil-pipe leakage problem. This complexity is due to variation in the flow regime, pipe material, and soil characteristics (van Zyl and Clayton, 2005). Therefore, a thorough understanding of the soil fluidisation around

leaking pressurised pipe should be achieved via an efficient numerical method that is applicable to simulate such a multiphase large deformation problem. This method should be capable of addressing the influence of different soil and pipe parameters on the soil-leakage system and the evolution of the soil fluidisation mechanism with effective computational time.

## 2.7 Parameters involved in soil-leakage interaction

Soil fluidisation associated with leakage from an underground water pipe is a complex phenomenon that involves various interacting soil and pipe parameters. There has been a multitude of studies related to the soil fluidisation process associated with pipe leakage. Considering all the factors involved in the pipe leakage problem in a single study is practically impossible. Therefore, this section aims to thoroughly discuss the influence of different contributing parameters including pipe-material behaviour, flow rate, leakage pressure, orifice size, orifice position, bed height, and soil properties (e.g., soil type, particle size distribution and shape, soil hydraulic conductivity, and relative density) on the soil-leakage interaction based on the extensive literature review.

### 2.7.1 Pipe-material behaviour

The pipe leakage behaviour, and particularly the pressure-leakage relation depends on the pipe material performance and properties (van Zyl and Clayton, 2005). The leakage exponents ($N_1$) are significantly dependent on the pipe material. For example, the variation in the pipe leakage exponent for a pipe with round, longitudinal and circumferential cracks have been numerically investigated by Cassa et al. (2010). It was concluded that an increase in the leakage exponent was caused by the expansion of the longitudinal and circular cracks. However, the water loss remains constant with the change in the size of the circular crack. Furthermore, the highest leakage exponent extent was validated in longitudinal cracks due to stresses in lower pipe compared to the circumferential cracks (Greyvenstein and van Zyl, 2007).

Water leakage is highly influenced by the type of pipe material. Greyvenstein and van Zyl (2007) mentioned that corroded steel pipes in contrast to HDPE pipes are characterised by the highest leakage exponents ($N_1$ = 0.9) due to the weakness of the supporting materials as a result of corrosion. In uPVC pipes, the leakage area will be reduced, and the crack will be elongated due to the circumferential stresses (Greyvenstein and van Zyl, 2007). To investigate the impacts of pipe material on the leak head-discharge relationships, different experiments were conducted at the Water Engineering Laboratory of the University of Perugia, Italy by Ferrante (2012). It has been concluded that a linear relationship exists between the leak area and the head in an elastic material pipe. However, other approaches were required for elastoplastic and viscoelastic materials such as polyethylene pipe where the leak head-discharge relationships could be dependent on the behaviour of the pipe-material (Ferrante, 2012). In addition, the strength of the pipe material influences the leakage behaviour as the pipe water pressure is taken up by its wall (Farley and Trow, 2003). Recently, Ilunga (2016) established the relationship between water leakage and the pipe-material behaviour in pressurised pipes with longitudinal cracks. The authors observed that increases in the leakage pressure results in the expansion of the longitudinal cracks and therefore, the water flow rate. This opposes the fixed orifice area assumption that is considered in the orifice equation. Thus, it is essential to understand the effect of pipe-material behaviour on the pipe leakage phenomenon that might affect the overall ground stability.

### 2.7.2 Flow rate

Flow rate has a significant influence on the fluidisation process. Based on the flow rates, Zoueshtiagh and Merlen (2007) defined three different regimes in granular soil bed. The first regime occurs at relatively low flow rates where the soil bed behaves as a porous medium, and thus stays motionless. The second regime occurs at a higher flow rate that resulted in local deformation at the bed surface. This regime was considered a transitional zone from the first regime to the fluidisation regime. As the flow rate was increased, the third regime occurs where the local fluidisation was observed at the bed surface above the area of the injection hole.

Alsaydalani (2010) studied the internal soil fluidisation caused by injecting fluid into granular soil. The increase in flow rate resulted in the surrounding particles mobilisation around the orifice and initiation of soil fluidisation. At high flow rates, the volume of the fluidised zone increases significantly, which might appear at the soil surface (Teeluckdharry, 2017). According to van Zyl et al. (2013), at a flow rate of 320 litres/h, the fluidisation area around the pipe is divided into the fluidised, mobilised, and static zones (Figure 2.16).

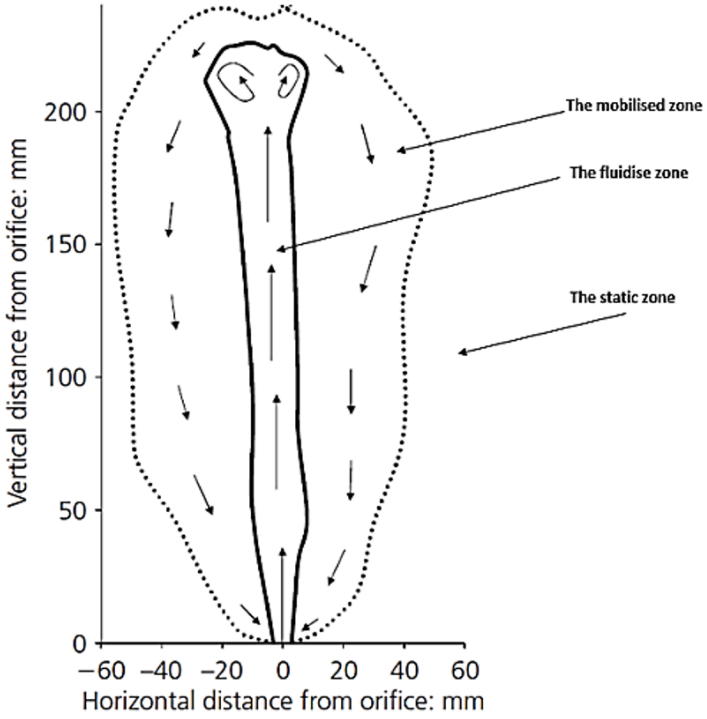



**Figure 2.16:** Three zones associated with fluidisation with a leak from an orifice (van Zyl et al., 2013)

A fluidised zone includes fluid-like particles, with height independent of the orifice diameter but affected by the flow rate (Alsaydalani, 2010). Furthermore, the fluidised zone is surrounded by a wider mobilised zone in which the granular particles are partially mobilised. Most of the head loss occurs in the fluidised and mobilised zones (Walski et al., 2006). The static zone surrounds the mobilised zone, where the soil particles remain stable. van Zyl et al. (2013) observed that the flow rate influences the distribution of the excess pore water pressure in the soil bed. In addition, it affects the volume of the fluidised zone that extends rapidly before it stabilizes. Teeluckdharry

(2017) showed that the flow rate controls the leakage paths in which high flow rates resulted in greater water spread in the soil bed.

### 2.7.3 Leakage pressure

In the water distribution system, pipe leakage is greatly influenced by water pressure. Previously, the effect of pressure on leakage by following the orifice equation (Eq. 2.1)was neglected.

$$q = C_d A \sqrt{2gh} \tag{2.1}$$

Where: $q$ = flow rate, $C_d$ = discharge coefficient, $A$ = orifice area, $g$ = gravitational acceleration and $h$ = pressure head differential over the orifice. The leakage parameter was proven to be proportional to the square root of the pipe pressure (Farley and Trow, 2003). However, van Zyl and Clayton (2005) showed the significant impact of water pressure on leakage in water distribution networks. Thus, the orifice equation was replaced by the following leakage exponent ($N_1$) power equation (Eq. 2.2) that was developed by Lambert (2001):

$$q = Ch^{N_1} \tag{2.2}$$

Where: $q$ = flow rate, $C$ = leakage coefficient and $h$ = pressure head. The leakage exponent and fixed coefficient can be derived after assessing the leakage system while the pressure varies. This method is commonly used in the leakage problem where the leakage exponent ($N_1$) can vary between 0.5 and 2.79 (Farley and Trow, 2003). The typical variation in the leakage exponent may be caused by different soil and pipe characteristics (Greyvenstein and van Zyl, 2007). High-pressure results in expanding the leakage area and thus increasing the flow rate (Cassa and van Zyl, 2014). The pore water pressure increases significantly as a result of the water leakage into the soil bed leading to the initiation of the fluidisation zone (Bailey and van Zyl, 2015). Alsaydalani (2010) proved that there was a linear relationship between the required pressure to create fluidisation and the bed height above the leakage point. In addition, it was concluded

that for fine granular material, a lower pressure is sufficient to create the onset of fluidisation compared to coarser particles.

Cui et al. (2018), experimentally and numerically investigated the excess pore water pressure distribution in a sand bed at different flow rate and water pressure. The authors observed that cavity formation at the pipe orifice initiates after exceeding a specific flow rate and pressure peak, which depends on the orifice diameter. This cavity expands to the soil surface due to the flow effect under a constant pressure distribution in the fluidised zone (Cui et al., 2018).

### 2.7.4 Orifice size

The orifice size significantly affects the energy loss that occurs across the orifice. A higher value of pressure head across the orifice is required for the occurrence of fluidisation associated with a smaller orifice (Zoueshtiagh and Merlen, 2007). However, the distribution of excess pore pressure in the soil bed is not dependent on the orifice size but influenced by the fluid flow rate (Alsaydalani, 2010). Furthermore, the extension of the fluidised zone is not affected by the orifice size (Zoueshtiagh and Merlen, 2007; van Zyl et al., 2013). This contradicts Tang et al. (2017)'s study which showed an expansion of the eroded zone with an increase in orifice size. Walski et al. (2006) and Alsaydalani (2010) stated that most of the pressure dissipation that occurs across the orifice is converted to the velocity head compared to the pressure loss through the soil. In addition, the onset of soil fluidisation is influenced by the flow rate rather than the pressure across the orifice (Alsaydalani, 2010). However, at the same flow rate, a lower pressure across the orifice is required to initiate the soil fluidisation in a larger orifice compared to that in a smaller orifice, as shown in Figure 2.17.

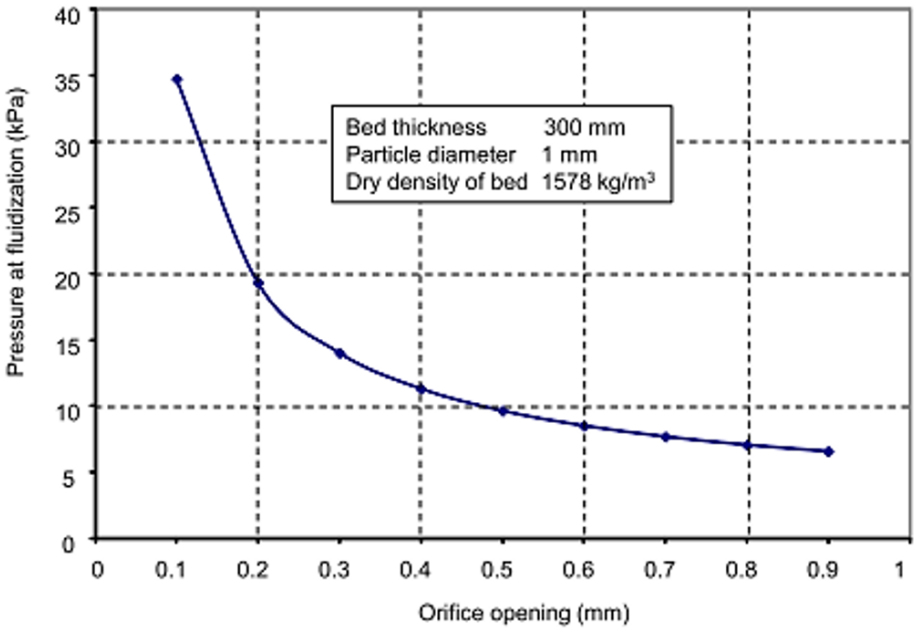



**Figure 2.17:** The variation in pressure (kPa) at the initiation of fluidisation with the change in orifice size (mm) (Alsaydalani and Clayton, 2014)

van Zyl et al. (2013) observed that the pressure head across the orifice is inversely proportional to its size and the crack shape in the pipe affects the flow rate. For instance, a rectangular crack results in a lower flow rate compared to a circular crack under the same pressure and leakage area (De Marchis and Milici, 2019). Previous studies have been limited to the effect of orifice size on the initiation of soil fluidisation induced by pipe leakage. However, these studies did not consider the impact of crack size on the post-local fluidisation mechanism until it reaches the soil surface.

### 2.7.5 Orifice position

Tang (2017) studied the impact of the pipe defect position on the soil fluidisation mechanism. In addition to the most common location of the pipe slot at the crown, Davies et al. (2001) have reported other locations of the pipe defect shifting from the crown to the springline. The effect of the changes in slot position on the water flow rate in the sand was experimentally studied by Tang (2017). As the orifice position varied from the crown (90°) to the springline (0°), the water flow rates and thus the soil fluidisation decreased with time (Figure 2.18). Therefore, the

duration of the soil fluidisation mechanism increases as the slot position shifts from the crown to the springline. Tang (2017) observed that the greatest area of the mobilised zone occurs when the orifice is the invert of the pipe. Alsaydalani (2010) confirmed that in pipe leakage, soil fluidisation may not appear at the bed surface if it is initiated around the orifice position, i.e. leakage location in the pipe, or in the middle of the soil bed.

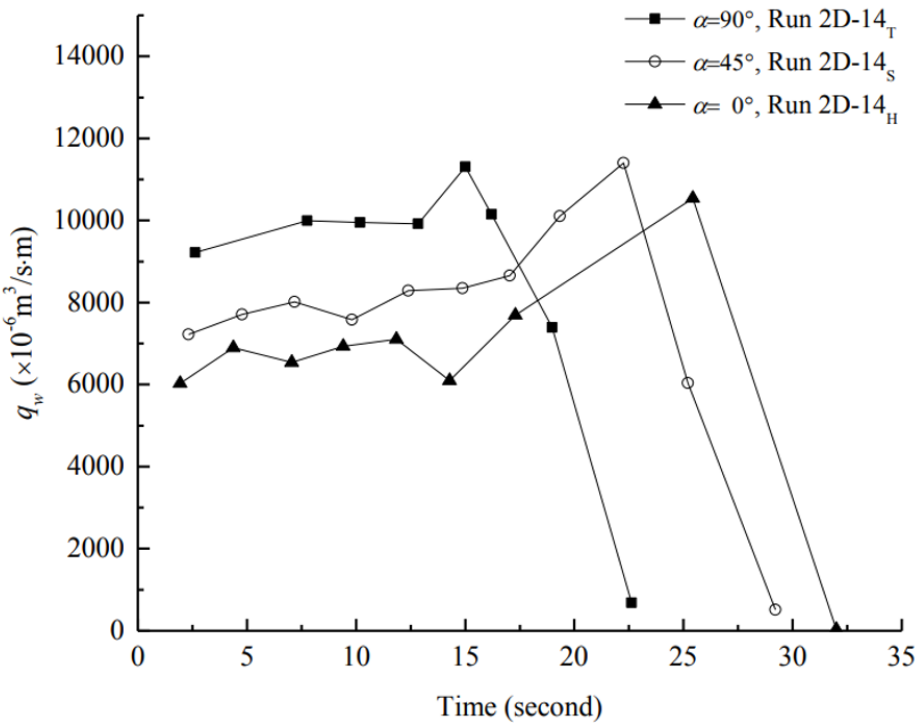



**Figure 2.18:** The change in water flow rate, $q_w$, for different orifice positions, $\alpha$, with time (Tang, 2017)

### 2.7.6 Bed height

Alsaydalani (2010) studied the influence of soil height on the fluidisation mechanism. The author concluded that the initiation of fluidisation in a thick soil bed requires a high flow rate due to the high bulk unit weight of the thick soil bed (Zoueshtiagh and Merlen, 2007). Figure 2.19 shows the influence of the sand bed height on the required pressure for the onset of fluidisation based on the experimental study carried out by van Zyl et al. (2013). In contrast to Darcy's flow, a nonlinear direct proportional relationship between the fluidisation pressure and the bed thickness was observed.

Tang (2017), in contrast with previous research (Philippe and Badiane, 2013; Cui et al., 2014), confirmed that a greater soil bed height requires higher water velocity to initiate soil fluidisation. This results from an increase in the resisting forces in the sand body. In addition, the propagation time of soil fluidisation to reach the top surface depends on the soil bed thickness (Tang, 2017).

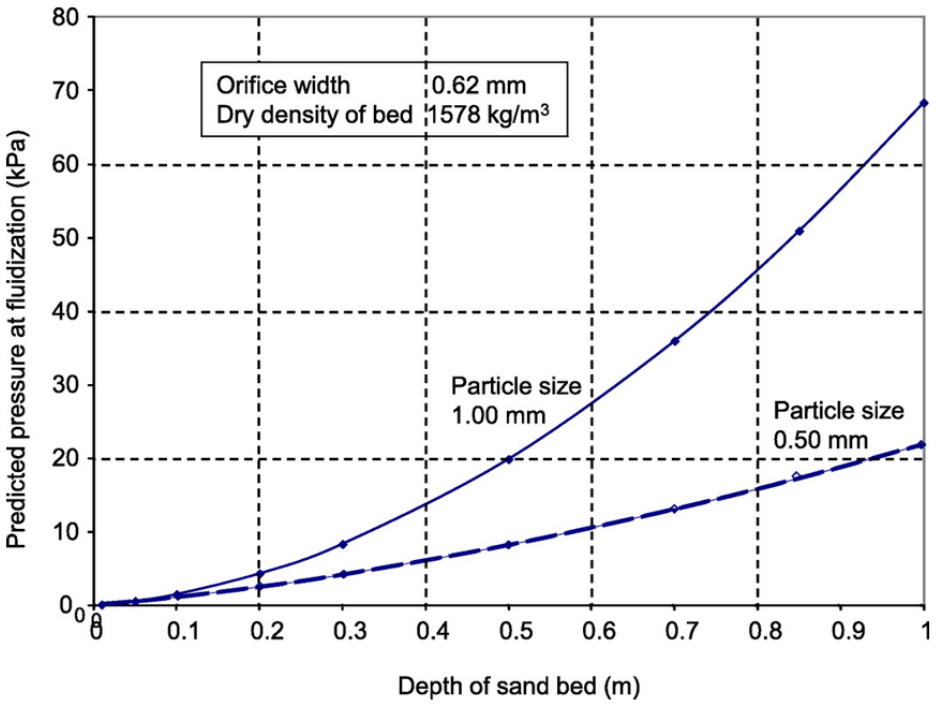



**Figure 2.19:** The variation in pressure (kPa) at the initiation of fluidisation with the change in bed height (m) and particle size (mm) (Alsaydalani and Clayton, 2014)

### 2.7.7 Soil properties

In addition to pipe characteristics, surrounding soil properties are important in the fluidisation mechanism due to the particle-fluid interaction. Few studies have been conducted on the effect of soil properties such as soil type, particle size distribution and shape, soil hydraulic conductivity and relative density on water leakage. Further, the impact of other geotechnical properties of soil, such as density and fines content on the leakage discharge must be investigated.

#### 2.7.7.1 Soil type

Walski et al. (2006); Zoueshtiagh and Merlen (2007); van Zyl et al. (2013); Ćipranić and Sekulić (2015) have thoroughly studied the significant impact of the granular soil on the leakage phenomenon. It was concluded that head losses between the orifice and the soil surface depend on the soil properties, such as hydraulic conductivity (Walski et al., 2006). A parameter denoted by the 'orifice/soil (OS) number' that is the coefficient between the orifice and soil head losses, was introduced by Walski et al. (2006). It has been observed that at a high flow rate in a low hydraulic conductivity soil, such as clay and silt, the orifice/soil number will be low; the soil head loss dominates over the orifice head loss (van Zyl and Clayton, 2005). This contradicts the study conducted by Walski et al. (2006) which did not consider the effect of soil properties on water leakage. In his studies, Alsaydalani (2010) observed that the onset of fluidisation requires sufficient input energy to overcome both the orifice and soil head losses. This coincides with experimental results obtained by Zoueshtiagh and Merlen (2007) that studied the soil fluidisation mechanism in the sand and glass grain.

The complex relationship between soil type and a leaking phenomenon was investigated by Greyvenstein and van Zyl (2007). The soil particle interaction with the pipe opening and hydraulic fracturing are the main causes of the non-linear relationship between the flow rate and the head loss. In addition, Latifi et al. (2017) established the relationship between water leakage on specific soil characteristics including the liquid limit, plastic limit, and plasticity index that depends on the soil type. For instance, it was observed that soil with a high fine content characterised with high plastic limit could lead to lower water leakage proving the inevitable influence of the surrounding soil properties on water leakage from pipes.

#### 2.7.7.2 Particle size distribution and shape

Soil fluidisation due to pipe leakage depends on particle size distribution (PSD) and form (Kezdi, 1969; Alsaydalani and Clayton, 2014). In terms of water leakage from pipes, water flows into the soil bed may result in the fluidisation of fine particles. The strength of the soil bed against the fluidisation mechanism is linearly related to its particle size distribution (Latifi et al., 2017). The

stability of the soil depends on its grading, which affects its density and hydraulic conductivity. Well-graded soil is characterised by lower hydraulic conductivity and thus making it more stable against soil fluidisation due to its good particle interlocking (Latifi et al., 2017). Alsaydalani (2010) observed that in a coarser-grained soil, initiation of fluidisation required higher flow rates compared to finer-grained soils. In addition, he observed the impact of PSD on the excess pore water pressure in the soil bed. The finer-grained soils are characterised by high fluidisation potential due to the higher pore water pressure generation (Latifi et al., 2017).
Latifi et al. (2017) mentioned that as particle roughness decreases, the pore water pressure generation in the granular bed increases and a lower flow rate is required for the onset of fluidisation in low sphericity particles (Alsaydalani and Clayton, 2014).

#### 2.7.7.3 Soil hydraulic conductivity

Soil hydraulic conductivity depends on the soil void ratio, pore size, and fabric (Knappett and Craig, 2020). According to Lambe and Whitman (1969), the proportional relationship between the soil hydraulic conductivity and the square of the particle size based on the Kozeny-Carman equation. The variation in soil hydraulic conductivity results from a change in particle size distribution that influences the soil fluidisation mechanism (Alsaydalani and Clayton, 2014). Flow velocity is derived from the soil hydraulic conductivity based on Darcy's law (Richards and Reddy, 2007). Teeluckdharry (2017) showed experimentally that the leakage paths are insensitive to the soil's hydraulic conductivity that is defined as the soil's capability to allow water movement through its pores. The hydraulic properties of soil, such as hydraulic conductivity, will significantly impact the leakage paths (van Zyl and Clayton, 2005). In low hydraulic conductivity soil, the water leakage will be less visible at the ground surface as opposed to the granular soil of high hydraulic conductivity. Richards and Reddy (2007) observed that high hydraulic conductivity soil is more sensitive to cavity formation due to the risk of fabric failure. This results in the movement of soil fines through the soil, which is known as suffusion. In contrast, Tang (2017) mentioned that high hydraulic conductivity soil is characterized by low soil movement due to the rapid dissipation of pore-water pressure.

#### 2.7.7.4 Soil relative density

The impact of the relative density (loose and dense) on the soil response before and at the initiation of soil fluidisation has been recently studied (Tehrani et al., 2018; Akrami et al., 2022). The previous experimental investigations conducted by Alsaydalani and Clayton (2014) focused only on dense granular soil. However, Tehrani et al. (2018) performed an experimental study on the fluidisation of saturated silica sand with three different initial relative densities. It has been observed that dense sand with high relative density (DR = 88%) resulted in a greater fluidised zone as shown in Figure 2.20. A similar finding was reported by Akrami et al. (2022) that noticed a considerably larger failure extent in finer sand with high relative density. Further studies are required to investigate the effect of relative density on the soil fluidisation mechanism in different types of soil.

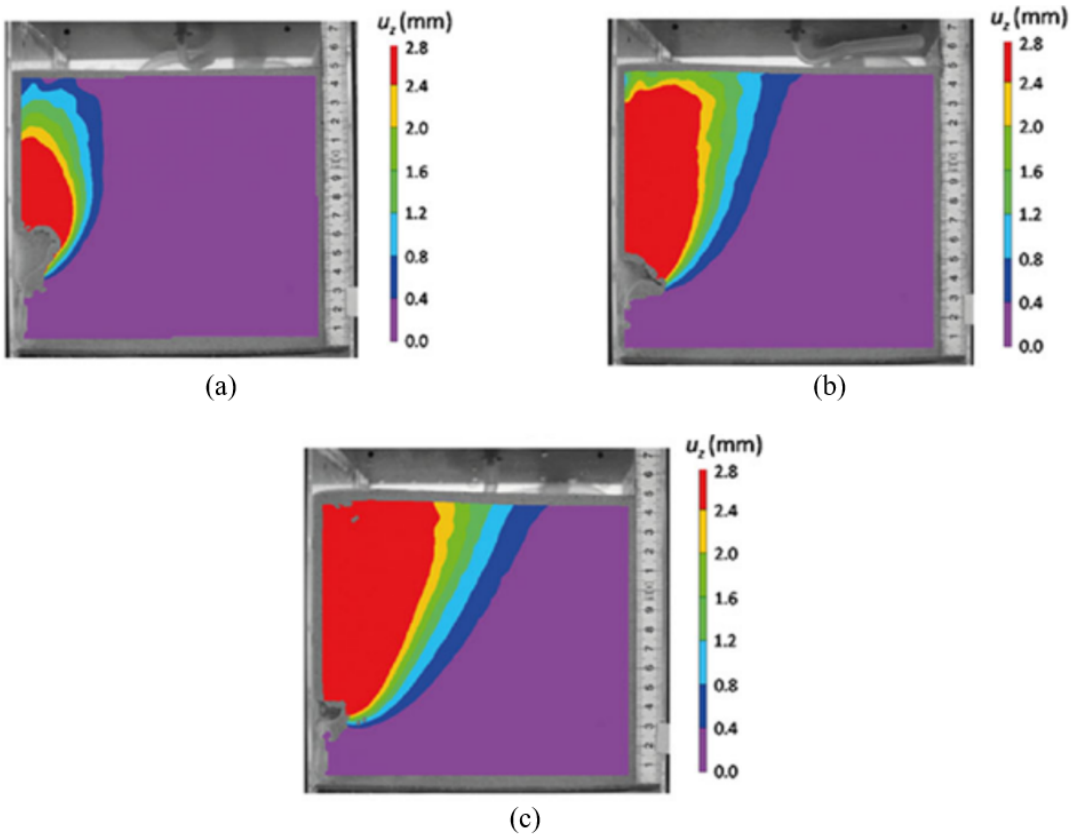



**Figure 2.20:** Sand vertical displacement ($U_z$) profile during the soil fluidisation for (a) loose soil with DR = 31%, (b) medium dense soil with DR = 61%, dense soil with DR = 88% (Tehrani et al., 2018)

In summary, soil fluidisation due to water leakage from a pipe is a complicated phenomenon that involves careful and comprehensive consideration of various pipe and soil parameters. Previous investigations conducted by Lambert (2001); Alsaydalani (2010); Ilunga (2016); Tang (2017) successfully studied the influence of pipe properties including the material behaviour, flow rate, water pressure, orifice size, crack location and bed thickness on the initiation of soil fluidisation due to pipe leakage. The change in the water flow rate and pressure result in different flow regimes of different extents (Farley and Trow, 2003). There is a contradiction between previous studies regarding head loss in the granular soils and across the orifice. In granular soil, Greyvenstein and van Zyl (2007) showed the dominance of the soil head loss on the head loss across the orifice, while Walski et al. (2006) did not consider the soil impact on the leakage discharge and thus considered the head loss across the orifice as a major loss. On the other hand, the soil influence on the fluidisation phenomenon due to water leakage from pipes has not been thoroughly addressed. Previous studies focused on limited soil parameters including the soil type, particle size distribution, hydraulic conductivity, and soil relative density (Zoueshtiagh and Merlen, 2007; Greyvenstein and van Zyl, 2007; Philippe and Badiane, 2013; Teeluckdharry, 2017; Tehrani et al., 2018). Further work is needed to investigate the impact of different pipe and soil characteristics on the development of soil fluidisation around a leaking pipe.

## 2.8 Key gaps of knowledge

Although various numerical and experimental investigations have been performed for the sake of understanding the pipe leakage problem, still little is known about the soil-pipe leakage interaction due to the complex nature of the problem. This complexity results from the variation in the flow regime, pipe material, and soil characteristics (van Zyl and Clayton, 2005). Based on the conducted literature review, the following key gaps of knowledge can be identified.

- Previously, most of the studies were focused on particular parameters involved in the internal soil fluidisation mechanism such as the effect of leakage rate, pipe materials, orifice size and water pressure in granular and poorly graded sand (van Zyl and Clayton,

2005; Alsaydalani, 2010; Cui et al., 2014; Bailey and van Zyl, 2015; Tang, 2017). However, the influence of soil properties has been relegated in the literature.

- The soil parameters including the soil density, fine content, and gradation are expected to highly influence the soil-leakage interaction (Rogers et al., 2008). These are not addressed properly in the previously conducted experimental and numerical research.

- Most of the previous studies performed the soil-leakage experiment using soil with mono-disperse grain sizes (Alsaydalani, 2010; Bailey and van Zyl, 2015; Tang, 2017). There is a lack of multi-scale simulations of granular soil in soil fluidisation phenomenon around leaking pressurised pipe.

- There is a contradiction in the study of head loss through the soil and the orifice. On the one hand, the head loss through the soil is considered much smaller compared to that in the orifice (Walski et al., 2006). On the other hand, Teeluckdharry (2017) showed the significant influence of soil properties on the leakage rate. Thus, they proved that water head loss through the orifice is dominated by the head loss through the soil.

- Recent experimental studies simulated the soil-leakage interaction using a vertical jet of water (Alsaydalani, 2010). However, this does not precisely resemble the real horizontal water flow from a longitudinal or circumferential crack in pressurised pipes.

- Numerical simulations are highly recommended to understand the complicated soil-leakage system due to the possibility and repeatability of data acquisition under different settings.

- Cui (2013); Li (2013) suggested that the micro-structural characteristics and inhomogeneities of the granular particles in the soil fluidisation around leaking pipe are difficult to determine using the continuum numerical methods. Accordingly, a numerical method was developed based on the DEM approach that can capture these properties and thus the local rheology. However, DEM is computationally expensive and requires a large computational time, especially for large-scale problems (Han and Cundall, 2013).

- There is a lack of a proper numerical simulation of soil fluidisation around leaking pressurised pipe that is capable of analysing different parameters together such as the flow rate and leakage relevant soil parameters. This is essential in understanding the influence of pipe leakage on ground stability.

Efficient simulations are needed for a buried water pipe enabling the detection, evaluation, and monitoring processes of the pipe leakage. Thus, a cumulative analysis of different parameters such as the leakage location, diameter, flow rate, leakage pressure, and Reynolds number in addition to the soil permeability, grain size, density, fine content, angle of friction and other factors that complicate the actual interpretation of this issue is needed to finalize this study (Li et al., 2007; Guo et al., 2013; van Zyl et al., 2013; Tang et al., 2017). The pipeline leakage problem should have early detection and repair, through knowing the initial pipe defects causes, to avoid ground collapse (Tang et al., 2017). Therefore, a numerical approach considering all the involved parameters must be developed to simulate the soil-leakage problem that is essential for the safety of pipeline utilisation. Previous approaches focused on particular leakage parameters independently such as pipe size, flow velocity and fluid pressure (Rogers et al., 2008; Alsaydalani, 2010; Cui et al., 2014; Teeluckdharry, 2017). However, the new developed model will properly study the overall pipe leakage issue covering different soil and pipe properties together. This includes orifice size, leakage rate/pressure, orifice location, bed height, soil cohesion, soil porosity, soil density and soil porosity. The conducted simulation will help identify the influence of pipe leakage on ground stability, prioritising the maintenance of the water network and evaluating the risk of water leakage on the adjacent infrastructure. Numerically simulating the development of soil-fluid interaction around leakage pipe, with a focus on the effect of soil and pipe properties on this mechanism is the most efficient method to adopt. It will help in early quantifying and assessing the leakage loss before it approaches the surface. This will be applicable and efficient in water, construction, insurance, and other utility companies.

## 2.9 Summary

The critical literature works conducted on soil fluidisation due to pipe leakage were thoroughly reviewed in this chapter. First, an overview of soil fluidisation and pipe leakage has been introduced. Second, the experimental studies conducted on soil fluidisation induced by a leaking pipe were discussed in detail. Moreover, the previously investigated numerical simulations of soil fluidisation around a leaking pipe using different approaches were presented. Finally, the effect of different pipe and soil parameters involved in the soil fluidisation mechanism triggered by a pipe leakage has been reported based on the related published literature. In general, previous studies have been limited to capturing the onset of the soil fluidisation induced by pipe leakage; while other works only presented the results of the analysis without focusing on understanding and investigating the fluidisation mechanism around a leaking pipe. The review has shown that little effort has been devoted in the previous investigations to analyse the effect of different soil and pipe parameters mainly on the post-local fluidisation mechanism until it reaches the soil surface. All of the key findings and gaps of knowledge have been summarised and linked to the objectives of this research.

# Chapter 3

# Methodology

## 3.1 Introduction

In this chapter, the research methodology adopted for this study is presented, followed by a review of the basis of the Material Point Method (MPM). Then, the frameworks of the two-phase (2P) MPM approaches available for modelling soil-fluid interaction problems are defined in terms of the concept and computational solution. The implementation of the advanced in/outflow boundary conditions (BCs) into the double-point approach for simulating the water inflow to the domain is described. Finally, the numerical procedure adopted in this research is provided at the end of this chapter.

## 3.2 Research methodology

In geotechnical problems, it is common to encounter soil-fluid interaction in which the solid phase is coupled with the fluid phase (Jassim et al., 2013). The properties of each phase are described by specific equations (Zienkiewicz and Shiomi, 1984; Verruijt, 2009), and previous studies showed the limitation of Discrete Element Method (DEM) and Finite Element Method (FEM) in simulating soil fluidisation around a leaking pipe. The DEM method, based on discrete mechanics, can capture the inhomogeneities of the granular particles in soil fluidisation phenomena around a leaking pipe. However, DEM is computationally expensive and requires a large computational time, especially for simulations of large-scale problems.

Soil fluidisation is characterised by large deformations of the ground (Martinelli et al., 2017). These deformations are not feasible to predict with traditional approaches such as FEM due to

mesh tangling. Even though remeshing techniques solve this issue to a certain degree, some accuracy issues still arise from projecting field variables between meshes in successive stages (Wang et al., 2015). This has prompted the development of particle-based numerical techniques such as the Material Point Method (MPM), which is applied in this research. The different steps of the research methodology are presented in Figure 3.1. It highlights the actions required to simulate the soil fluidisation around a buried pressurised water leaking pipe using a multiphase MPM approach to meet the research objectives.

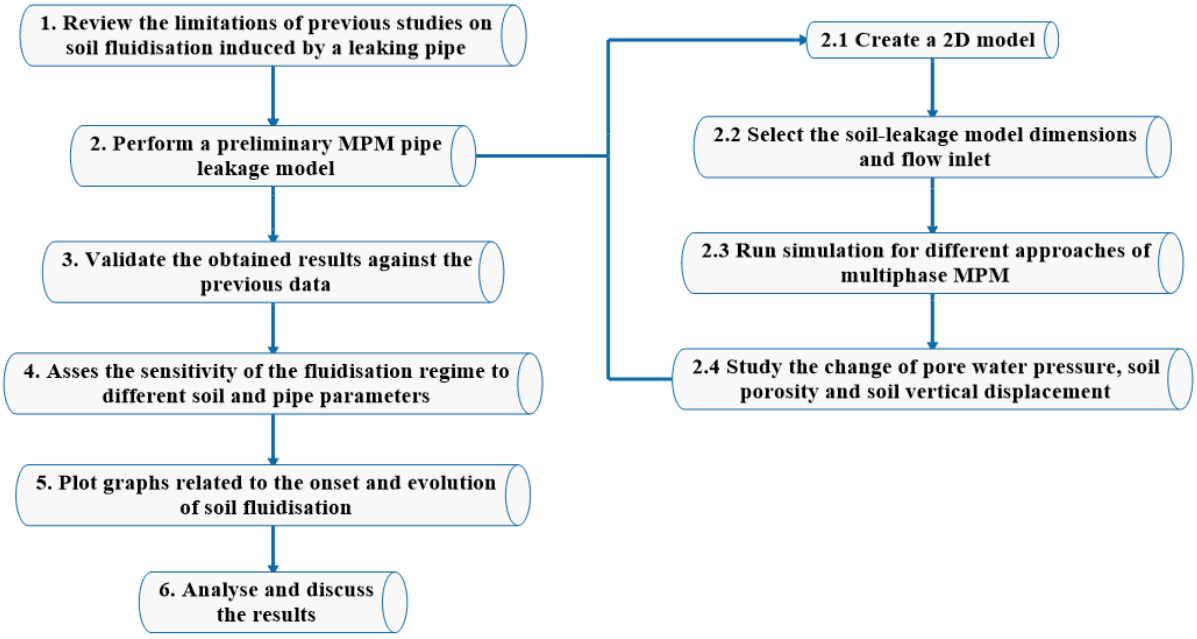



**Figure 3.1:** Overview of the research methodology followed in this research work

## 3.3 The Material Point Method: basic concept

The Material Point Method (MPM) is a particle-based method in which the time-dependent continuum where bodies are represented using a set of Lagrangian Material Points (LMPs) accompanied by a conventional finite element computational mesh (Martinelli and Rohe, 2015). The MPM was developed by Sulsky et al. (1994) for the purpose of modelling dynamic deformation in a solid medium. This process is an extension of the Particle-In-Cell (PIC) method, that was initiated by Harlow (1964) for implementation in fluid mechanics. The Lagrangian MPs are occasionally referred to as 'particles', however despite what the name implies, they

represent a part of a continuum rather than individual solid particles. A schematic representation of the discretisation of the media (continuum body) into MPs is presented in Figure 3.2. The MPs move through a fixed Eulerian mesh that is used to solve the main governing equations (i.e., momentum balance). These MPs convey the stress, strain, mass, energy, momentum, and other material parameters of the continuum. The size of the mesh can affect the obtained results similar to the Finite Element Method (FEM), but the Eulerian mesh is only utilised for formulation purposes without carrying any permanent information. The use of the background mesh decreases the computational cost compared to other meshless methods such as Smoothed Particle Hydrodynamics (SPH) (Fern and Soga, 2016). In addition, the boundary conditions can be defined on this mesh, which is also an advantage compared to SPH. The continuum in MPM complies with the basic conservation thermodynamical laws (Fern et al., 2019) that include mass, momentum, and energy conservation. The MPM weak and discrete formulation is consistent with the equation of the classic FEM (Sulsky and Schreyer, 1993). The Material Point Method (MPM) utilizes a mapping technique consisting of two primary steps (Sulsky et al., 1994; Fern et al., 2019). First, the Grid-to-Particle Mapping transfers information from the computational grid to particles by interpolating values like velocity and stress from grid nodes to corresponding particle locations. This interpolation can be performed using various techniques, including linear or higher-order interpolation. Second, the Particle-to-Grid Mapping updates grid values by interpolating particle-based information, such as velocity or mass, back to the grid nodes employing different interpolation methods. This process ensures a precise representation of material behaviour on the grid, enabling the application of conventional numerical approaches for solving equations, including partial differential equations.

One time step of the MPM computational cycle is illustrated in Figure 3.3. In the first stage, MPs properties are transmitted to the mesh nodes; in the second stage, accelerations at each node are determined after solving the momentum balance equations; in the third stage, the obtained velocity fields at nodes are mapped back to MPs; and in the final stage, the position and state parameters of MPs are updated. At the end of the last stage, the computational mesh is reset to its initial alignment (Martinelli and Rohe, 2015). The MPM incorporates the advantages of both

Lagrangian and Eulerian approaches while eliminating most of their drawbacks, including the mesh distortion and the advected quantities (Sulsky et al., 1994; Zhang et al., 2007; Fern et al., 2017). There are some disadvantages associated with MPM related to the application of moving boundary conditions, multiphase interaction, and large rotation problems (Bandara and Soga, 2015). Also, errors in spatial discretization might accumulate and affect the required continuity (Kashiwa, 2001; Zhang et al., 2008). MPM is computationally more expensive than FEM due to the dual discretisation framework (MPs and computational mesh) (Kularathna, 2018). The final drawback of the MPM approach is the cell crossing instability in which material points cross an element's boundary in the computational mesh leading to unphysical instability (Yerro, 2015). This can particularly occur in a problem involving a large deformation.

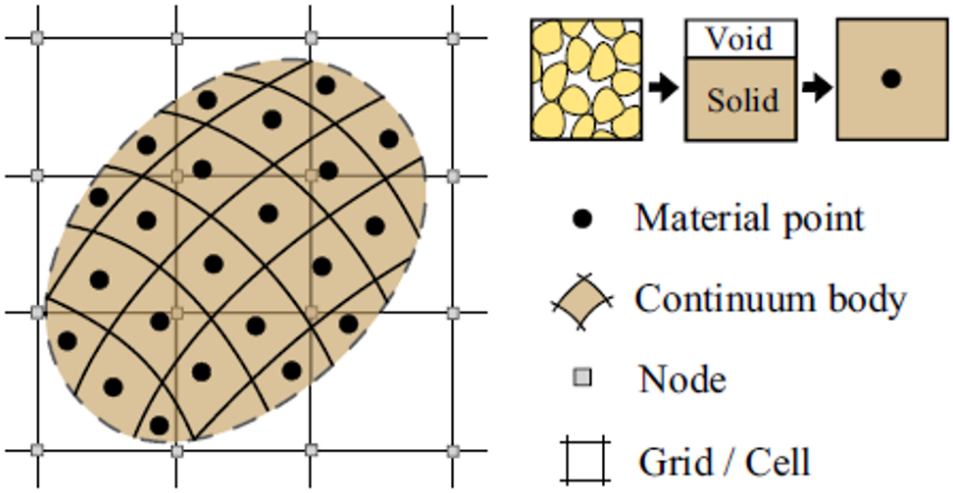



**Figure 3.2:** Schematic representation of the spatial discretization of MPM (Fern and Soga, 2016)

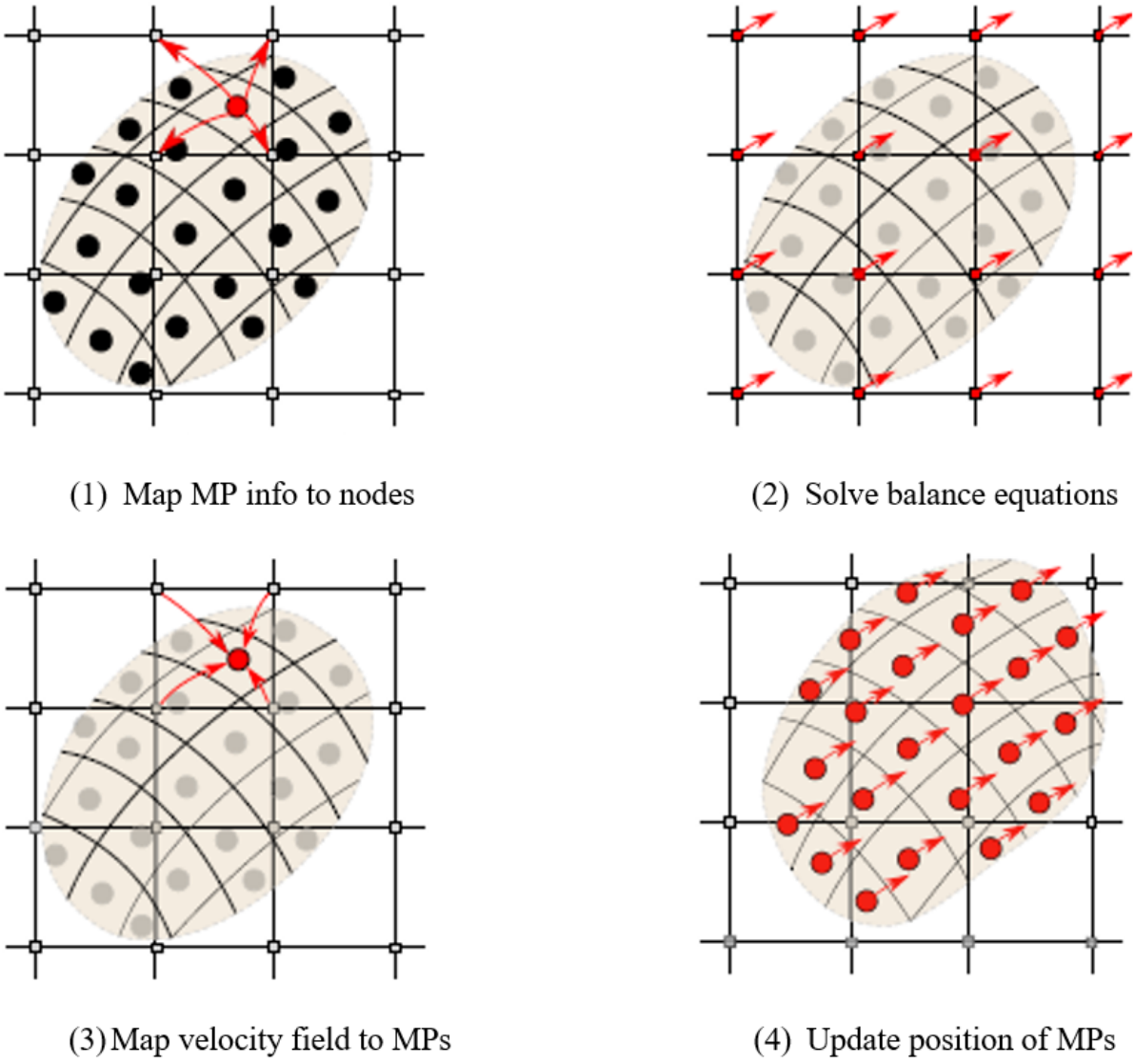



**Figure 3.3:** The computational strategy of MPM (Fern and Soga, 2016)

## 3.4 MPM multi-phase approaches

The Material Point Method (MPM) has shown to be a powerful technique in simulating and solving various problems in geotechnical and hydraulic fields, such as the study of granular flow (Więckowski, 2003; Phuong et al., 2014), landslides and slopes (Beuth et al., 2011; Yerro et al., 2014), columna collapse (Andersen and Andersen, 2010; Martinelli and Rohe, 2015), pile installations (Phuong et al., 2014), dike failure (Coelho et al., 2018), internal erosion (Yerro et al., 2017; Murphy et al., 2020), and soil liquefaction (C. di Prisco et al., 2022). MPM has

been applied to solve large deformation problems and multi-phase processes in saturated and unsaturated porous media (Abe et al., 2014; Yerro et al., 2015; Zhao and Liang, 2016).

The two-phase MPM formulation has been developed to model the soil-fluid interaction in saturated soils based on studies in continuum mechanics lately applied in Finite Element Method (FEM) (Terzaghi, 1943; Zienkiewicz et al., 1999). There are two distinct formulations for simulating the solid-fluid (two-phase) interaction in saturated porous media; two-phase single-point (2P-SP) approach and two-phase double-point (2P-DP) (Ceccato et al., 2018). The 2P-SP adopts one set of Material Points (MPs) (Zabala and Alonso, 2011; Jassim et al., 2013) while the 2P-DP consists of two sets of MPs as shown in Figure 3.4.

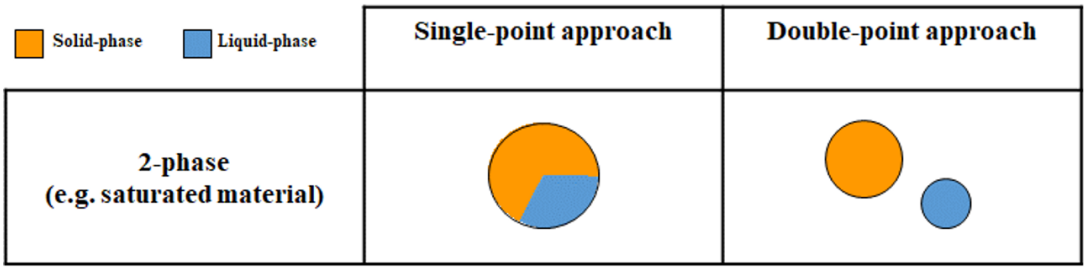



**Figure 3.4:** Schematic diagram of different multi-phase MPM approaches [after Yerro et al. (2015)]

## 3.4.1 Two-phase single-point MPM approach

### 3.4.1.1 Concept

In the two-phase single-point (2P-SP) formulation, the porous medium is simulated based on the macroscale continuum approach, where the saturated soil is defined by the solid skeleton kinematics using one set of material points (MPs) (Zabala and Alonso, 2011; Jassim et al., 2013). As shown in Figure 3.5, each MP represents a portion of the saturated media, and this media moves as a unit with the solid phase (i.e., Lagrangian description of the soil motion). The information from the liquid phase is also carried by the MPs using an Eulerian approach. In 2P-SP formulation, each MP satisfies the solid mass conservation, but the liquid flow may alter the total mass. This framework usually assumes the validity of Darcy's law; hence it is not valid when liquid flow is very rapid and non-laminar. The 2P-SP formulation is not appropriate

when dealing with the interaction between free water and porous water since the first one has no representation in the domain. The 2P-SP approach has proved to be an efficient technique for modelling geotechnical problems such as slope collapse (Soga et al., 2016) and the CPT (Cone Penetration Testing) testing (Ceccato et al., 2016).

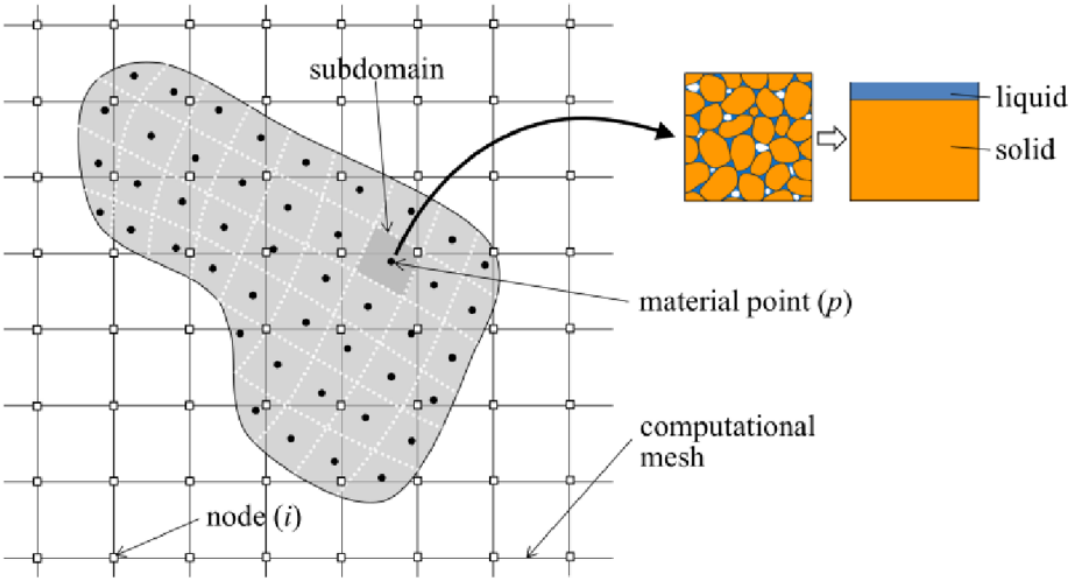



**Figure 3.5:** Scheme of the two-phase single-point formulation [after Yerro and Rohe (2019)]

### 3.4.1.2 Computational solution

The two-phase single-point (2P-SP) formulation is based on specific physical laws, including momentum balance and mass balances (Jassim et al., 2013). The dynamic momentum balances of both the liquid phase and mixture (solid and liquid) are solved at the nodes based on (Eq. 3.1) and (Eq. 3.2), respectively. This approach considers all the dynamic terms in which the acceleration of the solid skeleton ($a_S$) and the acceleration of the pore liquid ($a_L$) are the main unknown variables. These terms play a crucial role in accurately simulating fluid-solid interactions and porous materials. They enable the modelling of the coupling between the fluid and solid phases, ensuring mass conservation, capturing dynamic behaviour, and maintaining energy conservation within the system (Fern et al., 2019). Neglecting these inertia terms would result in inaccurate simulations and unrealistic material responses. The mass conservation of the solid and liquid phases in addition to their constitutive relationships are expressed in (Eq. 3.3) and (Eq. 3.4).

Eq. 3.3 is solved to update the volumetric concentration of liquid (porosity).

$$\rho_L a_L = \nabla_p - f^d + \rho_l b \tag{3.1}$$

$$n_S \rho_S a_S + n_L \rho_L a_L = \nabla.\sigma + \rho_m b \tag{3.2}$$

$$\frac{D^S n_L}{D_t} = n_S \nabla.v_S \tag{3.3}$$

$$\frac{D^S \varepsilon_{vol,L}}{D_t} = \frac{n_S \nabla.v_S + n_L \nabla.v_L}{n_L} \tag{3.4}$$

$D^S(.)/D_t$ represents the material time derivative following the motion of the solid phase that can be expressed as

$$\frac{D^S(.)}{D_t} = \frac{d(.)}{d_t} + \vec{v_S}\nabla(.)$$

Where, $\rho_S$ is the solid density, $\rho_L$ is the liquid density, $\rho_m$ is the mixture density, $n_S$ is the volumetric concentration ratio of solid, $n_L$ is the volumetric concentration ratio of liquid ($\rho_m = n_S\rho_S + n_L\rho_L$), $v_S$ is the solid velocity, $v_L$ is the liquid velocity, $f^d$ is the drag force, $\sigma$ is the Cauchy stress tensor, and $\varepsilon_{vol,L}$ is the volumetric strain of the liquid phase.

The flow in this formulation is assumed to be laminar; therefore, the drag force ($f^d$) is solved based on Darcy's law (Eq. 3.5).

$$f^d = \frac{n_L \mu_L}{\kappa_L}(v_L - v_S) \tag{3.5}$$

Where, $\mu_L$ is the constant liquid viscosity and $\kappa_L$ is the constant intrinsic permeability.

In the 2P-SP formulation, the solid mass is automatically conserved as the solid mass of each MP remains constant. This is not the case for the liquid where the liquid mass in MPs can vary depending on the change in porosity. In this approach, the liquid is considered to be weekly compressible, and the fluxes resulting from the change in spatial variations in liquid mass are ignored, as shown in (Eq. 3.4). The latest assumption might have some impact on the solution in problems that have a high gradient of porosity.

A Galerkin method is used to obtain a semi-discrete form of the field equations (Eq. 3.1) to (Eq. 3.4). Time integration is performed using an explicit time stepping algorithm. More details

about the implementation of these methods, in the context of the 2P MPM approach, are provided in Appendix A.1. In each time step, the solution scheme follows the following steps (Yerro, 2015; Ceccato et al., 2018).

1. Map the variables (such as positions, velocities, mass, material properties, state variables, etc) required to solve the governing equations in the mesh from the MPs to the nodes.
2. Calculate the nodal acceleration for solid ($a_S$) and liquid ($a_L$).
3. Update the velocity and momentum of the material particles from the obtained acceleration for solid and liquid phases.
4. Compute the nodal velocities from the resulted nodal momentum and then calculate the strain rate.
5. Update the excess pore pressure and effective stresses based on the solved liquid and solid constitutive laws at the MPs.
6. Update the displacement and location of MPs based on the solid velocity.

### 3.4.2 Two-phase double-point MPM approach

#### 3.4.2.1 Concept

Two-phase double-point (2P-DP) formulation (Bandara, 2013; Abe et al., 2014; Martinelli, 2016; Cao and Neilsen, 2021) uses two sets of MPs to represent the solid phase and the liquid phase separately; these are so-called solid material points (SMPs) and liquid material points (LMPs). The 2P-DP is based on the mixture theory, which assumes that each point in a body's space consists of a finite number of MPs that represent the mixture's constituents. The 2P-DP approach takes full advantage of the Lagrangian description for soil and liquid phases (Abe et al., 2014; Martinelli and Rohe, 2015). In the 2P-DP framework, the volume fractions theory (Truesdell and Toupin, 1960) is used to simulate the solid-liquid interaction. The SMPs and LMPs are used to compute the velocities of the solid skeleton and water independently, and they are allowed to

move separately and overlap, as shown in Figure 3.6. The LMPs can denote the free water as well as the pore water. If the SMPs and LMPs coincide in the same element in the computational mesh, the element is understood as saturated material; hence SMPs account for the pore water in the soil skeleton. The mechanical behaviour of the dry soil, saturated soil, free water, and pore water can all be represented in the 2P-DP MPM framework.

The 2P-DP approach has been efficiently employed in modelling soil fluidisation (Bolognin et al., 2017), development of crater development around a damaged pipeline (Martinelli et al., 2017), submerged column collapse (Martinelli and Rohe, 2015), and various geotechnical simulations.

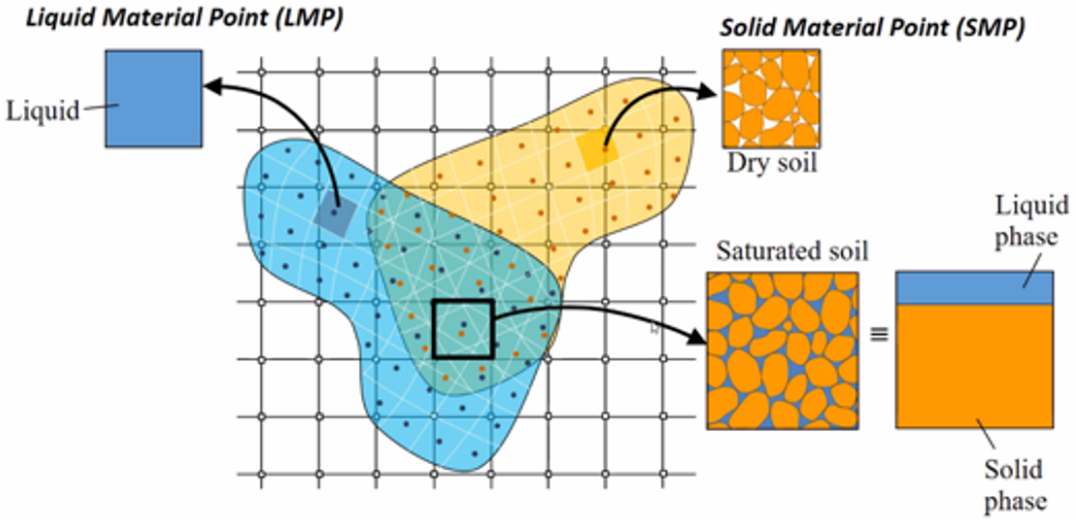



**Figure 3.6:** Scheme of the two-phase double-point formulation [after Yerro and Rohe (2019)]

#### 3.4.2.2 Computational solution

The 2P-DP double-point approach used in this research is the one proposed by Martinelli (2016). The main governing equations are the momentum and mass balances for the solid and liquid phases. This approach, similar to the 2P-SP formulation, considers all the dynamic terms in which the acceleration of the solid skeleton ($a_S$) and the acceleration of the pore liquid ($a_L$) are the main unknown variables. Contrary to the two-phase single-point, the mass conservation of both solid and liquid phases is automatically fulfilled in the double-point formulation (Ceccato et al., 2018). The solid and liquid momentum balances are solved based on Eq. 3.6 and Eq. 3.7, respectively. The momentum balance for solid is regarded in this formulation instead of the

mixture one. The solid (Eq. 3.4) and total (Eq. 3.8) mass balances and their respective constitutive equations are solved at the MPS.

$$n_S \rho_S a_S = \nabla . \bar{\sigma}_S + f^d + n_S \rho_S b \tag{3.6}$$

$$n_L \rho_L a_L = \nabla . \bar{\sigma}_L - f^d + n_L \rho_L g \tag{3.7}$$

$$\frac{D^L \varepsilon_{vol,L}}{D_t} = \frac{n_S \nabla . v_S + n_L \nabla . v_L + (v_L - v_S) . \nabla n_L}{n_L} \tag{3.8}$$

Where: $\bar{\sigma}_S$ is the partial stress for the solid phase ($\bar{\sigma}_S = \sigma' + n_S \sigma_L$),
$\bar{\sigma}_L$ is the partial stress for the liquid phase ($\bar{\sigma}_L = n_L \sigma_L$),
$\sigma'$is Terzaghi effective stress tensor, $\sigma_L$ is the liquid stress tensor that is equivalent to pore pressure ($p$) in saturated material, $f^d$ is the drag force, $g$ is the gravitational acceleration, and $D^L(.)/D_t$ represents the material time derivative following the motion for the liquid phase that can be expressed as

$$\frac{D^L(.)}{D_t} = \frac{d(.)}{d_t} + \vec{v_L} \nabla (.)$$

In contrast to the 2P-SP formulation, the liquid phase in the 2P-DP approach can change from porous liquid to free fluid. This transition results in important changes in the flow regime as well as the volumetric concentration ratios. Thus, the generalised drag force ($f^d$) in Eq. 3.5 is updated to account for the high flow regime resulting in Eq. 3.9.

$$f^d = \frac{{n_L}^2 \mu_L}{\kappa_L} (v_L - v_S) + \beta {n_L}^3 \rho_L |v_L - v_S| (v_L - v_S) + \sigma_L . \nabla n_L \tag{3.9}$$

Where: $\beta$ is the non-Darcy flow coefficient that is estimated based on Eq. 3.10.

$$\beta = \frac{B}{\sqrt{\kappa_L A {n_L}^3}} \tag{3.10}$$

Where: $n_L$ is the volumetric concentration ratio of the liquid and $\kappa_L$ is the intrinsic permeability that is calculated based on the Kozeny-Carman equation (Bear, 1988).

$$\kappa_L = \frac{\frac{D^2}{A} {n_L}^3}{(1-n_L)^2} \tag{3.11}$$

The liquid mass balance of the 2P-DP formulation is expressed in Eq. 3.8 and comprises all the convective terms. Contrary to the 2P-SP approach, the liquid fluxes due to the spatial variation of liquid mass are considered.

In the 2P-DP MPM approach proposed by Martinelli (2016), the transition between the solid-like or liquid-like state of the solid-liquid mixture is distinguished at the element level through a maximum porosity threshold $n_{max}$ (i.e., critical porosity). $n_{max}$ can be associated to the characteristic maximum void ratio of the soil. When the porosity is lower than $n_{max}$, the solid-liquid mixture is considered saturated soil (i.e., solid-like state). In a solid state, the effective stresses at the SMPs are calculated consistent with the material constitutive model associated with the solid skeleton; the porous liquid (represented by LMPs) is assumed weakly compressible, consistent with Eq. 3.8 and an imposed water bulk modulus. The liquid deviatoric stress is set to zero.

If the saturated mixture experiences an increase in porosity (e.g., triggered by the injection of water in the system), the intergranular contact between the soil grains can eventually vanish, the effective stress becomes zero, and the mixture fluidises. This transition from solid to liquid-like behaviour is assumed to happen when porosity reaches the threshold $n_{max}$. Consequently, when the porosity of the mixture is larger than $n_{max}$, the solid-liquid mixture is considered in a liquid state, and its momentum balance is described by the Navier-Stokes equation. The stresses at the SMPs (i.e., effective stress) are imposed to be zero, while the stresses at the LMPs are updated assuming that its constitutive behaviour is a Newtonian fluid. Consistently, the deviatoric part of the stress tensor of the liquid $\sigma_{dev,L}$ is computed using the following Eq. 3.12.

$$\sigma_{dev,L} = 2\mu_L \varepsilon_{dev,L} \tag{3.12}$$

Where: $\mu_L$ is the liquid viscosity that considers the solid concentration ratio of the mixture and $\varepsilon_{dev,L}$ is the deviatoric component of the liquid strain rate.

The liquid viscosity is, in fact, an equivalent viscosity ($\mu_e q$) assumed to depend on the volumetric concentration ratio of the solid material within the saturated mixture using the following Eq. 3.13 (Beenakker, 1984).

$$\mu_{eq}^{t} = 1 + \frac{5}{2}\tilde{n}_{S,el}^{L,t} + 5.2\left(\tilde{n}_{S,el}^{L,t}\right)^2 \tag{3.13}$$

where $\tilde{n}_{S,el}^{L}$ represents the interpolated element solid concentration ratio.

It is important to note that when the mixture is in a solid state, the effective stresses can vanish, but the state of the mixture changes to liquid only if the porosity is larger than $n_{max}$. Finally, liquid pressure in a LMP is also set to zero if belongs to a free surface.

The 2P-DP computational cycle follows the following steps (Ceccato et al., 2018; Fern et al., 2019).

1. Map the variables (such as positions, velocities, mass, material properties, state variables, etc) required to solve the governing equations in the mesh from the MPs to the nodes.

2. Calculate the nodal acceleration for solid ($a_S$) and liquid ($a_L$).

3. Update the velocity and momentum of the material particles from the obtained acceleration for solid and liquid phases.

4. Compute the nodal velocities from the resulted nodal momentum and then calculate the strain rate.

5. Update the liquid stress and effective stresses based on the solved liquid and solid constitutive laws at the LMP and SMP respectively.

6. Identify the free surface LMPs.

7. Update the displacement and location of MPs based on the solid velocity.

Both 2P-SP and 2P-DP formulations are generally integrated explicitly and consider a weakly compressible liquid. The SP formulation is only applicable to a laminar flow as the drag force

considers the validity of Darcy's law. In contrast, the drag force implemented in the 2P-DP approach accounts for the gradient of the concentration ratio, laminar flow (in a low-velocity regime) and non-linear flow (in a high-velocity regime). Therefore, the use of the 2P-DP formulation is vital when the flow velocity is high, and the spatial variability of concentrations is significant (Ceccato et al., 2018). In addition, an important feature of the 2P-DP formulation compared to the 2P-SP approach is the capability of capturing the interaction between the porous media and free water. This is an essential aspect in various geotechnical problems, such as erosion, scouring, and fluidisation. The number of MPs required to discretise the saturated media in the 2P-DP formulation is significantly higher (at least double) compared to the 2P-SP approach. This will inevitably impact computational time.

#### 3.4.2.3 Inflow/Outflow Boundary Condition

For the numerical study of soil response under pressurised leaking pipes, it is necessary to account for inflow and outflow BCs in the 2P-DP approach that can ensure consistent water flow through the orifice and a constant water head at the ground surface, respectively. The inflow/outflow boundary conditions (BCs) developed by Zhao et al. (2019) have been used here as a basis to model BCs.

In this analysis, the inflow and outflow zones are attached to the original model (Figure 3.7) to allow LMPs to enter and leave the computational domain. In the inflow region (Figure 3.7a, in green), a constant velocity is prescribed to the LMPs. Zero acceleration is prescribed at the inflow nodes that are shared with the regular elements of the computational region to maintain the imposed velocity field at the boundary, applied to the computation of the governing equation. The momentum balance equations are not solved in the inflow/outflow boundary elements. When an inflow element becomes empty, new LMPs are introduced at the Gauss point locations to refill the inflow elements. The momentum balance equations are only solved at the nodes shared between inflow and non-inflow elements, and the momentum is transferred from MPs in the inflow elements to the MP in the adjacent elements. On the other hand, outflow elements are indicated in Figure 3.7b, in red. The LMPs that enter the outflow elements are consistently

removed. The nodes shared between outflow elements and computational region have a constant pressure (zero) boundary condition and a zero pressure is defined at the LMPs on the free water surface.

It is worth mentioning that the in/outflow elements are not treated as part of the calculation domain boundaries, but instead as boundaries used to feed or remove MPs from the domain. In other MPM works, the water flow is modelled using a large water reservoir (Bolognin et al., 2017; Martinelli et al., 2017). However, the water level decreases as water flows throughout the model leading to a progressive drop of the total head at the inflow boundary. The use of the in/outflow BCs enables the modelling of constant velocity flows and optimizes the computational cost by simplifying the geometry and reducing the number of MPs in the system.

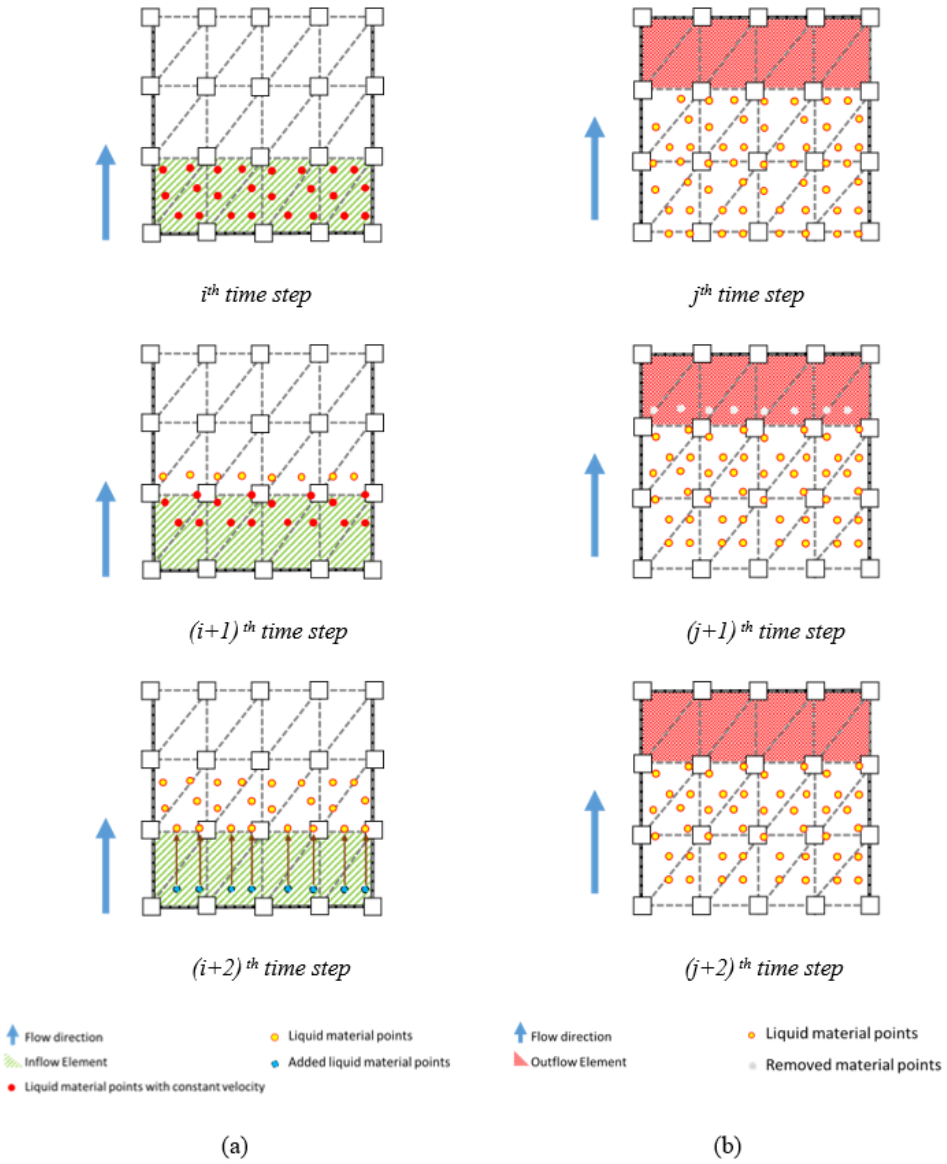



**Figure 3.7:** Schematic of (a) inflow BC and (b) outflow BC

## 3.5 MPM simulation process

In this research, MPM two-phase approaches are used to investigate the soil-fluid interaction mechanisms associated with a buried pressurised leaking water pipe embedded in a fully saturated soil bed. All analysis presented are performed with an in-house version of the open-source Anura3D MPM software (Anura3D, 2022). An overview of the main numerical procedure adopted in the present study is illustrated in Figure 3.8.

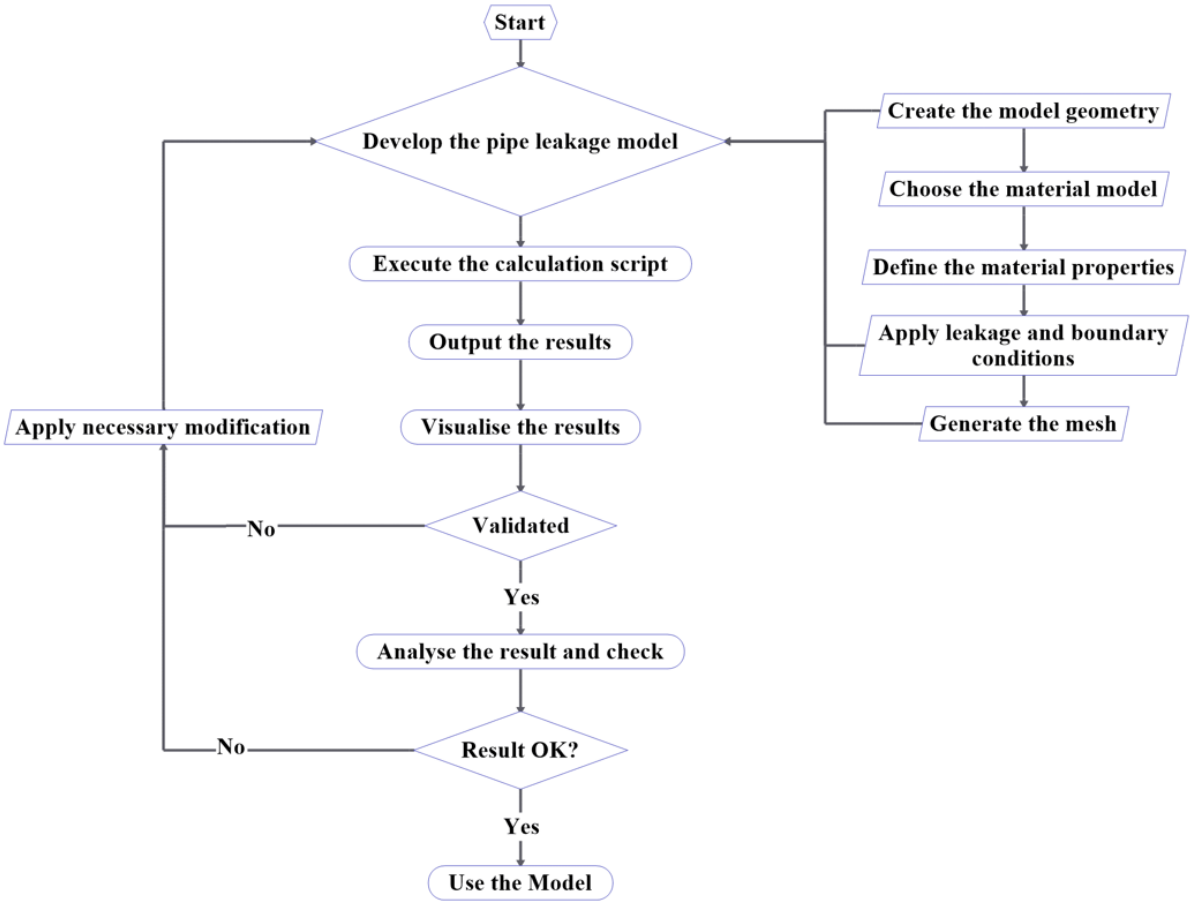



**Figure 3.8:** Flowchart illustration of the implemented MPM simulation

## 3.6 Summary

In this chapter, the research methodology, including the Material Point Method (MPM) adopted in the following chapters, has been discussed in detail. The two distinct MPM formulations for modelling the solid-fluid (two-phase) interaction problems were described and compared. In the two-phase single-point (2P-SP) approach, one set of MPs is adopted, and in the two-phase double-point (2P-DP) approach, two sets of MPs are considered. This chapter also introduced the advanced inflow and outflow boundary conditions (BCs) employed in the double-point approach to prescribing velocity-controlled inflow of material points (MPs) to the domain. Furthermore, the numerical procedures of the developed MPM simulation were provided in this chapter. In this

study, soil fluidisation induced by a leaking pressurised water pipe embedded in fully saturated soil is simulated using the two MPM approaches.

# Chapter 4

# Capability of Different MPM Approaches in Modelling Soil Fluidisation

## 4.1 Introduction

The aim of this chapter is to present capabilities of two-phase single-point (2P-SP) and two-phase double-point (2P-DP) Material Point Method (MPM) approaches to simulate the initiation and evolution of soil fluidisation around a leaking pipe. First, the description of the numerical model developed in each approach is presented. Then, the results are presented and discussed, where the displacement field and failure mechanism around the leaking pipe are analysed in terms of the soil porosity. Finally, the conclusions are summarised at the end.

## 4.2 Numerical model

The main objective of this study is to develop a validated MPM model that captures the key features of the soil fluidisation around a leaking pipe. The initial step in developing a model is conducting a thorough literature review of the recent numerical and experimental studies to study the requirements to build a robust MPM simulation. This is focused on previous studies that investigated soil-water interaction associated with pipe (see Sections 2.5 and 2.6). In particular, the numerical model presented below is mainly inspired by the work form Alsaydalani (2010), who successfully studied the soil fluidisation mechanism due to a localised flow in granular soil. Alsaydalani performed a two-dimensional flow experiment to interpret the internal fluidisation mechanism of the sand bed using the experimental apparatus that is shown in Figure 4.1. A

submerged soil bed with a range of different materials was connected to a water inlet pipe through an orifice ranging from 0.234 to 0.92 mm. The change in the pore water pressure along the soil bed was monitored using standpipes connected to the center line of the soil bed, as shown in Figure 4.1.

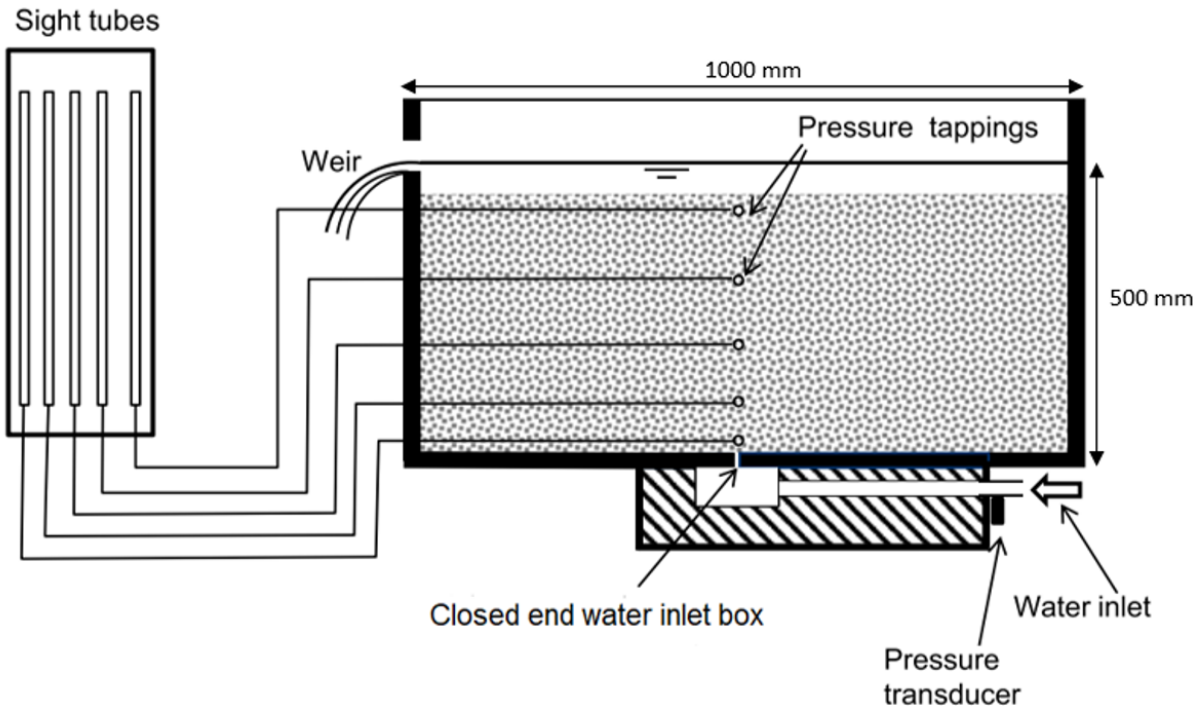



**Figure 4.1:** Experimental setup for internal fluidisation mechanism by Alsaydalani (2010)

The numerical simulation of soil fluidisation induced by a leaking pipe is conducted using two Material Point Method (MPM) formulations presented in the previous chapter, i.e., two-phase single-point (2P-SP) formulation and two-phase double-point (2P-DP) formulation with a two-dimensional model used in each approach. A fully submerged sand bed is connected to a pressurised inlet pipe through an orifice. As the aim of this research at this stage is to study the soil fluidisation around the leaking pipe, only the orifice is modelled and not the whole pipe. This approach significantly simplifies the model and reduces the computation time. The soil and water parameters used in the numerical model are extracted from the experiment conducted by Alsaydalani (2010), listed in Table 4.1.The dilation angle is prescribed as zero in the developed model to promote numerical stability and simplifies modelling by avoiding complexities associated with volumetric expansion. This assumption is supported by previous

studies (Fern et al., 2019; Bolognin et al., 2017; Feng et al., 2021) that validate the use of a dilatancy angle of zero for granular materials within the Material Point Method. Nevertheless, it is crucial to recognize that the applicability of this assumption varies and should be carefully assessed based on the specific material and simulation requirements.

**Table 4.1:** Material parameters of the model, equivalent for the silica sand and water (* parameters only required for the double-point formulation) (Alsaydalani, 2010)

| Material Parameter | Symbol | Unit | Value |
|---|---|---|---|
| Initial porosity | $n_0$ | - | 0.45 |
| Density soil | $\rho_s$ | kg/$m^3$ | 2660 |
| Liquid density | $\rho_l$ | kg/$m^3$ | 1000 |
| Intrinsic permeability | k | $m^2$ | $4.0 \times 10^{-11}$ |
| Water bulk modulus | $K_l$ | kPa | 50000 |
| Water viscosity | $\mu_d$ | kPa.s | $8.905 \times 10^{-7}$ |
| $K_0$-value | $K_0$ | - | 0.44 |
| Effective Poisson ratio | v' | - | 0.3 |
| Effective Young's modulus | E' | kPa | 69000 |
| Effective Cohesion | c' | kPa | 1.0 |
| Effective friction angle | $\phi'$ | degree | 34 |
| Dilatancy angle | $\psi$ | degree | 0 |
| Soil grain diameter* | $D_p$ | mm | 0.9 |
| Maximum soil porosity* | $n_{max}$ | - | 0.50 |

### 4.2.1 Two-phase single-point (2P-SP) model

In this section, a two-dimensional MPM model designed to study the capability of the 2P-SP approach to simulate the soil fluidisation around a leaking pipe is presented in Figure 4.2. The utilisation of a 2D modelling approach provides computational efficiency while offering valuable insights into the fundamental behaviour of the system. The soil bed is 500 mm in height and 1000 mm in length, and an empty space is modelled at the top of the soil bed that allows the

top vertical displacement of the material. The size of the empty space is chosen to be 100 mm, which is greater than the maximum expected displacement of the MPs at the surface. An orifice with a width of 100 mm is positioned in the middle of the soil base. Note that the size of the orifice is larger than in previous experimental and numerical studies (Alsaydalani, 2010; Cui, 2013), which is selected to reduce the computational cost.

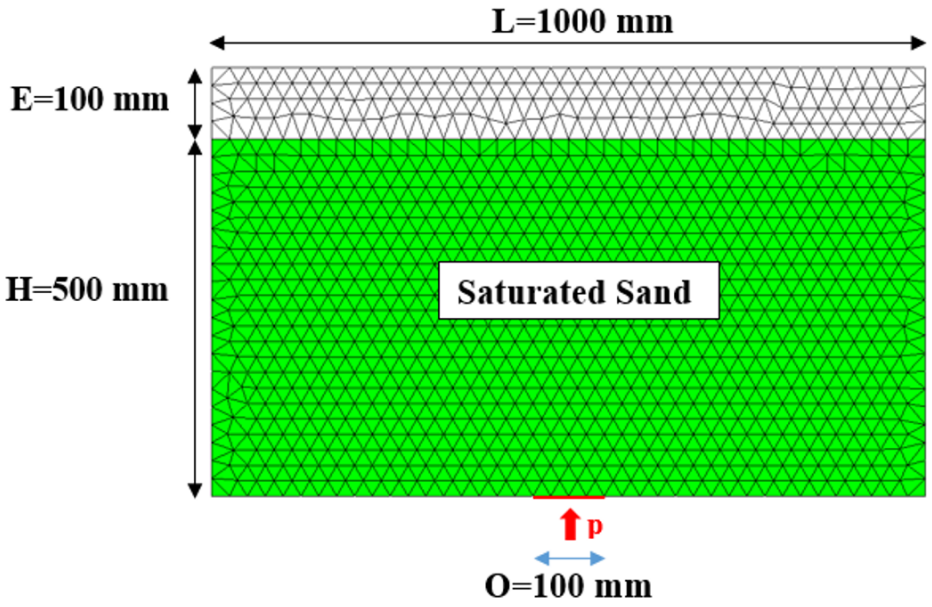



**Figure 4.2:** Discretised domain employed in the single-point modelled problem where 'p' is the applied water pressure, 'H' is the height, 'L' is the length, 'O' is the orifice, and 'E' is the empty space

A two-dimensional mesh comprising 2124 three-node triangular elements has been used as the computational grid. At the beginning of the simulation, three MPs are assigned within the filled elements with a nominal element sized at 0.025 m (Figure 4.2). A homogeneous saturated soil layer is considered, and soil behaviour is modelled using the Mohr-Coulomb elastic-perfectly plastic constitutive model (MC), which is simple and serves as a first-order model. Mohr-Coulomb is a failure criterion that is used to predict the shearing behaviour of soil and, thus, the soil deformation. The water bulk modulus is decreased by 40 times with respect to the real one to optimise the computational time. The influence of reducing the bulk modulus is analysed later in Chapter 5. The intrinsic permeability (k) is assumed constant throughout the 2P-SP simulation. Material properties are summarised in Table 4.1. Solid and liquid displacements on the left

and right sides of the model are fixed in the horizontal direction, whilst the bottom boundary is fully fixed in both horizontal and vertical directions. A vertical fixed boundary is also applied at the top of the model to avoid MPs leaving the mesh. A strain-smoothing algorithm is used to reduce the kinematic locking (Al-Kafaji, 2013). Stresses are initialised via an earth pressure coefficient at rest ($K_0$) procedure, and pore pressures are initially hydrostatic. The water leakage at the orifice is modelled by removing the vertical liquid fixity in the crack where excess water pressure is applied to the nodes. In each simulation, constant water pressure ranging from 5-15 kPa is applied at the orifice through the calculation.

First, a sensitivity analysis is performed to study the effect of the number of elements at the orifice (i.e., mesh-size dependency) on solution accuracy leading to the development of a validated MPM model that captures the soil fluidisation mechanism. The boundary conditions (e.g., fixities) in MPM are generally imposed at the mesh nodes. If nodes are affected by a fixity, the deformation of the MPs located in the surrounding elements is constrained. Note that if the corners of the orifice are fixed, therefore, all elements surrounding those corners will then be affected by these boundary conditions. If the mesh is too coarse, the excess water pressure cannot be properly transmitted. Therefore, a parametric analysis of the number of elements at the orifice is performed to identify the minimum mesh size required to accurately capture the inflow condition.

The impact of the element size in the orifice on the ratio of the transmitted water pressure is investigated by varying the number of elements at the orifice between one and ten elements. A parametric analysis is conducted with three different imposed excess water pressure (EWP) of 5, 8 and 10 kPa through a 100 mm orifice. The mesh dependency for the ratio of the transmitted water pressure with respect to the applied excess water pressure at the orifice is plotted in Figure 4.3. The ratio of the transmitted water pressure in the modelled problem is expected to be equal to one imposed at the boundary as the energy loss through the orifice is not considered.

In this numerical model, the ratio of the transmitted water pressure through the orifice is 0.40 when only one element is considered. This ratio increases significantly to 0.9 when the number of elements increases to four. This simulation further investigates the impact on the ratio of

transmitted water beyond four elements, however, a constant ratio is observed beyond this value. The obtained results are consistent for different imposed excess water pressure. The mesh dependency reduces as the mesh is refined with a reasonable transmission of water pressure. Therefore, four elements are considered at the orifice in all the presented simulations to optimise the computational effort while maximising the accuracy of the results.

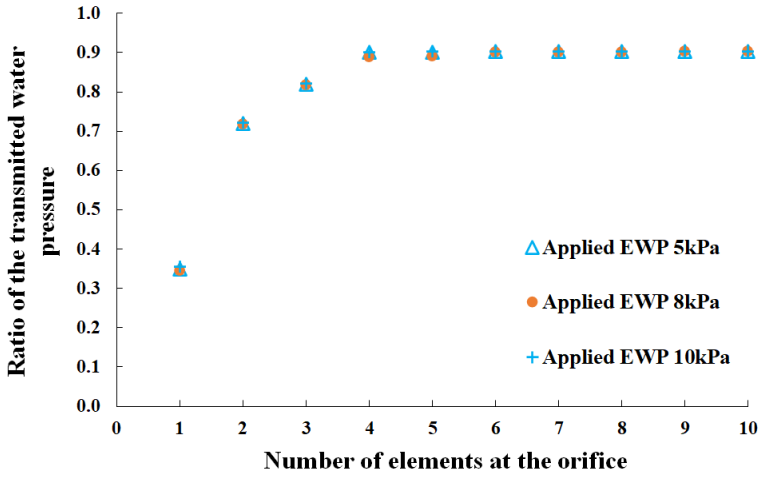



**Figure 4.3:** Effect of the number of elements at the orifice on the transmitted water pressure under different imposed excess water pressure (EWP)

### 4.2.2 Two-phase double-point (2P-DP) model

A similar problem is modelled using the two-phase double-point (2P-DP) approach (Figure 4.4). In this model, the fluid flow is induced by applying a constant water flow through the orifice, and the in/outflow boundary conditions (BCs) introduced by Zhao et al. (2019) are used. The implementation of inflow/outflow Boundary Conditions (BCs) have helped the simulation of constant velocity flows and optimised the computational cost compared to other methods of modelling water leakage such as water reservoir (see Appendix B). Furthermore, inflow and outflow zones are included in the model to allow the Liquid Material Points (LMPs) to enter and leave the computational mesh. The length of the soil bed is 2000 mm. In the inflow element (Figure 4.4, in green) ensure a constant free water table (pressure zero at the water surface) by automatically removing those LMPs that enter the outflow zone. Water elements (Figure 4.4, in blue) represent those elements initially filled with LMPs representing free water. The saturated

soil region (Figure 4.4, in purple) is initialised by placing both Solid Material Points (SMPs) and LMPs to represent the two-phase media. The inflow velocities prescribed in the 2P-DP are used to target the equivalent pressure as the 2P-SP analysis. Thus, both models of the two MPM approaches considered in this study are equivalent despite using different MPM frameworks and boundary conditions.

The soil bed is set to be a fully saturated homogenous layer and a linear elastic-perfectly plastic Mohr-Coulomb constitutive model (MC) is used to model the constitutive behavior of soil (solid-like state). Mohr-Coulomb is a simple failure criterion that predicts the shearing behavior of soil and thus the overall soil deformation. The free water is modelled with a Newtonian fluid model, while the porous water is assumed linear elastic. The material parameters (Table 4.1) and the orifice size (100mm) are the same as those used in the single-point approach. The intrinsic permeability (k) is set as a function of the diameter of the solid grains ($D_p$) and the solid porosity (n) with the Kozeny-Carman formula (Bear, 1988). In this formulation, the maximum porosity ($n_{max}$) is used as an additional parameter to differentiate between the solid and liquid state of the mixture. This parameter is determined based on the provided maximum void ratio from Alsaydalani (2010)'s experiment. The model comprised of 3510 three-node triangular elements with an element size of 0.025 m. Six MPs per element (three LMPs and three SMPs) are initially assigned to the saturated soil domain, and six liquid MPs are assigned to the free water and inflow elements. Solid and liquid displacements are constrained in the normal direction and free in the longitudinal direction in the lateral boundaries. The bottom of the saturated soil region is fully fixed except for the orifice region in which LMPs are allowed to move vertically. The effective stresses are initialised via the $K_0$ procedure, and pore pressures are initially hydrostatic. The prescribed flow velocity ranges from $10^{-3}$ m/s to $10^{-2}$ m/s.

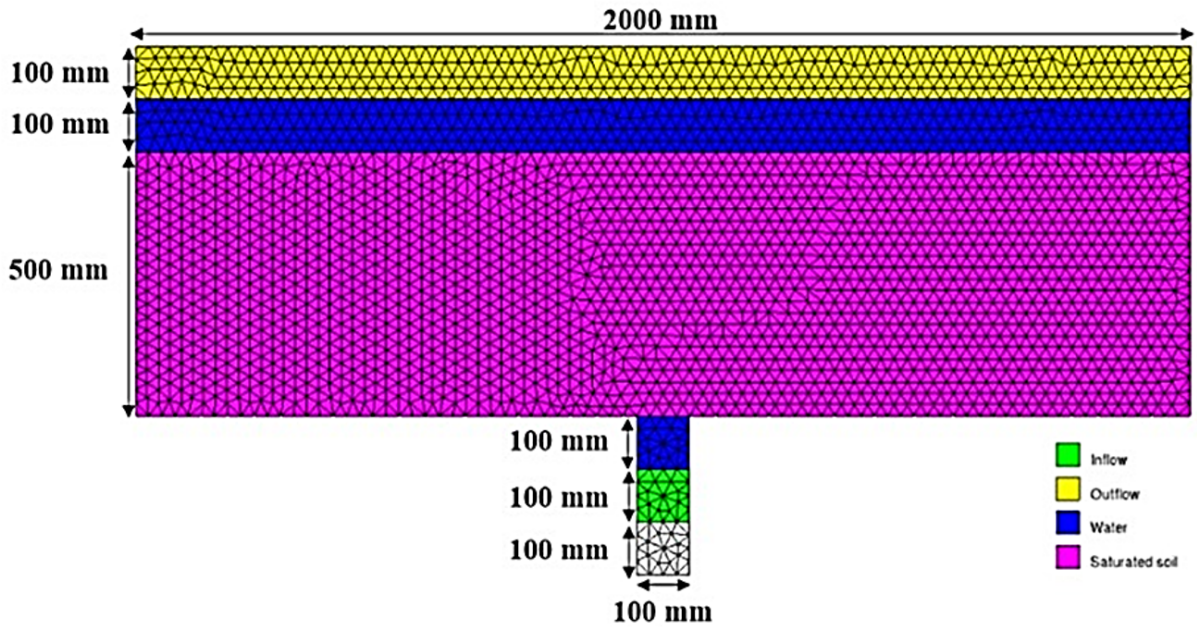



**Figure 4.4:** Discretised domain employed in the double-point modelled problem

In a similar approach to 2P-SP, a parametric analysis is conducted using the 2P-DP to study the influence of the element size at the orifice on the results obtained. For this numerical model, special attention to the corners of the orifice is required (Figure 4.5). Due to the boundary conditions of the two nodes located at the corners between the base of the soil bed and the inlet (Figure 4.5, red nodes), the mobility of the MPs located in the neighboring elements is restricted by this boundary condition (zone of influence of corner nodes). In particular, if a LMP is moving vertically from the inflow zone with a prescribed inflow velocity ($v_i$) enters an element containing one of the corner nodes; it will artificially slow down. This means that $v_i$ is not fully transmitted to the soil. The comparison of Figure 4.5a and Figure 4.5b illustrates that the smaller the elements in the orifice, the smaller the zone of influence restricted by the corner nodes (Figure 4.5b).

To fully understand the effect of the zone of influence of the corner boundaries in the inflow liquid velocity ($v_i$), a parametric analysis is performed, varying the number of elements at the orifice between one to ten elements. In this analysis, the LMPs are prescribed with three different inflow velocities ($v_i$) of 0.001, 0.005, and 0.010 m/s through a 100 mm orifice. The mesh dependency

for the ratio of the transmitted water velocity at the orifice ($v_o$) with respect to the inflow velocity ($v_i$) at the inflow BC is shown in Figure 4.6.

In the model, the energy losses through the orifice are not considered. Thus, the flow velocity at the orifice ($v_o$) is expected to be equal to the applied inflow velocity ($v_i$). The water velocity at the orifice ($v_o$) is measured by averaging the velocity of the material points passing the orifice region. The obtained results are in agreement with the parametric analysis performed in the 2P-SP simulation where four is the required optimal number of elements allowing up to the ratio of 0.9 for the transmitted water velocity. As stated previously, increasing the number of elements beyond four does not significantly improve the results but impacts and increases the computational cost. To optimise the computational time while having reasonable results, all models presented in this study consider four elements at the orifice.

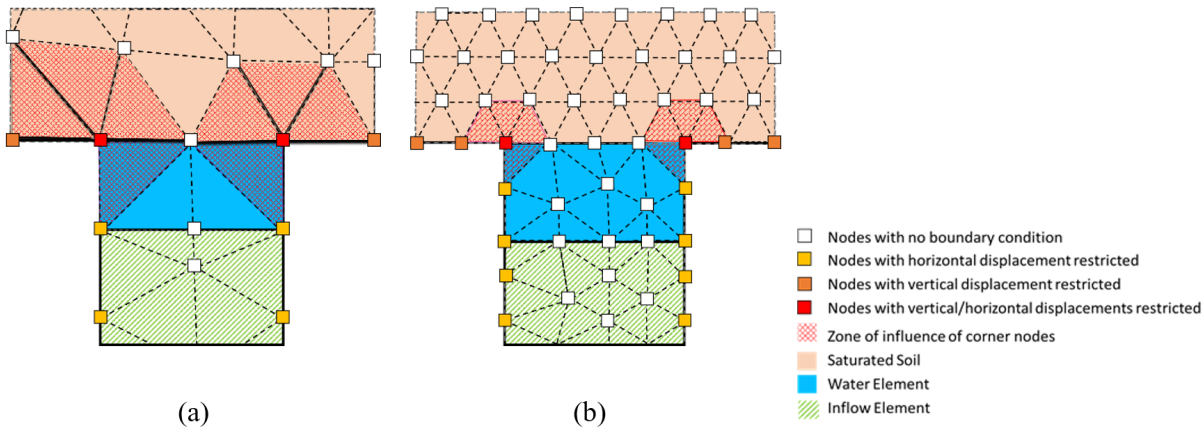



**Figure 4.5:** Schematic of the effect of (a) two elements and (b) four elements at the orifice on the MPM simulation

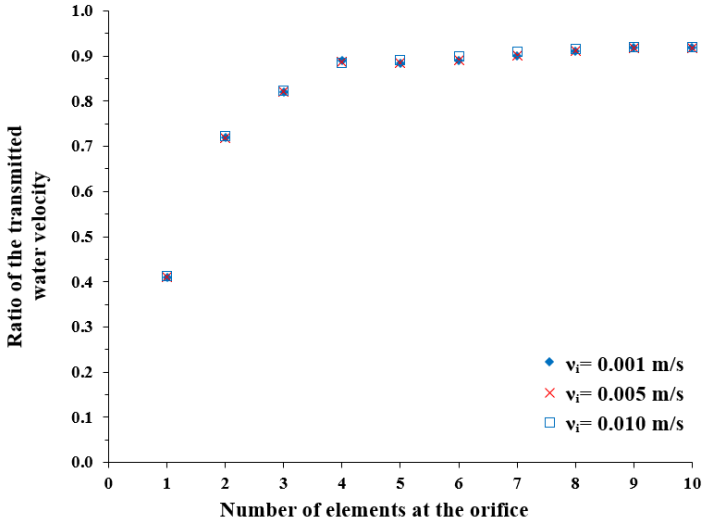



**Figure 4.6:** Effect of the number of elements at the orifice on the transmitted water velocity under different inflow velocities ($v_i$)

## 4.3 Results and discussion

This section presents and discusses the results obtained with the 2P-SP and 2P-DP MPM approaches. The capabilities of the two approaches to simulate the soil fluidisation mechanism are investigated and compared in terms of vertical soil displacements, excess pore water pressures, and porosity developed during the initiation of fluidisation and post fluidisation.

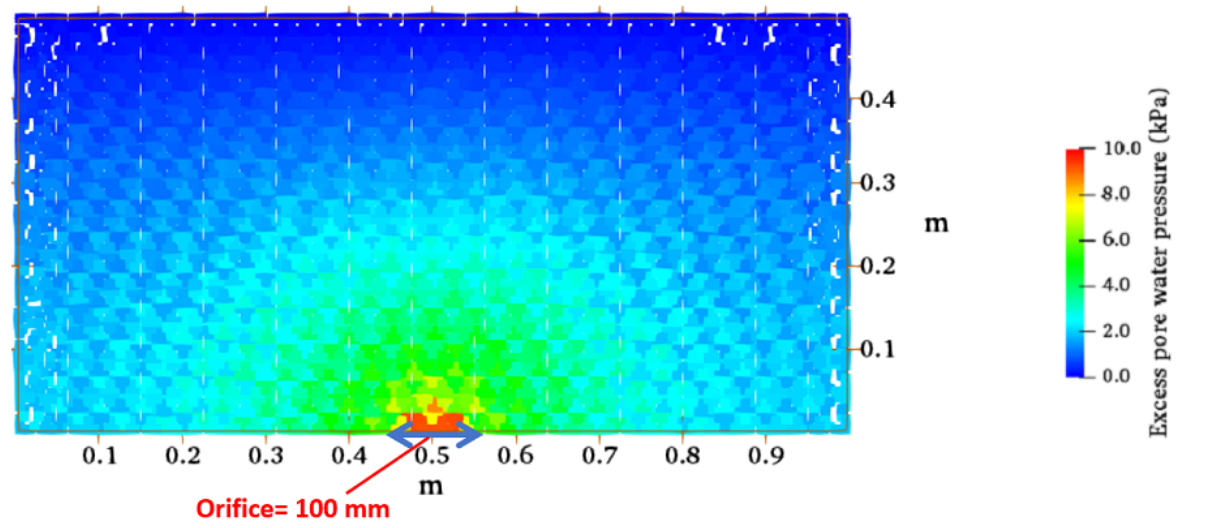
### 4.3.1 Two-phase single-point (2P-SP) MPM results

In this section, results obtained with the 2P-SP approach are presented. The MPM results of fluidisation initiation are compared with the Finite Element Method (FEM) results for validation purposes. Note that at this stage of the problem, only small deformations are developed in the soil. The MPM model (geometry and material parameters) is replicated using the standard FEM using ABAQUS FEA software suite. A two-dimensional mesh consisting of 800 four-nodded quadrilateral elements is used in the model discretisation where constant water pressure is applied at an orifice of 100 mm width that is connected to a saturated soil bed.

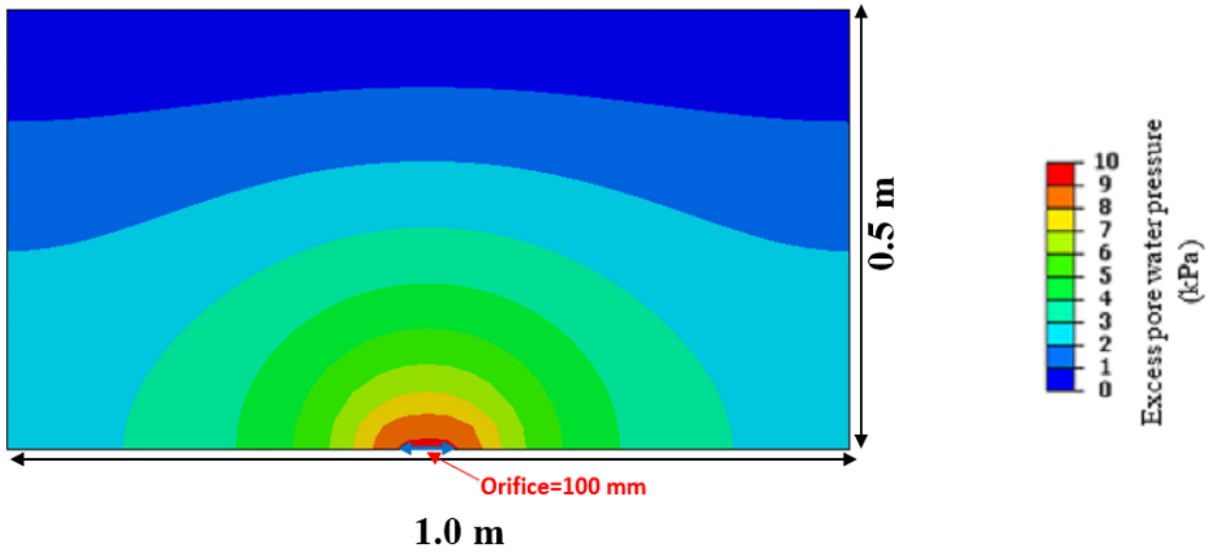
Figure 4.7 shows the excess pore water pressure distribution in the soil bed subjected to an excess water pressure of 10 kPa at a 100 mm orifice after 2s of simulation based on the 2P-SP MPM

(Figure 4.7a) and FEM (Figure 4.7b) results. It is demonstrated that the pore pressure is highly accumulated in the vicinity of the orifice, which quickly dissipates, moving up the soil bed away from the pressure source. Figure 4.8 presents the change in the excess pore water pressure after 2s of MPM and FEM simulations at different heights in the soil bed for different applied water pressures (p= 5 kPa to 15 kPa). It is observed that the excess pore water pressure increases correspondingly with the increase in the applied pressure at the orifice. As the controlled water pressure is increased from 5 kPa to 14.5 kPa, the excess pore water pressure expands within the soil bed. Beyond these values, the excess pore water pressure at 25 mm above the orifice drops from a peak of 12.4 kPa to 11.2 kPa, corresponding to an applied pressure of 14.5 kPa and 15 kPa, respectively. However, an approximately steady state of the excess pore water pressure is noticed near the soil surface. This is due to the localized nature of the problem. The slight difference between the MPM and FEM results is regarded as a consequence of the location difference in data acquisition. This inconsistency in the location of the reference points induces variations in pore pressure.

Based on the previous experimental (Alsaydalani, 2010) and numerical (Cui, 2013) studies, the onset of fluidisation that occurred in the vicinity of the orifice is associated with a peak in excess pore water pressure that is attributed to the uplift mechanism of the soil bed above the pipe orifice. In the presented example, an applied pressure of 14.5 kPa results in a peak excess pore water pressure. Thus, 14.5 kPa is defined as the minimum pressure that is required for the onset of soil fluidisation. This is followed by an abrupt drop in the excess pore water pressure in the vicinity of the orifice. Both 2P-SP MPM and FEM approaches identified the required water pressure for the onset of soil fluidisation (14.5 kPa). Although the orifice size and the applied water pressure are not exact values as in the previous studies, a consistent fluidisation process is recognised in this study with the 2P-SP MPM and FEM results. The observed mechanism is consistent with the previous experimental (Alsaydalani, 2010) and numerical (Cui, 2013; Li, 2013) solutions. Results showed that for higher values of applied water pressure, i.e., post-fluidisation conditions, no equilibrium can be reached in the FEM solution due to the large deformation and mesh tangling.




(a)




(b)

**Figure 4.7:** Excess pore water pressure distribution in a submerged soil bed based on (a) MPM and (b) FEM results where an excess water pressure (10 kPa) is imposed at an orifice

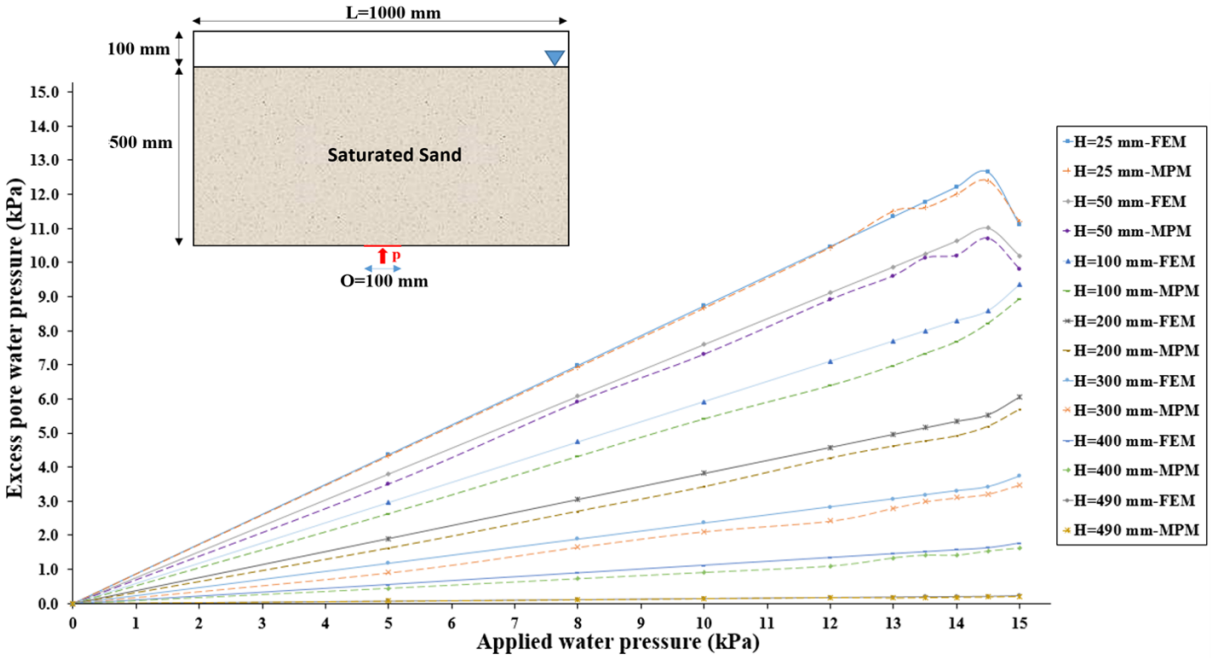
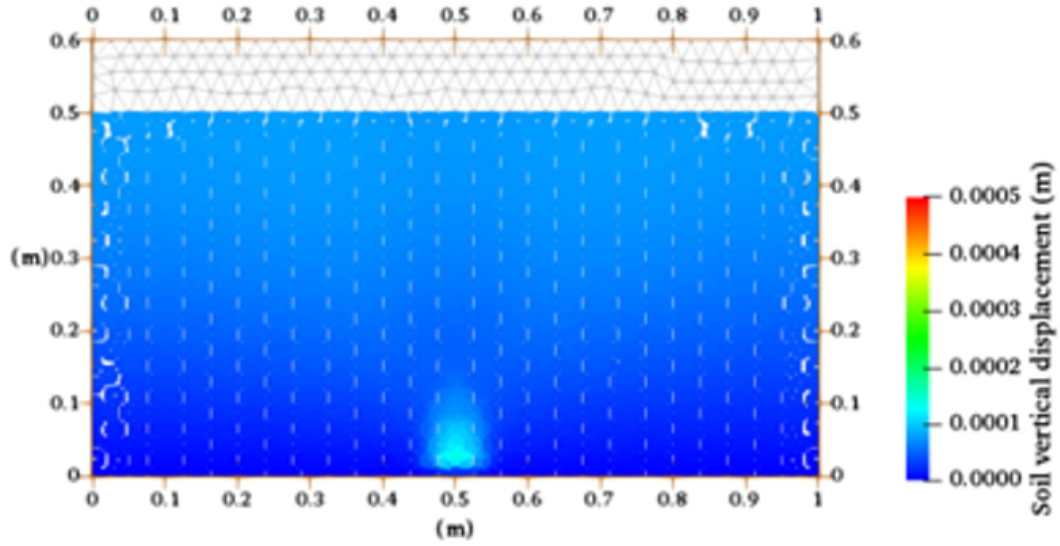
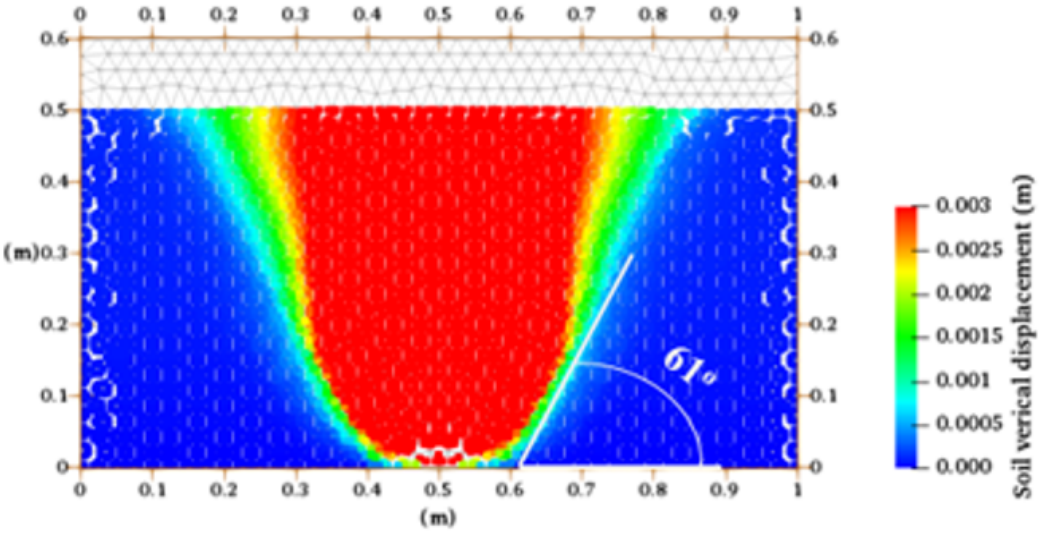



**Figure 4.8:** Excess of pore water pressure distribution at different heights (H) for a centred cross-section considering different applied pressures. FEM versus single-point MPM results

Figure 4.9 shows the soil vertical displacement after 2s of simulation for two different applied pressures (p=10 and 14.5 kPa). Displacements are relatively small (maximum of 0.15 mm) in the vicinity of the orifice before the onset of fluidisation at an applied water pressure of 10 kPa (Figure 4.9a). These soil displacements increase at the onset of fluidisation to 0.3 mm at an applied water pressure of 14.5 kPa (Figure 4.9b). The uplift mechanism in the soil bed is attributed to the peak in pore pressure where the soil is lifted in an upward direction above the orifice leading to the formation of the fluidised zone. The angle of the mobilised zone is 61° as drawn from the edge of the orifice to the soil surface along the boundary of the distributed zone (Figure 4.9b). The inclination angle of the wedge is consistent with Alsaydalani (2010) and Cui (2013), that used the same soil parameters. In addition, the resulting angle is expected theoretically based on the angle of shear failure that is related to the angle of internal friction of the soil (34°), i.e. [45° + (34/2)] = 62°.




(a)




(b)

**Figure 4.9:** Soil vertical displacement after 2s of simulation in a submerged soil bed where an excess water pressure of (a) p=10 kPa or (b) p=14.5 kPa is imposed at the orifice

The 2P-SP MPM calculation crashes before reaching quasistatic conditions when the applied pressure on the orifice is just beyond the pressure that triggers global fluidisation (p=14.5 to 15.0 kPa). Figure 4.10 shows the vertical displacement distribution immediately prior to termination of calculation for p=16 kPa. During the uplift mechanism, MPs are dragged vertically through the computational mesh, and elements near the orifice may become empty resulting in numerical

instability in this scenario. This causes the formation of unrealistic voids within the continuum that affects the continuity of the stress and strain fields (Yerro, 2015). The empty elements near the orifice also cause a disconnection between the boundary nodes (where the pressure p is applied) and the actual soil, which means that the applied pressure will not dissipate into the soil bed. This numerical issue has been previously addressed by the addition of virtual MPs (Beuth, 2012). Virtual MPs are integration points with a small mass that are added in the empty elements to enhance the continuity of the solution. However, another limitation of the current 2P-SP model that prevents the calculation from proceeding after the fluidisation onset is that a unique linear elastic-perfectly plastic constitutive law (Mohr-Coulomb) is considered to describe soil behaviour. This is not realistic at the post-fluidisation stage when solid grains are not in contact, and the soil has a liquid-like behaviour. Therefore, the inability of the constitutive model to transition from 'solid-like' to 'liquid-like' behaviour leads to the calculation to crash. In the next section, the ability of the SP-DP approach to simulate the progression of the onset of fluidisation is discussed.

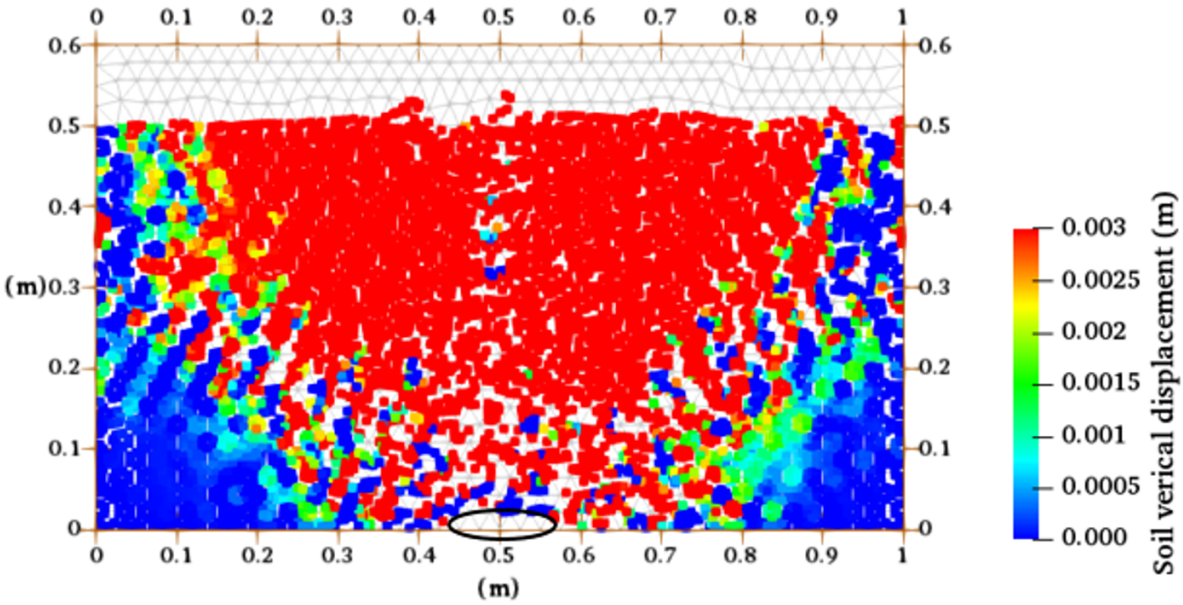



**Figure 4.10:** Soil vertical displacement during the post-local fluidisation mechanism in submerged soil bed where an excess water pressure of 16 kPa is imposed at the orifice

### 4.3.2 Two-phase double-point (2P-DP) MPM results

In this section, the results obtained with the double-point approach are presented. The 2P-DP approach distinguishes between the solid-like and liquid-like behaviour of the soil (represented by the SMPs) based on the maximum porosity value $n_{max}$. In order to visualise the state of the soil, Figure 4.11 shows the porosity field at the maximum development of fluidisation for two different inflow velocities.

Figure 4.11a considers an inflow velocity of $10^{-3}$ m/s, which is equivalent to a water pressure of 14.5 kPa that was identified as the pressure required for the onset of soil fluidisation in the 2P-SP simulation. In this case, the maximum porosity ($n_{max} = 0.50$) is only reached locally in the vicinity of the orifice, indicating that the fluidisation starts but does not progress.

If the prescribed inflow velocity increases to $10^{-2}$ m/s, the fluidisation mechanism progresses and reaches the surface. This is demonstrated in Figure 4.11b, where the porosity field is presented at the time of maximum fluidisation. The liquid-like zone (represented by those SMPs with the maximum porosity) connects the orifice with the top of the model. At this point, the fluidised zone forms an inclined wedge-shaped failure surface that breaks through the soil surface. Afterwards, the fluidised zone is consequently dragged away by the LMPs flow along the soil surface.

The soil fluidisation mechanism is associated with an uplift mechanism of the soil bed (due to the reduction in effective stress) above the pipe orifice (maximum of 80 mm), as shown in Figure 4.12. The prediction from the MPM simulation shows a good qualitative agreement with the previous experimental study conducted by Alsaydalani (2010), who observed that the soil fluidisation is attributed to an uplift mechanism of the grains in the fluidised region of the soil. These results qualitatively show the 2P-DP MPM formulation's capability in identifying the soil fluidisation mechanism induced by a leaking pressurised water pipe. Some drawbacks of the 2P-DP MPM approach include some numerical instabilities that originate due to grid crossing and volumetric locking. These instabilities can reduce the accuracy of the results, including the pore pressure distribution in water. A proper strategy needs to be identified in the extension

of this study to minimise the numerical noise. Also, the possibility of having artificially dry elements in the saturated soil can create spurious oscillations. The later noise has been minimised by increasing the number of SMPs.

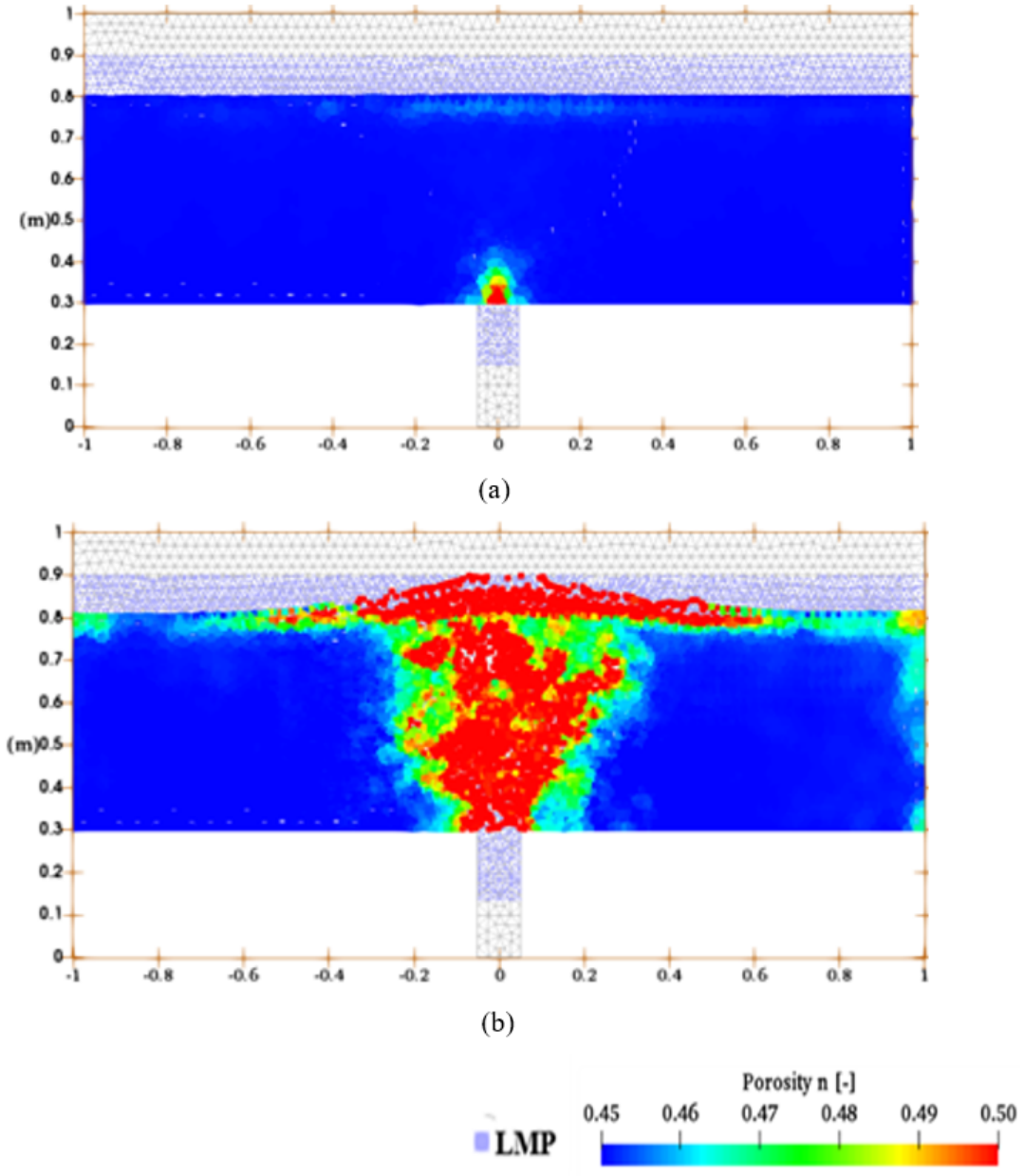



**Figure 4.11:** Soil porosity after 2s of simulation at the SMPs (a) at the onset of fluidisation considering an inflow of $10^{-3}$ m/s and (b) when the fluidisation reaches the surface considering an inflow velocity of $10^{-2}$ m/s

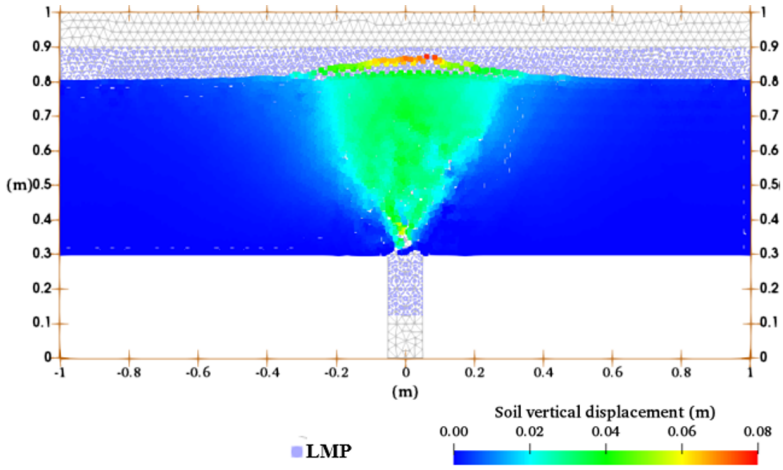



**Figure 4.12:** Soil vertical displacement after 2s of simulation at the SMPs when fluidisation reaches the surface (inflow velocity of $10^{-2}$ m/s)

## 4.4 Summary

This chapter demonstrates and compares the capabilities of the two-phase single-point (2P-SP) and two-phase double-point (2P-DP) MPM formulations to simulate the progression of soil fluidisation associated with a buried and pressurised leaking water pipe embedded in fully saturated sand. The results show that the 2P-SP formulation is applicable for identifying the leak pressure required for the initiation of the local fluidisation in the vicinity of the orifice. However, it is not capable of capturing the post-local fluidisation mechanism due to the formation of empty elements near the orifice and the inability of the constitutive model to represent the transition from solid-like to liquid-like behaviour. The 2P-DP MPM formulation, together with the use of in/outflow boundary conditions, can capture the evolution of soil fluidisation around a leaking pipe until it reaches the soil surface. The MPM results demonstrate how vertical soil displacements, excess pore water pressures, and porosity develop during the onset of fluidisation and post-fluidisation. It can be observed that the excess pore water pressure close to the orifice drops at the onset of fluidisation. The results are qualitatively consistent with previous experimental and numerical works. The 2P-DP MPM model is further expanded for this application in Chapter 5 to study the effect of different soil and pipe parameters on the soil fluidisation mechanism around a leaking pipe.

# Chapter 5

# Implementing the Proposed 2P-DP MPM Approach for Modelling Pipe Leakage

## 5.1 Introduction

In this chapter, the two-phase double-point (2P-DP) Material Point Method (MPM) technique is considered to investigate the soil fluidisation mechanism around a leaking and pressurised water pipe embedded in fully saturated soil. In the model, the inflow water velocity leading to the initiation and evolution of soil fluidisation around the leaking pipe is identified based on the changes in soil porosity and soil bed expansion ratio. This chapter demonstrates that the MPM results are consistent with published experimental studies. Finally, a parametric study is undertaken to investigate the influence of different parameters, including the orifice size, bed height, soil porosity, soil cohesion, leakage direction, and pipe depth, on the soil fluidisation process.

## 5.2 Numerical model

The 2P-DP MPM model presented in this section is also inspired by the experiments conducted by Alsaydalani (2010). A similar problem to the model presented in Chapter 4 is simulated with the same material parameters. The two-dimensional model is shown in 5.1, where a saturated homogeneous soil bed is connected to an inlet pipe through an orifice. The soil bed is 300 mm in height and 1500 mm in length. A sensitivity analysis was conducted to examine the effect of the length of the soil bed on the solution. A careful increase in the bed length was considered to

minimise boundary condition effects. An orifice with a size of 10 mm is located at the middle of the soil base. As the focus of this study at this stage is to investigate the soil behaviour around the leaking pipe, only the orifice is modelled and not the whole pipe. Note that the width of the smallest modelled orifice is 5 mm, which is 15 times larger than previous experimental and numerical studies (Alsaydalani, 2010; Cui, 2013). The smaller the orifice, the finer the mesh is required to discretise the domain, and the higher the computational cost. For instance, the physical time for simulating a model with the smallest orifice (5 mm) is compared to that of the largest orifice (15 mm) using an Intel Core i7 at 2.50 GHz CPU with 8 GB RAM. The model with a 5 mm orifice consists of 5,153 linear triangular non-structured elements; where the minimum element size is 0.00125 m and increases towards the edges of the model up to 0.033 m. On the other hand, the model with a 15 mm orifice consists of 2,415 elements ranging from 0.00375 m to 0.033 m. The computational time decreases by 94% from 162 hours to 10 hours, when changing the orifice size (o) from 5 mm to 15 mm. A parametric analysis is presented in the results section to study the effects of the orifice size.

The water flow is injected through the orifice by applying an upward constant fluid flow at the inflow BC. In the inflow elements (Figure 5.1, in green), a prescribed velocity ($v_i$) is assigned to the Liquid Material Points (LMPs). An empty domain, which does not have any MPs, is attached to the bottom of the inflow elements to avoid the effect of the boundary conditions on the inflow elements. At the top of the model, the outflow region (Figure 5.1, in pink) defines a constant free water table consistent with the experiment from Alsaydalani (2010) by removing those LMPs that enter the outflow elements. Free water zones (Figure 5.1, in blue) include elements initially filled with only LMPs. A saturated soil domain (Figure 5.1, in light brown) is initialised by placing both SMPs and LMPs to represent the saturated medium. The model consists of 4,753 linear triangular non-structured elements. A mesh is refined around the orifice to better capture the size of the crack and the inflow process. The minimum element size is 0.0025 m increasing towards the edges of the model up to 0.033 m (more details on mesh sensitivity analysis are presented in Appendix C). Six MPs per element (three LMPs and three SMPs) are initially assigned to the saturated soil domain, and six LMPs are assigned to the free water and inflow

elements. A sensitivity analysis of different types of boundary conditions, i.e., fixed and contact boundary conditions, on the accuracy of results is conducted (see Appendix C). Mechanical fixities are applied at the boundaries as follows:

- At all boundaries except for the orifice region, solid and liquid displacements are constrained in the normal direction and are free in the longitudinal direction.
- At the orifice region, LMPs are allowed to move vertically. The nodes located at the corners between the base of the soil bed and the inlet pipe are fully fixed.

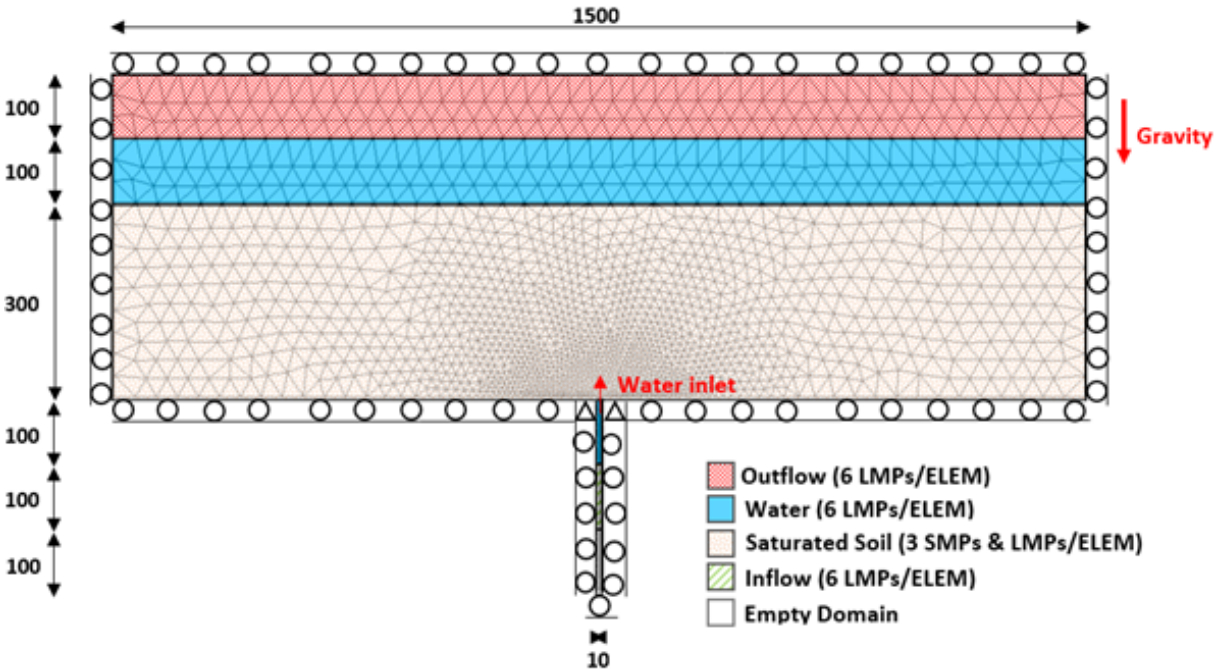



**Figure 5.1:** Geometry of the MPM model (unit: millimetres)

The bulk modulus of water considered in the simulation is 50000 kPa which is 40 times lower than the real bulk modulus to increase the critical time step and optimise the computational time with the explicit MPM integration scheme. This does not have a significant influence on the results as it is still considerably larger than the effective bulk modulus of the solid matrix. In order to analyse the effect of bulk modulus of water, the original model is compared with a higher bulk modulus of 25000 kPa (reduced by 20 times). The computational time required to analyse the problem with lower bulk modulus of water is 10 hours compared to 97 hours for the problem with higher bulk modulus of water, which is almost 10 times faster. This is due to

the critical time step dependence on the bulk modulus of the material, therefore, the higher the bulk modulus, the larger the critical time step (Liang, 2010). However, the observed fluidisation mechanism in both cases is consistent in terms of the porosity distribution and ground movement. This approach of reducing the water bulk modulus to speed up the simulation has been used previously by Liang (2010) and Martinelli et al. (2017). According to Liang (2010), the increased compressibility of water has marginal impacts on the results as the speed of sound is over ten times greater than the maximum flow speed. In addition, a lower bulk modulus of the water is reasonable to incorporate the possible inclusion of air and, therefore, higher compressibility of the water (Ceccato, 2015; Ceccato et al., 2016). Thus, it is concluded that using a reduced water bulk modulus by a factor of 40 is an acceptable approximation.

As described in Chapter 3, the 2P-DP MPM formulation considered here is consistent with the one proposed by Martinelli (2016), in which Darcy's law is generalised with a non-linear term (Ergun, 1952) to account for laminar and steady flow in high-velocity regime. The soil intrinsic permeability (k) is updated using the Kozeny-Carman formula (Bear, 1988) which depends on the solid grain diameter ($D_p$) in addition to soil porosity ($n$). Lastly, the maximum soil porosity ($n_{max}$) that differentiates the solid and liquid states of the mixture is determined based on the provided maximum void ratio from Alsaydalani (2010). A strain-smoothing algorithm is also applied to reduce the kinematic locking (Al-Kafaji, 2013). The effective stresses are initialised via an earth pressure coefficient at rest ($K_0$) procedure, and pore pressures are initially hydrostatic. In each simulation, a constant inflow velocity ($v_i$) is prescribed at the orifice throughout the calculation.

## 5.3 Results and discussion

The results obtained with the 2P-DP MPM approach are presented below. First, the soil fluidisation mechanism for a reference scenario is discussed. Then, the effects of orifice size, soil-bed height, and soil porosity on the soil fluidisation process are investigated through parametric analysis.

### 5.3.1 Soil fluidisation mechanism

Soil fluidisation initiates when the drag forces exerted by an upward fluid balance the gravitational forces of the bed. This process loosens the soil packing, which results in increasing the soil's porosity. In this research, by using the 2P-DP MPM approach, the transition between solid-like and the liquid-like response of the soil is based on the porosity threshold value $n_{max}$ ; $n < n_{max}$ has a solid-like behaviour, while when $n \geq n_{max}$ the soil is fluidised. Therefore, tracking the evolution of porosity in the soil mass (SMPs) is an efficient approach to representing the soil state in the model.

A set of numerical models subjected to different inlet velocities through a 10 mm orifice is simulated to investigate the onset and development of soil fluidisation mechanism. The porosity distribution at different inlet velocities after 2s of simulation through the centreline of the soil bed is plotted in Figure 5.2. It is observed that the soil porosity increases with the increase in the inflow velocity ($v_i$) and increases faster in those points located closer to the orifice (i.e., 0.05 m above the orifice). The maximum soil porosity ($n_{max} = 0.50$) corresponds to critical porosity. When $v_i$ increases from 0.002 m/s to 0.020 m/s, the soil porosity immediately above the orifice exceeds (for the first time) the maximum porosity, indicating that fluidisation has initiated at the orifice. The porosity across the bed height remains constant and equal to the initial value of 0.45. As $v_i$ increases, the fluidised zone expands and develops upward through the soil bed. When $v_i$ reaches to 0.040 m/s, the first point situated above the orifice (0.05 m) reaches the critical porosity, which is considered the onset of soil fluidisation in the vicinity of the orifice (i.e., onset or initiation of soil fluidisation of the soil bed).

At the initiation of soil fluidisation, the particles above the orifice are mobilised and moved with the leakage of water. This was identified by Alsaydalani (2010) as an 'internally fluidised zone' where the soil within this region was uplifted, while those outside the region remained steady (Figure 5.3a). Similarly, Figure 5.3b shows the distribution of the porosity after 2s of the MPM simulation across the whole domain for $v_i = 0.04$ m/s; the fluidised zone localised around the orifice is clearly distinguished in red. Finally, when the $v_i$ increases up to 0.10 m/s, the fluidised

zone reaches ground level (i.e., surface fluidisation). Figure 5.3c demonstrates the movement of the fluidised region beyond the extent of the orifice to the ground surface. The LMPs flow along the ground surface and are consequently dragged away from the fluidised zone.

The inflow velocity required for the initiation of soil fluidisation is also identified by monitoring the soil bed expansion ratio, which is the ratio between the final soil-bed height H and the initial bed height $H_0$ (Taghipour et al., 2005). The soil fluidisation initiates when the expansion ratio exceeds a value of one resulting in a significant heave of the bed (Chen et al., 2011). The heaving of the soil bed occurs when the upward drag force applied by the water exceeds the bulk weight of the soil. In the numerical model, the soil bed expansion starts when $v_i = 0.040$ m/s, as noticed in Figure 5.4, which is in good agreement with the porosity results. The soil bed heaves significantly (10%) by the time the fluidisation reaches the surface at an inflow velocity of 0.10 m/s. The soil fluidisation mechanism is associated with the uplift of the granular materials above the orifice, and this was recognised by Alsaydalani (2010) as shown in Figure 5.5a. The vertical soil displacement for $v_i = 0.040$ m/s based on the MPM simulation is presented in Figure 5.5b; displacements are relatively small (maximum of 1.0 m) in the vicinity of the orifice at the onset of fluidisation. The MPM prediction is consistent with the experimental result by Alsaydalani (2010). It is worth mentioning that Alsaydalani (2010) assessed the effect of orifice size on the onset of the soil fluidisation mechanism. It was concluded that the fluidisation zone is not influenced by orifice size under tested conditions. The inclination angle of the mobilised zone measured from the MPM result is 63° (Figure 5.5b), which is consistent with Alsaydalani (2010)'s experiment using the same soil properties (Figure 5.5a). Furthermore, the obtained angle is expected theoretically based on the angle of shear failure that depends on the angle of friction of the soil (34°), i.e., [45°+34/2] = 62°. The soil displacements increase as the fluidisation reaches the soil surface to 10 m at an inlet velocity of 0.10 m/s (Figure 5.5c). The uplift mechanism in the soil bed occurs when the soil is lifted in an upward direction above the orifice leading to the formation of the fluidised zone. Previous studies (Zoueshtiagh and Merlen, 2007; Montellà et al., 2016) have described the significant uplift as a chimney, which is a narrow zone of upward movement of water and soil. The upward progression of the fluidised

region results in the entire erosion and instability of the soil in the chimney. Overall, these results qualitatively validate the observations from previous experimental results.

The fluidisation mechanism is also attributed to an abrupt drop in the effective stress where the contact forces between the grains vanish. The effective stress at different inflow velocities through the centerline of the soil bed is plotted in Figure 5.6 after 2s of simulation. It is found that the effective stress decreases with the increase in the inflow velocity ($v_i$) and drops faster at the vicinity of the orifice. When $v_i$ increases from 0.002 m/s to 0.040 m/s, the effective stress at 0.05 m above the orifice decreases to zero, indicating the onset of the soil fluidisation at which the leakage force exerted by the upward flow balances the bulk weight of the soil. When the $v_i$ increases, up to 0.10 m/s, the effective stress across the bed height becomes null at the point where the fluidisation reaches the ground surface.

It is worth noting that this study focuses on the initiation and progression of the fluidisation mechanism up to the ground surface. Once the fluidised zone reaches the bed surface, the simulation becomes unstable, and the post-fluidisation mechanism (i.e., behaviour after the fluidisation reaches the ground surface) cannot be analysed. A possible explanation for the numerical instabilities is that the 2P-DP MPM approach used here considers the liquid as weakly compressible, which can generate pressure oscillations when simulating nearly incompressible pressurised flows (Kularathna and Soga, 2017; Yamaguchi et al., 2020; Kularathna et al., 2021; Sołowski et al., 2021).

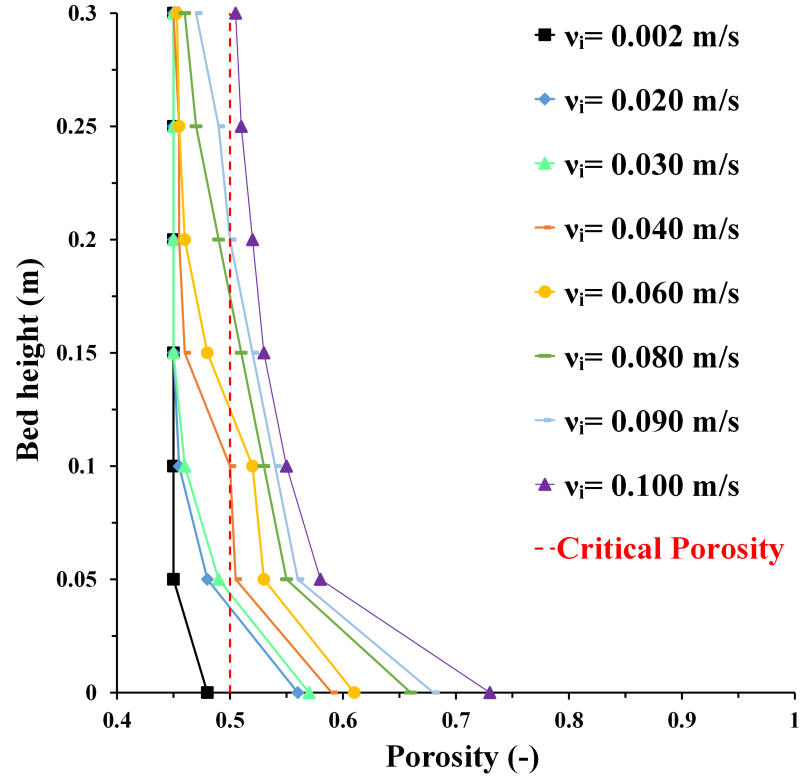



**Figure 5.2:** Porosity distribution at different inflow velocities ($v_i$) through the centreline of the soil bed

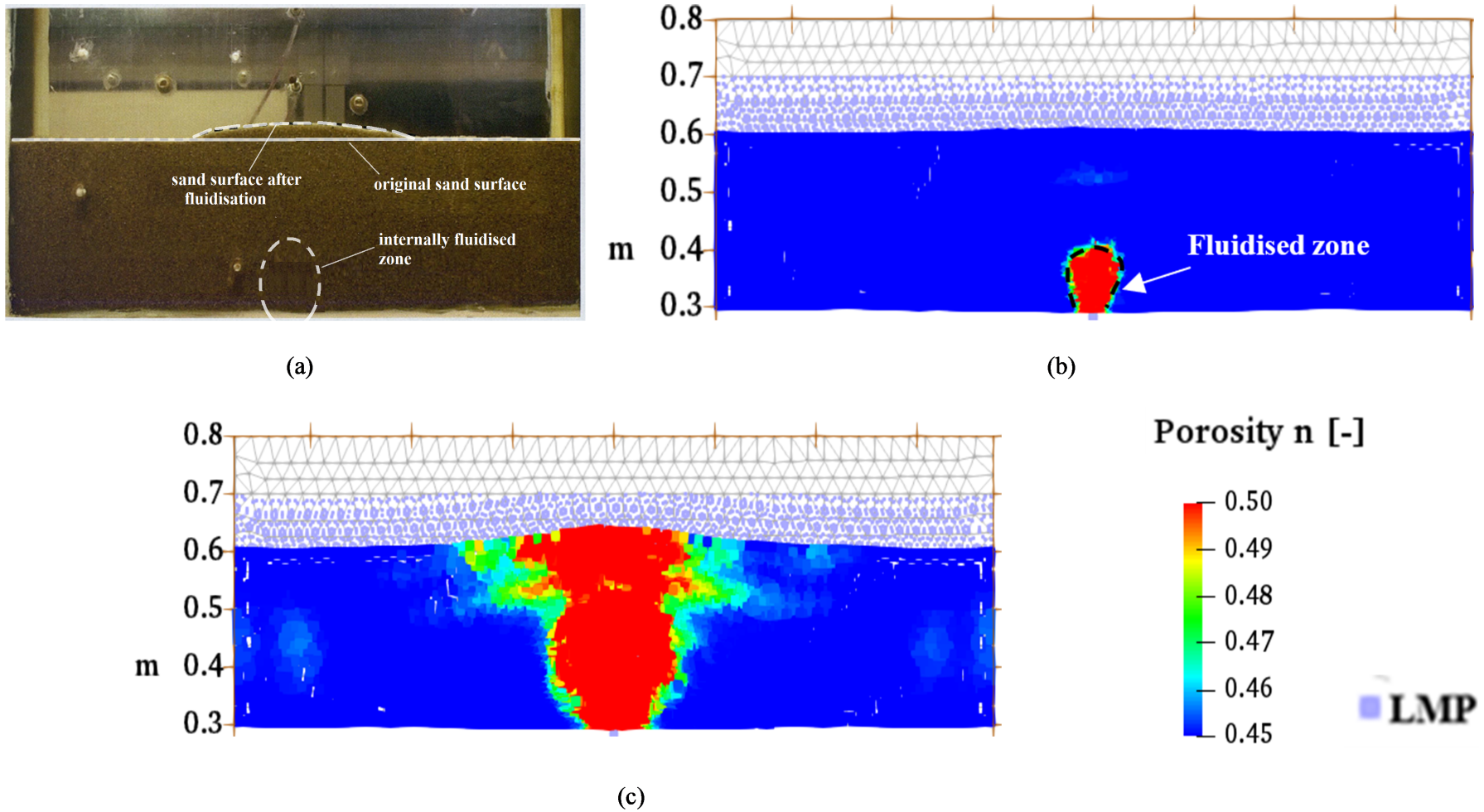



**Figure 5.3:** Fluidised zone at the onset of fluidisation for (a) Alsaydalani (2010)'s experimental result with an orifice of 0.336 mm and (b) MPM result with an orifice of 10 mm after 2s of simulation (c) Fully developed fluidised zone based on MPM simulation after 2s of simulation

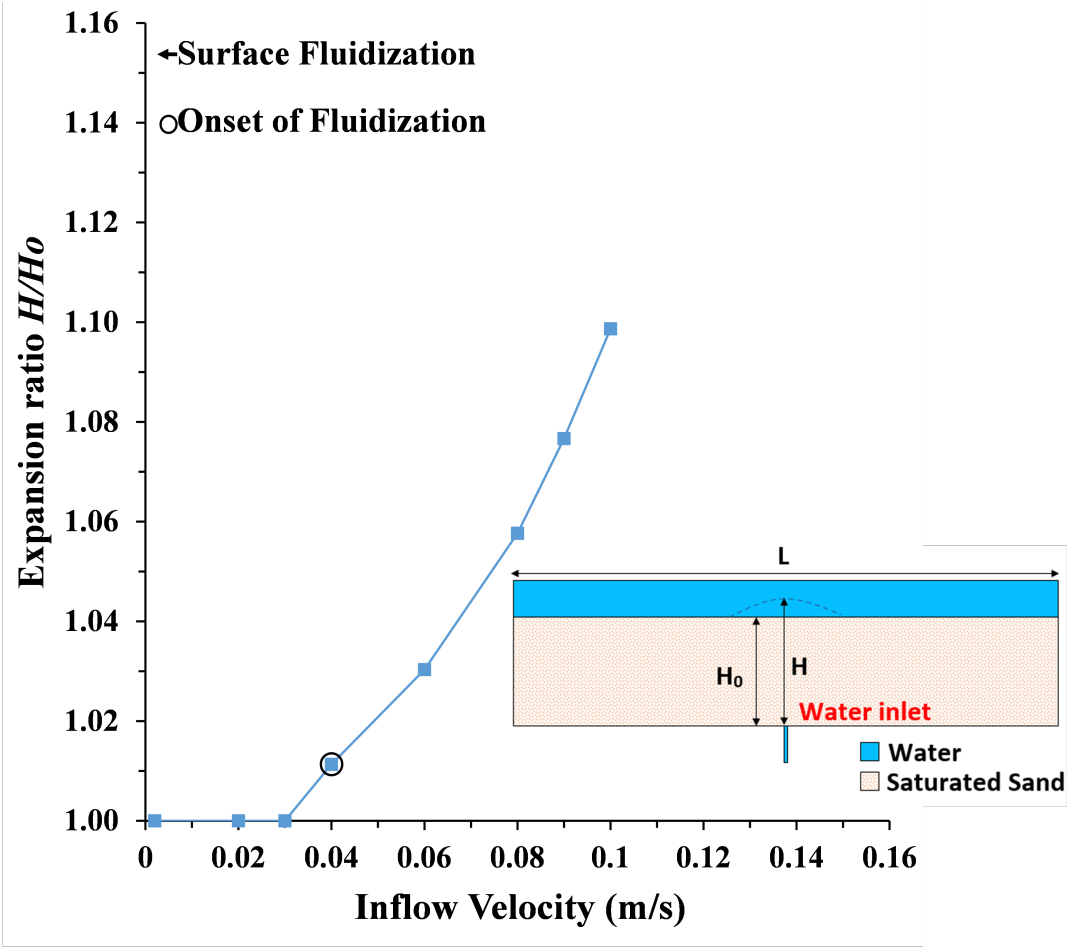



**Figure 5.4:** Change in soil bed expansion ratio with different prescribed inflow velocities at a 10 mm orifice

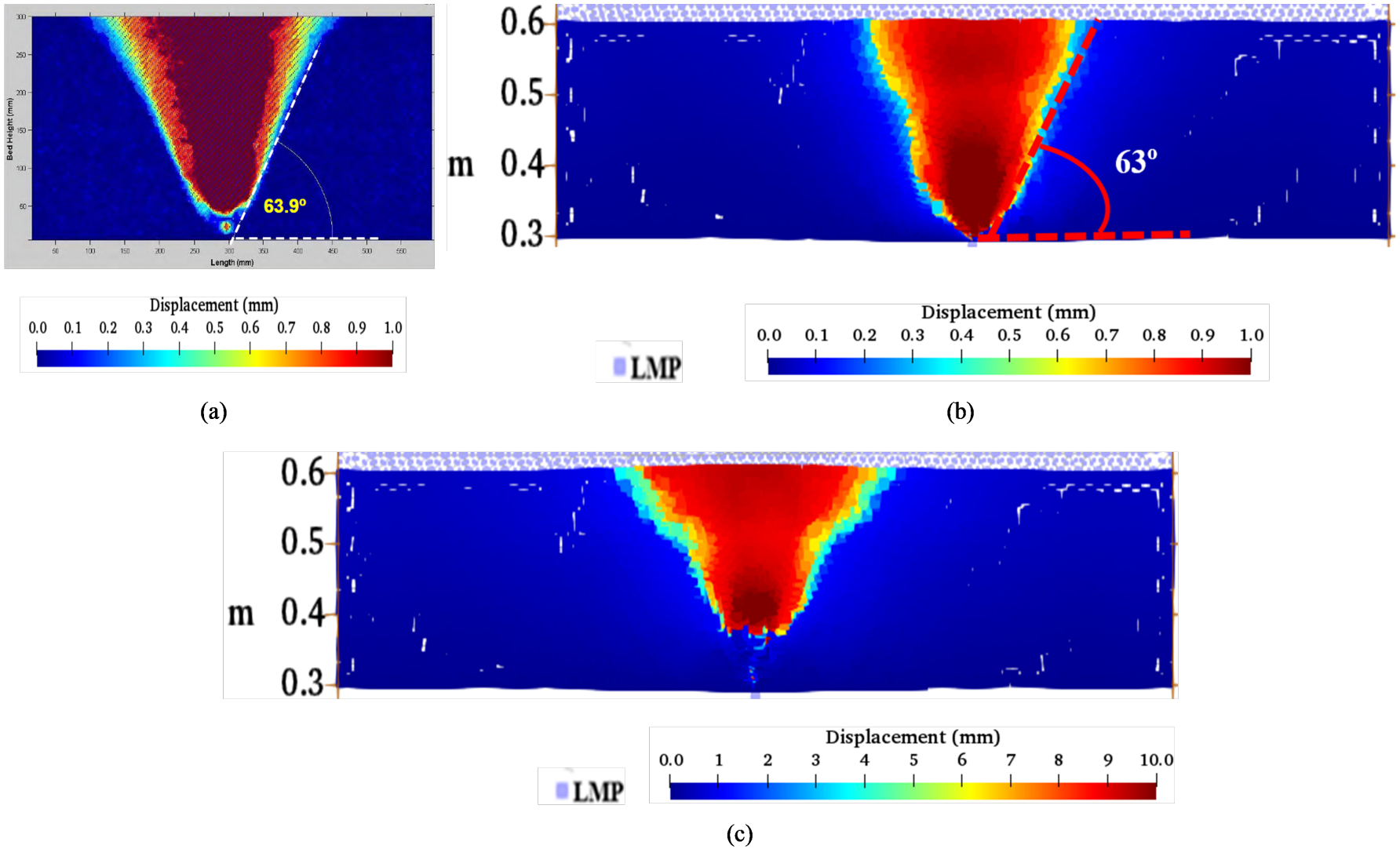



**Figure 5.5:** Soil vertical displacement at the onset of fluidisation for (a) Alsaydalani (2010)'s experimental result and (b) MPM result at an inflow velocity of 0.04 m/s. (c) MPM soil vertical displacement when fluidisation reaches the surface at an inflow velocity of 0.10 m/s

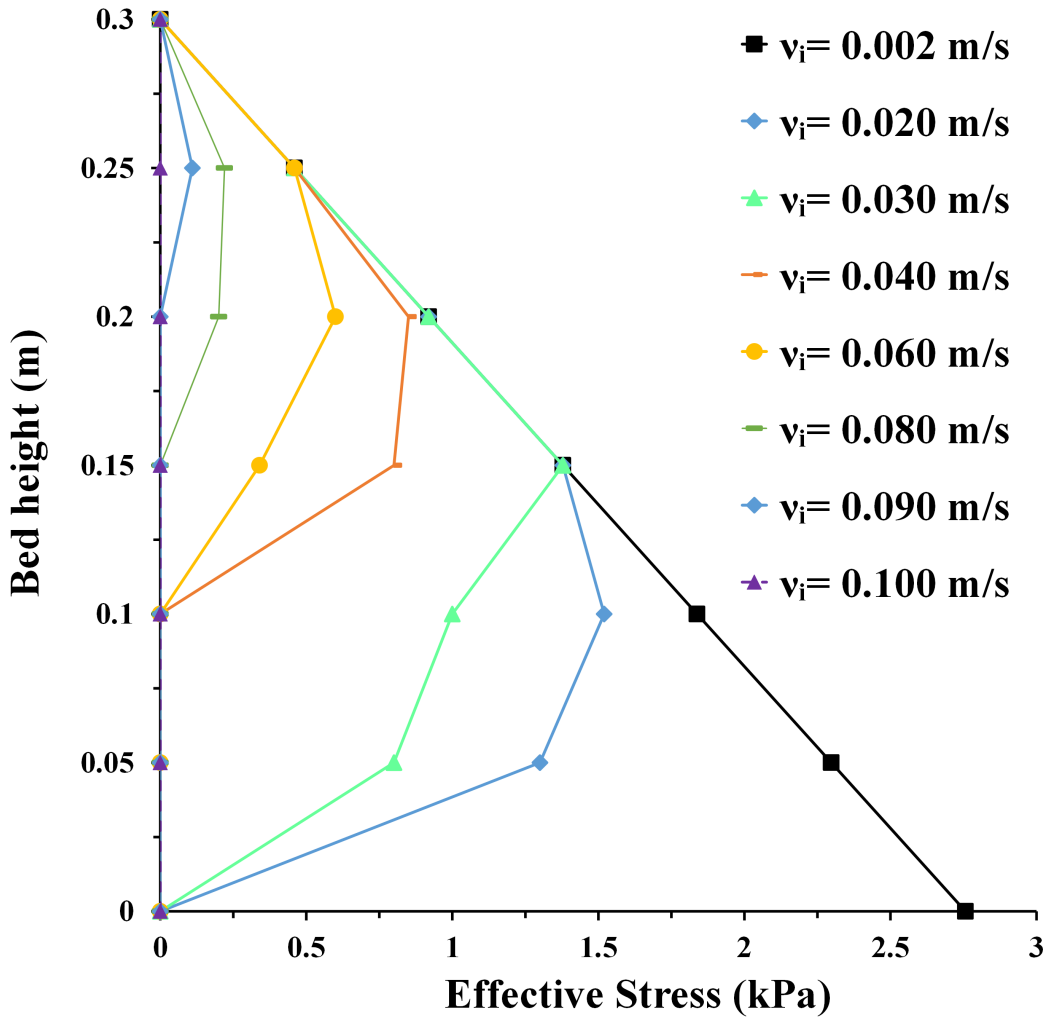



**Figure 5.6:** Effective stress at different inflow velocities ($v_i$) through the centreline of the soil bed

## 5.3.2 Parametric study

### 5.3.2.1 Effect of orifice size

Five simulations with different orifice sizes (5.0, 7.5, 10.0, 12.5, and 15.0 mm) are conducted to investigate the effect of orifice size on the soil fluidisation process induced by a pressurised leaking water pipe. The numerical results of the porosity at different inflow velocities through the centreline of the soil bed for different orifice sizes (o) are plotted in Figure 5.7. Consistent with the results presented in the previous section, the onset of soil fluidisation is determined

when the SMPs at 0.05 m above the orifice fluidises ($n \geq n_{max}$), while surface fluidisation is determined when all SMPs through the centreline of the soil bed are fluidised ($n \geq n_{max}$).

The inflow required for the onset ($v_{io}$) and surface fluidisation ($v_{is}$) in models with different orifice sizes are presented in Figure 5.8. The vertical lines represent the accuracy of the inflow velocity that is calculated based on ranges of values of soil porosity (Figure 5.8). It is observed that the inflow velocity triggering the onset of the soil fluidisation ($v_{io}$) decreases with an increase in the orifice size. As the orifice size increases from 5 mm to 15 mm, $v_{io}$ decreases from 0.08 m/s to 0.02 m/s. It is of interest to note that the inflow flow rate is a function of the orifice area multiplied by the inflow velocities. The critical flow rate to initiate soil fluidisation decreases considerably from 1440 l/h to 1080 l/h, corresponding to an orifice size of 5 mm and 15 mm, respectively. The inflow velocity inducing the surface fluidisation ($v_{is}$) decreases from 0.16 m/s to 0.08 m/s as the orifice size increases from 5 mm to 15 mm. Therefore, the larger the orifice size, the smaller the inflow velocities required to trigger the onset and surface fluidisation. These results are consistent with the analytical predictions developed by Tang et al. (2017) in their study of sand erosion caused by an upward water jet. If the orifice is large enough, the soil fluidisation progresses rapidly and reaches the surface at minimal leakage velocity. In contrast, smaller orifices provide less water flow to fluidise the soil bed.

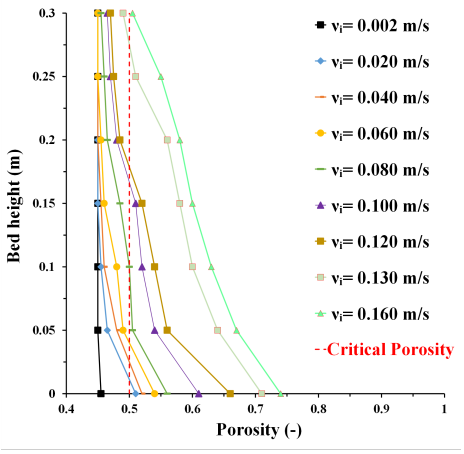
The range of orifice sizes considered in this study is at least 15 times larger than the experimental study used for reference (Alsaydalani, 2010), which used an orifice size (o) of 0.336 mm. This is selected to reduce the computational cost of the models as smaller orifice requires finer mesh to discretise the domain. From the numerical results, a second-order polynomial trendline for the inflow required for the onset of soil fluidisation ($v_{io}$) is plotted in Figure 5.8. This trendline is represented using the following Eq. 5.1.

$$v_{io} = 0.0003o^2 - 0.0129o + 0.136 \tag{5.1}$$

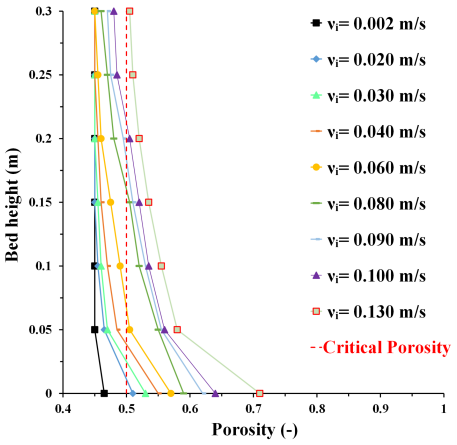
Where, $v_{io}$ is in m/s, and o is the orifice size in mm. Note that Eq. 5.1 is specific for the material properties and soil bed height considered in the MPM model, which are consistent with

Alsaydalani (2010), and it is not a generic expression. The experimental results from Alsaydalani (2010) indicate that $v_{io}$ = 0.12 m/s was required to initiate soil fluidisation through a 0.336 mm orifice. This value is derived after deducting the velocity loss measured through the orifice. Based on Eq. 5.1, the predicted inflow velocity causing the initiation of soil fluidisation ($v_{io}$) for an orifice size of 0.336 mm is 0.13 m/s (Figure 5.8), which is very similar to the experimental results reported by Alsaydalani (2010). This exercise further validates the consistency of the model with the available data.

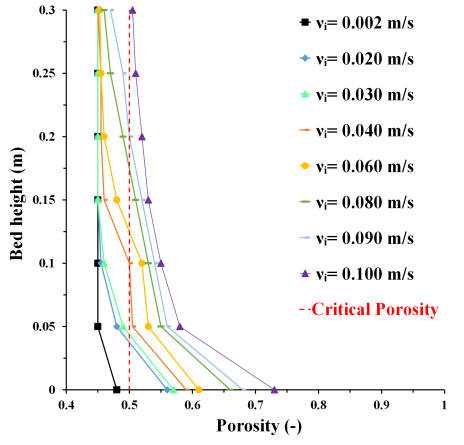
The change in expansion ratio $H/H_0$ with the inflow velocity for different orifice sizes is presented in Figure 5.9. The larger orifice size results in more heaving of the soil bed at the same inflow velocity. This is in agreement with the experiment conducted by Weisman and Lennon (1994) in the development of fluidiser systems. As the orifice size increased, the soil fluidisation occurred rapidly at minimal leakage velocity. An increase in the orifice opening leads to a lower expansion ratio at the onset of fluidisation. The final expansion ratio as the fluidisation reaches the ground level is not significantly affected by the orifice size. Therefore, the orifice size mainly affects the initiation of the soil fluidisation process.



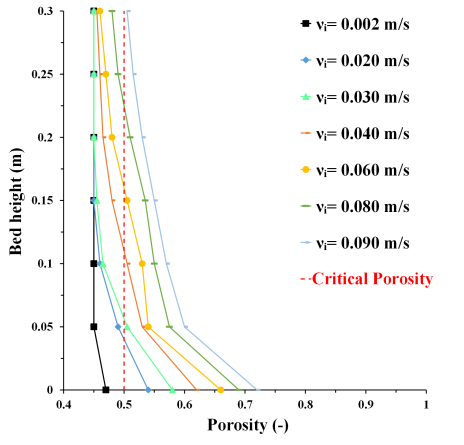

(a) o = 5.0 mm



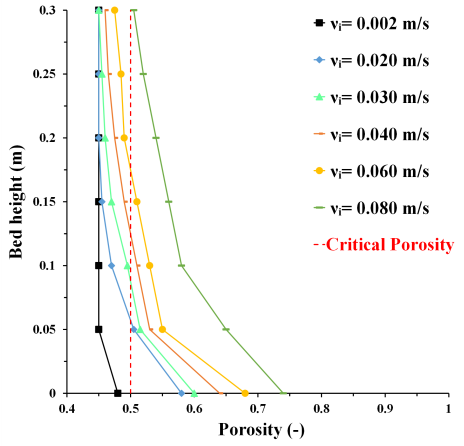

(b) o = 7.5 mm




(c) o = 10.0 mm




(d) o = 12.5 mm




(e) o = 15.0 mm

**Figure 5.7:** Porosity distribution at different inflow velocities ($v_i$) through the centreline of the soil bed with different orifice sizes (o)

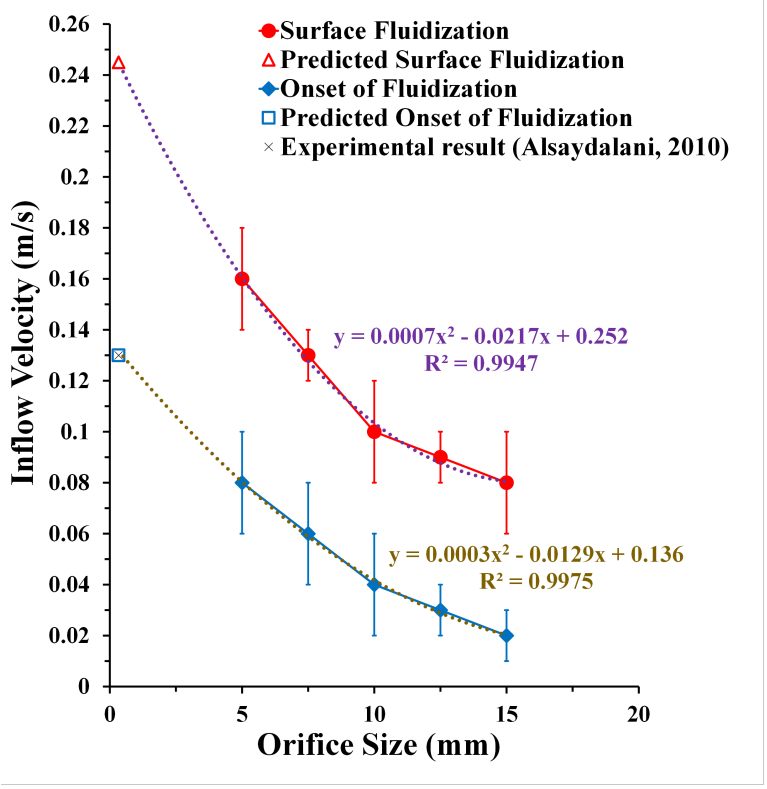



**Figure 5.8:** Inflow velocity through different orifice sizes at the onset of fluidisation and when the fluidisation reaches the surface of the soil bed. The vertical lines demonstrate the variability of the inflow velocity

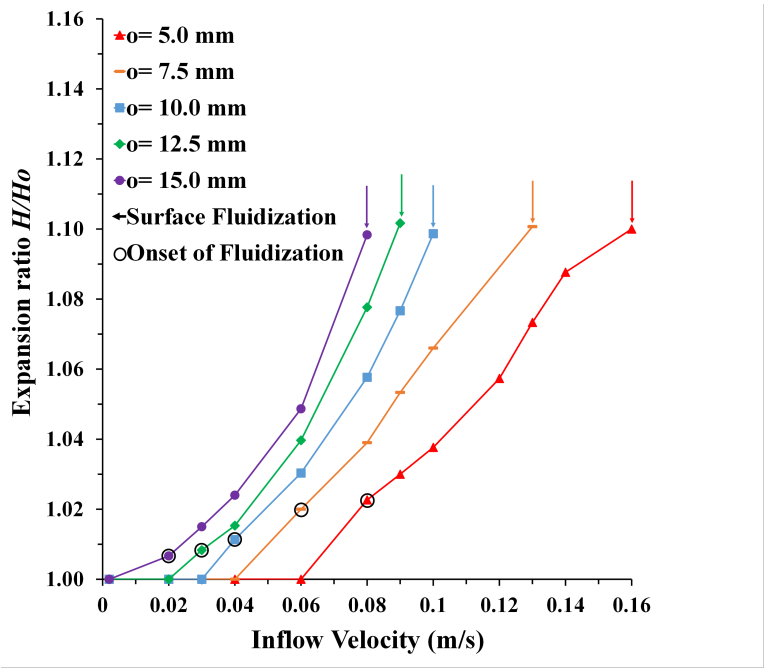



**Figure 5.9:** Change of soil bed expansion ratio at different inflow velocities through different orifice sizes (o)

#### 5.3.2.2 Effect of soil-bed height

Five numerical models with different soil-bed heights are simulated to explore the effect of bed height on the soil fluidisation mechanism. To eliminate the effect of boundary conditions on the fluidisation zone, the ratio length/height of the soil bed is kept constant for all simulations. Thus, four simulations with different bed heights of 300, 400, 500, 600, and 700 mm are conducted with a soil-bed length of 1500, 2000, 2500, 3000, and 3500 mm, respectively. Figure 5.10 presents the change in the inflow velocity needed for the onset ($v_{io}$) and surface ($v_{is}$) fluidisation at a 10 mm orifice with the change of the bed height. In this model, the inflow velocity leading to the initiation of the soil fluidisation ($v_{io}$) increases with an increase in the soil bed height. As the bed height increases from 300 mm to 700 mm, $v_{io}$ increases from 0.04 m/s to 0.10 m/s. Similarly, the water velocity at the orifice required to observe surface fluidisation ($v_{is}$) increases considerably from 0.10 m/s to 0.40 m/s, corresponding to a bed height of 300 mm and 700 mm, respectively. Thus, the velocity required to induce surface fluidisation significantly increases with the bed height.

The variation in the expansion ratio $H/H_0$ with the inflow velocity is plotted for different bed heights in Figure 5.11. The thicker the soil bed, the lower the expansion ratio $H/H_0$ at the same inflow velocity. As the height of the soil bed increases, higher leakage velocity is required to initiate soil fluidisation. The effect of the soil-bed height is not significant in terms of the expansion ratio at the onset of fluidisation. However, the thicker the soil-bed height results in a lower expansion ratio when the fluidisation reaches the surface. This agrees with the previous study conducted by Tang et al. (2017) that concluded a thicker soil bed is characterised by more resistance of the mobilised soil region. Therefore, a larger inflow velocity is required to fluidise the above soil bed.

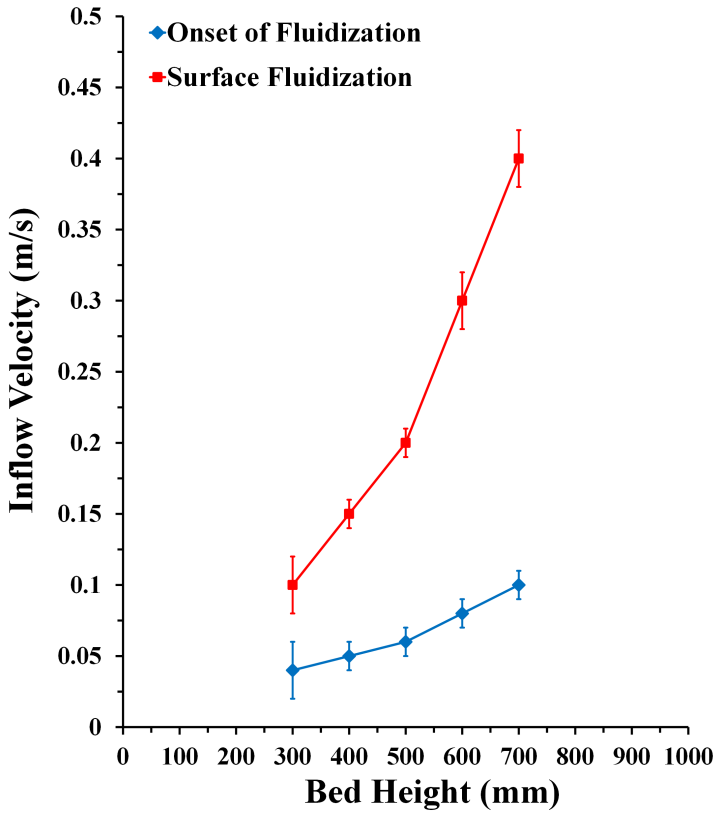



**Figure 5.10:** Inflow velocity through different soil bed height at the onset of fluidisation and when the fluidisation reaches the surface in soil bed

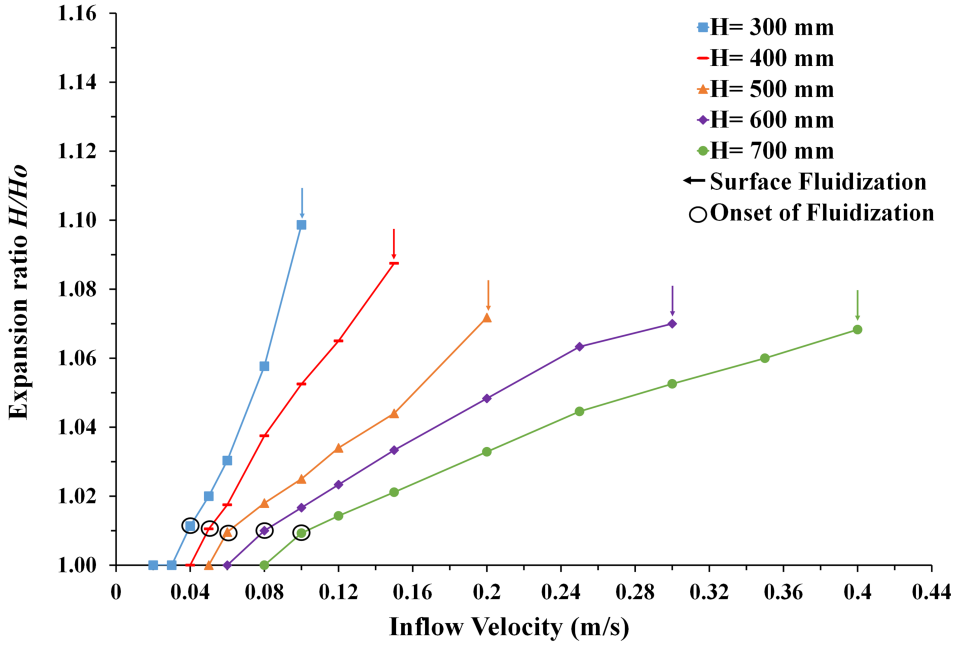



**Figure 5.11:** Change of soil bed expansion ratio at different inflow velocities through different soil-bed height (H)

#### 5.3.2.3 Effect of soil porosity

Four models with four different initial soil porosity (0.30, 0.35, 0.40, and 0.45) have been conducted to explore the effects of soil porosity on soil fluidisation induced by a leaking pipe. In this simulation, the intrinsic soil permeability (k) depends on the solid grain diameter ($D_p$) and the soil porosity (n) (Bear, 1988). Alsaydalani and Clayton (2014) stated that permeability, and therefore soil porosity, can be expected to have a large effect on the water flowing into the soil bed. Water seepage in the soil bed with higher porosity is easily dissipated, which can expedite soil bed fluidisation at the lower inflow velocity. For example, an inflow velocity ($v_{io}$) of 0.10 m/s at a 10 mm orifice in a soil bed with 0.30 initial porosity is sufficient to initiate the soil fluidisation (Figure 5.12a). For higher soil porosity (0.45), the soil fluidisation is initiated at a lower inflow velocity ($v_{io}$) of 0.04 m/s. Soil fluidisation initiates under a lower inflow velocity in a higher porosity soil bed. Similarly, the inflow velocity ($v_{is}$) required to develop fluidisation reaching the bed surface decreases with an increase in the soil porosity. The inflow velocity inducing the surface fluidisation ($v_{is}$) decreases from 0.16 m/s to 0.10 m/s as the soil porosity increases from 0.30 (Figure 5.12b) to 0.45 (Figure 5.12e). Thus, the inflow velocity required for the onset ($v_{io}$) and surface ($v_{is}$) fluidisation decreases linearly with the increase of the soil porosity. Hence, soil porosity is an essential parameter in soil fluidisation, and lowering the soil porosity can effectively improve the stability of the soil bed.

The effect of porosity on the surface heaving at the onset of fluidisation is also investigated. Figure 5.13a shows the change in soil-height expansion ratio as the inflow velocity increases in the soil bed with different initial soil porosity. The inflow velocity that induces soil fluidisation ($v_{io}$) is determined when the soil bed expansion ratio $H/H_0$ exceeds one. Water can easily flow through the soil when the soil porosity is large, and soil-bed fluidisation is initiated at a lower inflow velocity, as shown in Figure 5.13a. This higher water velocity results in an increase in the expansion ratio. On the other hand, flow is more difficult through the lower porosity soil because of the lower permeability. The higher the porosity of the soil bed, the lower the expansion ratio at the same leakage velocity. The expansion ratio is lower as the soil fluidisation reaches the surface in highly porous soil. Figure 5.13b and Figure 5.13c demonstrate the vertical soil displacement

as the fluidisation reaches the soil surface in the soil bed with an initial soil porosity of 0.30 and 0.35, respectively. The soil vertical displacements in lower porous soil are relatively high (maximum of 0.06 m) compared to the vertical displacements that occurred in highly porous soil (maximum of 0.05 m). Chen et al. (2011) stated that the driving force exerted by the water on the solid skeleton decreases as the soil porosity increases, and this decrease in driving force makes the soil bed more difficult to heave.

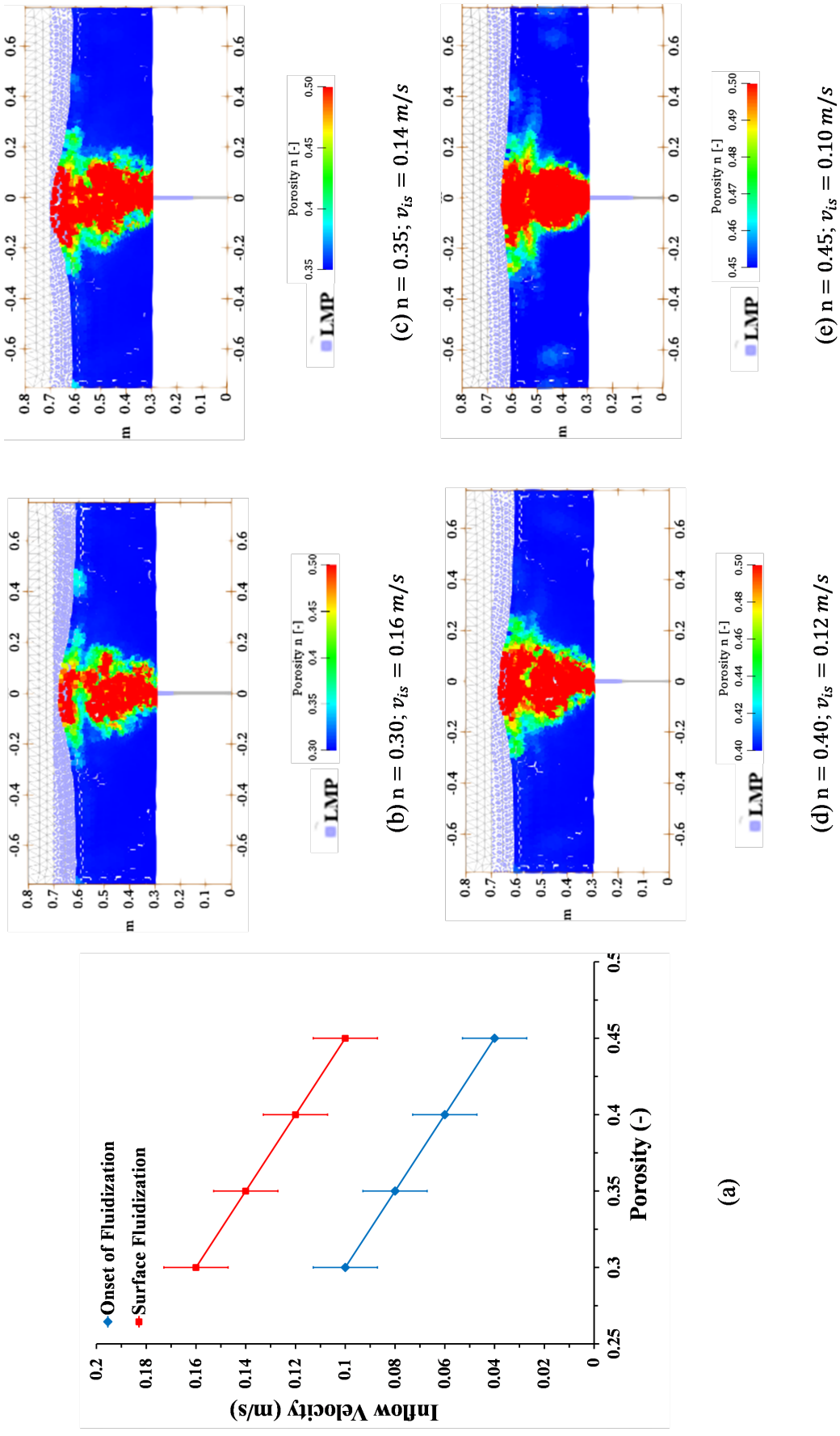
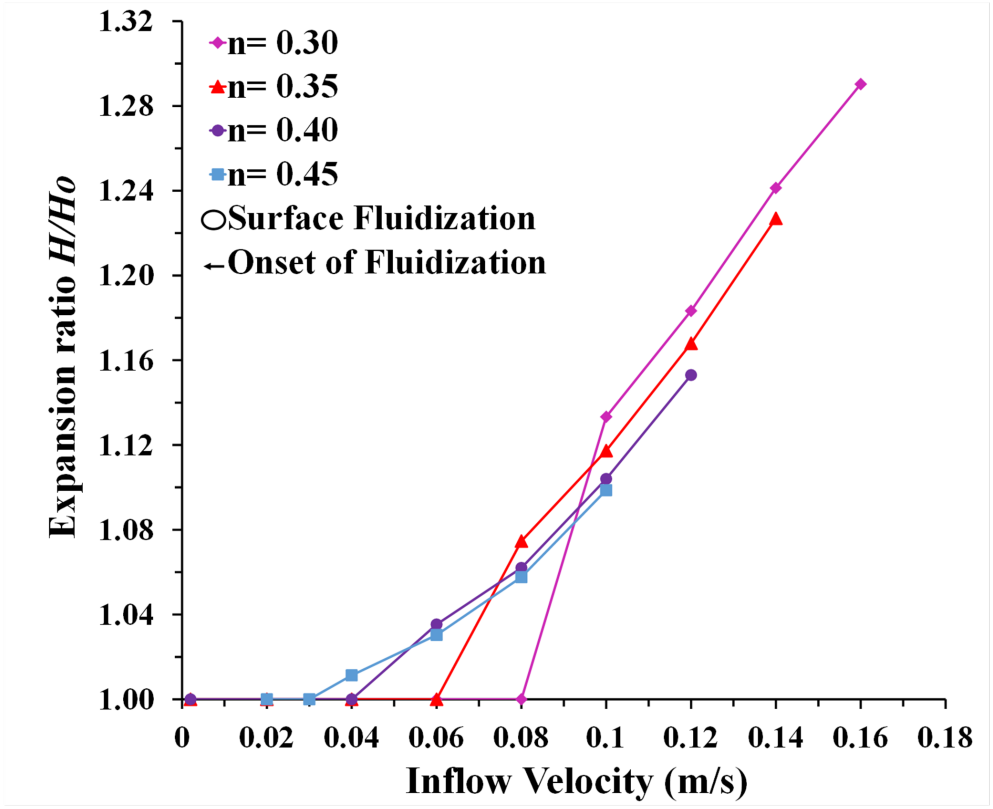
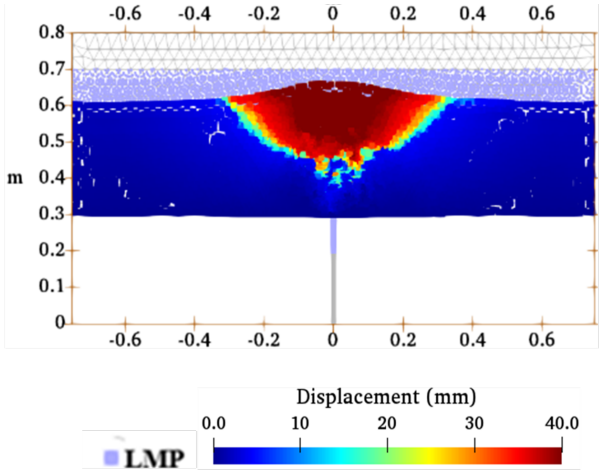


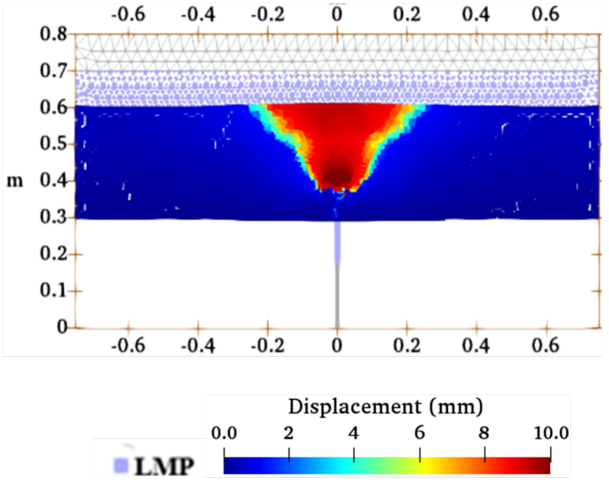

**Figure 5.12:** (a) Inflow velocity at the onset of fluidisation and when the fluidisation reaches the surface in soil bed with different initial soil porosity. (b, c, d and e) Soil porosity in soil bed with different initial porosity




(a)




(b) n = 0.30; $v_{is} = 0.16\ m/s$




(c) n = 0.45; $v_{is} = 0.10\ m/s$

**Figure 5.13:** (a) Change in soil bed expansion ratio at different inflow velocities in soil bed with different initial soil porosity (n). Soil vertical displacement at an initial porosity of (b) 0.30 and (c) 0.45

#### 5.3.2.4 Effect of soil cohesion

The cohesion of soil is a measure of the internal resistance to erosion that is a complementary parameter of the soil friction forces (Nouwakpo, 2010). To study the effect of soil cohesion on soil fluidisation induced by a leaking pipe, seven simulations with varying soil cohesion values ranging from 1 kPa to 50 kPa have been modelled. It is worth noting that a cohesion value of 50 kPa can be realistic for certain cohesive soils, considering factors such as mineral composition, compaction, and clay content. Figure 5.14a shows the inflow velocity for initiation ($v_{io}$) and surface ($v_{is}$) fluidisation at a 10 mm orifice for different cohesion values. As expected, higher inflow velocity is required for the onset ($v_{io}$) and full development ($v_{is}$) of fluidisation in more cohesive soil. As the soil cohesion increases from 1kPa to 50 kPa, $v_{io}$ increases from 0.04 m/s to 0.12 m/s. The results in Figure 5.14b and Figure 5.14c show the full development of soil fluidisation represented by those SMPs with the maximum porosity. For a soil bed with the lowest cohesion value (1 kPa), a wider fluidisation region at minimal inflow speed is observed (Figure 5.14b). For the soil with larger cohesion (50 kPa), the propagation of the fluidised zone is slower and is observed at higher leakage velocity (Figure 5.14c). This shows the significant effect of soil cohesion on the evolution of soil fluidisation that can provide internal resistance to material fluidisation (Rogers et al., 2008; Brunier-Coulin et al., 2016).

The change in the expansion ratio versus the inflow velocity in a soil bed with different cohesion values is plotted in Figure 5.15. The higher the material cohesion, the lower the bed expansion at the same leakage velocity. The cohesion between soil particles stabilises the soil layer above the fluidised region by increasing the resistance of the soil bed (Philippe and Badiane, 2013). The effect of the cohesion parameter on the expansion ratio at the onset of fluidisation is not significant. However, the final expansion ratio at surface fluidisation increases by 2% when the effective cohesion increases from 1 kPa to 5 kPa. Beyond these values, the final expansion ratio is independent of the cohesion value.

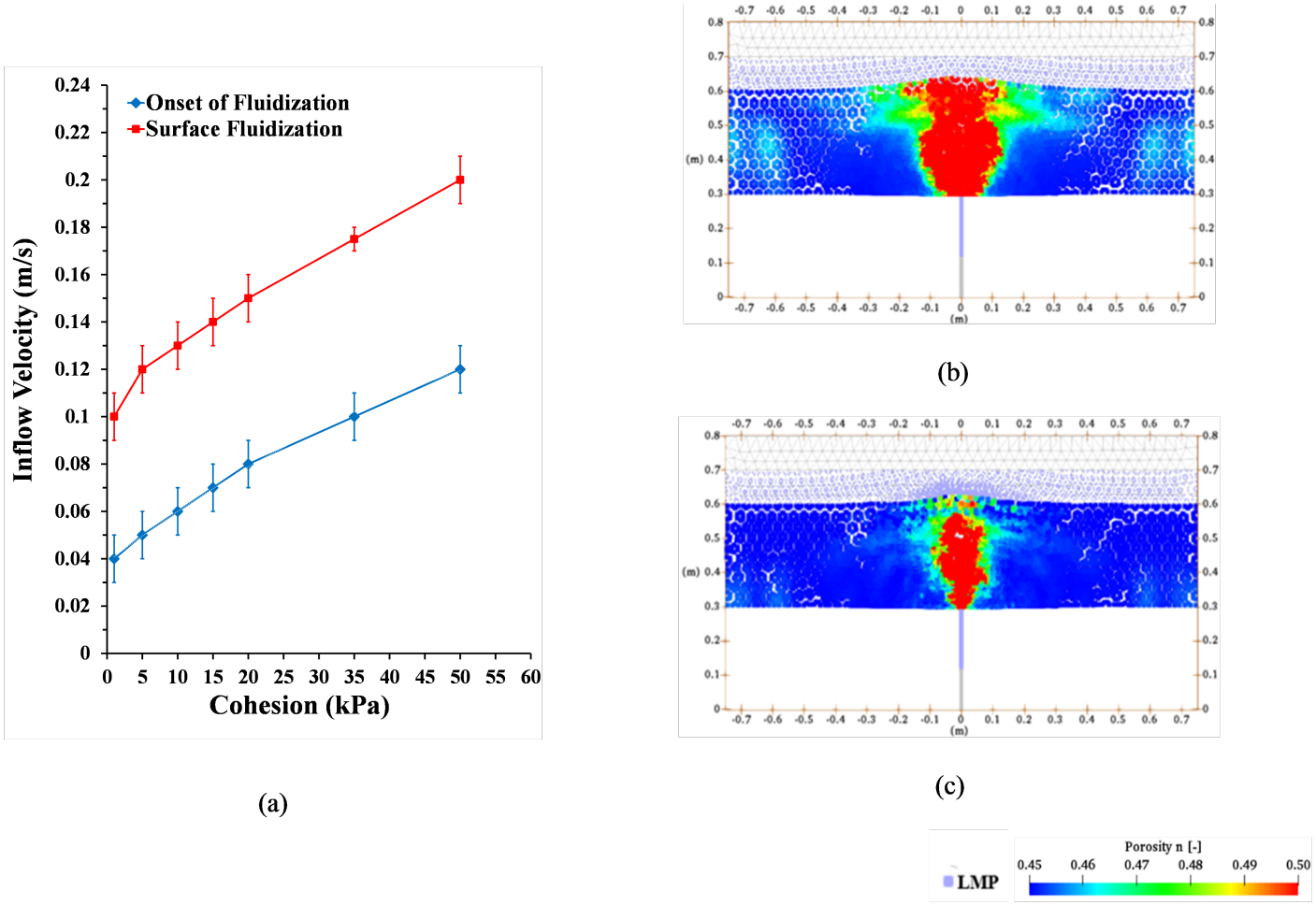



**Figure 5.14:** (a) Inflow velocity at the onset and surface fluidisation in soil with different effective cohesion. Soil porosity at an inflow velocity of (b) 0.10 m/s and (c) 0.20 m/s in soil with the cohesion of 1 kPa and 50 kPa, respectively. The LMPs are represented with blue dots

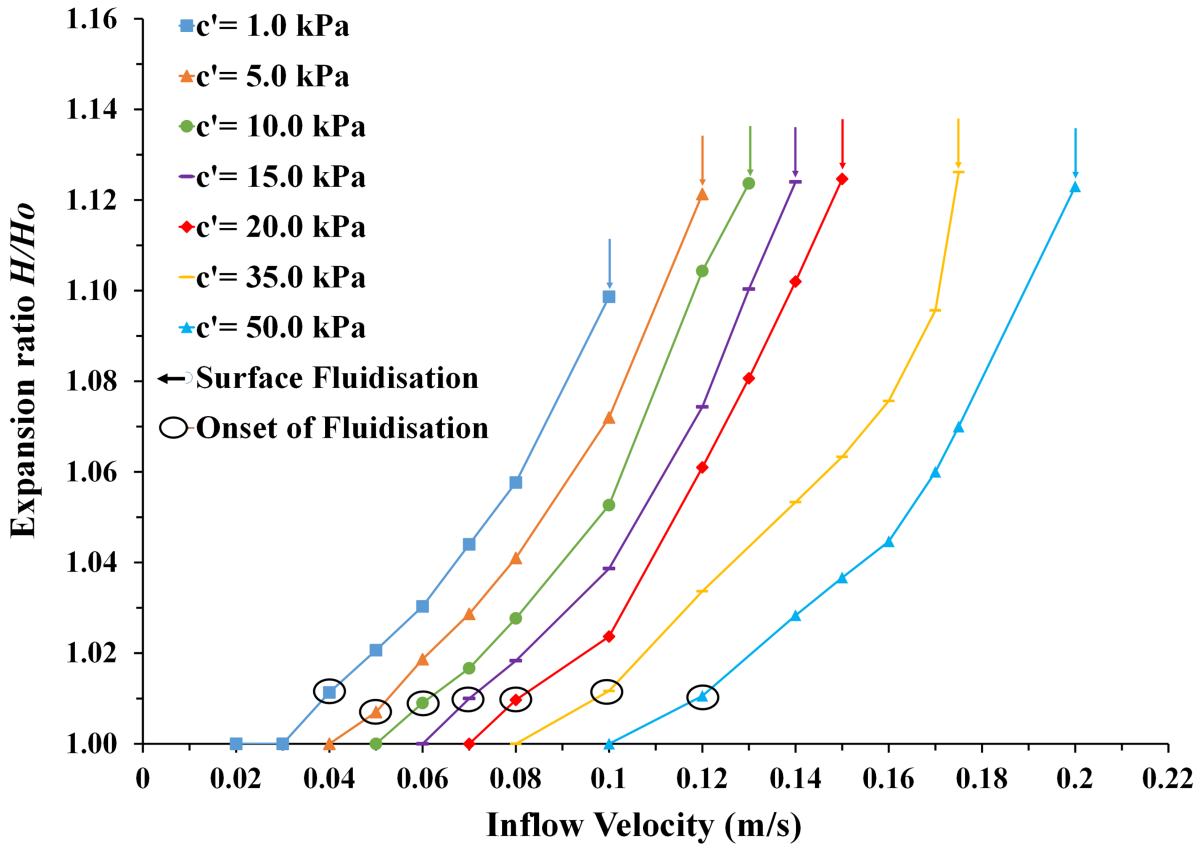



**Figure 5.15:** Change of soil bed expansion ratio at different inflow velocities in soil bed with different effective cohesion (c')

#### 5.3.2.5 Effect of leakage direction

Two numerical simulations have been conducted using the 2P-DP MPM approach coupled with the use of inflow/outflow boundary conditions, to investigate the effect of leakage direction on the fluidised regime and soil behaviour. A pipeline with a diameter of 50 mm is embedded at a burial depth ($H_p$) of 150 mm below the ground surface in a saturated soil bed. Two cases are studied considering the locations of the orifice located at the crown (upward leakage) and springline (lateral leakage) of the pipe with the (o) fixed at 10 mm. The MPM models of both cases are presented in Figure 5.16, where the pipe is replaced by an equivalent square with a 50 mm long side. The model designed to study the impact of the upward leakage where the orifice is located at the crown of the pipe is presented in Figure 5.16a. A similar problem is modelled to interpret the effect of the lateral leakage, demonstrated in Figure 5.16b. The inflow/outflow boundary conditions (BCs) were tested to model a lateral leakage as shown in Appendix E. The porosity

field at the onset and surface fluidisation for the two scenarios at different inflow velocities ($v_i$) is compared in Figure 5.17. An inflow velocity ($v_{io}$) of 0.25 m/s at a 10 mm orifice in a soil bed subjected to an upward leakage is required to initiate the soil fluidisation (Figure 5.17a). For lateral leakage, the soil fluidisation is initiated at a higher inflow velocity ($v_{io}$) of 0.04 m/s (Figure 5.17c). Soil fluidisation initiates under a lower inflow velocity in a soil bed subjected to an upward leakage. Similarly, the inflow velocity ($v_{is}$) required to develop fluidisation reaching the bed surface increases with the lateral leakage. The inflow velocity inducing the surface fluidisation ($v_{is}$) increases from 0.05 m/s to 0.09 m/s as the leakage direction changes from upward (Figure 5.17b) to lateral leakage (Figure 5.17d). Thus, the inflow velocity required for the onset ($v_{io}$) and surface ($v_{is}$) fluidisation increases linearly with the change of leakage direction from crown to springline. In addition, the area of the fluidised zone increases as the leakage direction changes from upward to lateral flow. Hence, orifice location is an essential factor in soil fluidisation, and determining the leakage location can effectively improve the interpretation of the fluidisation mechanism.

Alsaydalani (2020) experimentally investigated the impact of lateral water flow from an impermeable vertical surface on the failure mechanism of a granular bed using the Particle Image Velocimetry (PIV) technique. The sequences of failure were observed in horizontal leakage under an increasing flow rate, as presented in 5.18, are as follows: (i) outward movement (horizontally and vertically upwards) of soil particles away from the orifice, (ii) cavity formation in the vicinity of the orifice, (iii) cavity enlargement, and (iv) surface fluidisation. Consistent behaviour is observed in the MPM simulation presented in Figure 5.17c and Figure 5.17d. As the inflow rate increases, the fluidised zone expands horizontally and vertically upwards through the soil bed. This expansion primarily occurs horizontally in the leakage direction. However, as the fluidised zone develops away from the orifice it gradually propagates upwards to reach the soil surface.

The influence of leakage direction on the soil bed expansion at the onset of fluidisation is also investigated. Figure 5.19 plots the change in bed-height expansion ratio as the inflow velocity increases with different leakage directions. Water can easily flow upwards through the soil subjected to an upward leakage, and soil-bed fluidisation is initiated at a lower inflow velocity,

as shown in Figure 5.19. This higher water velocity results in an increase in the expansion ratio. However, upward flow is more difficult through soil subjected to lateral water leakage. In an upward leakage, the expansion ratio is higher at the same leakage velocity. The final surface heave as the fluidisation reaches the ground level in lateral leakage is higher than the surface heave that occurs in upward leakage. It is inferred from this section that the change in the orifice location from the crown (upward leakage) to the springline (lateral leakage) of the pipe plays a significant role in the development of the soil fluidisation triggered by a leaking pipe.

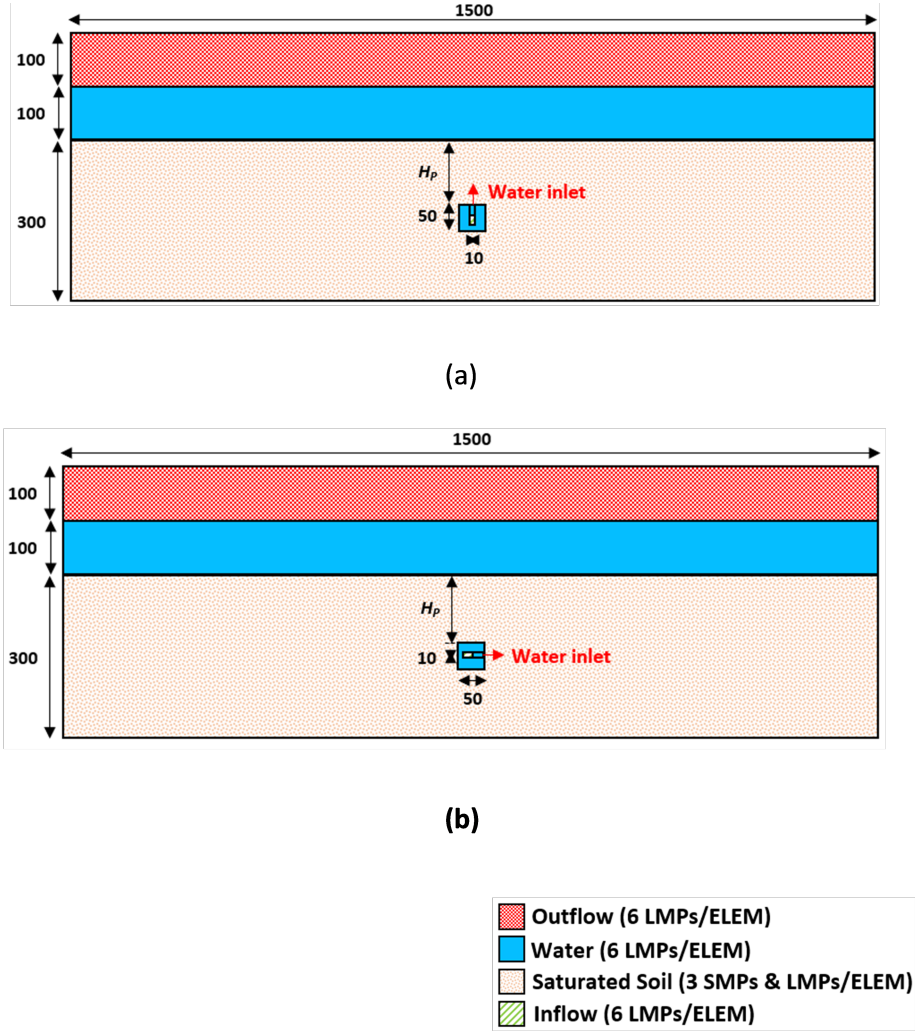



**Figure 5.16:** Geometry of the MPM model of soil bed subjected to (a) upward leakage and (b) lateral leakage where Hp is the pipe burial depth (unit: millimetres)

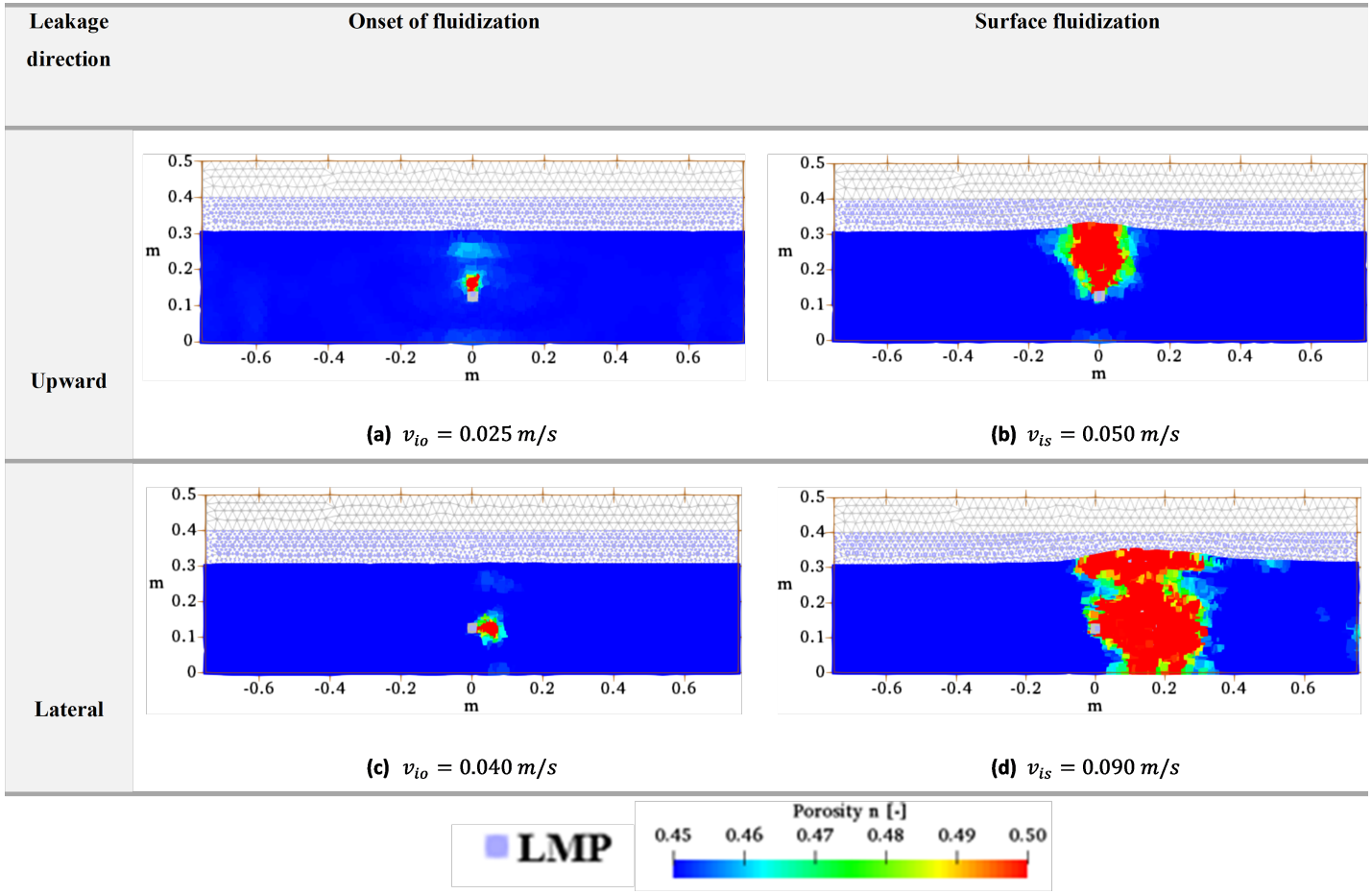



**Figure 5.17:** Soil porosity at the onset and surface fluidisation in soil bed subjected to upward (a, b) and lateral (c, d) leakage at the different inflow velocities

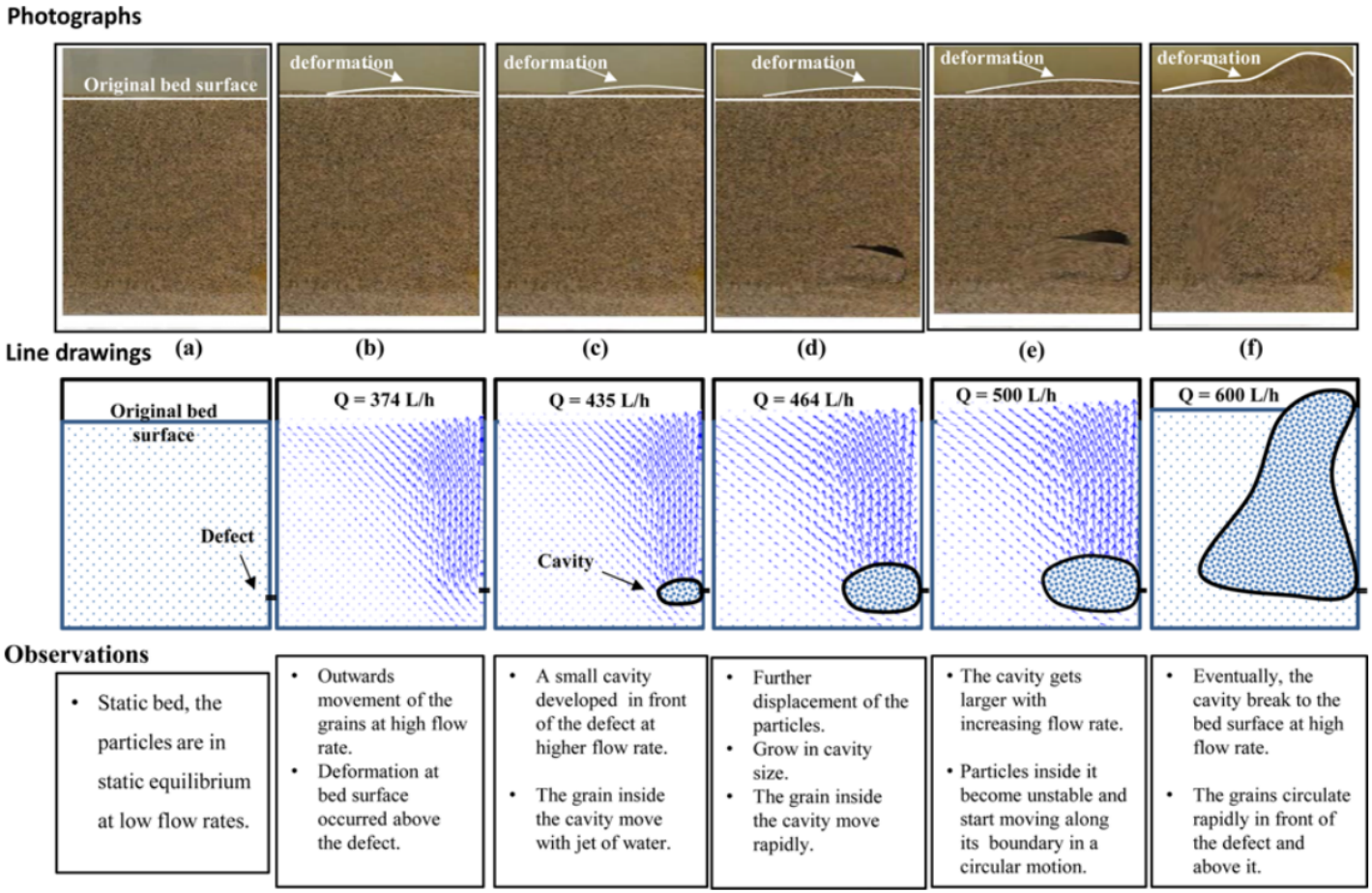



**Figure 5.18:** Different phases of the failure mechanisms of granular beds caused by lateral leakage: (a) static bed, (b) outwards movement of the grains, (c) creation of cavity, (d) and (e) enlargement of cavity, (f) cavity breaking the surface of the bed with a height of 200 mm and a defect opening of 0.23 mm (Alsaydalani, 2020)

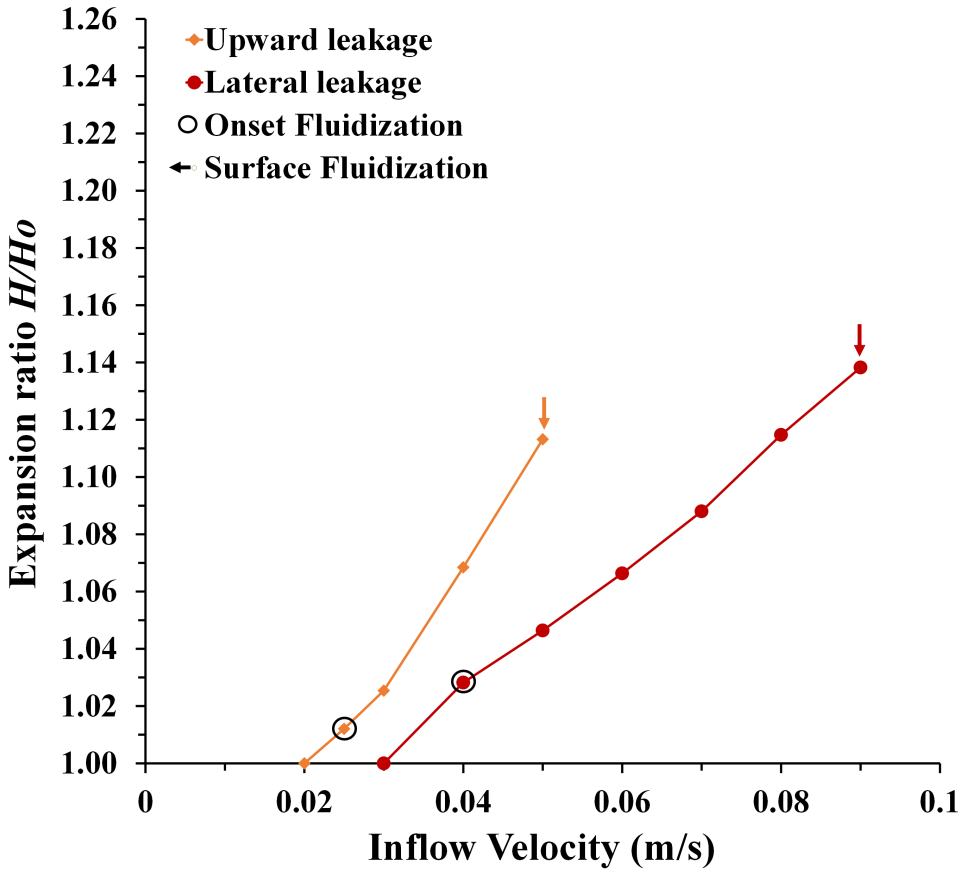



**Figure 5.19:** Change of soil bed expansion ratio is soil bed subjected to different flow directions

#### 5.3.2.6 Effect of pipe depth

The effect of pipe depth on the fluidisation of the soil bed is studied by varying the pipe burial depth ($H_p$) for different leakage directions; upward and horizontal flow through a 10 mm orifice.

##### 5.3.2.6.1 Upward leakage

Four simulations with different embedded depths of pipe of 50, 100, 200 and 300 mm are modelled with an orifice located at the crown (upward leakage) of the pipe. The change in the inflow velocity required for the onset ($v_{io}$) and surface ($v_{is}$) fluidisation at a 10 mm orifice with the change of the pipe depth is shown in Figure 5.20 and Figure 5.21. The 300 mm burial depth resulted in a greater fluidised zone than the shallower burial depths, as shown in Figure 5.20. This agrees with the experimental study conducted by Pike et al. (2018) that observed the intensity of the soil movement is increased in a pipe with greater cover depth. As the pipe

depth increases from 50 mm to 300 mm, the inflow velocity inducing the soil fluidisation ($v_{io}$) increases linearly from 0.01 m/s to 0.04 m/s. Similarly, the inflow velocity required to expand the fluidisation zone reaching the soil surface ($v_{is}$) increases considerably from 0.02 m/s to 0.10 m/s, corresponding to a pipe depth of 50 and 300 mm, respectively. Therefore, the shallower the pipe depth, the lower the water velocity required to induce fluidisation, and the smaller the influence on the surrounding soil in the fluidisation developing stage. However, the deeper the pipe burial depth, the higher the inflow velocity needed to initiate fluidisation, and the greater the fluidised zone.

The variation in surface heave versus the inflow velocity in a soil bed subjected to an upward leakage with different pipe depths is illustrated in Figure 5.22. The greater the pipe depth, the lower the bed expansion at the same water velocity. As the pipe depth increases, higher leakage velocity is required to induce soil fluidisation. The expansion ratio at the onset of fluidisation is not significantly affected by the depth of the pipe. However, as the burial depth increases from 50 mm to 100 mm, the final expansion ratio at surface fluidisation increases by 6%. Beyond these values, the final surface heave is not significantly affected by the pipe depth.

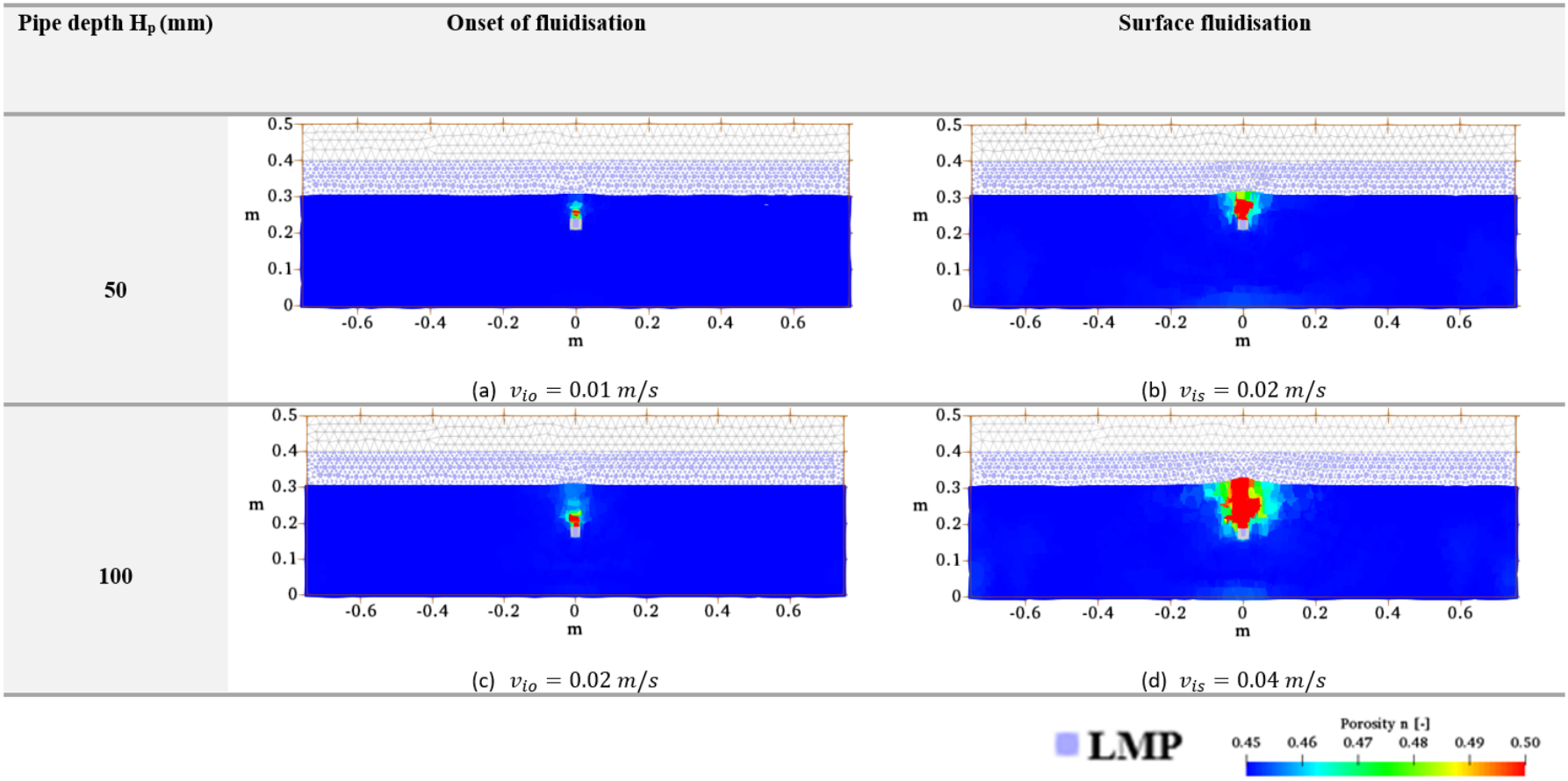



**Figure 5.19:** Soil porosity at the SMPs in the soil bed subjected to an upward leakage from a pipe with different burial depths

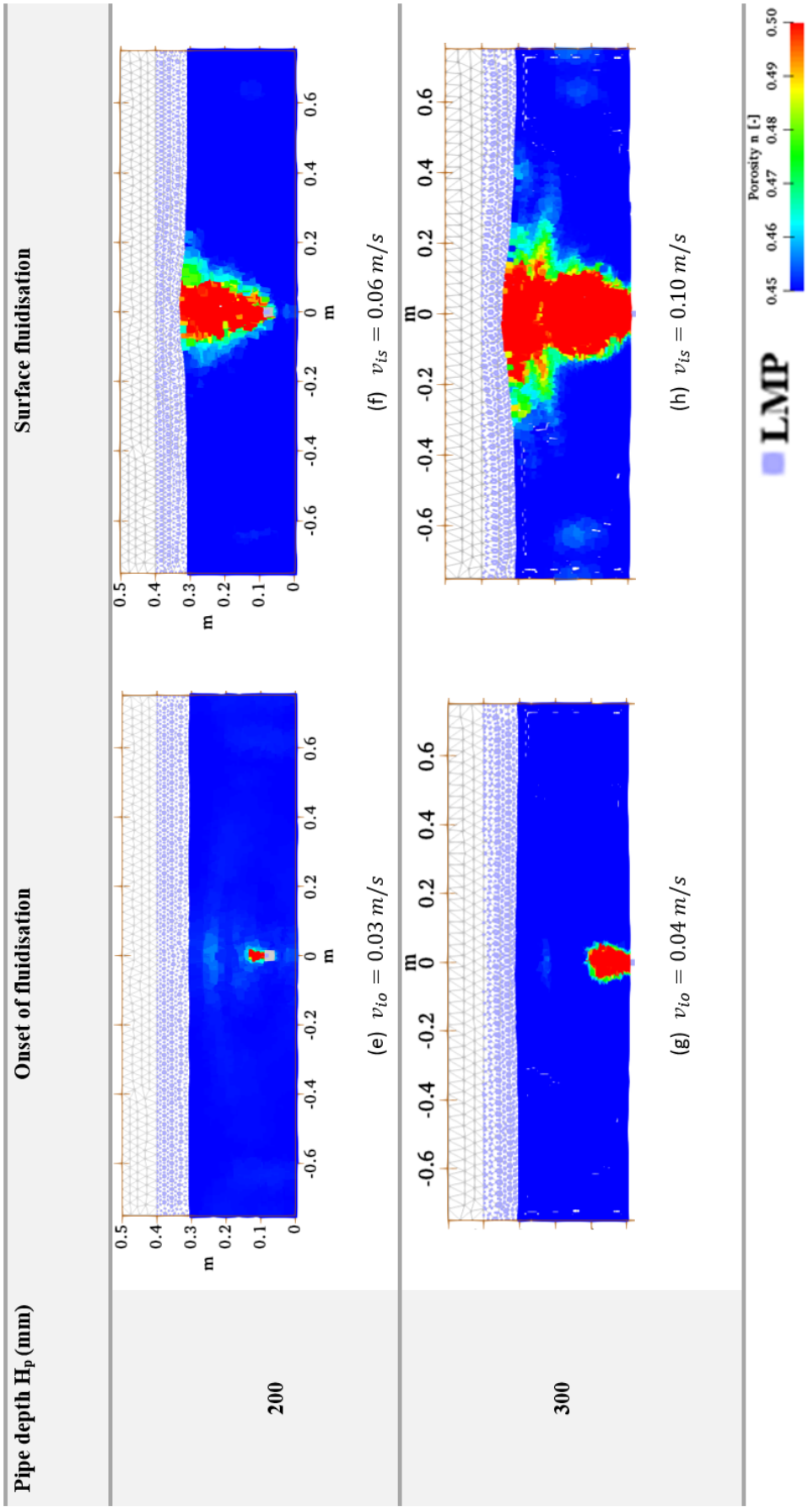



**Figure 5.20:** Soil porosity at the SMPs in the soil bed subjected to an upward leakage from a pipe with different burial depths

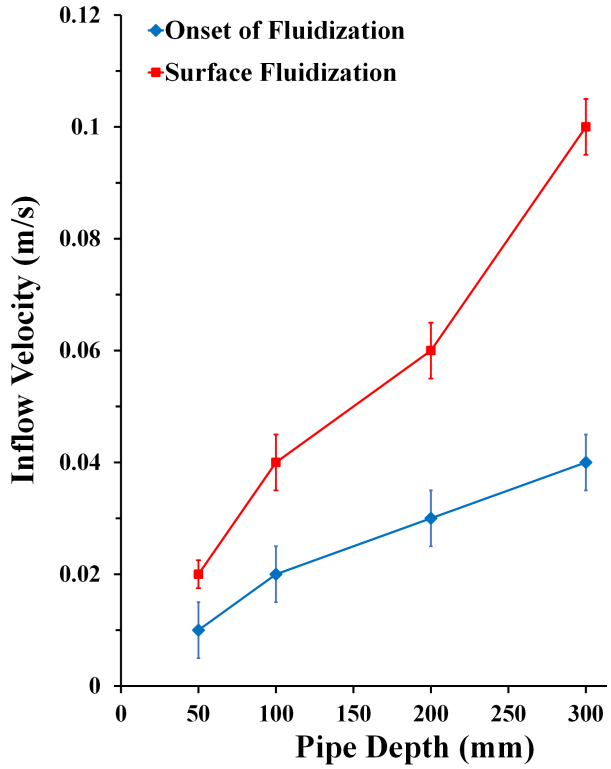



**Figure 5.21:** Upward inflow velocity through a pipe located at different burial depths at the onset of fluidisation and when the fluidisation reaches the bed surface

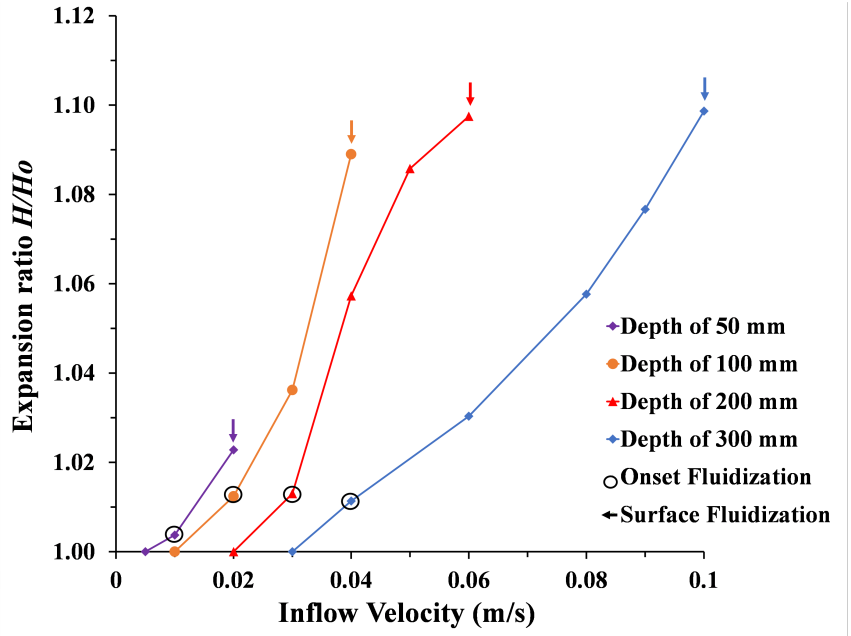



**Figure 5.22:** Change of soil bed expansion ratio through a pipe located at different depths

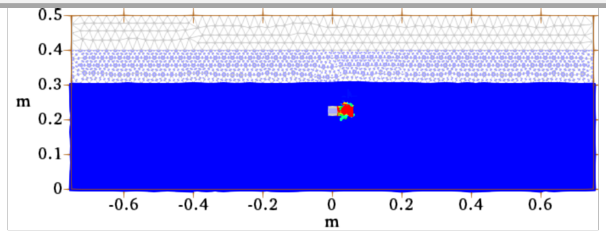
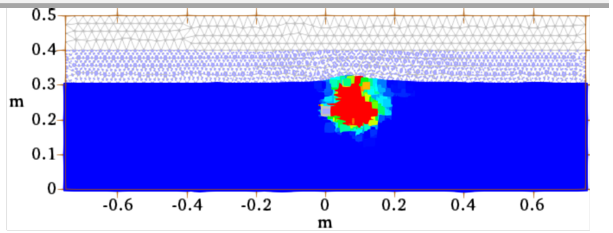
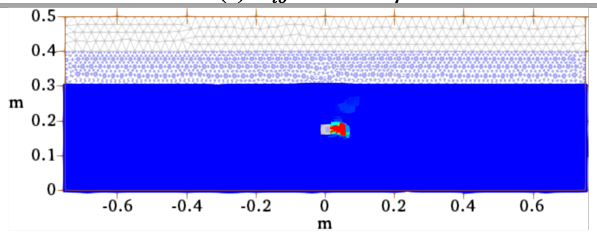
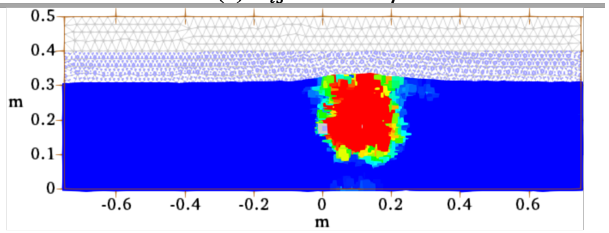
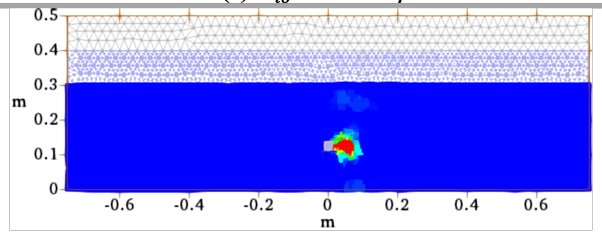
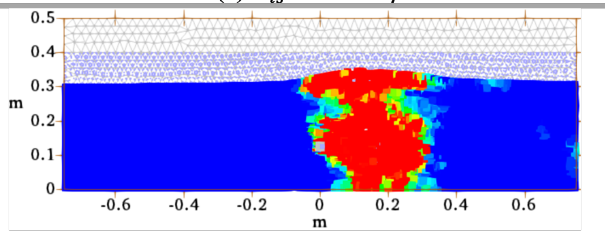
#### 5.3.2.6.2 Lateral leakage

Four simulations with different embedded depths of pipe of 50, 100, 200 and 300 mm are modelled with an orifice located at the crown (upward leakage) of the pipe. The change in the inflow velocity required for the onset ($v_{io}$) and surface ($v_{is}$) fluidisation at a 10 mm orifice with the change of the pipe depth is shown in Figure 5.23 and Figure 5.24. The 300 mm burial depth resulted in a greater fluidised zone than the shallower burial depths as shown in Figure 5.23. This agrees with the experimental study conducted by Pike et al. (2018) that observed the intensity of the soil movement is increased in a pipe with greater cover depth. As the pipe depth increases from 50 mm to 300 mm, the inflow velocity inducing the soil fluidisation ($v_{io}$) increases linearly from 0.01 m/s to 0.04 m/s. Similarly, the inflow velocity required to expand the fluidisation zone reaching the soil surface ($v_{is}$) increases considerably from 0.02 m/s to 0.10 m/s, corresponding to a pipe depth of 50 and 300 mm, respectively. Therefore, the shallower the pipe depth, the lower the water velocity required to induce fluidisation, and the smaller the influence on the surrounding soil in the fluidisation developing stage. However, the deeper the pipe burial depth, the higher the inflow velocity needed to initiate fluidisation, and the greater the fluidised zone. The variation in surface heave versus the inflow velocity in a soil bed subjected to an upward leakage with different pipe depths is illustrated in Figure 5.25. The greater the pipe depth, the lower the bed expansion at the same water velocity. As the pipe depth increases, higher leakage velocity is required to induce soil fluidisation. The expansion ratio at the onset of fluidisation is not significantly affected by the depth of the pipe. However, as the burial depth increases from 50 mm to 100 mm, the final expansion ratio at surface fluidisation increases by 6%. Beyond these values, the final surface heave is not significantly affected by the pipe depth.

The effect of burial depth on the soil fluidisation triggered by lateral leakage from an orifice located at the springline of the pipe is shown in Figure 5.23 and Figure 5.24 for different pipe depths: 50, 100 and 150 mm. The depth of the modelled pipe is limited to 150 mm to avoid the effect of the lower boundary condition during the development of fluidisation. It can be observed that the deeper the pipe, the higher the leakage velocity required to initiate fluidisation. In the presented simulations, an inflow velocity ($v_{io}$) of 0.02 m/s is required to induce the soil

fluidisation in a pipe buried 50 mm below the ground level (Figure 5.23a). This value increases linearly to 0.04 m/s with the increase of pipe depth from 50 mm to 150 mm (Figure 5.23e). The deeper the buried depth of the pipe, the slower the development of the fluidised zone that occurred at higher water velocity. However, the greater the pipe depth, the greater the fluidised zone induced by lateral leakage.

The influence of the pipe depth on the expansion ratio versus the inflow velocity is plotted in Figure 5.25. Soil-bed fluidisation is initiated at a lower water velocity through the soil bed subjected to lateral leakage from a pipe located at a shallower depth. The deeper the pipe depth, the lower the surface heave at the same leakage velocity. As the soil fluidisation is fully developed, the expansion ratio is higher in the soil bed with greater pipe depth. For example, the expansion ratio increases by 8% as the pipe depth increases from 50 mm to 150 mm. Thus, the greater the depth of the pipe, the greater the effect on the soil bed. This shows the significant impacts of the leakage location and pipe depth on the fluidisation process.

| Pipe depth $H_p$ (mm) | Onset of fluidization | Surface fluidization |
|---|---|---|
| 50 |  |  |
| | (a) $v_{io} = 0.02\ m/s$ | (b) $v_{is} = 0.04\ m/s$ |
| 100 |  |  |
| | (c) $v_{io} = 0.03\ m/s$ | (d) $v_{is} = 0.07\ m/s$ |
| 150 |  |  |
| | (e) $v_{io} = 0.04\ m/s$ | (f) $v_{is} = 0.09\ m/s$ |

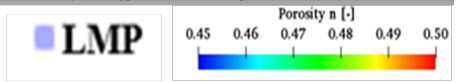



**Figure 5.23:** Soil porosity at the SMPs in soil bed subjected to a lateral leakage from a pipe with different burial depths

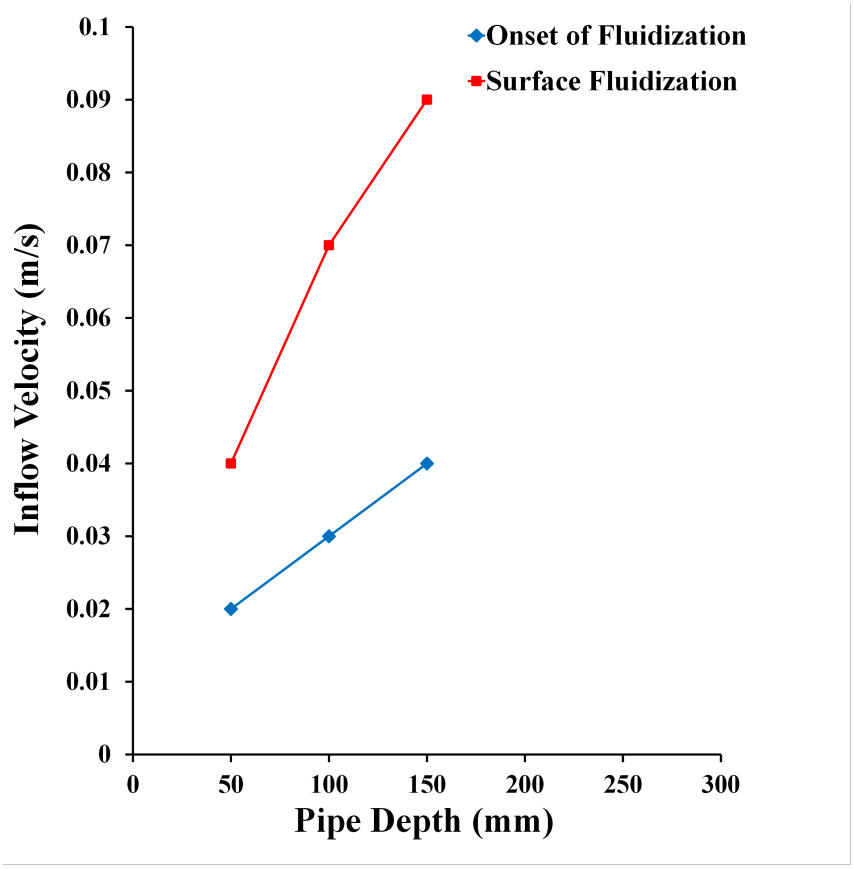



**Figure 5.24:** Lateral inflow velocity through a pipe located at different depths at the onset of fluidisation and when the fluidisation reaches the surface of the soil bed

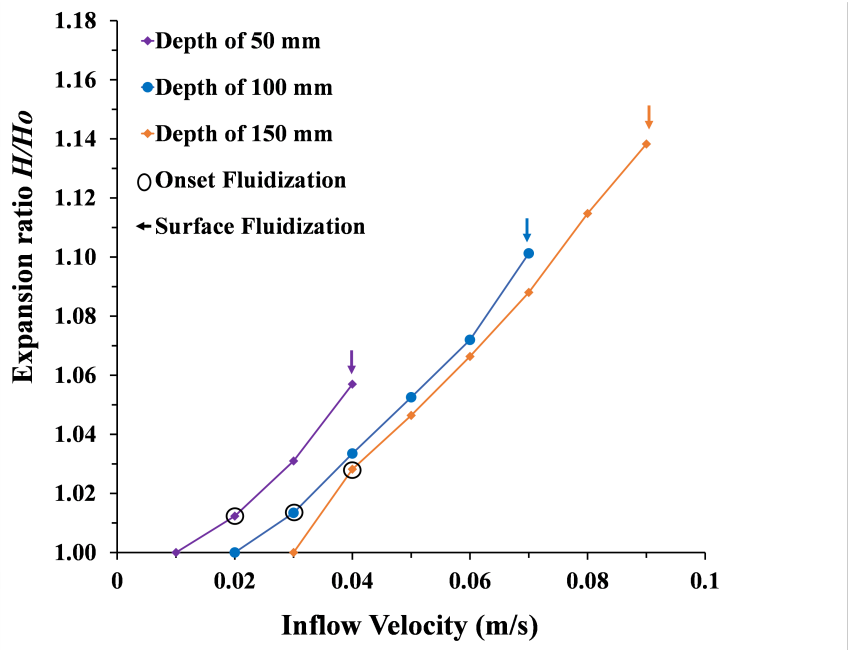



**Figure 5.25:** Change of soil bed expansion ratio through a pipe located at different depths

## 5.4 Summary

In this chapter, the onset and development of soil fluidisation induced by a pressurised and leaking water pipe embedded in fully saturated soil are simulated using the two-phase double-point (2P-DP) MPM approach coupled with the use of inflow/outflow boundary conditions. This formulation captures the transition from solid to liquid behaviour resulting from the fluidisation mechanism considering a threshold porosity; beyond this value, the material is considered a Newtonian fluid. The MPM results capture the initiation and evolution of soil fluidisation and soil bed expansion changes during the infiltration process. As the leakage velocity increases, the soil porosity close to the orifice increases until it exceeds the maximum porosity at the onset of fluidisation. Soil fluidisation results in a significant soil bed expansion that increases with the propagation of the fluidised zone. Based on this analysis, an equation is proposed to predict the inflow velocity at which fluidisation starts to verify the numerical model against previous experimental works. Furthermore, the MPM model is used to investigate the impacts of the orifice size, soil bed height, and soil porosity on the soil fluidisation mechanism around a leaking pipe. Based on the numerical simulations, the following key points are concluded:

- An increase in orifice size can considerably decrease the inflow velocity resulting in soil fluidisation. However, the surface fluidisation mechanism is not significantly affected by the orifice size.

- The inflow leakage velocity required for the onset and evolution of soil fluidisation significantly increases with an increase in the soil-bed height. The impact of the soil-bed height is higher compared to the effect of orifice size, hence, it is more effective to increase the pipe burial depth to reduce fluidisation risk.

- Soil porosity is a significant parameter in soil fluidisation, and the decrease in soil porosity can effectively strengthen the stability of the soil bed. Thus, soil with lower porosity should be used around underground pipes.

- The inflow leakage velocity required for the onset and evolution of soil fluidisation significantly increases with an increase in soil cohesion.
- A higher leakage velocity is required for the soil fluidisation induced by lateral leakage compared to upward leakage. The shallower the pipe depth, the lower the inflow velocity required for the onset and development of fluidisation, but the greater the ground displacement.

These results contribute to the understanding of the consequences of pipe leakage in pressurised water pipes and support identifying the most important parameters contributing to the initiation and propagation of soil fluidisation.

# Chapter 6

# Conclusions and Future Research

This chapter summarises the main outcomes of the conducted research. These outcomes correspond to the general and detailed objectives outlined in Chapter 1. In addition, some potential directions for future research are suggested to pursue and expand on, the work carried out in this research.

## 6.1 Research outcomes and conclusions

This study proposes a novel approach for numerical simulation of soil fluidisation around buried and pressurised leaking water pipe using the Material Point Method (MPM). The primary focus of this study is to advance knowledge in understanding of soil fluidisation progression induced by a leaking buried pipe, and to determine critical state that leads to a ground failure as well as identifying the role and importance of contributing parameters. The key achievements and conclusions of this study are as follows.

In Chapter 2, a comprehensive review of the literature on soil-fluid interaction associated with leaking pipes and other related experimental and numerical studies was conducted, it was demonstrated that the mechanism of soil fluidisation is still not fully understood. Previous studies have focused on investigating the initiation of soil fluidisation induced by pipe leakage. However, limited studies focused on progression of the fluidisation mechanism until it reaches the soil surface i.e. post fluidisation. There are relatively fewer studies concerned with the effect of different soil and pipe parameters on the pipe leakage and soil fluidisation problems.

In Chapter 3, the numerical modelling methodology was discussed, including an overview of the Material Point Method (MPM). MPM is proven to be a powerful numerical tool among traditional

and commonly used numerical methods in simulating large deformation in multi-phase problems. Therefore, this method is applied to investigate and achieve the aim of this research through modelling the soil fluidisation triggered by leaking pressurised pipes. Different multiphase MPM approaches, including the concept and the solution procedure for two-phase single-point MPM and two-phase double-point MPM, were presented and discussed in detail in this chapter. Additionally, the implementation of developed inflow/outflow Boundary Conditions (BCs) into the double-point approach was provided in this chapter. This enabled the modelling of constant velocity flows and optimised the computational cost by simplifying the geometry and reducing the number of material points (MPs). The numerical process of the conducted simulation using the MPM two-phase approaches was presented in this chapter.

In Chapter 4, the capabilities of the two-phase single-point and double-point MPM formulations to simulate the onset and progression of soil-fluid interaction around a leaking pipe have been demonstrated and compared. The two-dimensional model used in each formulation was presented in which the soil and water parameters were extracted from a previous experimental study conducted by Alsaydalani (2010). The results were compared against standard finite element analysis for reference and to highlight the advantages of MPM. The following conclusions can be drawn based on the results of the numerical simulations.

- The pore pressure is highly accumulated in the vicinity of the orifice in a soil bed subjected to a leaking pressurised buried pipe. This quickly dissipates, as it is moved upwards through the soil bed and away from the pressure source.

- The onset of fluidisation that occurred in the vicinity of the orifice is associated with a peak in excess pore water pressure that is attributed to the uplift mechanism of the soil bed above the pipe orifice.

- Both single-point MPM approach and FEM are applicable for identifying the leak pressure required for the onset of the local fluidisation in the vicinity of the orifice.

- The single-point MPM approach is not capable of capturing the post-local fluidisation mechanism due to the formation of empty elements near the orifice and the inability of the constitutive model to represent the transition from solid-like to liquid-like behaviour.
- The two-phase double-point MPM formulation captures the transition from solid to liquid behaviour resulting from the fluidisation mechanism considering a threshold porosity value beyond which the material is considered a Newtonian fluid.
- The two-phase double-point MPM formulation, coupled with the implementation of inflow/outflow boundary conditions, was proven to be an effective tool in capturing the progression of soil fluidisation induced by a leaking pipe until it reaches the soil surface.
- The MPM results demonstrated how vertical soil displacements, excess pore water pressure, and porosity develop during the onset of fluidisation and post-fluidisation.
- The soil fluidisation mechanism is associated with an uplift mechanism (due to the reduction in effective stress) of the grains in the fluidised region of the soil. The obtained results agree well qualitatively with the previous experimental and numerical solutions.

In Chapter 5, a robust model was developed using the two-phase double-point (DP) MPM approach to model the soil-fluid interaction around a leaking pressurised water pipe embedded in fully saturated soil. The MPM model was validated against published experimental data to replicate the realistic pipe leakage problem. In the numerical simulation, the inflow water velocity leading to the onset and progression of soil fluidisation around leaking pipe was identified based on the changes in soil porosity and soil bed expansion ratio. The model was then enhanced to conduct extensive parametric assessment on the effects of the orifice size, bed height, soil porosity, soil cohesion, leakage direction and pipe depth on the soil fluidisation mechanism. The key findings from this investigation were as follows.

- The larger the orifice size, the smaller the inflow velocities required to trigger the onset and surfacing of soil fluidisation. These results are consistent with the previous experimental

and analytical studies on soil erosion caused by an upward water jet and show that the MPM model has been able to capture the behaviour correctly.

- An increase in the orifice opening leads to a lower expansion ratio at the onset of fluidisation. The final expansion ratio as the fluidisation reaches the ground level is not significantly affected by the orifice size.

- The leakage velocity required for the initiation and progression of soil fluidisation considerably increases with the height of the soil bed. The thicker soil bed is characterised by higher bed stability and lower fluidisation risk.

- The initiation and progression of soil fluidisation occurred at higher leakage velocity in a lower porosity soil bed. Thus, the decrease in soil porosity increases the stability of the soil bed against fluidisation.

- The soil cohesion can provide internal resistance to material fluidisation. The higher the soil cohesion, the higher the water velocity required to fluidise the soil bed.

- The occurrence of soil fluidisation is dependent on the leakage direction. A lower leakage velocity is required for the soil fluidisation induced by upward leakage compared to lateral leakage.

- The inflow velocity required for the onset and progression of fluidisation increase with the increase in pipe depth. Additionally, the deeper the pipe, the lower the surface heave that is attributed to pipe leakage.

These results proved the significance of the fluidisation mechanism triggered by a defective pressurised water pipe and support the identification of the critical state that causes the ground subsidence. The model developed in this study can be used as a robust prediction tool to model the onset and progress of the fluidisation zone and to determine critical parameters involved in this mechanism. This tool could have a significant value to asset managers that are responsible for the maintenance of buried pipes, the supporting ground, and surface transportation infrastructure.

## 6.2 Recommendations for future research

This research contributes to the knowledge of soil fluidisation around a buried and pressurised leaking water pipe, specifically the associated soil fluidisation mechanism, using the Material Point Method (MPM). Based on the knowledge and experience acquired from this study, the following future works are proposed.

1. Although it was shown that the developed two-dimensional model provides a good understanding of the pipe leakage problem, future work should be carried out to perform a three-dimensional analysis by which the fluidisation mechanism can be captured more accurately.

2. This research has focused on investigating the fluidisation mechanism in a uniform soil material. Further research is essential to investigate the influence of different types of materials as well as soil layering on the fluidisation mechanism.

3. More simulations could be conducted in the future to investigate the impacts of initial soil density and orifice shape on soil-fluid interaction. Furthermore, the effect of soil friction on the progression of the fluidised zone is recommended to be adopted in future works.

4. The effect of leakage direction has been limited to the upward and lateral flow. However, it has been anticipated that different fluidisation processes would associate with downward and inclined leakage which needs further investigation.

5. In the presented study, the pipe is simply modelled as a source of leakage in the soil-fluid interaction. However, the pipe may experience external soil loads, which could cause additional leaks. Thus, future work should consider the soil-pipe interaction effects to obtain a representative model of the pipe leakage problem.

6. In the adopted two-phase double-point MPM approach, there is a sudden transition between the solid-phase and liquid-phase by a porosity threshold. The formulation used in this study is based on the theory of porous media and therefore the accuracy of this approach

in representing fluidisation must be within the range of its application. The use of a more advanced constitutive model may alleviate the error and capture the fluidisation mechanism more accurately. However, the implementation of an advanced constitutive model requires calibration against additional experimental data that are not provided in the validated experimental study. Therefore, the implementation of more advanced constitutive models is required to improve the transition process from solid to fluid states during fluidisation.

7. All the models presented use two-phase MPM formulations where only solid-liquid phases are considered to simulate a fully saturated soil bed. Further work is needed to extend the simulations to partially saturated materials by incorporating the three-phase MPM approach (solid, liquid and air) by means of using advanced constitutive models.

8. An important aspect that future work should focus on is the validation of the developed problem against real-world data rather than controlled laboratory tests. This could reveal the practical applications and limitations of the proposed model. However, this requires an improvement of the computational efficiency of the developed MPM model by avoiding unnecessary storage and computation.

9. The observation that the fluidised zone is confined within a shear band, indicating strain localisation, is intriguing. As post-fluidisation progresses, localised shear strains can lead to instability of the entire structure comprising the fluidised zone and shear band. Therefore, it is important to investigate the critical mode of failure to determine whether soil collapse is primarily caused by shear failure or full soil fluidisation extending up to the soil surface.

10. In dynamic scenarios involving plastic strains, particularly in perfect plasticity or softening with non-associated flow rules, the mathematical problem based on field equations is known to be ill-posed. Consequently, numerical predictions of shear bands become highly dependent on the mesh, and achieving convergence becomes challenging. Simulating the post-fluidisation response inherits these difficulties, necessitating the development of robust numerical models. One potential approach to address these challenges is to regularise the

problem, and the simplest methods involve visco-plastic regularisation. Other alternatives include incorporating gradient-dependent plasticity and non-local constitutive laws.

# References


Abe, K., Soga, K. and Bandara, S. (2014), 'Material Point Method for Coupled Hydromechanical Problems', *Journal of Geotechnical and Geoenvironmental Engineering* **140**(3).

Adedeji, K. B., Hamam, Y., Abe, B. T. and Abu-Mahfouz, A. M. (2017), Burst leakage-pressure dependency in water piping networks: Its impact on leak openings, *in* '2017 IEEE AFRICON', IEEE, pp. 1502–1507.

Akrami, S., Bezuijen, A., Tehrani, F. S. and Terwindt, J. (2022), 'The effect of relative density on the response of sand to internal fluidization', *Acta Geotechnica* **0123456789**.
**URL:** *https://doi.org/10.1007/s11440-022-01574-w*

Al-Farraji, A. (2017), Chemical engineering and reactor design of a fluidised bed gasifier, PhD thesis, Cardiff University.

Al-Kafaji, I. K. J. (2013), *Formulation of a Dynamic Material Point Method ( MPM ) for Geomechanical Problems*.

Ali, H. and Choi, J.-h. (2019), 'Risk prediction of sinkhole occurrence for different subsurface soil profiles due to leakage from underground sewer and water pipelines', *Sustainability* **12**(1), 310.

Almeida, A. B. and Ramos, H. M. (2010), 'Water supply operation: diagnosis and reliability analysis in a Lisbon pumping system', *Journal of Water Supply: Research and Technology—AQUA* **59**(1), 66–78.

Alsaydalani, M. (2010), Internal fluidisation of granular material, PhD thesis, University of Southampton.
**URL:** *https://eprints.soton.ac.uk/385439/*

Alsaydalani, M. O. (2020), 'Failure Mechanism of a Granular Bed Induced by a Horizontal Water Jet Using Particle Image Velocimetry', *KSCE Journal of Civil Engineering* **24**(6), 1696–1705.

Alsaydalani, M. O. A. and Clayton, C. R. I. (2014), 'Internal Fluidization in Granular Soils', *Journal of Geotechnical and Geoenvironmental Engineering* **140**(3), 1–10.

Andersen, S. and Andersen, L. (2010), 'Modelling of landslides with the material-point method', *Computational Geosciences* **14**(1), 137–147.

Anderson, T. B. and Jackson, R. (1967), 'Fluid mechanical description of fluidized beds. Equations of motion', *Industrial & Engineering Chemistry Fundamentals* **6**(4), 527–539.

Andrade, J. E., Avila, C. F., Hall, S. A., Lenoir, N. and Viggiani, G. (2011), 'Multiscale modeling and characterization of granular matter: from grain kinematics to continuum mechanics', *Journal of the Mechanics and Physics of Solids* **59**(2), 237–250.

Andreou, S. A., Marks, D. H. and Clark, R. M. (1987), 'A new methodology for modelling break failure patterns in deteriorating water distribution systems: Theory', *Advances in Water Resources* **10**(1), 2–10.

Anura3D (2022), 'Anura3D MPM Research Community'.
**URL:** *http://www.anura3d.com/*

Armero, F. and Love, E. (2003), 'An arbitrary Lagrangian–Eulerian finite element method for finite strain plasticity', *International Journal for Numerical Methods in Engineering* **57**(4), 471–508.

Aubram, D., Rackwitz, F. and Savidis, S. A. (2017), Contribution to the non-Lagrangian formulation of geotechnical and geomechanical processes, *in* 'Holistic Simulation of Geotechnical Installation Processes', Springer, pp. 53–100.

Awad, A. S. and Karni, A. (2000), 'Stability of saturated cohesionless soil layer due to water flowing from a broken underground pipeline', *J. King Saud Univ., Eng. Sci* **12**(1), 27–44.

Bailey, N. D. and van Zyl, J. E. (2015), 'Experimental investigation of internal fluidisation due to a vertical water leak jet in a uniform medium', *Procedia Engineering* **119**(1), 111–119.
**URL:** *http://dx.doi.org/10.1016/j.proeng.2015.08.860*

Bandara, S. S. (2013), Material point method to simulate large deformation problems in fluid-saturated granular medium, PhD thesis, University of Cambridge Cambridge.

Bandara, S. and Soga, K. (2015), 'Coupling of soil deformation and pore fluid flow using material point method', *Computers and geotechnics* **63**, 199–214.

Barbosa, P. (2022), 'Listening for Leaks'.
**URL:** *https://www.waterworld.com/drinking-water/distribution/article/14235456/2204wwft2*

Bardenhagen, S. G., Brackbill, J. U. and Sulsky, D. (2000), 'The material-point method for granular materials', *Computer Methods in Applied Mechanics and Engineering* **187**(3), 529–541.
**URL:** *https://www.sciencedirect.com/science/article/pii/S0045782599003382*

Bathe, K.-J. and Wilson, E. L. (1976), *Numerical methods in finite element analysis*, Prentice Hall.

Bear, J. (1988), *Dynamics of fluids in porous media*, Courier Corporation.

Beenakker, C. W. J. (1984), 'The effective viscosity of a concentrated suspension of spheres (and its relation to diffusion)', *Physica A: Statistical Mechanics and its Applications* **128**(1-2), 48–81.

Berardi, L., Giustolisi, O., Kapelan, Z. and Savic, D. A. (2008), 'Development of pipe deterioration models for water distribution systems using EPR', *Journal of Hydroinformatics* **10**(2), 113–126.

Beuth, L. (2012), 'Formulation and application of a quasi-static material point method'.

Beuth, L., Wikeckowski, Z. and Vermeer, P. A. (2011), 'Solution of quasi-static large-strain problems by the material point method', *International Journal for Numerical and Analytical Methods in Geomechanics* **35**(13), 1451–1465.

Bolognin, M., Martinelli, M., Bakker, K. J. and Jonkman, S. N. (2017), 'Validation of material point method for soil fluidisation analysis', *Journal of Hydrodynamics* **29**(3), 431–437.
**URL:** *http://dx.doi.org/10.1016/S1001-6058(16)60753-9*

Boxall, J. B., O'Hagan, A., Pooladsaz, S., Saul, A. J. and Unwin, D. M. (2007), Estimation of burst rates in water distribution mains, *in* 'Proceedings of the Institution of Civil Engineers-Water Management', Vol. 160, Thomas Telford Ltd, pp. 73–82.

Bruaset, S. and Sægrov, S. (2018), 'An analysis of the potential impact of climate change on the structural reliability of drinking water pipes in cold climate regions', *Water* **10**(4), 411.

Bruce, D. A., di Cervia, A. R. and Amos-Venti, J. (2006), 'Seepage remediation by positive cut-off walls: A compendium and analysis of North American case histories', *ASDSO Dam Safety, Boston, MA, September* pp. 10–14.

Brunier-Coulin, F., Cuéllar, P. and Philippe, P. (2016), Local mechanisms of cohesive soil erosion, *in* '8th International Conference on Scour and Erosion', John Harris, Richard Whitehouse & Sarah Moxon, p. 7.

Bui, H. H., Sako, K. and Fukagawa, R. (2007), 'Numerical simulation of soil–water interaction using smoothed particle hydrodynamics (SPH) method', *Journal of Terramechanics* **44**(5), 339–346.

C. di Prisco, L., Flessati, L. and Marveggio, P. (2022), 'Onshore pipelines in liquefied soil: experimental tests and numerical study', *Journal of Geotechnical and Geoenvironmental Engineering* (In Preparation).

Campbell, C. S. and Brennen, C. E. (1985), 'Computer simulation of granular shear flows', *Journal of Fluid Mechanics* **151**, 167–188.

Campbell, D. and Belcher-BM, A. (2016), 'Selly Oak burst water main: No estimate on when road will reopen as homes hit by flooding'.
**URL:** *https://www.birminghammail.co.uk/news/midlands-news/selly-oak-burst-water-main-12221484*

Cao, C. and Neilsen, M. (2021), 'Dam breach simulation with the material point method', *Computation* **9**(2), 8.

Cassa, A. M. and van Zyl, J. E. (2014), 'Predicting the leakage exponents of elastically deforming cracks in pipes', *Procedia Engineering* **70**, 302–310.

Cassa, A. M., Van Zyl, J. E. and Laubscher, R. F. (2010), 'A numerical investigation into the effect of pressure on holes and cracks in water supply pipes', *Urban Water Journal* **7**(2), 109–120.

Cathala, J. (1953), 'Fluidization and the research methods of Chemical Engineering Science', *Chemical Engineering Science* **2**(6), 273–281.

Ceccato, F. (2015), 'Study of large deformation geomechanical problems with the material point method', *Universita degli Studi di Padova* .

Ceccato, F., Beuth, L. and Simonini, P. (2016), 'Analysis of piezocone penetration under different drainage conditions with the two-phase material point method', *Journal of Geotechnical and Geoenvironmental Engineering* **142**(12), 4016066.

Ceccato, F., Yerro, A. and Martinelli, M. (2018), 'Modelling soil-water interaction with the material point method. Evaluation of single-point and double-point formulations', *Numerical Methods in Geotechnical Engineering IX* (July), 351–357.

Cerquaglia, M. L., Deliège, G., Boman, R., Papeleux, L., Terrapon, V. and Ponthot, J.-P. (2015), On some drawbacks and possible improvements of a Lagrangian Finite Element method for simulating incompressible flows, *in* 'Particles 2015'.

Chen, S. and Doolen, G. D. (1998), 'Lattice Boltzmann method for fluid flows', *Annual review of fluid mechanics* **30**(1), 329–364.

Chen, X.-Z., Shi, D.-P., Gao, X. and Luo, Z.-H. (2011), 'A fundamental CFD study of the gas–solid flow field in fluidized bed polymerization reactors', *Powder Technology* **205**(1-3), 276–288.

Chen, Y., Ohashi, H. and Akiyama, M. (1995), 'Heat transfer in lattice BGK modeled fluid', *Journal of statistical physics* **81**(1-2), 71–85.

Chenot, J. L. and Massoni, E. (2006), 'Finite element modelling and control of new metal forming processes', *International Journal of Machine Tools and Manufacture* **46**(11), 1194–1200.

Ćipranić, I. and Sekulić, G. (2015), 'The Analysis of the Influence of Soil on Leakage in Water Supply Systems', *Technical Gazette* **22**(5), 1179–1184.

Clark, R. M., Stafford, C. L. and Goodrich, J. A. (1982), 'Water distribution systems: A spatial and cost evaluation', *Journal of the Water Resources Planning and Management Division* **108**(3), 243–256.

Clarke, B. G., Magee, D., Dimitrova, V., Cohn, A. G., Du, H., Mahesar, Q.-a., Sadeghioon, A. M., Rogers, C. D. F., Gunn, D., Enwisle, D. and Others (2017), A decision support system to proactively manage subsurface utilities, *in* 'International Symposium for Next Generation Infrastructure 2017 Conference Proceedings', ISNGI, pp. 99–108.

Cleve R. Wootson Jr. (2016), 'San Antonio sinkhole swallows two cars, killing a sheriff's deputy'. **URL:** *https://www.washingtonpost.com/news/post-nation/wp/2016/12/05/no-way-they-were-going-to-survive-texas-sinkhole-swallows-2-cars-killing-a-sheriffs-deputy/*

Coelho, B. Z., Rohe, A. and Aboufirass, A. (2018), Assessment of dike safety within the framework of large deformation analysis with the material point method, *in* 'Numerical Methods in Geotechnical Engineering IX', CRC Press, pp. 657–663.

Coetzee, C. J., Vermeer, P. A. and Basson, A. H. (2005), 'The modelling of anchors using the material point method', *International journal for numerical and analytical methods in geomechanics* **29**(9), 879–895.

Colombo, A. F. and Karney, B. W. (2002), 'Energy and costs of leaky pipes: Toward comprehensive picture', *Journal of Water Resources Planning and Management* **128**(6), 441–450.

Cook, B. K., Noble, D. R. and Williams, J. R. J. E. C. (2004), 'A direct simulation method for particle-fluid systems', *Engineering Computations* **21**(2/3/4), 151–168.

Cremonesi, M., Franci, A., Idelsohn, S. and Oñate, E. (2020), 'A state of the art review of the particle finite element method (PFEM)', *Archives of Computational Methods in Engineering* **27**(5), 1709–1735.

Crespo, A. J. C. (2008), 'Application of the smoothed particle hydrodynamics model SPHysics to free-surface hydrodynamics', *Universidade de Vigo* .

Cui, X. (2013), Numerical simulation of internal fluidisation and cavity evolution due to a leaking pipe using the coupled DEM-LBM technique, PhD thesis, University of Birmingham.

Cui, X. L., Tao, G. L. and Li, J. (2018), Experiment and numerical simulation on seepage failure of sand caused by leakage of underground water pipe, *in* 'IOP Conference Series: Earth and Environmental Science', Vol. 153, IOP Publishing, p. 32033.

Cui, X., Li, J., Chan, A. and Chapman, D. (2012), 'A 2D DEM-LBM study on soil behaviour due to locally injected fluid', *Particuology* **10**(2), 242–252.
**URL:** *http://dx.doi.org/10.1016/j.partic.2011.10.002*

Cui, X., Li, J., Chan, A. and Chapman, D. (2014), 'Coupled DEM-LBM simulation of internal fluidisation induced by a leaking pipe', *Powder Technology* **254**, 299–306.

Cundall, P. A. (1971), A computer model for simulating progressive, large-scale movement in blocky rock system, *in* 'Proceedings of the International Symposium on Rock Mechanics, 1971'.

Daoudi, A., Benbrahim, M. and Benjelloun, K. (2005), 'An intelligent system to classify leaks in water distribution pipes', *Small* **7**(13), 20.

Das, B. M. and Sivakugan, N. (2018), *Principles of foundation engineering*, Cengage learning.

Dave, M. M. and Solanki, C. H. (2020), Protection of Buried Pipelines Using Geosynthetics Under Different Loading Conditions—A Review BT - Advances in Computer Methods and Geomechanics, Springer Singapore, Singapore, pp. 249–262.

Davies, J. P., Clarke, B. A., Whiter, J. T. and Cunningham, R. J. (2001), 'Factors influencing the structural deterioration and collapse of rigid sewer pipes', *Urban water* **3**(1-2), 73–89.

De Marchis, M. and Milici, B. (2019), 'Leakage estimation in water distribution network: effect of the shape and size cracks', *Water Resources Management* **33**(3), 1167–1183.

Deen, N. G., Annaland, M. V. S., Van der Hoef, M. A. and Kuipers, J. A. M. (2007), 'Review of discrete particle modeling of fluidized beds', *Chemical engineering science* **62**(1-2), 28–44.

Dewey, R. (1988), 'Installation of a deep cutoff wall at Navajo Dam', *Trans. of 16th ICOLD, San Francisco, CA, June* **5**, 230–237.

DiscoverWater (2022), 'Find out how water companies in England & Wales are performing'.
**URL:** */discoverwater.co.uk*

Donea, J., Giuliani, S., methods in applied mechanics Halleux, J.-P. J. C. and Engineering (1982), 'An arbitrary Lagrangian-Eulerian finite element method for transient dynamic fluid-structure interactions', **33**(1-3), 689–723.

Doyle, G., Seica, M. V. and Grabinsky, M. W. F. (2003), 'The role of soil in the external corrosion of cast iron water mains in Toronto, Canada', *Canadian geotechnical journal* **40**(2), 225–236.

Duran, J. (2012), *Sands, powders, and grains: an introduction to the physics of granular materials*, Springer Science Business Media.

El Shamy, U. (2002), 'Discrete element simulations of water flow through granular soils'.

Ergun, S. (1952), 'Fluid flow through packed columns', *Chem. Eng. Prog.* **48**, 89–94.

EurEau (2021), 'Europe's water in figures - An overview of the European drinking water and waste water sectors'.
**URL:** *https://www.eureau.org/resources/publications/1460-eureau-data-report-2017-1/file*

Fang, Q., Zhang, D. and Wong, L. N. Y. (2011), 'Environmental risk management for a cross interchange subway station construction in China', *Tunnelling and Underground Space Technology* **26**(6), 750–763.

Farley, M. and Trow, S. (2003), *Losses in water distribution networks*, IWA publishing.

Feng, K., Huang, D. and Wang, G. (2021), 'Two-layer material point method for modeling soil–water interaction in unsaturated soils and rainfall-induced slope failure', *Acta Geotechnica* **16**(8), 2529–2551.

Feng, Y. Q. and Yu, A. B. (2006), 'Discrete particle simulation of size segregation of particle mixtures in a gas fluidized bed', *China Particuology* **4**(03n04), 122–126.

Fern, E. J., de Lange, D. A., Zwanenburg, C., Teunissen, J. A. M., Rohe, A. and Soga, K. (2017), 'Experimental and numerical investigations of dyke failures involving soft materials', *Engineering Geology* **219**, 130–139.

Fern, E. J. and Soga, K. (2016), 'The role of constitutive models in MPM simulations of granular column collapses', *Acta Geotechnica* **11**(3), 659–678.

Fern, J., Rohe, A., Soga, K. and Alonso, E. (2019), *The material point method for geotechnical engineering: a practical guide*, CRC Press.

Ferrante, M. (2012), 'Experimental Investigation of the Effects of Pipe Material on the Leak Head-Discharge Relationship', *Journal of Hydraulic Engineering* **138**(8), 736–743.

Germanopoulos, G. and Jowitt, P. W. (1989), 'LEAKAGE REDUCTION BY EXCESS PRESSURE MINIMIZATION IN A WATER SUPPLY NETWORK.', *Proceedings of the Institution of Civil Engineers* **87**(2), 195–214.

Gernon, T. M., Gilbertson, M. A., Sparks, R. S. J. and Field, M. (2009), 'The role of gas-fluidisation in the formation of massive volcaniclastic kimberlite', *Lithos* **112**, 439–451.

Gingold, R. A. and Monaghan, J. J. (1977), 'Smoothed particle hydrodynamics: theory and application to non-spherical stars', *Monthly notices of the royal astronomical society* **181**(3), 375–389.

Giustolisi, O., Laucelli, D. and Savic, D. A. (2006), 'Development of rehabilitation plans for water mains replacement considering risk and cost-benefit assessment', *Civil Engineering and Environmental Systems* **23**(3), 175–190.

Global Water Leakage Summit, . (2008), 'Adapting the most effective strategies for water efficiency and leakage management', *Proceedings of the 3rd Annual Leakage Summit for International Water Utilities, London, UK, see http://www. global-leakage-summit. com/index. asp (accessed 06/04/2008)* .

Goodarzi, M., Kwok, C. Y., Tham, L. G. and Chen, F. (2013), Fluid coupling in DEM simulation using Darcy's law: Formulation, and verification, *in* 'AIP Conference Proceedings', Vol. 1542, AIP, pp. 1134–1137.

Gould, S. J. F., Boulaire, F. A., Burn, S., Zhao, X.-L. and Kodikara, J. K. (2011), 'Seasonal factors influencing the failure of buried water reticulation pipes', *Water Science and Technology* **63**(11), 2692–2699.

Greyvenstein, B. and van Zyl, J. E. (2007), 'An experimental investigation into the pressure-leakage relationship of some failed water pipes', *Journal of Water Supply: Research and Technology—AQUA* **56**(2), 117–124.

Guo, N. and Zhao, J. (2014), 'A coupled FEM/DEM approach for hierarchical multiscale modelling of granular media', *International Journal for Numerical Methods in Engineering* **99**(11), 789–818.

Guo, S., Shao, Y., Zhang, T., Zhu, D. Z. and Zhang, Y. (2013), 'Physical modeling on sand erosion around defective sewer pipes under the influence of groundwater', *Journal of Hydraulic Engineering* **139**(12), 1247–1257.

Guo, Y. and Yu, X. B. (2016), Coupled DEM and CFD Simulations of Soil Erosion, *in* K. R. Reddy, N. Yesiller, D. Zekkos, A. Farid and A. De, eds, 'Geo-Chicago 2016', Vol. 2016-, Reston, VA: American Society of Civil Engineers, Reston, pp. 661–670.

Hakuno, M. and Tarumi, Y. (1988), 'A granular assembly simulation for the seismic liquefaction of sand', *Doboku Gakkai Ronbunshu* **1988**(398), 129–138.

Han, K., Feng, Y. T. and Owen, D. R. J. (2007), 'Coupled lattice Boltzmann and discrete element modelling of fluid–particle interaction problems', *Computers structures* **85**(11-14), 1080–1088.

Han, Y. and Cundall, P. A. (2013), 'LBM–DEM modeling of fluid–solid interaction in porous media', *International Journal for Numerical and Analytical Methods in Geomechanics* **37**(10), 1391–1407.

Harlow, F. H. (1964), 'The particle-in-cell computing method for fluid dynamics', *Methods Comput. Phys.* **3**, 319–343.

Hazay, M. and Munjiza, A. (2016), Introduction to the combined finite-discrete element method, *in* 'Computational Modeling of Masonry Structures Using the Discrete Element Method', IGI Global, pp. 123–145.

He, Y., Bayly, A. E. and Hassanpour, A. (2018), 'Coupling CFD-DEM with dynamic meshing: A new approach for fluid-structure interaction in particle-fluid flows', *Powder Technology* **325**, 620–631.

He, Y., Zhu, D. Z., Zhang, T., Shao, Y. and Yu, T. (2017), 'Experimental Observations on the Initiation of Sand-Bed Erosion by an Upward Water Jet', *Journal of Hydraulic Engineering* **143**(7), 4–9.

Hecke, B. V. (2020), 'Lose the leaks'.
**URL:** *https://nickelinstitute.org/en/blog/2020/january/lose-the-leaks/ on the way to,treated drinking water they produce.*

Hu, H. H. (1996), 'Direct simulation of flows of solid-liquid mixtures', *International Journal of Multiphase Flow* **22**(2), 335–352.

Hu, Y. and Hubble, D. W. (2007), 'Factors contributing to the failure of asbestos cement water mains', *Canadian Journal of Civil Engineering* **34**(5), 608–621.

Hu, Z., Yang, Z. X., Guo, N. and Zhang, Y. D. (2022), 'Multiscale modeling of seepage-induced suffusion and slope failure using a coupled FEM–DEM approach', *Computer Methods in Applied Mechanics and Engineering* **398**, 115177.

Ibrahim, A. and Meguid, M. (2021), 'Continuum-based approach to model particulate soil–water interaction: Model validation and insight into internal erosion', *Processes* **9**(5), 1–15.

Ibrahim, A. and Meguid, M. A. (2020), 'Coupled flow modelling in geotechnical and ground engineering: an overview', *International Journal of Geosynthetics and Ground Engineering* **6**(3), 1–25.

Ilunga, T. D. (2016), *The Effect of Pipe Material on the Behaviour of Water Leakage through Longitudinal Cracks under Pressure*, University of Johannesburg (South Africa).

Jain, R., Kumari, K., Kesharwani, R. K., Kumar, S., Pal, S. K., Singh, S. B., Panda, S. K. and Samantaray, A. K. (2015), Friction stir welding: scope and recent development, *in* 'Modern Manufacturing Engineering', Springer, pp. 179–229.

Jassim, I., Stolle, D. and Vermeer, P. (2013), 'Two-phase dynamic analysis by material point method', *International journal for numerical and analytical methods in geomechanics* **37**(15), 2502–2522.

Jenkins, L., Gokhale, S. and McDonald, M. (2015), 'Comparison of pipeline failure prediction models for water distribution networks with uncertain and limited data', *Journal of Pipeline Systems Engineering and Practice* **6**(2), 4014012.

Jensen, R. P. and Preece, D. S. (2000), Modeling sand production with Darcy-flow coupled with discrete elements, Technical report.

Jesson, D., Farrow, J., Mulheron, M., Nensi, T. and Smith, P. (2017), 'Achieving Zero Leakage by 2050: Basic Mechanisms of Bursts and Leakage'.

Kafui, K. D., Thornton, C. and Adams, M. J. (2002), 'Discrete particle-continuum fluid modelling of gas–solid fluidised beds', *Chemical engineering science* **57**(13), 2395–2410.

Kakoudakis, K. (2019), 'Pipe failure prediction and impacts assessment in a water distribution network', (March), 1–190.

Karoui, T., Jeong, S.-Y., Jeong, Y.-H. and Kim, D.-S. (2018), 'Experimental study of ground subsidence mechanism caused by sewer pipe cracks', *Applied Sciences* **8**(5), 679.

Kashiwa, B. A. (2001), 'A multifield model and method for fluid-structure interaction dynamics', *Los Alamos National Laboratory, Los Alamos, Tech. Rep. LA-UR-01-1136* .

Kawaguchi, T., Tanaka, T. and Tsuji, Y. (1998), 'Numerical simulation of two-dimensional fluidized beds using the discrete element method (comparison between the two-and three-dimensional models)', *Powder Technology* **96**(2), 129–138.

Kezdi, A. (1969), 'Increase of protective capacity of flood control dikes', *Department of Geotechnics, Technical University of Budapest, Report* (1).

Kingdom, B., Liemberger, R. and Marin, P. (2006), 'The Challenge of Reducing Non-Revenue Water in Developing Countries', *Water Supply and Sanitation Board Discussion Series* .

Kleiner, Y., McDonald, S., Rajani, B., Kleiner, Y., Mcdonald, S. and Others (2003), 'Cathodic protection of water mains in Ottawa: analysis and planning', *Corrosion control for enhanced reliability and safety* pp. 1–14.

Knappett, J. and Craig, R. F. (2020), *Craig's Soil Mechanics*, 9 edn, CRC Press, Milton.

Kuipers, J. A. M., Van Duin, K. J., Van Beckum, F. P. H. and Van Swaaij, W. P. M. (1992), 'A numerical model of gas-fluidized beds', *Chemical engineering science* **47**(8), 1913–1924.

Kularathna, S. (2018), Splitting solution scheme for material point method, PhD thesis, University of Cambridge.

Kularathna, S., Liang, W., Zhao, T., Chandra, B., Zhao, J. and Soga, K. (2021), 'A semi-implicit material point method based on fractional-step method for saturated soil', *International Journal for Numerical and Analytical Methods in Geomechanics* **45**(10), 1405–1436.

Kularathna, S. and Soga, K. (2017), 'Comparison of two projection methods for modeling incompressible flows in MPM', *Journal of Hydrodynamics, Ser. B* **29**(3), 405–412.

Kunkel, G., Laven, K. and Mergelas, B. (2008), 'Does Your City Have High-risk Pipes?', *Journal-American Water Works Association* **100**(4), 70–74.

Kwon, Y. W. and Hosoglu, S. (2008), 'Application of lattice Boltzmann method, finite element method, and cellular automata and their coupling to wave propagation problems', *Computers structures* **86**(7-8), 663–670.

Lambe, T. W. and Whitman, R. V. (1969), 'Soil mechanics, 553 pp'.

Lambert, A. (2001), What do we know about pressure-leakage relationships in distribution systems, *in* 'IWA Conf. n Systems approach to leakage control and water distribution system management'.

Latifi, M., Mohammadbeigi, S., Farahi Moghadam, K., Naeeni, S. T. Kilanehei, F. (2022), 'Experimental Study of Pressure and Soil Effects on Fluidization and Mobile Bed Zones around Buried Leaking Pipes', *Journal of Pipeline Systems Engineering and Practice* **13**(4), 4022034.

Latifi, N., Eisazadeh, A., Marto, A. and Meehan, C. L. (2017), 'Tropical residual soil stabilization: A powder form material for increasing soil strength', *Construction and Building Materials* **147**, 827–836.

Ledwith, C., Weisman, R. N. and Lennon, G. P. (1990), Selection of hole size for fluidization pipes, *in* 'Hydraulic engineering', ASCE, pp. 933–938.

Lennon, G. P. and Weisman, R. N. (1995), 'Head requirement for incipient fluidization of fine sands in unbounded domains', *Journal of Hydraulic Engineering* **121**(11), 838–841.

Leva, M. (1959), *Fluidization*, McGraw-Hill Book Co., New York.

Li, J. (2013), Numerical investigations of the coupled DEM-LBM technique with application to leakage-soil interaction due to a leaking pipe, PhD thesis, University of Birmingham.

Li, X., Chu, X. and Sheng, D. C. (2007), 'A saturated discrete particle model and characteristic-based SPH method in granular materials', *International Journal for Numerical Methods in Engineering* **72**(7), 858–882.

Liang, D. (2010), Evaluating shallow water assumptions in dam-break flows, *in* 'Proceedings of the Institution of Civil Engineers-Water Management', Vol. 163, Thomas Telford Ltd, pp. 227–237.

Liemberger, R., Marin, P. and Others (2008), 'Reducing Water Loss in Developing Countries Using Performance-Based Service Contracting'.

Liu, G.-R. and Liu, M. B. (2003), *Smoothed particle hydrodynamics: a meshfree particle method*, World Scientific.

Liu, H. (2017), *Pipeline engineering*, CRC Press.

Liu, Z., Sadiq, R., Rajani, B., Najjaran, H. and Others (2010), 'Exploring the relationship between soil properties and deterioration of metallic pipes using predictive data mining methods', *Journal of Computing in Civil Engineering* **24**(3), 289.

Lominé, F., Scholtes, L., Sibille, L., Poullain, P. J. I. J. f. N. and in Geomechanics, A. M. (2013), 'Modeling of fluid–solid interaction in granular media with coupled lattice Boltzmann/discrete element methods: application to piping erosion', **37**(6), 577–596.

Lowe, D. R. (1976), 'Subaqueous liquefied and fluidized sediment flows and their deposits', *Sedimentology* **23**(3), 285–308.

Lucy, L. B. (1977), 'A numerical approach to the testing of the fission hypothesis', *The astronomical journal* **82**, 1013–1024.

Makar, J. M. (2001), Investigating large gray cast-iron pipe failures: A step-by-step approach, *in* 'AWWA Infrastructure Conference, Orlando, Fla', Citeseer.

Malm, A., Ljunggren, O., Bergstedt, O., Pettersson, T. J. R. and Morrison, G. M. (2012), 'Replacement predictions for drinking water networks through historical data', *Water research* **46**(7), 2149–2158.

Martinelli, M. (2016), 'Soil-water interaction with material point method', *Double-Point Formulation. Report on EU-FP7 research project MPM-Dredge PIAP-GA-2012-324522* (May).

Martinelli, M. and Rohe, A. (2015), 'Modelling fluidisation and sedimentation with the material point method', *Incontro Annuale dei Giovani Ingegneri Geotecnici* pp. 1–4.

Martinelli, M., Tehrani, F. S. and Galavi, V. (2017), 'Analysis of Crater Development Around Damaged Pipelines Using the Material Point Method', *Procedia Engineering* **175**, 204–211.

Meguro, K. and Ravichandran, N. (2000), '3-Dimensional distinct element simulation of liquefaction phenomena', *SEISAN KENKYU* **52**(12), 598–601.

Mercier, F., Bonelli, S., Golay, F., Anselmet, F., Philippe, P. and Borghi, R. (2015), 'Numerical modelling of concentrated leak erosion during Hole Erosion Tests', *Acta Geotechnica* **10**(3), 319–332.

Montellà, E. P., Toraldo, M., Chareyre, B. and Sibille, L. (2016), 'Localized fluidization in granular materials: Theoretical and numerical study', *Physical Review E* **94**(5), 52905.

Mora-Rodríguez, J., Delgado-Galván, X., Ramos, H. M., López-Jiménez, P. A., Mora-Rodr´, J., Delgado-Galván, X., Ramos, H. M. and López-Jiménez, P. A. (2014), 'An overview of leaks and intrusion for different pipe materials and failures', *Urban Water Journal* **11**(1), 1–10.

Mordak, J. and Wheeler, J. (1988), 'Deterioration of asbestos cement water mains. Final report to the Department of the Environment', *Water Research Center, Wiltshire, UK* .

Morris, J. and Johnson, S. (2009), 'Dynamic simulations of geological materials using combined FEM/DEM/SPH analysis', *Geomechanics and Geoengineering: An International Journal* **4**(1), 91–101.

Mourgues, R. and Cobbold, P. R. (2006), 'Sandbox experiments on gravitational spreading and gliding in the presence of fluid overpressures', *Journal of Structural Geology* **28**(5), 887–901.

Mukunoki, T., Kumano, N. and Otani, J. (2012), 'Image analysis of soil failure on defective underground pipe due to cyclic water supply and drainage using X-ray CT', *Frontiers of Structural and Civil Engineering* **6**(2), 85–100.

Murphy, J., Yerro, A. and Soga, K. (2020), 'A New Approach to Simulate Suffusion Processes with MPM', (February 2022), 482–490.

Nairn, J. A. (2003), 'Material point method calculations with explicit cracks', *Computer Modeling in Engineering and Sciences* **4**(6), 649–664.

Nath, P. (1983), 'Trench excavation effects on adjacent buried pipes: Finite element study', *Journal of Geotechnical Engineering* **109**(11), 1399–1415.

Niven, R. K. and Khalili, N. (1998), 'In situ fluidisation by a single internal vertical jet', *Journal of Hydraulic Research* **36**(2), 199–228.

Noack, C. and Ulanicki, B. (2008), Modelling of soil diffusibility on leakage characteristics of buried pipes, *in* 'Water Distribution Systems Analysis Symposium 2006', pp. 1–9.

Nouwakpo, S. (2010), 'Pore Water Effects on Soil Erodibility and Its Implication in Ephemeral Gully Erosion Modeling', (1996).

O'Day, D. K. (1989), 'External corrosion in distribution systems', *Journal-American Water Works Association* **81**(10), 45–52.

OECD (2016), 'Water governance in cities'.
**URL:** *www.read.oecd-ilibrary.org/governance/water-governance-in-cities.com*

OFWAT (2022), 'Leakage – Ofwat'.
**URL:** *https://www.ofwat.gov.uk/households/supply-and-standards/leakage/.*

Olivera Bonilla, R. R. (2004), 'Numerical simulations of undrained granular media'.

Oñate, E., Celigueta, M. A. and Idelsohn, S. R. (2006), 'Modeling bed erosion in free surface flows by the particle finite element method', *Acta Geotechnica* **1**(4), 237–252.

Osher, S. and Sethian, J. A. (1988), 'Fronts propagating with curvature-dependent speed: algorithms based on Hamilton-Jacobi formulations', *Journal of computational physics* **79**(1), 12–49.

O'Sullivan, C. (2011), 'Particle-based discrete element modeling: geomechanics perspective', *International Journal of Geomechanics* **11**(6), 449–464.

Owen, D. R. J. and Feng, Y. T. (2001), 'Parallelised finite/discrete element simulation of multi-fracturing solids and discrete systems', *Engineering computations* **18**(3/4), 557–576.

Owen, D. R. J., Leonardi, C. R. and Feng, Y. T. J. I. J. f. N. M. i. E. (2011), 'An efficient framework for fluid–structure interaction using the lattice Boltzmann method and immersed moving boundaries', **87**(1-5), 66–95.

Peche, A., Graf, T., Fuchs, L. and Neuweiler, I. (2017), 'A coupled approach for the three-dimensional simulation of pipe leakage in variably saturated soil', *Journal of Hydrology* **555**, 569–585.

Philippe, P. and Badiane, M. (2013), 'Localized fluidization in a granular medium', *Physical Review E* **87**(4), 42206.

Phuong, N., van Tol, A., Elkadi, A. and Rohe, A. (2014), 'Modelling of pile installation using the material point method (MPM)', *Numerical methods in Geotechnical engineering* **271**, 276.

Pike, S. M., van Zyl, J. E. and Clayton, C. R. I. (2018), 'Scouring Damage to Buried Pipes Caused by Leakage Jets: Experimental Study', *Journal of Pipeline Systems Engineering and Practice* **9**(4), 1–11.

Pirnia, P., Duhaime, F., Ethier, Y. and Dubé, J.-S. (2019), 'ICY: An interface between COMSOL multiphysics and discrete element code YADE for the modelling of porous media', *Computers & Geosciences* **123**, 38–46.

Pirnia, P., Duhaime, F., Ethier, Y. and Dubé, J.-S. (2020), 'Hierarchical multiscale numerical modelling of internal erosion with discrete and finite elements', *Acta Geotechnica* **15**(10), 2877–2889.

Preece, D. S., Jensen, R. P., Perkins, E. D. and Williams, J. R. (1999), 'Sand production modeling using superquadric discrete elements and coupling of fluid flow and particle motion', *The 37th U. S. Symposium on Rock Mechanics (USRMS)* .

Premnath, K. N., Nave, J.-C. and Banerjee, S. (2005), Computation of multiphase flows with lattice Boltzmann methods, *in* 'ASME 2005 International Mechanical Engineering Congress and Exposition', American Society of Mechanical Engineers, pp. 403–420.

Priyadarshini, A., Pal, S. K. and Samantaray, A. K. (2012), Finite element modeling of chip formation in orthogonal machining, *in* 'Statistical and computational techniques in manufacturing', Springer, pp. 101–144.

Rajani, B. and Kleiner, Y. (2001), 'Comprehensive review of structural deterioration of water mains: physically based models', *Urban water* **3**(3), 151–164.

Rajani, B. and Tesfamariam, S. (2004), 'Uncoupled axial, flexural, and circumferential pipe soil interaction analyses of partially supported jointed water mains', *Canadian geotechnical journal* **41**(6), 997–1010.

Rajani, B., Zhan, C. and Kuraoka, S. (1996), 'Pipe soil interaction analysis of jointed water mains', *Canadian Geotechnical Journal* **33**(3), 393–404.

Rajeev, P., Kodikara, J., Robert, D., Zeman, P. and Rajani, B. (2014), 'Factors contributing to large daimeter water pipe failure', *Water Asset Management International* **10**(3), 9–14.

Rezaei, H. (2016), 'Impact of pressure fluctuations on pipe failures in water distribution networks', (July).

Richards Jr, R., Elms, D. G. and Budhu, M. (1990), 'Dynamic fluidization of soils', *Journal of Geotechnical Engineering* **116**(5), 740–759.

Richards, K. S. and Reddy, K. R. (2007), 'Critical appraisal of piping phenomena in earth dams', *Bulletin of Engineering Geology and the Environment* **66**(4), 381–402.

Robinsona, M., Ludinga, S. and arXiv preprint arXiv:. Ramaiolib, M. J. (2013), 'Fluid-particle flow and validation using two-way-coupled mesoscale SPH-DEM'.

Rogers, C. D. F., Chapman, D. N. and Royal, A. C. D. (2008), 'Experimental investigation of the effects of soil properties on leakage: final report [R]', *Report prepared for Thames Water Limited and Three Valleys Water Limited. Department of Civil Engineering, The University of Birmingham, Edgbaston Birmingham* .

Rogers, D. (2014), 'Leaking water networks: an economic and environmental disaster', *Procedia Engineering* **70**, 1421–1429.

Røstum, J. (2000), 'Statistical modelling of pipe failures in water networks'.

Ruchti, G. F. (2017), 'Water pipeline condition assessment', *Am. Soc. Civil Eng.(ASCE)* .

Shafipour, R. and Soroush, A. (2008), 'Fluid coupled-DEM modelling of undrained behavior of granular media', *Computers and Geotechnics* **35**(5), 673–685.

Soga, K., Alonso, E., Yerro, A., Kumar, K. and Bandara, S. (2016), 'Trends in large-deformation analysis of landslide mass movements with particular emphasis on the material point method', *Géotechnique* **66**(3), 248–273.

Sołowski, W. T., Berzins, M., Coombs, W. M., Guilkey, J. E., Möller, M., Tran, Q. A., Adibaskoro, T., Seyedan, S., Tielen, R. and Soga, K. (2021), 'Material point method: Overview and challenges ahead', *Advances in Applied Mechanics* **54**, 113–204.

St. Clair, A. M. and Sinha, S. (2014), 'Development of a standard data structure for predicting the remaining physical life and consequence of failure of water pipes', *Journal of Performance of Constructed Facilities* **28**(1), 191–203.

Stelloh, T. and Bacallao, A. (2016), 'Massive Texas Sinkhole Swallows Two Cars, Killing Sheriff's Deputy'.
**URL:** *https://www.nbcnews.com/news/us-news/massive-texas-sink-hole-swallows-two-cars-killing-sheriff-s-n692231*

Stuart, J. (2011), Bursts per 1000km project report, Technical report, Severn Trent Water.

Sulsky, D., Chen, Z. and Schreyer, H. L. (1994), 'A particle method for history-dependent materials', *Computer methods in applied mechanics and engineering* **118**(1-2), 179–196.

Sulsky, D. and Schreyer, H. L. (1993), 'The particle-in-cell method as a natural impact algorithm', *ASME APPLIED MECHANICS DIVISION-PUBLICATIONS-AMD* **180**, 219.

Sulsky, D. and Schreyer, H. L. (1996), 'Axisymmetric form of the material point method with applications to upsetting and Taylor impact problems', *Computer Methods in Applied Mechanics and Engineering* **139**(1-4), 409–429.

Suzuki, K., Bardet, J. P., Oda, M., Iwashita, K., Tsuji, Y., Tanaka, T. and Kawaguchi, T. (2007), 'Simulation of upward seepage flow in a single column of spheres using discrete-element method with fluid-particle interaction', *Journal of Geotechnical and Geoenvironmental Engineering* **133**(1), 104–109.

Taghipour, F., Ellis, N. and Wong, C. (2005), 'Experimental and computational study of gas–solid fluidized bed hydrodynamics', *Chemical engineering science* **60**(24), 6857–6867.

Tang, Y. (2017), 'Mechanisms of Soil Erosion due to Defective Sewer Pipes'.
**URL:** *https://era.library.ualberta.ca/files/cb5644r94z*

Tang, Y., Zhu, D. Z. and Chan, D. H. (2017), 'Experimental study on submerged sand erosion through a slot on a defective pipe', *Journal of Hydraulic Engineering* **143**(9), 4017026.

Tao, H. (2018), NUMERICAL MODELING OF SOIL INTERNAL EROSION MECHANISM, PhD thesis.

Teeluckdharry, S. (2017), An experimental investigation of leakage flow paths in soil surrounding leaks in water distribution systems, Master's thesis, University of Cape Town.

Tehrani, F. S., Askarinejad, A. and Schenkeveld, F. (2018), 'Preliminary results of laboratory analysis of sand fluidisation', *Physical Modelling in Geotechnics* **1**(September), 461–464.

Telegraph, T. (2022), 'Fury as burst water main triggers mini 'tsunami' and two sinkholes in Islington'.
**URL:** *https://www.telegraph.co.uk/news/2022/08/08/islington-flood-burst-water-main-triggers-3ft-tsunami-two-sinkholes/*

Terzaghi, K. (1943), 'Theoretical Soil Mechanics John Wiley and Sons Inc', *New York* **314**.

Truesdell, C. and Toupin, R. (1960), The classical field theories, *in* 'Principles of classical mechanics and field theory/Prinzipien der Klassischen Mechanik und Feldtheorie', Springer, pp. 226–858.

Tsinker, P. (1988), 'Pile jetting', *Journal of Geotechnical Engineering Division, ASCE* **11**(3), 326–334.

Tsuji, Y., Kawaguchi, T. and Tanaka, T. (1993), 'Discrete particle simulation of two-dimensional fluidized bed', *Powder Technology* **77**(1), 79–87.

Twort, A. C., Ratnayaka, D. D. and Brandt, M. J. (2001), 'Water Supply, 2000', *Arnold: London, reprinted by Butterworth-Heinemann: Oxford* .

van Zyl, J. E., Alsaydalani, M. O. A., Clayton, C. R. I., Bird, T. and Dennis, A. (2013), Soil fluidisation outside leaks in water distribution pipes–preliminary observations, *in* 'Proceedings of the Institution of Civil Engineers-Water Management', Vol. 166, Thomas Telford Ltd, pp. 546–555.

van Zyl, J. E. and Clayton, C. R. (2005), The effect of pressure on leakage in water distribution systems, *in* 'Proceedings of the 8th International Conference on Computing and Control for the Water Industry, CCWI 2005: Water Management for the 21st Century', Vol. 2, Thomas Telford Ltd, p. 77.

Verruijt, A. (2009), *An introduction to soil dynamics*, Vol. 24, Springer Science & Business Media.

Vreeburg, J. H. G., Vloerbergh, I. N., Van Thienen, P. and De Bont, R. (2013), 'Shared failure data for strategic asset management', *Water Science and Technology: Water Supply* **13**(4), 1154–1160.

Walski, T., Bezts, W., Posluszny, E. T., Weir, M. and Whitman, B. E. (2006), 'Modeling leakage reduction through pressure control', *Journal-American Water Works Association* **98**(4), 147–155.

Waltham, A. C. (1993), 'Crown hole development in the sandstone caves of Nottingham', *Quarterly Journal of Engineering Geology and Hydrogeology* **26**(4), 243–251.

Wang, D., Bienen, B., Nazem, M., Tian, Y., Zheng, J., Pucker, T. and Randolph, M. F. (2015), 'Large deformation finite element analyses in geotechnical engineering', *Computers and Geotechnics* **65**, 104–114.

Wang, K. and Sun, W. (2016), 'A semi-implicit discrete-continuum coupling method for porous media based on the effective stress principle at finite strain', *Computer Methods in Applied Mechanics and Engineering* **304**, 546–583.

Wang, T., Zhang, F., Furtney, J. and Damjanac, B. (2022), 'A review of methods, applications and limitations for incorporating fluid flow in the discrete element method', *Journal of Rock Mechanics and Geotechnical Engineering* .

Weisman, R. N. and Lennon, G. P. (1994), 'Design of fluidizer systems for coastal environment', *Journal of waterway, port, coastal, and ocean engineering* **120**(5), 468–487.

Weisman, R. N., Lennon, G. P. and Roberts, E. W. (1988), 'Experiment on fluidization in unbounded domains', *Journal of Hydraulic Engineering* **114**(5), 502–515.

Wengström Rd, T. (1993), 'Comparative Analysis of Pipe Break Rates-A Literature Review'.

Więckowski, Z. (2003), 'Modelling of silo discharge and filling problems by the material point method', *Task Quarterly* **7**(4), 701–721.

Wols, B. A. and Van Thienen, P. (2014), 'Impact of weather conditions on pipe failure: a statistical analysis', *Journal of Water Supply: Research and Technology—AQUA* **63**(3), 212–223.

Wu, K., Yang, D., Wright, N. J. C. and Structures (2016), 'A coupled SPH-DEM model for fluid-structure interaction problems with free-surface flow and structural failure', **177**, 141–161.

Xu, B. H. and Yu, A. B. (1997), 'Numerical simulation of the gas-solid flow in a fluidized bed by combining discrete particle method with computational fluid dynamics', *Chemical engineering science* **52**(16), 2785–2809.

Xu, Q., Liu, R., Chen, Q. and Li, R. (2014), 'Review on water leakage control in distribution networks and the associated environmental benefits', *Journal of Environmental Sciences* **26**(5), 955–961.

Yamaguchi, Y., Takase, S., Moriguchi, S. and Terada, K. (2020), 'Solid–liquid coupled material point method for simulation of ground collapse with fluidization', *Computational Particle Mechanics* **7**(2), 209–223.

Yamijala, S., Guikema, S. D. and Brumbelow, K. (2009), 'Statistical models for the analysis of water distribution system pipe break data', *Reliability Engineering & System Safety* **94**(2), 282–293.

Yamini, H. and Lence, B. J. (2010), 'Probability of failure analysis due to internal corrosion in cast-iron pipes', *Journal of Infrastructure Systems* **16**(1), 73–80.

Yerro, A. (2015), MPM modelling of landslides in brittle and unsaturated soils, PhD thesis, Universitat Politecnica de Catalunya.

Yerro, A., Alonso, E. E. and Pinyol, N. M. (2015), 'The material point method for unsaturated soils', *Geotechnique* **65**(3), 201–217.

Yerro, A., Alonso, E. E. and Pinyol, N. M. (2016), 'Run-out of landslides in brittle soils', *Computers and Geotechnics* **80**, 427–439.

Yerro, A., Alonso, E. and Pinyol, N. (2014), Modelling progressive failure with MPM, *in* 'Proc. 8th Eur. Conf. Numerical Methods in Geotechnical Engineering', London, CRC Press, pp. 319–323.

Yerro, A. and Rohe, A. (2019), Fundamentals of the Material Point Method, *in* J. Fern, A. Rohe, K. Soga and E. Alonso, eds, 'Material Point Method Geotechnical Eng. A Practical Guide', Taylor & Francis Group, London, chapter 2, pp. 23–56.

Yerro, A., Rohe, A. and Soga, K. (2017), Modelling Internal Erosion with the Material Point Method, *in* 'Procedia Engineering', Vol. 175, Elsevier Ltd, pp. 365–372.

Zabala, F. and Alonso, E. E. (2011), 'Progressive failure of Aznalcóllar dam using the material point method', *Géotechnique* **61**(9), 795–808.

Zhang, D. Z., Zou, Q., VanderHeyden, W. B. and Ma, X. (2008), 'Material point method applied to multiphase flows', *Journal of Computational Physics* **227**(6), 3159–3173.

Zhang, H. W., Wang, K. P. and Zhang, Z. (2007), Material point method for numerical simulation of failure phenomena in multiphase porous media, *in* 'Computational Mechanics', Springer, pp. 36–47.

Zhao, X., Bolognin, M., Liang, D., Rohe, A. and Vardon, P. J. (2019), 'Development of in/outflow boundary conditions for MPM simulation of uniform and non-uniform open channel flows', *Computers and Fluids* **179**, 27–33.

Zhao, X. and Liang, D. (2016), MPM modelling of seepage flow through embankments, *in* 'The 26th International Ocean and Polar Engineering Conference', OnePetro.

Zhu, H., Zhang, L., Chen, C. and Chan, K. (2018), 'Three-dimensional modelling of water flow due to leakage from pressurized buried pipe', *Geomechanics & engineering* **16**(4), 423–433.

Zienkiewicz, O. C., Chan, A. H. C., Pastor, M., Schrefler, B. A. and Shiomi, T. (1999), *Computational geomechanics*, Vol. 613, Citeseer.

Zienkiewicz, O. C. and Morice, P. B. (1971), *The finite element method in engineering science*, Vol. 1977, McGraw-hill London.

Zienkiewicz, O. C. and Shiomi, T. (1984), 'Dynamic behaviour of saturated porous media; the generalized Biot formulation and its numerical solution', *International journal for numerical and analytical methods in geomechanics* **8**(1), 71–96.

Zoueshtiagh, F. and Merlen, A. (2007), 'Effect of a vertically flowing water jet underneath a granular bed', *Physical Review E - Statistical, Nonlinear, and Soft Matter Physics* **75**(5), 1–12.

# Appendix A

# MPM numerical implementation

## A.1 2P-SP MPM approach

In this Appendix, the momentum balances for the liquid and the mixture are integrated and discretised using the two-phase single-point (2P-SP) MPM approach. This process results in the formulation of a system of equations. Additionally, an explicit time discretization scheme is provided.

### A.1.1 Spatial discretisation

In the 2P-SP MPM approach, both a computational mesh and a set of material points are employed to represent the continuum. A set of standard linear shape functions ($N_j$) is utilised to discretise all the primary unknowns at the mesh nodes. As an example, solid and liquid displacements can be approximated as follows

$$u_s(x.t) = \sum_{j=1}^{N_n} u_{s_j}(t) N_j(x,t) \tag{A.1}$$

$$u_l(x.t) = \sum_{j=1}^{N_n} u_{s_j}(t) N_j(x,t) \tag{A.2}$$

where $u_{s_j}(t)$ and $u_{s_j}(t)$ are the solid and liquid displacements at node $j$. During the discretisation process, each material point is assigned to a specific portion of the saturated porous media. It is important to note that the mass of the mixture, which includes both the solid and liquid components, is concentrated at the position of the corresponding material point. Consequently,

the density of the mixture ($\rho_m$) can be described as follows

$$\rho_m(x,t) = \sum_{p=1}^{N_p} m_p \delta(x - x_p) \tag{A.3}$$

where $m_p$ is the total mass of the material point $p$, $x_p$ is the position of the material point p, ($\delta$) is the Dirac delta function, and $N_p$ is the total number of material points.

Additionally, in the 2P-SP MPM approach, it is crucial to take into account the liquid density ($\rho_l$) and the solid density ($\rho_s$) as

$$\rho_l(x,t) = \sum_{p=1}^{N_p} \tilde{m}_{lp} \delta(x - x_p) \tag{A.4}$$

$$\rho_s(x,t) = \sum_{p=1}^{N_p} \tilde{m}_{sp} \delta(x - x_p) \tag{A.5}$$

Where $\tilde{m}_{lp}$ and $\tilde{m}_{lp}$ represent the masses that a material point would possess if it were composed entirely of liquid or solid, respectively. These values can be calculated using the provided expressions.

$$\tilde{m}_{lp} = \rho_l V_p \tag{A.6}$$

$$\tilde{m}_{sp} = \rho_s V_p \tag{A.7}$$

Furthermore, the real masses of liquid and solid within a material point can be expressed as

$$m_{lp} = n\tilde{m}_{lp} \tag{A.8}$$

$$m_{sp} = (1-n)\tilde{m}_{sp} \tag{A.9}$$

### A.1.2 Discretisation of the momentum balance equations

The Galerkin method of Weighted Residuals has been utilized to derive the weak form of the momentum balance equations. Considering the discretisation at the nodes (Eq. A.1) and

(Eq. A.2), the momentum balances for the liquid and mixture can be expressed as

$$\begin{aligned}\sum_{j=1}^{N_n}\int_{\Omega}\rho_l N_i^p N_j^p d\Omega a_{lj} = \int_{\partial\Omega^{Pl}} N_i^p \hat{p}_l d\partial\Omega^{pl} - \int_{\Omega} B_i^p \rho_{lp} m d\Omega \\ -\sum_{j=1}^{N_n}\int_{\Omega}\frac{n\mu_l}{k_l} N_i^p N_j^p d\Omega(v_{lj}-v_{sj}) + \int_{\Omega}\rho_l N_i^p b d\Omega\end{aligned} \tag{A.10}$$

$$\begin{aligned}\sum_{j=1}^{N_n}\int_{\Omega}(1-n)\rho_s N_i^p N_j^p d\Omega a_{sj} + sum_{j=1}^{N_n}\int_{\Omega} n\rho_l N_i^p N_j^p d\Omega a_{lj} = \\ \int_{\partial\Omega^t} N_i^p \hat{t} d\partial\Omega^t - \int_{\Omega} B_i^p . \sigma_p d\Omega + \int_{\Omega}\rho_m N_i^p b d\Omega\end{aligned} \tag{A.11}$$

By utilising (Eq. A.3) and (Eq. A.4) to approximate the integrals across the domain as a quadrature on the material points, the resulting system of equations can be expressed in a concise manner as follows.

$$\widetilde{\mathrm{M}_l} = \sum_{p=1}^{N_p} \tilde{m}_{lp} \mathrm{N}^p \tag{A.12}$$

$$\mathrm{M}_s = \sum_{p=1}^{N_p} m_{sp} \mathrm{N}^p \tag{A.13}$$

$$\mathrm{M}_l = \sum_{p=1}^{N_p} m_{lp} \mathrm{N}^p \tag{A.14}$$

$$\mathrm{Q}_l = \sum_{p=1}^{N_p} \frac{n\mu}{k_l} \mathrm{N}^{pT} . \mathrm{N}^p V_p \tag{A.15}$$

$$\mathrm{F}_l^{ext} = \int_{\partial\Omega^{Pl}} \mathrm{N}^p . \hat{p}_l d\partial\Omega^{pl}|_p + \sum_{p=1}^{N_p} \tilde{m}_{lp} \mathrm{N}^p . b \tag{A.16}$$

$$\mathrm{F}^{ext} = \int_{\partial\Omega^t} \mathrm{N}^p . \hat{t} d\partial\Omega^t|_p + \sum_{p=1}^{N_p} m_p \mathrm{N}^p . b \tag{A.17}$$

$$\mathrm{F}_l^{int} = \sum_{p=1}^{N_p} B^p . p_{lp} m V_p \tag{A.18}$$

$$\mathrm{F}^{int} = \sum_{p=1}^{N_p} B^p . \sigma_p V_p \tag{A.19}$$

### A.1.3 Time discretisation

To perform time integration of the equations, an explicit Euler scheme is employed. The liquid and solid velocities are updated using the accelerations at time $t^k$ (refer to Eq. A.20 and Eq. A.21), while the liquid and solid displacements are updated using the velocities calculated at time $t^{k+1}$ (refer to Eq. A.22 and Eq. A.23).

$$v_l^{k+1} = v_l^k + \triangle t a_l^k \tag{A.20}$$

$$v_s^{k+1} = v_s^k + \triangle t a_s^k \tag{A.21}$$

$$u_l^{k+1} = u_l^k + \triangle t v_l^{k+1} \tag{A.22}$$

$$u_s^{k+1} = u_s^k + \triangle t v_s^{k+1} \tag{A.23}$$

## A.2 2P-DP MPM approach

In the two-phase double-point (2P-DP) MPM approach, each set of material points (MPs) (i.e. LMPs and SMPs) is used to represent either liquid or solid phase. The mass associated with each MP is concentrated at its respective position. As a result, the densities of the liquid and solid can be expressed in terms of mass. The momentum balance equations are discretised at the nodes of the computational mesh and integrated at the material points. This integration results in the formulation of the following system of equations

$$M_L \vec{a}_L = f_L^{ext} - f_L^{int} - f_L^n - Q_L(\vec{v}_L - \vec{v}_S) \tag{A.24}$$

$$M_S\vec{a}_S = \vec{f}_S^{ext} - \vec{f}_S^{int} - \vec{f}_S^{n} - Q_L(\vec{v}_L - \vec{v}_S) \tag{A.25}$$

where $\vec{a}_S$ is the solid nodal acceleration, where $\vec{a}_L$ is the liquid nodal acceleration, $M_S$ and $M_L$ corresponds to the lumped mass matrices for the solid and liquid phases. $\vec{f}_l^{ext}$, $\vec{f}_l^{int}$, $\vec{f}_S^{ext}$ and $\vec{f}_S^{int}$ represent the internal and external nodal force vectors for the liquid and solid phases, respectively. $\vec{f}_l^{n}$ and $\vec{f}_S^{n}$ denote the vectors of solid-liquid interaction forces associated with the concentration ratio gradient, and $Q_L$ represents the nodal drag force matrix. The specific expressions for all these matrices and force vectors can be found below

$$M_L \approx \sum_{MP=1}^{n_{LMP}} m_L^{MP} N \tag{A.26}$$

$$M_S \approx \sum_{MP=1}^{n_{MP}} m_S^{MP} N \tag{A.27}$$

$$\vec{f}_L^{ext} \approx \int_{\partial\Omega^{PL}} N^T \vec{\hat{P}}_L d\partial\Omega^{PL} \mid_{M\ P} + \sum_{MP=1}^{n_{MP}} m_L^{MP} N^T \vec{g} \tag{A.28}$$

$$\vec{f}_S^{ext} \approx \int_{\partial\Omega^{T}} N^T (\vec{T} + n_S^{MP} \vec{\hat{P}}_L) d\partial\Omega^{T} \mid_{M\ P} + \sum_{MP=1}^{n_{MP}} m_S^{MP} N^T \vec{g} \tag{A.29}$$

$$\vec{f}_L^{int} \approx \sum_{MP=1}^{n_{MP}} B^T \bar{\sigma}_L^{MP} V_{MP} \tag{A.30}$$

$$\vec{f}_S^{int} \approx \sum_{MP=1}^{n_{MP}} B^T \bar{\sigma}_S^{MP} V_{MP} \tag{A.31}$$

$$\vec{f}_L^{n} \approx \sum_{MP=1}^{n_{MP}} N^T \bigtriangledown n_L^{MP} \sigma_L^{MP} V_{MP} \tag{A.32}$$

$$\vec{f}_S^{n} \approx \sum_{MP=1}^{n_{MP}} N^T \bigtriangledown n_S^{MP} \sigma_L^{MP} V_{MP} \tag{A.33}$$

$$Q_L \approx \sum_{MP=1}^{n_{MP}} N^T \left(\frac{(n_L^{MP})^2 \mu_L^{MP}}{K_L^{MP}} + \beta (n_L^{MP})^3 \rho_L^{MP} \mid \vec{v}_L - \vec{v}_S \mid\right) N V_{MP} \tag{A.34}$$

where $\vec{T}$ is the prescribed traction vector, $\vec{\hat{P}}_L$ represents the prescribed liquid pressure, $(N)$ refers to the matrix of nodal shape functions, $(B)$ is the matrix that incorporates the gradients of the nodal shape functions. One numerical challenge in this approach is the computation of the concentration ratio gradient $(\bigtriangledown n_L)$. The effective liquid concentration ratio field $(n_L)$ exhibits discontinuities at the interface between free surface water and porous medium. The liquid concentration ratio field, $(n_L)$, exhibits two constant values: 1 in the free surface water and the porosity value, $(n)$, in the porous medium. To address the transition between free surface water and groundwater, (Martinelli, 2016) introduced the concept of a transition zone. In this zone, an interpolated liquid concentration ratio is introduced, enabling a smooth transition of $(n_L)$ between the free surface water and the groundwater regions.

# Appendix B

# Pipe leakage modelling using a water reservoir

In this Appendix, the representation of pipe leakage with a water reservoir using the two-phase double-point (2P-DP) Material Point Method (MPM) formulation is presented and discussed. The pipe leakage is represented by a water reservoir that is large enough to roughly maintain the initial water height throughout the calculation. This approach was adopted from the numerical study conducted by Martinelli et al. (2017) that investigated the crater development around a leaking pipe embedded in sand using the MPM. The model geometry designed to model the pipe leakage problem is presented in Figure B.1. The soil bed is 12.5 m in height and 2.5 m in length. An orifice with a width of 0.5 m is positioned in the middle of the soil base connected to a 12 m height water reservoir.

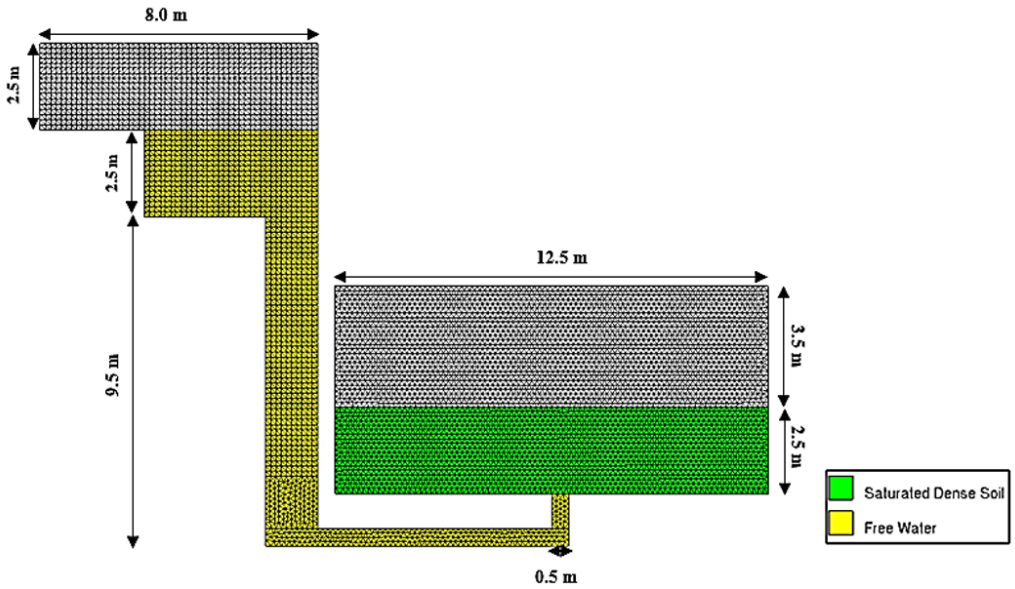



**Figure B.1:** Discretised domain of pipe leakage problem

The soil and water properties used in this model are similar to the parameters used in previous simulations (see Section 4.2). Stresses are initialised via an earth pressure coefficient at rest (K0) procedure, and pore pressures are initially hydrostatic. At all boundaries, including the water reservoir, the displacements are fixed in normal directions and free in the longitudinal direction. The water leakage is modelled by removing the vertical liquid fixity at the orifice.

Figure 4.11 shows the displacement field associated with the water leakage for t = 1, 2 and 3 seconds, together with the location of the liquid material points. The soil fluidisation process is associated with an uplift mechanism of the soil bed above the orifice (maximum of 10 mm), as shown in Figure 4.12. The fluidisation mechanism is consistent with the presented results in this thesis. However, the water reservoir approach does not provide constant water flow during the simulation. This limitation impacts the accuracy of simulating the soil fluidisation progression around a pressurised leaking pipe. Therefore, advanced inflow/outflow Boundary Conditions (BCs) have been implemented into the double-point approach that is described in this thesis (Section 3.4.2.3). This helped the simulation of constant velocity flows and optimised the computational cost by simplifying the geometry.

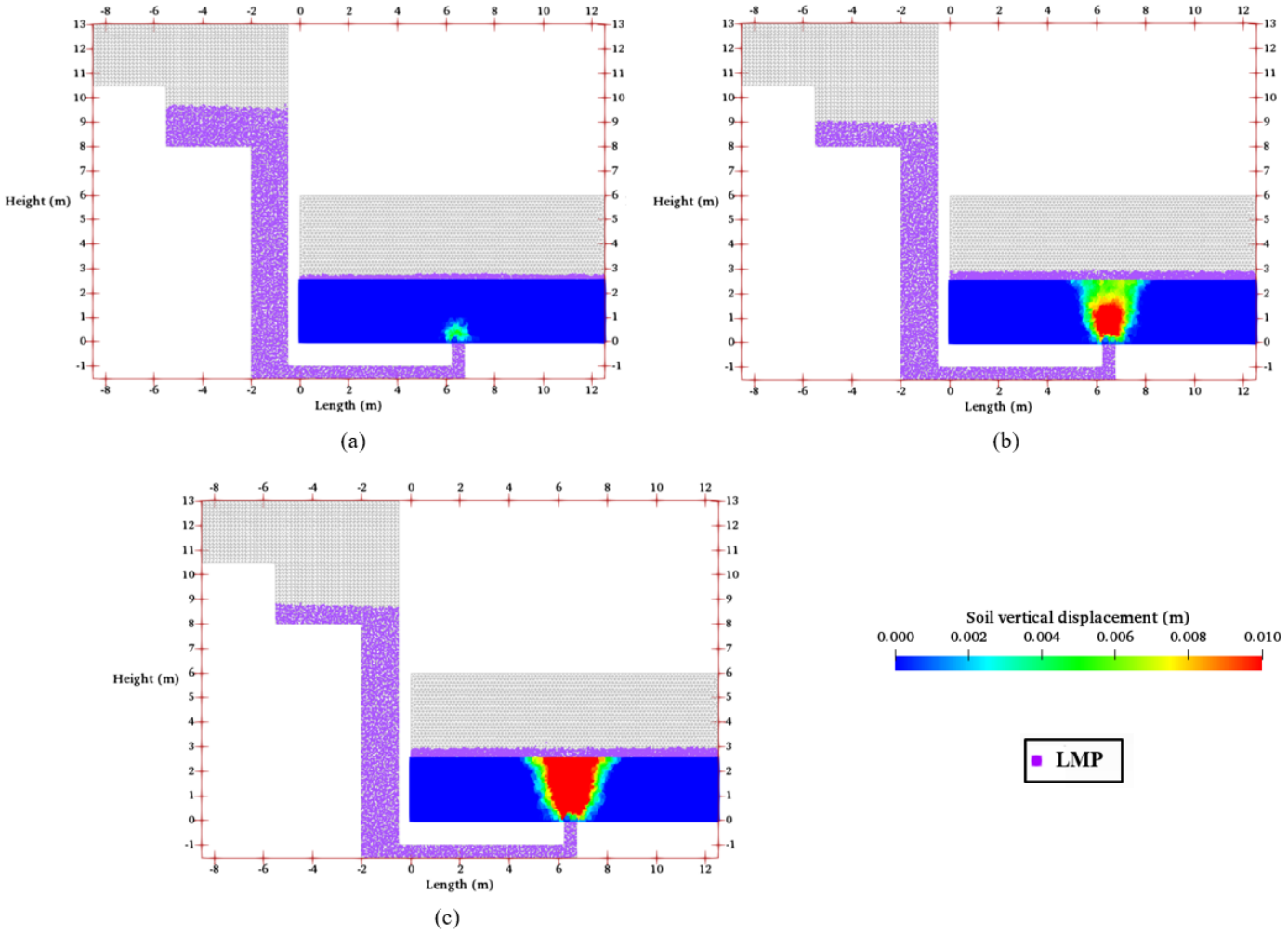


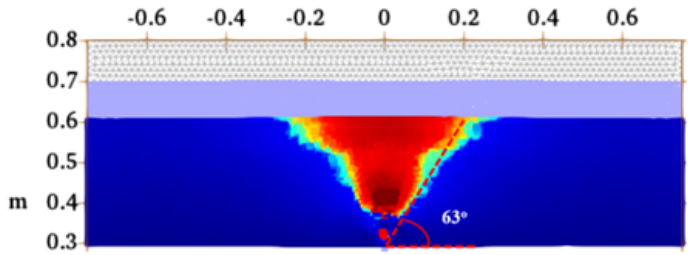
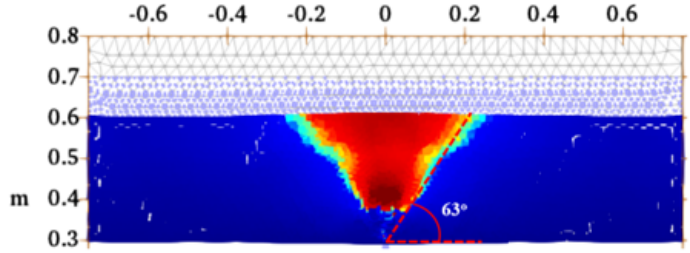
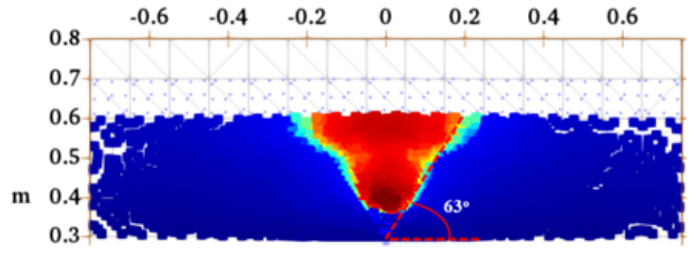

**Figure B.2:** Soil vertical displacement in pipe leakage problem at different time; (a) 1s, (b) 2s, and (c) 3s

# Appendix C

# Mesh sensitivity analysis

In this Appendix, the conducted mesh sensitivity analysis is demonstrated to examine the impact of mesh size on solution accuracy. The parameters of the mesh sensitivity analysis are listed in Table C.1. The mesh is varied between 0.015 m and 0.100 m, which results in the number of material particles varying between 18,414 and 49,044. The inclination angle of the fluidised zone obtained from MPM simulations with different mesh sizes is consistent with Alsaydalani (2010)'s experiment. Therefore, it has been concluded that the shape of the fluidised zone is independent of the mesh size. The shape of the fluidised zone depends on the material properties among other parameters. For instance, the inclination angle of the wedge of the uplift zone above the orifice depends on the angle of shear failure that depends on the angle of friction of the soil (Cui, 2013).

**Table C.1:** Mesh sensitivity analysis parameters

| Case | Mesh size (m) | Time increment (s) | Total number of material particles |   |
|---|---|---|---|---|
| **1** | 0.015 | $3.2 \times 10^{-4}$ | 49,044 |   |
| **2** | 0.030 | $3.9 \times 10^{-4}$ | 25,002 |   |
| **3** | 0.100 | $4.7 \times 10^{-4}$ | 18,414 |   |

# Appendix D

# Boundary condition analysis

A comparison between the MPM results for different types of boundary conditions is presented here. In Figure D.1a, a fixed boundary condition has been used at the base of the soil bed. However, a contact algorithm implemented in Anura3D has been applied between the base of the soil bed and the added base (Figure D.1b, in grey). The contact boundary would be a better representation of the boundary condition which may release the particle if they move upwards and provide some constraints if they move downwards. However, this does not have a significant impact on the results as there is generally no uplift of the soil at the bottom of the soil bed during the fluidisation mechanism. The obtained results were consistent with both types of boundary conditions. Therefore, a simplified fixed boundary condition is selected to reduce the computational cost of the simulations.

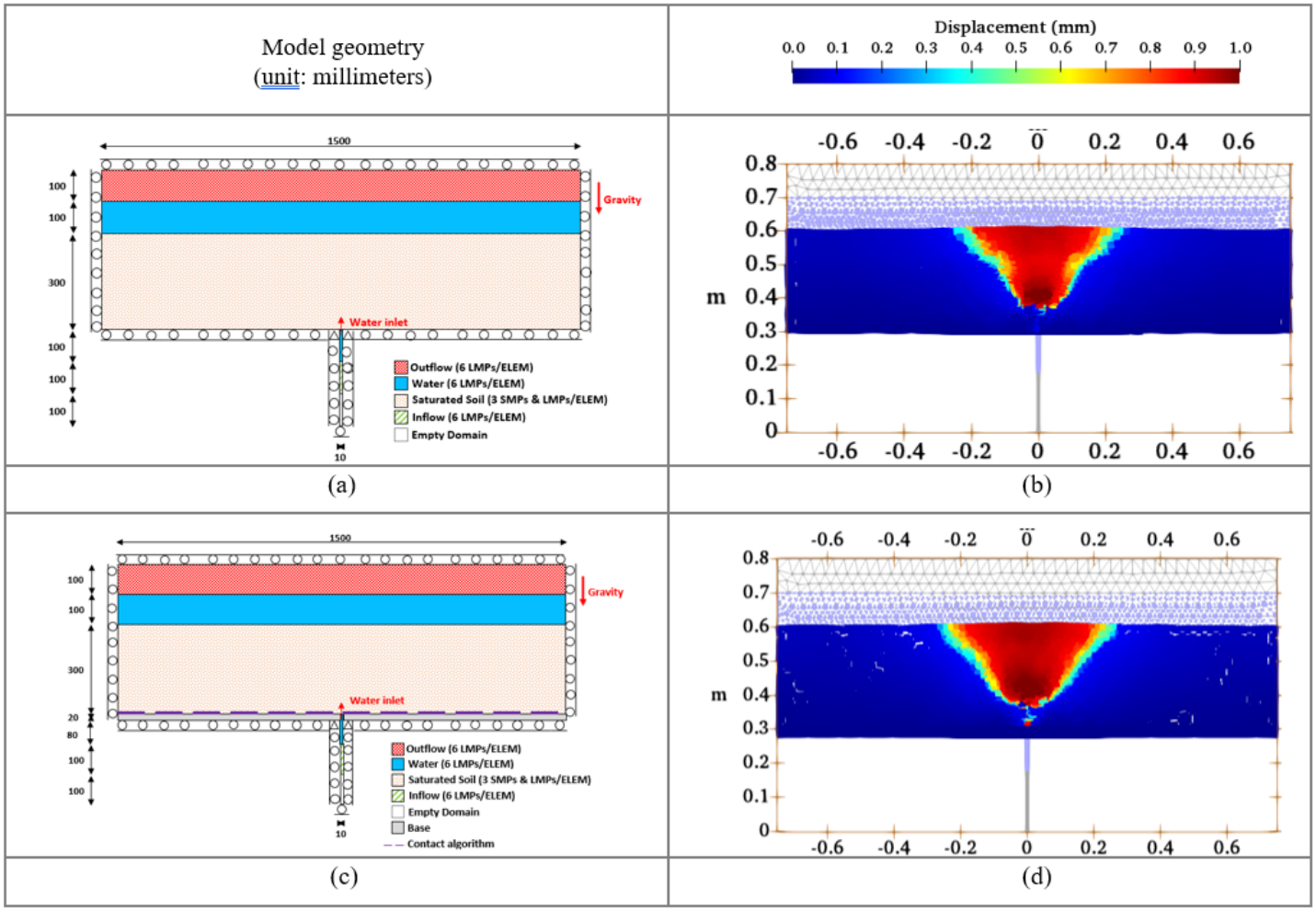



**Figure D.1:** Soil vertical displacement when fluidisation reaches the surface at an inflow velocity of 0.10 m/s for MPM model with (a, b) fixed boundary and (c, d) contact boundary at the base of the soil bed

# Appendix E

# Lateral leakage simulation

In this Appendix, the soil fluidisation process triggered by a lateral water leakage is investigated using the two-phase double-point (2P-DP) Material Point Method (MPM) formulation. The inflow/outflow boundary conditions (BCs) were developed to model a lateral flow. This is a preliminary model that was conducted prior to studying the effect of leakage direction on the fluidisation process (Section 5.3.2.5).

The 2P-DP MPM model presented in Figure E.1 is similar problem as the model presented in (Chapter 4) with the same material parameters. The soil bed is 300 mm in height and 1500 mm in length. A set of numerical simulations subjected to different lateral inflow velocities through a 10 mm orifice is simulated to investigate the onset and development of soil fluidisation mechanism.

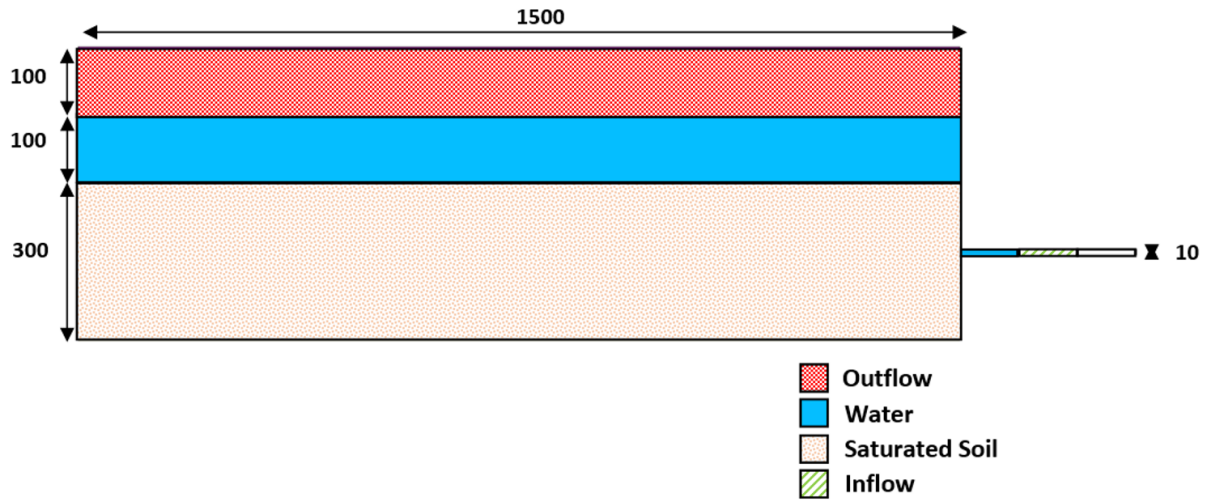
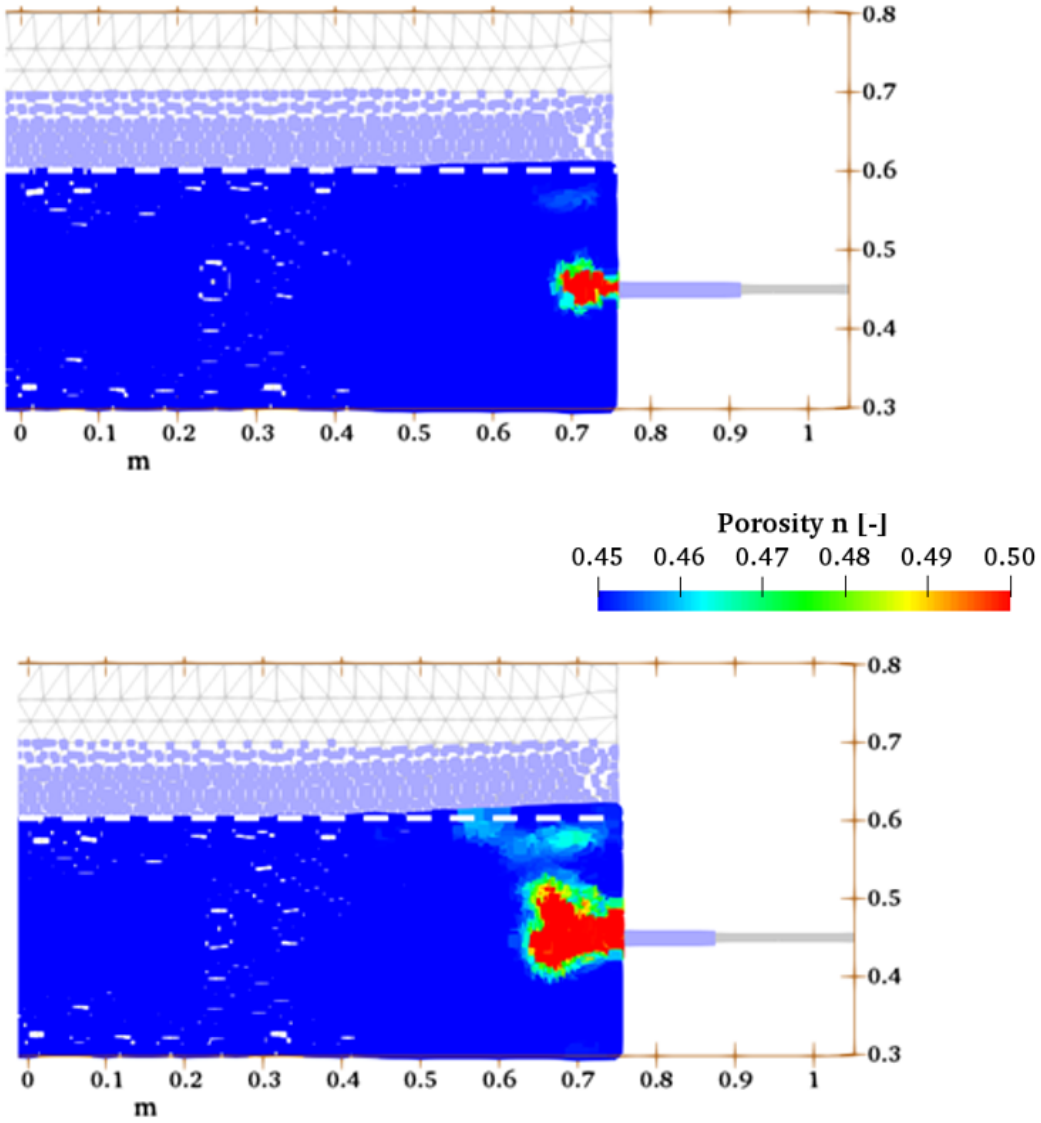



**Figure E.1:** Geometry of the lateral leakage model (unit: mm)

The porosity distribution at different inlet velocities after 2s of simulation through the centreline of the soil bed is plotted in Figure E.2. The soil porosity increases with the increase in the inflow velocity and increases faster around the orifice. Figure E.2 demonstrates the observed stages of

fluidisation progression with the increase in the leakage velocity: a) outwards initiation of the fluidised zone in lateral and vertical directions, b) enlargement of the fluidised region, c) rapid progression of fluidisation, and d) surface fluidisation. The observed mechanism is consistent with the experimental result by Alsaydalani (2020) that studied the effect of horizontal seepage on the failure mechanism of a granular bed. The presented investigation provides valuable insights into the fluidisation mechanism of the soil bed induced by lateral leakage.



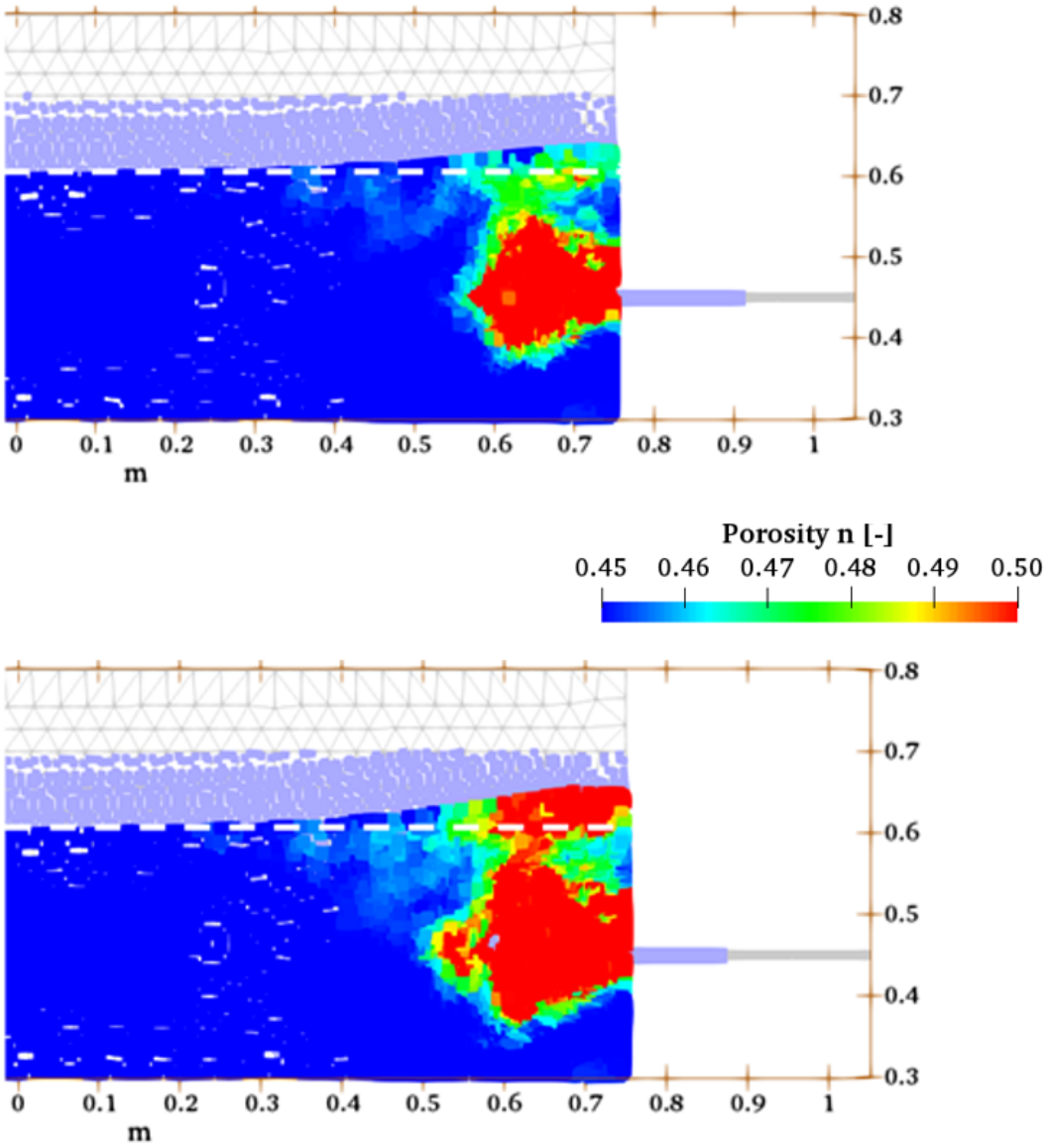

(a) 0.02 m/s

Onset of fluidisation that is associated with slight deformation of the bed surface above the office.

(b) 0.04 m/s

Enlargement of the fluidised zone at higher water velocity with a further uplift of the bed surface.

**Figure E.2:** Change of soil porosity in the soil bed subjected to a lateral leakage at different inflow velocities




(a) 0.08 m/s

Rapid progress of the fluidised zone

(b) 0.10 m/s

Emergence of the fluidised zone at the bed surface at high leakage velocity

**Figure E.3:** Change of soil porosity in the soil bed subjected to a lateral leakage at different inflow velocities